Online ISSN : 2395-602X
Print ISSN : 2395-6011
www.ijsrst.com

INTERNATIONAL VIRTUAL CONFERENCE ON MATERIALS AND NANOTECHNOLOGY IVCMN-2021

Jointly Organized by
Guru Nanak College of Science, Ballarpur
In Association with
P. R. Pote (Patil) College of Engineering and Management, Amravati

VOLUME 9, ISSUE 7, MARCH-APRIL-2021

INTERNATIONAL JOURNAL OF SCIENTIFIC RESEARCH IN SCIENCE AND TECHNOLOGY

Email : editor@ijsrst.com Website : http://ijsrst.com

International Virtual Conference on Materials and Nanotechnology

IVCMN – 2021

29 th and 30 th April 2021

Jointly Organized by
Guru Nanak College of Science, Ballarpur
In Association with
P. R. Pote (Patil) College of Engineering and Management, Amravati
In Association with
International Journal of Scientific Research in Science and Technology
Print ISSN : 2395-6011 Online ISSN : 2395-602X
Volume 9, Issue 4, March-April-2021
International Peer Reviewed, Open Access Journal

Published By
Technoscience Academy

(The International Open Access Publisher)

Website : www.technoscienceacademy.com

About the Conference

It's our great pleasure to announce that our Guru Nanak College of Science, Ballarpur is going to celebrate the golden jubilee year of opening of college. We are pleased to inform you that on this occasion Department of Physics, GNC Ballarpur is going to organize two days international virtual conference on materials and nanotechnology on 29th& 30th of April 2021. We have invited seven guest speakers from the country and outside the country.

Aims and Objectives

The main aim of this conference is to make everyone familiar with new researches that are being carried out in the field of material science and nanotechnology and their basic applications. The objectives of IVCOMN- 2021 are to bring about the sharing of views and researches carried out by eminent researchers, scientists, scholars and technologists by bringing them together on the dice and to develop curiosity among new researchers to bring about research in this field. The conference will cover healthy and useful discussion on theoretical and experimental aspects in the field of material science and nanotechnology. We take great pleasure in inviting you to submit original research papers on the topics given. You are requested to send an abstract of you.

The main aim of this conference is to make everyone familiar with new researches that are being carried out in the field of material science and nanotechnology and their basic applications. The objectives of IVCOMN- 2021 are to bring about the sharing of views and researches carried out by eminent researchers, scientists, scholars and technologists by bringing them together on the dice and to develop curiosity among new researchers to bring about research in this field. The conference will cover healthy and useful discussion on theoretical and experimental aspects in the field of material science and nanotechnology.

We take great pleasure in inviting you to submit original research papers on the topics given. You are requested to send an abstract of your research paper so as to reach us latest by 25 April 2021. All research papers will be published in UGC-approved, Google scholar, Research gate, Academia, DOAJ and Copernicus indexed journal.

We are looking forward for your positive response, active participation and valuable contribution for this conference.

-: Guru Nanak College of Science, Ballarpur :-

Guru Nanak Sewa Samitti is a multifocal diversified, being involved in various community & social activities to mankind. Guru Nanak College of Science, Ballarpur was established by veteran Late Sardar Ajit Singh Soni ji in 1971. Under the able guidance of Sardar Naginder Singh Soni ji, the institute is flourishing and blooming healthier, brighter & shiner. The Institution since its inception has help creating 1000+ success stories as doctors. engineers, diversified professional & country server through its NCC & NSS programmes shaping their careers & futures endurance ability.

-: P. R. Pote (Patil) College of Engeening and Management, Amravati :-

P. R. Pote (Patil) Group of Educational Institutes Amravati, is a foremost name in higher education in Maharashtra. Since its inception, the trust has been successfully conducting undergraduate and post graduate courses in emerging areas. It has 10 institutes under one roof. The Group offers undergraduate as well as post graduate courses in various disciplines of Engineering, Management and Technology. Various courses offered by the Group include ME, BE, MBA, MCA, Pharmacy, Architecture, Agriculture, B. Arch, B.Ed., CBSE Schooling, Polytechnic. By the blessings of Shri Sant Gajanan Maharaj, We aim at developing a pursuit of knowledge in Students, commitment to Economic, Social &Cultural uplifting of masses. The Institute highly believes in nurturing ethics and moral values in students. The P. R. Pote (Patil) Group has its branches at Amravati & Talegaon. We realize that education is the basis for the complete development of individual and for this purpose we have dedicated teaching staff, Digital Classrooms, Sophisticated Equipment, Wi-Fi campus, Finishing School, Placement Cell, State-of-Art Auditorium, Well Equipped Laboratories, Classrooms, International Quality Infrastructure and 24 hours Library. Our constant endeavor is to provide a gamut of opportunities for our students to make them practical engineers, top class managers and also good citizens.

Editorial Board

Invited Speakers

Dr. Konstantin Ivonovskikh
Ural Federal, Russia

Prof. Ramchandra Pode
Kyung Hee University
Kyung Hee. Univ. South Korea

Prof. S. J. Dhoble
Dept. of Physics,
RTMNU, Nagpur

Dr. Manish Shinde
Scientist B,
C – MET, Pune

Dr. C. Gayner
Material Scientist
Israel

Dr. Harnath D.
Physics Dept.
NIT,Warangal, India

Dr. R. G. Tanguturi
Dept. of Material Science
and Engg. Wuhan, China

Dr. Preeti Gupta
Leibniz Institute for Solid State
& Material research, Germany

Chairman of session

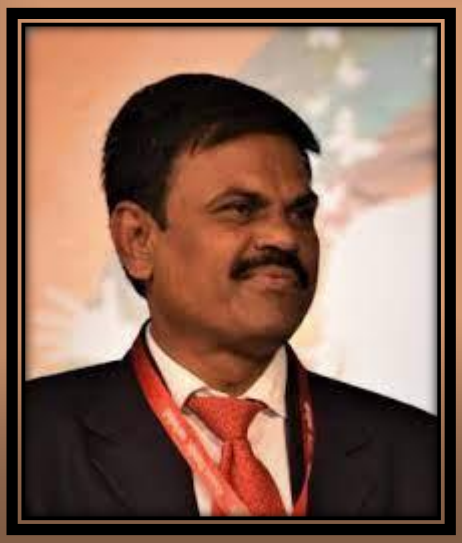

Dr. Ishwar S. Mohurley
Ex-Registrar
Gondwana University,
Gadchiroli

Dr. Sachin S. Wazalwar
Assistant Professor
Dept. of Applied Chemistry
RCERT, Chandrapur

Dr. N. R. Pawar
Head
Department of Physics
ACS College,Maregao

Dr. A. U. Bajpeyee
HOD
ACS College
Amravati

Organizing Secretory

Dr. Shobha Gaikwad

Dr. Amol Bhoyar

Convenor

Dr. Nilesh Takare

Dr. Amol Nande

Advisory Committee

Prof. S. J. Dhoble
Dr. R.S. Meshram
Dr. Manish Matte
Prof. L.K. Bedre
Dr. Amrut Gaddamwar
Dr. Prerna Modak
Prof. B.V. Tupte
Dr. D.B. Zade
Dr. R.A. Mandal
Prof. Atul Khobragade
Dr. P.K. Singh
Dr. Sanjay Singh
Dr. S. Pathak
Dr. R.R. Kherani
Prof. Pavan Chatare
Dr. U.P. Manik
Dr. P.R. Moharkar
Dr. K.C. Patil
Dr. S.R. Gawli
Dr. Ajay Dahegaonkar
Prof. V.S. Dhabarde
Dr. Madhamshettiwar

Dr. Atram
Dr. Jogi
Dr. Shende
Dr. Mrs. Katkamwar
Prof. Shambharkar
Dr. Thawari
Dr. Parwate
Dr. Batra
Dr. Deshmukh
Dr. Hunge
Dr. Kamlesh Dabre
Dr. Suyash Mullenwar
Prof. D.D. Bhoyar
Dr. G.S. Gond
Prof. Pramod Khirade
Dr. P.S. Katkar
Dr. Dipti Ingole
Dr. Ritesh Kohale
Dr. Deepak Taikar
Dr. Prerna Modak
Dr. K. M. Kulkarni
Dr. Mrs. S. A. Ghosh

Dr. I.S. Mohurley
Dr. F. C. Raghuwanshi
Dr. Pradip Khedkar
Dr. Ajay Lad
Dr. N. G. Belsare
Dr. Deepak Dhote
Dr. G. G. Muley
Dr. C. S. Ulhe
Dr. N. R. Pawar
Dr. A. U. Bajpeyee
Dr. G. R. Dhokane
Dr. P. R. Gandhi
Dr. N. B. Ingole
Dr. N. A. Patil
Dr. P. R. Rajput
Dr.Nandkishor Thakare
Dr. S. S. Thakare
Dr. Amrut Gaddamwar
Dr. Prashant Netankar
Dr. Manoj Munde
Dr. Pravin Bodhakhe
Dr. Mangesh Yerpude

Technical Committee

Dr. Dinesh Deshmukh
Ms. Sapana Sharma

Dr. Nilesh Jadhao
Mr. Nilesh B. Shelke

Mr. Avinash S. Ratthe
Ms. Seema Bhagat

CONTENTS

Sr. No	Article/Paper	Page No
1	**Nanotechnology for Herbal Drug and Its Uses** D. T. Sakhare	01-07
2	**Study of Nanotechnology with the Help of Cartoons** Dipak Nath	08-18
3	**Structural, Morphological, Dielectric and Magnetic Behaviour of Rare Earth Substituted Cobalt Ferrite Nanoparticles - A Brief Review** Y. S. Bopche, M. S. Bisen, A. M. Shahare, D. S. Choudhary	19-24
4	**Ultrasonic Study of 'Molecular Interaction of 2- Substituted 4, 5-Diphenyl Imidazole with Ethanol at Different Temperature'** T. M. Bhagat, Kalyani K. Kumbhare, Pradip B. Rathod	25-29
5	**Band gap of $Bi_2Al_4O_9$** S. G. Revankar, K. A. Gedekar, S. P. Puppulwar, S. P. Wankhede, P. D. Belsare , S. V. Moharil	30-32
6	**Synthesis, Structural and Magnetic Study of Nickel Substituted Magnesium Spinel Ferrites** Pranali K. Tembhurne, Nomdeov M. Gahane, Kishor G. Rewatkar, Sanjay J. Dhoble	33-38
7	**Literature Survey on Aspect Based Sentiment Analysis for Products on E-Commerce Business Platform** Shraddha H. Ingle, Prof. Mayur S. Burange, Dr. Ajay B. Gadicha	39-42
8	**A Prominent Overlapping of Red Phosphor Emission with the Absorption Spectra of Green Plants Useful for Artificial LED Plant Lighting** P. J. Yadav, N. D. Meshram, S. V. Moharil	43-45
9	**Study on Optical Properties of CDS Annealed Thin Films by Spray Pyrolysis** Dr. L. M. Shanware, Dr. R. S. Meshram, Dr. R. M. Thombre	46-48
10	**A Review on Mn3O4 and Its Composite Nano materials of Different Morphologies as an Electrode Material in Super capacitors** Tanaji S. Patil, Satish A. Gangawane, Mansing Takale	49-55
11	**Low Temperature Photoluminescence Analysis of CDS Nano Crystals** Nilesh Pote	56-62
12	**Stability Constants and Thermodynamic Parameters of Lanthanides (III) Complexes with 5-Bromo, Ortho Hydroxy Acetophenone - N - (4'- Methyl Phenyl) Imine at 250C** S.B. Maulage, S V Gayakwad, R G Machale, S V Kshirsagar	63-65

13	**Synthesis and Reactivity of 2-Imino-3-(6-Methyl-1, 3-Benzothiazol-2-Yl)-1, 3-Thiazolidin-4-One** T. M. Bhagat	66-69
14	**State of The Art : Phase Change Material as Means of Thermal Energy Storage** Punam Mehta	70-78
15	**A Floristic Survey of Dicotyledonous Plants from Guru Nanak College Of Science, Ballarpur Campus Dist. Chandrapur (Maharashtra) India** S. S. Dudhe, P. D. Khirade, N. S. Dudhe	79-86
16	**The Cloud-Based Health Tracking and Monitoring System with AWS** Vaishnavi Raosaheb Thoke, Prof. Prachi V. Kale	87-94
17	**Applications of Nanotechnology in Diabetes - A Review** A. D. Suryawanshi, V. B. Sanap, D. D. Suryawanshi, B. H. Pawar	95-99
18	**Structural and Morphological Properties of Spray Deposited Lead Telluride Thin Films** Syed Ghause Ibrahim, S. A.Waghuley, M. M. Hasan Farooqi, A.V. Kadu	100-103
19	**Determination of Macronutrients in Soil Samples at Tiwasa Region** N. A. Kalambe	104-108
20	**Determination of Nitrogen in Soil Samples of Tiwasa Region in Amravati District** N. A. Kalambe	109-110
21	**The Different Phases of Lithium Sulphate and Its Transition at Different Temperature** N R Thakare, A.V Nande, A D Bhoyar, S A Patil	111-114
22	**Synthesis, Spectral and Thermal Degradation Kinetics Studies of Copolymer Resin** Jyotsana Khobragade, W. B. Gurnule	115-122
23	**Synthesis and Physio-Chemical Aspects of Chlorosubstituted 1-Phenyl-Δ2-Pyraoles and 1-Phenyl-Δ2-Pyraolines on Plant Pathogen Cerscopora Personata** Amol D. Bhoyar, Vishal S. Bhoyar, Smita A. Patil, Nilesh R. Thakare	123-126
24	**Synthesis and Antifungal Activity of Chlorosubstituted 1-Phenyl-Δ2-Pyraoles and 1-Phenyl-Δ2-Pyraolines on Plant Pathogen Alternaria Solani** Amol D. Bhoyar, Vishal S. Bhoyar, Nilesh R. Thakare, Amol Nande	127-131
25	**Recent Development and Scope of Transition Metal Oxide Based Cathode Material - A Review** Nitesh P. Sawadekar, Anil R. Bari, Sushil P. Bhavsar	132-136
26	**Raman Spectroscopic Technique for Cancer Diagnosis** Patil S A, Thakare N R, Bhoyar A D	137-146

27	**Generalized Fractional Sine Transform and its Applications** Dr. S. A. Khapre, Milind K.Tatte	147-154
28	**The Cloud-Based Health Tracking and Monitoring System With AWS** Vaishnavi Raosaheb Thoke, Prof. Prachi V. Kale	155-162
29	**A Study of Green Inhibitor for Acidic Corrosion of Mild Steel** R. Anto Maria Jesili, J. Antony Rajam1	163-169
30	**A Comparative Analysis of Optimization Technique in Large Scale Transportation Problem to Optimize Mathematical Manipulation** Prof. Yogita D. Shahakar	170-177
31	**Synthesis, Spectral and Thermal Degradation Kinetics Studies of Copolymer Resin** Jyotsana Khobragade, W. B. Gurnule	178-185
32	**Dielectric Behaviour of Amides in Hexane: A Theoretical Study** Sanjay H Bagade	186-190
33	**Photo catalytic Degradation of Methylene Blue Using Mixed Metal Nano Ferrite** S. B. Narde	191-198
34	**Analysis of Heat Transfer and Human Comfort in Warehouse** Vivek Bhide, Prof. Prakash Ingle	199-203
35	**Comparative Study of Electrical Properties of Substituted Calcium Hexaferrites** Moharkar P. R., Gawali S. R.	204-208
36	**Solvent (Water) Effect on Geometry Properties of Patuletin Dyes for Formation of Metal Complex by DFT Method** Nilesh U. Jadhao, Dinesh W. Deshmukh, Manisha M. Jiwatode, B. M. Bahirwar	209-213
37	**To Study the Effect of Substrate Temperature on Optical Properties of Spray Pyrolitically Deposited $CdZnSe_{2x}Te_{2(1-X)}$ Thin Films for X=0.25** Gaikwad S. A.	214-220

International Virtual Conference on Materials and Nanotechnology
In Association with International Journal of Scientific Research in Science and Technology
Volume 9 | Issue 4 | Print ISSN: 2395-6011 | Online ISSN: 2395-602X (www.ijsrst.com)

Nanotechnology for Herbal Drug and Its Uses

D. T. Sakhare

U.G, P.G. & Research Centre, Department of Chemistry, Shivaji Art's, Comm. & Science College Kannad, Dist. Aurangabad-431103, Maharashtra, India

ABSTRACT

Nanotechnology is the new emerging technology in the drug discovery and it has the property of self-targeting in the sense that without the attachment of a specific ligand, the nanoparticles can be used for targeting, due to their distinctively small size, at the infected pathological areas. Drug delivery system fetched a novel drug delivery system, a novel approach to overcome the drawbacks of the traditional drug delivery systems. Treatment of chronic diseases like cancer using targeted drug delivery nanoparticles is the latest achievement. By analysing the relationship between nanotechnology and biological medicine, the application of Nano technological methods for bioavailability enhancement of herbal drugs can be brought about. "Bhasma", a natural product, is a metallo-medicine in powder form of Nano to submicron size. At present, several Nano drugs are under investigation for drug delivery and more specifically for cancer therapy. Interestingly, pharmaceutical sciences are using nanoparticles to reduce toxicity and side effects of drugs.

Keywords : Cancer, Diseases, Herbal Drugs, Nanoparticles/Nanotechnology, Plants, Uses.

I. INTRODUCTION

The term "nanotechnology" was derived by Greek word "nanos", meaning "dwarf". The nano device and nano strategy are one billionth of a meter or 10-9 m. The nanotechnology involves the clumps of atoms, molecules and molecular fragments into the extremely small particles between 1 and 100 nm, and puts forward to the interactions of molecular level matters and engineered materials characteristically. Nanotechnology is the new emerging technology in the drug discovery and it has the property of self-targeting in the sense that without the attachment of a specific ligand, the nanoparticles can be used for targeting, due to their distinctively small size, at the infected pathological areas. Drug delivery system fetched a novel drug delivery system, a novel approach to overcome the drawbacks of the traditional drug delivery systems. Treatment of chronic diseases like cancer using targeted drug delivery nanoparticles is the latest achievement in the pharmaceutical drug delivery field [1].

Nanotechnology is an advanced scientific technique in the 21st century. By analyzing the relationship between nanotechnology and biological medicine, the application of nanotechnological methods for bioavailability enhancement of herbal drugs can be brought about. It is indicated that nanotechnology is one of the fastest developmental, the most potential and the far-reaching high and new technology in the present era, and it greatly promotes the development of biological medicine and bioavailability enhancement of herbal drugs. With the application of nanotechnology of nanomization of herbal drugs, it will make the development of nanoherbal drugs

possessing high bioavaibility, which consequently will open the new era of herbal drug discovery [2].

The breakthrough in this regard will be achieved from the research of the nanomization of herbal drugs against cancer and various other diseases. “Ayurveda” is the ancient Indian medical science based on herbs and herbo-mineral preparations. In Ayurveda, seven metals used therapeutically are: gold (Au), silver (Ag), copper (Cu), iron (Fe), lead (Pb), tin (Sn) and zinc (Zn). These are passed through many processes and finally transformed into therapeutic form. “Bhasma” is the metal based medicine prepared from metals after many systematic processes to raw metal into therapeutic form. “Swarna bhasma” (gold ash) is a therapeutic form of gold metal of nanosized particles when evaluated through various tools and techniques. The size of particle was found to be about 56 nm. Swarna bhasma was also analyzed qualitatively and found that the final product is almost pure gold (Au). “Bhasma” is a metallo-medicine in powder form of nano to submicron size. The raw metal is converted into therapeutic form through classical process by repeated incineration and grinding with some herbal juices and other specified matters. Specialty of preparation process is that the whole process is not a chemical based, rather it is fully a mechanical process and chemical properties much differ to nanoparticles prepared through chemical process [3].

Use of nanotechnology in medicine and more specifically drug delivery is set to spread rapidly. Presently, many substances are under investigation for drug delivery and more specifically for cancer therapy. Interestingly, pharmaceutical sciences are using nanoparticles to reduce toxicity and side effects of drugs. From a positive view point, especially the potential to cross the blood brain barrier may open new ways for drug delivery into the brain. In addition, the nanosize also allows for access into the cell and various cellular compartments, including the nucleus. A multitude of substances are currently under investigation for the preparation of nanoparticles for drug delivery, varying from biological substances like albumin, gelatin and phospholipids for liposomes, and more substances of a chemical nature like various polymers and solid metal containing nanoparticles [4].

Herbal drugs have now occupied lead positions in the pharmacopoeia and the improvement in this concern through nanoformulations using nanotechnology have been done. Known effects and no side effects have made natural products/herbal drugs a powerful therapeutic solution to the organisms. But the delivery of plant/herbal therapeutic molecules as drugs is problematic due to poor solubility, poor permeability, low bioavailability, instability in biological milieu and extensive first pass metabolism. These limitations of herbal drugs can be overcome by attaching or encapsulating them with suitable nanomaterials. The nanomaterial’s can significantly enhance the pharmacokinetics and therapeutic index of plant drugs. Targeted delivery and combination therapy can drastically improve the performance of herbal drugs [5].

II. NANOTIZED HERBAL DRUG SOME CONDITIONS / DISEASES

The use of nanotechnology in medicine and more specifically drug delivery is set to spread rapidly. Presently, many substances are under investigation for drug delivery and more specifically for cancer therapy. Interestingly, pharmaceutical sciences are using nanoparticles to reduce toxicity and side effects of drugs. From a positive view point, especially the potential to cross the blood brain barrier may open new ways for drug delivery into the brain. In addition, the nano size also allows for access into the cell and various cellular compartments, including the nucleus. A multitude of substances are currently under investigation for the preparation of nanoparticles for drug delivery, varying from biological substances like albumin, gelatine and phospholipids for liposomes

and more substances of a chemical nature like various polymers and solid metal containing nanoparticles[6]

In Ayurveda, seven metals, viz., gold, silver, copper, iron, lead, tin and zinc are used therapeutically. These metals are passed through many process and finally transformed into therapeutic form for various diseases. “Bhasma” are the metal based medicine prepared from metals after many systematic processes to raw metal into therapeutic form. The particle size of “Swarna Bhasma” (gold ash, a therapeutic form of gold metal of nano size particles when evaluated through various tools and techniques) is about 56 nm. The “Bhasma” are metalomedicine in powder form of nano to submicron size particles. Raw metal is converted into therapeuticform through the classical process by repeated incineration and grinding with some herbal juices and other specified matters. Speciality of the preparation process is that the whole process is not a chemical based rather it is fully a mechanical process and chemical properties much differ to the nanoparticles prepared through chemical process [7].

The chemists are using nanotechnology for plant research to be applied as “phytotherapy”. The new breakthrough solution uses what are called “mesoporous” nanoparticles. These nanoparticles both introduce the gene and activate it at the same time, in a precise and controlled manner and without toxic after effects. The scientists could potentially use this as an aid in imaging analysis of plants, which have been activated with the appropriate materials. The nanoparticles are chemically coated and act as containers for the genes that are delivered to the plants. The coating induces the plants to swallow the particles, effectively ingesting them inside the plant cell walls, where the genes could be inserted. To date the biologists have succeeded in using this technology to introduce DNA to tobacco and corn plants, among others. With nanotechnology, researchers are able to impart several substances to the plants all at once and release them in a time controlled manner. Being able to penetrate the cell wall of the plant enables biologists to view the world of plant biology in all of its complex and intricate detail, opening vast new frontiers of discoveries for agriculture and other industries that rely on biotechnology [7]

Further, the researchers (at university of Delaware) have indicated that plants can undertake nanoparticles and accumulate these nanoparticles in their tissues and this shows that these can enter into human food chain. Lots of nanoparticles occur naturally in environment, however, presently a large number of applications from electronics to energy are based on nanoparticles and therefore, these are largely being manufactured by commercial organizations for “phytotherapy”. The researchers used low frequency monotone for vibrating the dried pumpkin plant and unique magnetic signals were able to revel the location of nanoparticles inside the plants. The researcher further carried out the research on pumpkin grown in sand and soil and found that there is little and no uptake of nanoparticles in comparison to the strong uptake in pumpkin plants grown in aqueous solution. Although this is a preliminary study, there is much scope for extending the study in a complete range of plants and other soil conditions. Nanotechnology can also be useful in detecting various plant diseases. The researchers are using nanotechnology for detecting plant disease at an early stage so that the food is protected from the possible damage [7].

In a study, the effect of synthesized silver nanoparticles together with plant products and commercially available drugs were evaluated against biofilm inhibition and its biochemical composition of clinical isolates of Candida tropicalis and Staphylococcus aureus. The silver nanoparticles were synthesized from Lactobacillus acidophilus 01 strain and tested with aqueous extracts of Aloe vera, ginger (Zingiber officinale), garlic (Allium sativum), tulsi (Ocimum tenuiflorum), oils (e.g., coconut oil),

antifungal drugs (e.g., fluconazole and itraconazole) for C. tropicalis and antibacterial antibiotics (e.g., tetracycline and chloramphenicol) for S. aureus. The synthesized silver nanoparticles, together with plant products and commercially available drugs, showed a maximum inhibitory effect against both the tested clinical isolates. In case of C. tropicalis, the maximum inhibition was seen for silver nanoparticles with itraconazole, fluconazole and garlic, followed by silver nanoparticles with itraconazole and garlic. Total carbohydrates and total proteins of biofilm matrix were highly reduced in respective treatments. In S. aureus, silver nanoparticles with tetracycline, chloramphenicol and garlic recorded the maximum inhibition, followed by silver nanoparticles with chloramphenicol and garlic. Distinct reduction in total carbohydrates and proteins of biofilm matrix was also recorded in respective treatments. This indicates that the biologically synthesized nanoparticles with plant products have better chemotherapeutic effects against microbial diseases [8]

In Africa, Artemisia annua plants are used as "phytotherapy" to treat malaria. The yield of artemisinin in wild population of A. annua plant is low (0.01-0.8%). So, there is a considerable limitation to commercialization of this herbal drug. The semi-synthetic production of artemisinin from its precursor artemisinic acid has been documented. Artemisinic acid is present in 10-fold excess in the plants. Hence, the semi-synthetic artemisinin yield is considerably higher than the isolation of artemisinin from plants. To preserve the natural resources of A. annua plants, artemisinin-like endoperoxides, e.g., arteflene have been synthesized chemically. Other possibilities for meeting the high demand for artemisinin are found in the natural production of artemisinin by phytotherapeutical and agricultural approaches and in biotechnological approaches. The phytotherapeutical and agricultural approaches allow the cultivation of wild-type plants in fields and greenhouses. The breeding of highyield cultivars and the cultivation of transgenic plants are done.

By nanotechnology, genetically modified plants deliver considerably higher amounts of artemisinin than wild-type plants. Biotechnological (or nanotechnological) approaches provide attractive possibilities for the largescale production of artemisinin. Hairy root cultures of A. annua can be generated by infection of roots with Agrobacterium rhizogens. Hairy roots grow quickly, reach high densities and can produce significant amounts of secondary metabolites like artemisinin. Due to this approach, the production of artemisinin in cell cultures can also be done in vitro. The expression of the biosynthetic pathway for artemisinin or related metabolites in genetically modified organisms, i.e., E. coli and Aspergillus flavipes or Saccharomyces cerevisiae has been reported. With the use of genetically engineered organisms, it should be possible to produce 25 kg artemisinin within an 8-hours working day. Therefore, with the implementation of sophisticated biotechnological (or nanotechnological) production techniques, it will be possible to meet the high demand for artemisinin for malaria treatment and hopefully in the future for cancer chemotherapy as well [9].

Using nanotechnology for "phytotherapy", the researchers (at Kaohsiung's Medical University, Graduate School of Biochemistry) ensured that a new herbal medicine compound was able to enter cancer cells without damaging the healthy cells of the human body. They explained that the new drug is produced by extracting cancer fighting ingredients of Chinese herbs such as milk veteh root, sealwort, cassia twigs and liquorice root and uses nanotechnology to reduce these ingredients to their smallest size, enabling them to enter cancerous cells without damaging healthy cells. The researchers said that this new drug has four advantagesit only kill cancerous cells; has rapid medicinal effects; does not

harm other organs and can be ingested orally without a physician's supervision. When taken together with western medicine, this drug is also able to lower the dosage and reduce resistance to cancer drugs, thereby enhancing overall efficiency.

However, this medicine has not been found to be effective for all forms of cancer. During the experiments, this drug was reportedly found to be effective in alleviating symptoms of pulmonary cancer, breast cancer, bone cancer, liver cancer, tounge cancer, primary or metastatic lymphoma, cervical cancer, ovarian cancer, brain cancer and skin cancer. The medicine was also reported to work especially well in the case of lymphoma, where the tumour was to have softened, grown smaller in size or disappeared altogether after 2 months of treatment. [7]

Highly stable micelles with the size of 10-40 nm can be prepared from poly (ethylene glycol)/phosphatidyl ethanolamine (PEGPE) conjugates. These micelles easily solubilize and firmly retain substantial quantities of various poorly soluble anticancer drugs (m-porphyrin, tamoxifen, taxol). The micelles with encapsulated drugs have the size and size distribution very close to that of original 'empty' micelles. Stable drug-loaded polymeric micelles may represent a convenient drug delivery system into tumours utilizing the enhanced permeability and retention effect [10].

Although the antitumour activity of camptothecin has been intensively studied for nearly fifty years, recent advances in drug delivery systems of camptothecin have considerably improved this drug's efficiency due to development in nano-sized dosage forms of camptothecinderived drugs. DNA topoisomerase is one of drug targets in cancer therapy. Camptothecin is a plant alkaloid derived from the Chinese tree Camptotheca acuminate. The alkaloid camptothecin caused DNA damage by specifically targeting DNA topoisomerase, effectively devastating a broad spectrum of tumors [11].

Recently, nanotechnology has drafted plant viruses for drug delivery in cancer. Plant viruses are a new addition to the long list of types of nanoparticles being investigated as next generation nanotech cancer therapies. From North Carolina State University, "Nanoparticle 'smart bomb' targets drug delivery to cancer cells". Researchers (at North Carolina State University) have successfully modified a common plant virus to deliver drugs only to specific cells inside the human body, without affecting surrounding tissue. These tiny "smart bombs"- each one thousands of times smaller than the width of a human hair- could lead to more effective chemotherapy treatments with greatly reduced, or even eliminated, side effects.

The researchers say that the virus is appealing in both its ability to survive outside of a plant host and its built-in "cargo space" of 17 nm, which can be used to carry chemotherapy drugs directly to tumour cells. The researchers deploy the virus by attaching small proteins, called "signal peptides", to its exterior that cause the virus to 'seek out' particular cells, such as cancer cells. Those same "signal peptides" serve as 'passwords' that allow the virus to enter the cancer cell, where it releases its cargo. Out of different nanoparticles as cell-targeting vectors used, the plant virus is superior in terms of stability, ease of manufacture, ability to target cells and ability to carry therapeutic cargo. Calcium is the key to keeping the virus' cargo enclosed. When the virus is in the bloodstream, calcium is also abundant. Inside individual cells, however, calcium levels are much lower, which allows the virus to open, delivering the cancer drugs only to the targeted cells. Another factor that makes the virus unique is the toughness of its shell. When the virus is in a closed state, nothing will leak out of the interior and when it does open, it opens slowly, which means that the virus has time to

enter the cell nucleus before deploying its cargo, which increases the drug's efficacy.

The researchers believe that their method will alleviate the side effects of common chemotherapy treatments, while maximizing the effectiveness of the treatment. The nanoparticles can be stabilized and targeted to specific cells (such as cancer cells) by attachment of specific proteins to the nanoparticles. Viruses that lack a lipid envelope (i.e., they consist of a genome surrounded by a protein capsid and other protein structures) provide a molecularly precise container of known structure and organization to which targeting molecules can be attached.

The encapsidation of various nanoparticles up to 17 nm in diameter by the 36 nm diameter "Red Clover Necrotic Mosaic Virus" (RCNMV) has been reported. This plant virus has a genome consisting of two single strand RNA molecules. The two genomic RNA molecules form a complex that binds the viral capsid protein and initiates the assembly of the virion. A small RNA molecule that mimics the site on the second genomic RNA required to initiate virion assembly can be tethered to various nanoparticles and then serve to initiate virion assembly, forming uniform virus-like particles about 33 nm in diameter- slightly smaller than the native virus particles- that encapsidate the nanoparticle within the protein shell. The relatively small size of the virus-like particles is an advantage because particles in the 30 nm range can be delivered directly to the cell nucleus via the nuclear pore complex. The virus-like particles are also sturdy enough to facilitate purification [12].

III.CONCLUSION

Nanotechnology has the property of self-targeting in the sense that without the attachment of a specific ligand, the nanoparticles can be used for targeting, due to their distinctively small size, at the infected pathological areas. Treatment of chronic diseases like cancer using targeted drug delivery nanoparticles is the latest achievement of nanotechnology. By analyzing the relationship between nanotechnology and biological medicine, the application of nanotechnological methods for bioavailability enhancement of herbal drugs can be brought about. With the application of nanotechnology of nanomization of herbal drugs, it will make the development of nanoherbal drugs possessing high bioavaibility, which consequently will open the new era of herbal drug discovery. At present, several nano drugs are under investigation for drug delivery and more specifically for cancer therapy.

IV. REFERENCES

[1]. Yadav D, Suri S, Choudhary AA, Sikender M, Hemant, Beg NM, et al. Novel approach: Herbal remedies and natural products in pharmaceutical science as nano drug delivery systems. Int J Pharm Technol. 2011;3(3):3092-116.

[2]. Bhadoriya SS, Mangal A, Madoriya N, Dixit, P. Bioavailability and bioactivity enhancement of herbal drugs by "Nanotechnology": A review. J Current Pharm Res. 2011;8(1):1-7.

[3]. Garg GP. Nanotechnology in herbal medicines. Herbal Tech Industry (English Monthly Newspaper). 2010 March.

[4]. De Jong WH, Borm PJA. Drug delivery and nanoparticles: Applications and hazards. Int J Nanomedicine. 2008;3(2):133-49.

[5]. Kumari A, Kumar V, Yadav SK. Nanotechnology: A tool to enhance therapeutic values of natural plant products. Trends in Medical Res. 2012;7:34-42.

[6]. Jong, W. H. and P. J. A. Borm (2008). Drug delivery and nanoparticles: Applications and hazards. Int. J. Nanomedicine, 3(2) : 133-149.

[7]. Garg, G. P. (2010). Nanotechnology in herbal medicines. Herbal Tech Industry (English Monthly Newspaper), March, 2010.

[8]. Raja, K., N. Selvaraj, E. Krishnamoorthi and B. K. Singh (2011). Effect of biologically synthesized nanoparticles with plant products and chemotherapeutics against biofilm of clinical isolates of Staphylococcus aureus and Candida tropicalis. IJPI'S J. Biotech. Biotherapeu, 1(3) : 1-10.

[9]. Efferth, T. (2007). Willmar Schwabe Award 2006: Antiplasmodial and antitumor activity of artemisinin- from bench to bedside. Planta Med., 73(4) : 299-309.

[10]. Gao, Z., A. N. Lukyanov, A. Singhal and V. P. Torchilin (2002). Diacyllipid-polymer micelles as nanocarriers for poorly soluble anticancer drugs. Nano Letters, 2(9) : 979-982.

[11]. Cuong, N. V., M. F. Hsieh and C. M. Huang (2013). Recent development in nano-sized dosage forms of plant alkaloid camptothecin-derived drugs. Publishing Technology Website.

[12]. Foresight Institute (2013). Nanotechnology drafts plant viruses for drug delivery. Website.

International Virtual Conference on Materials and Nanotechnology
In Association with International Journal of Scientific Research in Science and Technology
Volume 9 | Issue 4 | Print ISSN: 2395-6011 | Online ISSN: 2395-602X (www.ijsrst.com)

Study of Nanotechnology with the Help of Cartoons

Dipak Nath
Head, Department of Physics, Sao Chang College, Tuensang, Nagaland, India

ABSTRACT

Nanotechnology is field of research and innovation which covers a vast and diverse array of devices derived from engineering, biology, physics and chemistry. These devices include Nano vectors for the targeted delivery of anticancer drugs and imaging contrast agents. Nanowires, Nano robot, Nano eggs and Nano cantilever arrays are among the leading approaches under development for the early detection of precancerous and malignant lesions from biological fluids. These and other Nano devices can provide essential breakthroughs in the fight against cancer. This paper mainly contains about Nanotechnology and its 'various' applications. And this tells about the history of Nanotechnology and its necessity. This also discusses how it will improve our lives and about the applications in wide range. Here in my study I use cartoons to make nanotechnology an easy and interesting one.

I. INTRODUCTION

While delivering a lecture in an Asian conference held at National University of Singapore, Singapore, Pradeep K. Srivastava used few science cartoons in order to make his lecture more informative, interesting and impactful. He coined a new name for such cartoons - SCIENTOONS.

Pradeep K. Srivastava

Scientoons are the cartoons, based on science. they not only make you smile and laugh but also provide information about new researches, subjects, data & concepts in a simple, understandable and interesting thought provoking way.

Scientoonics is a new branch of science that deals with effective science communication by using a novel class of science cartoons called scientoons.

NOODLE NOT DNA

On April 2, 1953, American Biologist James D. Watson and French Physicist Francis H. Crick proposed a double helical structure of DNA (Deoxy Ribo Nucleic Acid), which is tightly packed in the 46 chromosomes in each of the 100 trillion cells of human body. DNA is a hereditary material through which traits are transferred from one generation to another.

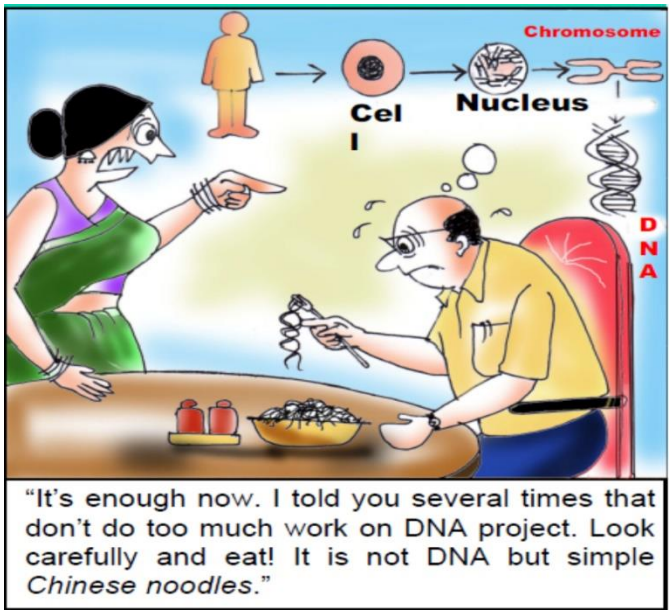

ROAD NOT LAB

The Zig Zag movement of the suspended particles in a fluid medium is called Brownian Movement

II. FAMOUS TALK OF RICHARD FEYNMAN

In 1959 Richard P. Feynman with his famous talk "There is plenty of room at the bottom" predicted that one day we will be making things at the atomic level. And since these small things will build upwards we will be able to make them more precisely and control what we want them to do. This prediction became true at the turn of the century with the onset of nanoscience and technology and the rest is history. Nanotechnology deals with the design, characterization, production, and application of structures, devices, and systems by controlled manipulation of size and shape at the nanometer scale (atomic, molecular, and macromolecular scale) that produces structures, devices, and systems with at least one novel/superior characteristic or property. The most important characteristic of materials that are produced from nanotechnology is that they have bigger surface/volume relation desirable for many applications. Another important characteristic is related with quantum physics because nanotechnology allows us to make materials in one dimension (nanowires), in two dimensions (nanotubes) or in all three dimensions (nanoparticles), very desirable in products related with industrial uses.

Physicist Richard Feynman

ORIGIN OF NANOTECHNOLOGY

K. Eric Drexler author of the book Engines of Creation (1985) which has advocated nanotechnology as a solution to a vast range of problems of mankind, popularized the word 'NANOTECHNOLOGY' in the 1980's, he was talking about building machines on the scale of molecules, a few nanometers wide—motors, robot arms, and even whole computers, far smaller than a cell. Drexler spent the next ten years describing and analyzing these incredible devices, and responding to accusations of science fiction

Nanotechnology is the design, characterization, production, and application of structures, devices and systems by controlling shape and size at nanometer scale. Nano in Greek means “dwarf”. A nanometer is one-billionth of a meter (10-9 m): ten times the diameter of hydrogen atom. The diameter of human hair is, on an average 80,000 nanometer.

III. BASIC STRATEGIES OF NANOTECHNOLOGY

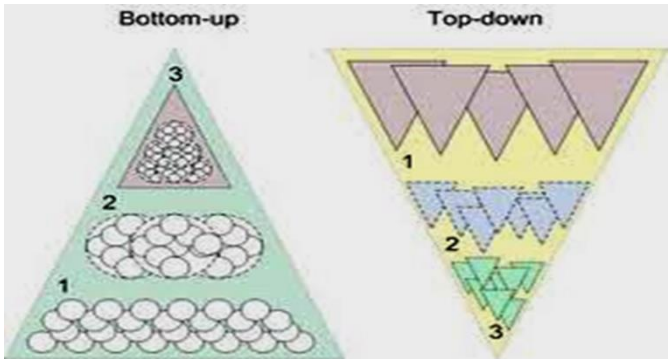

1. Top-Down Approach

A top-down is essentially the breaking down of a system to gain insight into its compositional sub-systems. In a top-down approach an overview of the system is formulated, specifying but not detailing any first-level subsystems. Each subsystem is then refined in yet greater detail, sometimes in many additional subsystem levels, until the entire specification is reduced to base elements. A top-down model is often specified with the assistance of "black boxes", these make it easier to manipulate. However, black boxes may fail to elucidate elementary mechanisms or be detailed enough to realistically validate the model. Top down approach starts with the big picture. It breaks down from there into smaller segments.

2. Bottom- Up Approach

A bottom-up approach is the piecing together of systems to give rise to grander systems, thus making the original systems sub-systems of the emergent system. Bottom-up processing is a type of information processing based on incoming data from the environment to form a perception. Information enters the eyes in one direction (input), and is then turned into an image by the brain that can be interpreted and recognized as a perception (output). In a bottom-up approach the individual base elements of the system are first specified in great detail. These elements are then linked together to form larger subsystems, which then in turn are linked, sometimes in many levels, until a complete top-level system is formed. This strategy often resembles a "seed" model, whereby the beginnings are small but eventually grow in complexity and completeness. However, "organic strategies" may result in a tangle of elements and subsystems, developed in isolation and subject to local optimization as opposed to meeting a global purpose.

IV. NANOMATERIALS:

Materials reduced to the nanoscale can suddenly show very different properties compared to what they exhibit on a macroscale, enabling unique applications. At such scales, the ordinary rules of physics and chemistryno longer apply.The materials characteristics such as colour, strength,conductivity and reactivity can differ substantially between the nano-scale and the macro scale. Opaque substances become transparent (copper). Insulators become conductors (silicon). Gold is chemically inert at normal scales, can serve as a potent chemical catalyst at nanoscales. Opaque substances become transparent (copper) Insulators become conductors (silicon). Gold is chemically inert at normal scales, can serve as a potent chemical catalyst at nanoscales.

V. TYPES OF NANOMATERIALS

1. CARBON BASED MATERIALS

These nano particles are composed of entirely carbon taking the form of hollow sphere, ellipsoid, or tube. Ex Fullerenes, Buckminster Fullerenes, Carbon Nano Tubes, etc

2. METAL BASED MATERIALS

These nano particles' are generally composed of conductors and semiconductors. Ex Quantum dots, Gold, silver, iron, platinum and titania nano particles

VI. CARBON NANOTUBES

A tube with nano scale dimensions, which are sheets of graphite rolled upto make a tube. The dimensions are variable. With remarkable tensile strength, carbon nanotubes exhibit varying electrical properties. These can be insulating, semiconducting or conducting.

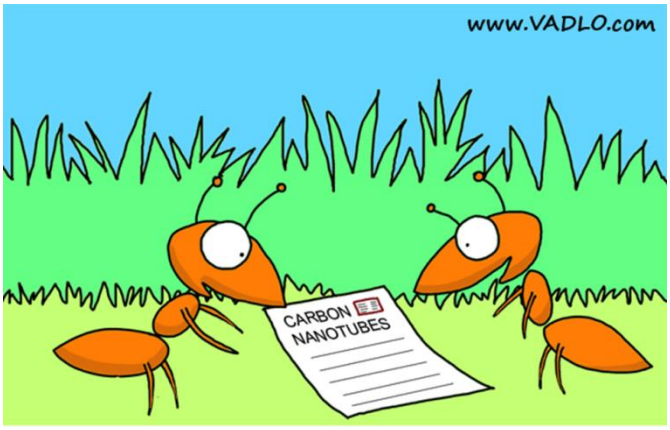

"Finally, we can drink Coke with a straw."

HYDROGEN STORAGE

Over the past few decades, the fields of science and engineering have been seeking to develop new and improved types of energy technologies that have the capability of improving life all over the world. In order to make the next leap forward from the current generation of technology, scientists and engineers have been developing energy applications of nanotechnology.

Nanotecnology will play an important role in the field of " Energy". Natural resources like oil, coal, natural gas etc required for all transportation, communication, agriculture, industry, houses and many other human activities are limited and depleting very fast. The future generation will have to look for alternative energy sources. Hydrogen has great potential as an

alternative source. Unlike petroleum it can be easily generated from renewable energy sources. It is non polluting.

"We have already used alternative source of energy"

Hydrogen as a part of water molecule is abundant on earth. Dissociation of water into hydrogen and oxygen is not a difficult process. Therefore abundant hydrogen fuel can be made available. When hydrogen fuel is burnt, it can only produce harmless water vapour. However main problem of using hydrogen fuel is its storage. Hydrogen gas is normally stored in a metal cylinder under high pressure. Carrying metal cylinders under high pressure not only can add to the weight of the vehicle but it dangerous also. Hydrogen in contact with air can catch fire. So the only solution is to store it in "Nanocylinder" of carbon nanotube. This could be a potent source of aero space engines and other industrial processes.

NANOBREEZE

To purify the indoor environment, the NanoBreeze Room Air Purifier uses patented photocatalytic nanotechnology to clean and purify indoor air.
Technology consists Titanium dioxide (TiO2) crystals, only 40 nanometers in size, form a molecular machine powered by light. TiO2 is a semiconductor charged by ultraviolet photons. When these nanoparticles are charged, powerful oxidizing agents called hydroxyl radicals are produced. These free radicals destroy airborne germs and pollutants that circulate over the surface of the patented light tube inside the NanoBreeze Air Purifiers.

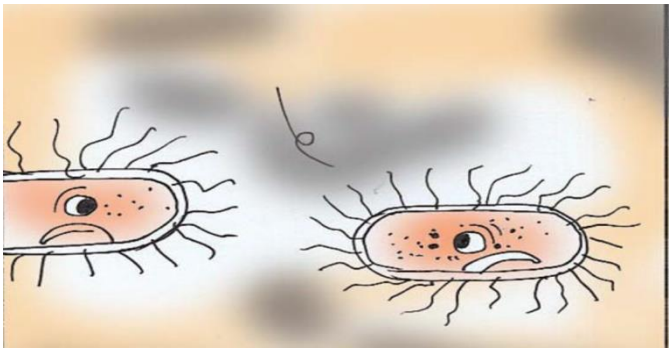

"We must leave this country immediately and Settle in any most backward countries only then we can survive."

NANOBATTERIES

Numerous gadgets like laptops, cellular phones, cordless phones, portables radios, calculators etc need rechargeable light weight batteries or cells. Presently , the batteries for such gadgets need to be either replaced with new ones recharged quite frequently due to their low energy density or storage capacity. Attempts are being made to increase their energy density using metal hydride nano particles(Nickel hydride, aerogel etc)
Nano structured materials offer a tremendous potential for developing high power density Lithium ion batteries with high rate capabilities.
Trapped lithium in carbon nanostructures could help to make rechargeable nano battery for next generation communication and remote sensing devices. Or simply evaporate. Even drops of water on gass give hazy look.

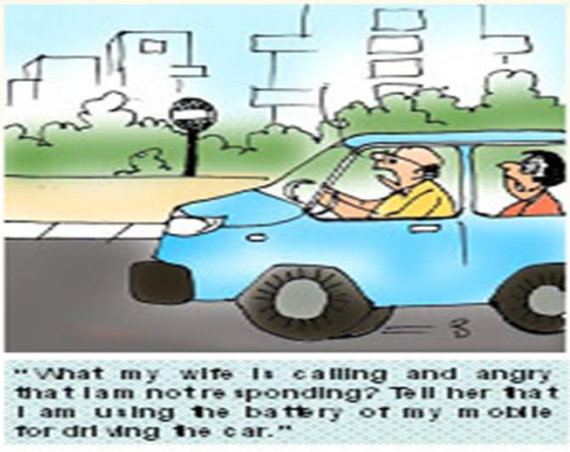

NANO EGGS

The core shell nanostructure could be considered as nanoeggs. Honkong university of science and technology has developed a nanoscale egg that could safely deliver platinum a known Anticancer agent to tumar cell. The nanoscale egg having the hard cobalt shell surrounding a yolk of platinum and iron, show that it is seven more toxic than the Anticancer agent Cis platin to cancer cell.

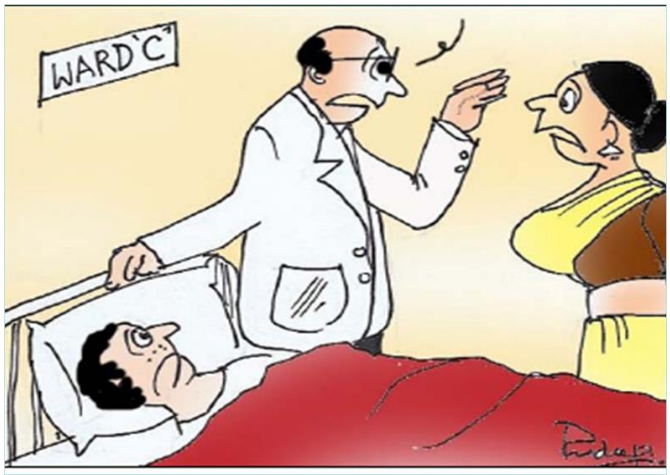

Not at all. Don't worry if he is a strictly vegetarian. This is just a term coined for it. It has nothing to do with the real eggs

NANOFOODS

Nanofood is that nanotechnology techniques or tools are used during cultivation, production, processing, or packaging of the food . It is not atomically modified food or food produced by nanomachines.

Nanofoods fall into four categories. First, and most obviously, there's the use of nanotechnology directly in a food that we eat. Second, there are supplements that use nanotechnology. And the last two categories, which are similar, are comprised of things we don't eat that use nanotechnology: food packaging and cookware.

"Take it Sir! Whatever you like, Veg, None veg, Italian, Thai, Continental! Everything is in plenty. See carefully! It is Nano food Sir."

MEMORY MATERIALS

Shape Memory materials have the ability to return to some previously defined shape or size when subjected to the appropriate thermal procedure. Alloys of Ni-Mn-Sn, Ni-Mn-In etc or molecular magnets such as A[M1(II) M2(III)(C2O4)3] etc are examples shape memory materials

The materials could find applications in Aircraft, Robotics, Telecommunication, Automotive, Piping, Cardio-vascular surgery, Orthopedic surgery, Dentistry etc.

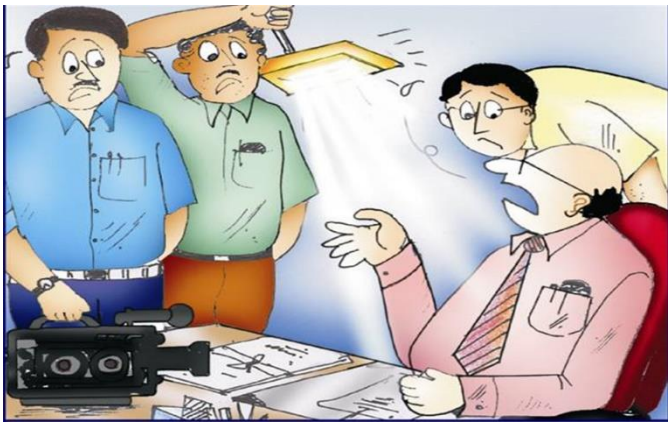

"Look! They have come to take our interview on that memory enhancer! Do you remember anything about that?"

NANOGELS

Nanoparticles are also important in cosmetic industry. Zinc oxide and titanium oxide nanoparticles of fairly uniform size are able to absorb ultraviolet light and

protect the skin. Due to their small size, nanoparticles based creams are preferred as they can be used in small amount and do not leave any gaps between them. This gives a smooth appearance. These small particles in some of the creams scatter light in such a way that appearance of the wrinkles is diminished. Some creams using nanoparticles are already marketed. Nano based dyes and colours quite harmless to skin and can be used in hair creams or gels. SUNSCREENS utilize nanoparticles which are extremely effective at absorbing light, especially in the ultra-violet (UV) range. Due to the particle size, they spread more easily, cover better, and save money. These are transparent, unlike traditional screens which are white.

These sunscreens are so successful that by 2001 they had captured 60% of the Australian sunscreen market.

"Be careful! He is a famous nanotechnologist. I doubt that he might have made see-through nano-spex."

NANOCLOTH

Nano-textiles is an emerging and interesting application of nanotechnology. It involves dealing with nano fibers at the atomic and molecular levels in order to tweak their properties. This novel technology can give rise to incredible clothing such as water-resistant and dirt-free clothes, odor-less socks, and intelligent clothes that can perfom climate control for us.

The ever-increasing demand for sophisticated fabrics with special features and exceptional comfort drives the need for the use of nanotechnology in this industry. More and more companies are utilizing nanoadditives to enhance the surface characteristics of clothes such as water/stain-resistance, UV-protection, wrinkle resistance, color durability, flame retardancy, and better thermal performance.

Although these nanofabrics are antimicrobial, strong and intelligent, they also pose some risks to the user and the environment.

"Oh no, my God! You are traveling in these SAME clothes for the last six month. Darling I am extremely sorry. I forgot to tell that these are not nano clothes but ordinary one."

NANOBRAIN

A nano brain is a conceptual device that executes massively parallel/ simultaneous computing following the information processing principles of human brain This machine assembly would serve as an intelligent decision making unit for the nano-robots, and could be programmed to execute particular operation for which it is designed.

This machine assembly would serve as an intelligent decision making unit for nanorobots. One essential feature of a nano brain is that it would acquire all sensory inputs from the external environment, and in processing that information, generate distinct instructions for every single execution unit connected to the nano brain simultaneously.Thus, the computing machine will communicate with the external world in a similar fashion to our central nervous system.

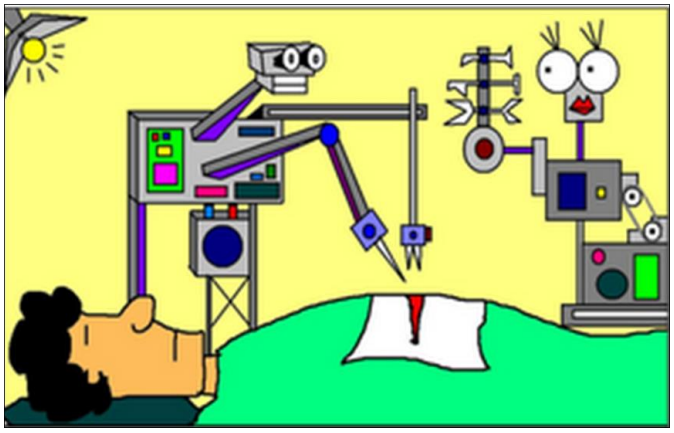

"Nurse, hand me another pair of scissors. I think I dropped the one you gave me earlier. Your pretty LEDs are distracting me today."

QUANTUM DOTS

Another minuscule molecule that will be used to detect cancer is a quantum dot. Quantum dots are tiny crystals that glow when they are stimulated by ultraviolet light. The wavelength, or color, of the light depends on the size of the crystal. Latex beads filled with these crystals can be designed to bind to specific DNA sequences. By combining different sized quantum dots within a single bead, scientists can create probes that release distinct colors and intensities of light. When the crystals are stimulated by UV light, each bead emits light that serves as a sort of spectral bar code, identifying a particular region of DNA.

To detect cancer, scientists can design quantum dots that bind to sequences of DNA that are associated with the disease. When the quantum dots are stimulated with light, they emit their unique bar codes, or labels, making the critical, cancer-associated DNA sequences visible. The diversity of quantum dots will allow scientists to create many unique labels, which can identify numerous regions of DNA simultaneously. This will be important in the detection of cancer, which results from the accumulation of many different changes within a cell. Another advantage of quantum dots is that they can be used in the body, eliminating the need for biopsy.

NANOSHELLS

Nanoshells are miniscule beads coated with gold. By manipulating the thickness of the layer making up the nanoshells, scientists can design these beads to absorb specific wavelengths of light. The most useful nanoshells are those that absorb near-infrared light, which can easily penetrate several centimeters of human tissue. The absorption of light by the nanoshells creates an intense heat that is lethal to cells. Researchers can already link nanoshells to antibodies that recognize cancer cells. Scientists envision letting these nanoshells seek out their cancerous targets, then applying near-infrared light. In laboratory cultures, the heat generated by the light-absorbing nanoshells has successfully killed tumor cells while leaving neighboring cells intact.

NANOROBOT

Nanotechnology is also being used to develop robots of nanosize called Nanorobots. They are of special interest to researcher in the medical industry. This has given rise to the field of nanomedicine. It has been suggested that a fleet of nanorobots might serve as antibodies or antviral agents in patients with compromised immune system, or in deseases that do not respond to more conventional measures.

These nanorobots can interact with tissues in a human body and deliver drugs and diagnose the precise nature of injury. They can also repair an organ without any surgical intervention. In theory they can remain operational for years, decade or centuries.

One more feather on the cap of nanotechnology is curing cancer with the help of a new method Trojan Horse Therapy. This therapy has the potential to directly target cancer cells with chemotherapy, rather than the current treatment that chemotherapy drugs injected into a cancer patient and attacking both cancer and healthy cells.

INTELLIGENT NANOMATERIALS

'Intelligent' Nanomaterial's which Have Sensing Properties. These could have intrinsic sensing properties, programmable optical, thermal and mechanical characteristics and self-healing properties. Nano composites consisting of conjugated polymers in a nanostructured silicate matrix changes the colour with respect to mechanical, chemical or thermal stress.

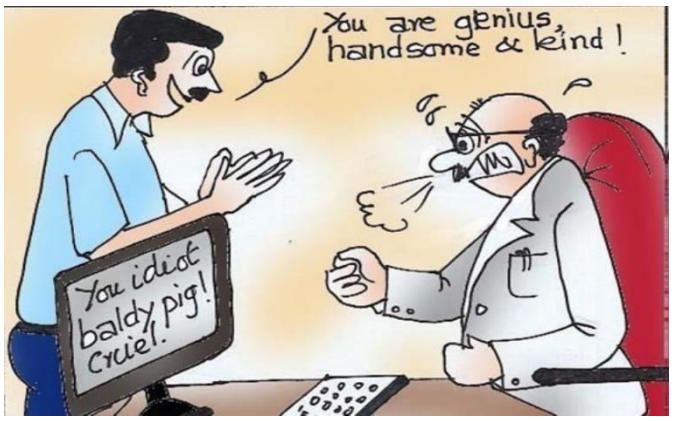

"Don't speak even a word further. I know you very well now"

VII. CONCLUSION

Since Nanotechnology is at the verge creating a significant change in our lives in near future, so it is utmost essential to popularize it among the young learners. In many parts of the world, science is being taught in such a way that most of the times students get a horrifying image of science. Scientoonic presentation would be of great help to make students believe that science is not only interesting but fun as well.

VIII. REFERENCES

[1]. Drexler, K. Eric (1986). Engines of Creation: The Coming Era of Nanotechnology. Doubleday. ISBN 978-0-385-19973-5.

[2]. Drexler, K. Eric (1992). Nanosystems: Molecular Machinery, Manufacturing, and Computation. New York: John Wiley & Sons. ISBN 978-0-471-57547-4.

[3]. Hubler, A. (2010). "Digital quantum batteries: Energy and information storage in nanovacuum tube arrays". Complexity. 15 (5): 48–55. doi:10.1002/cplx.20306. S2CID 6994736.

[4]. Shinn, E. (2012). "Nuclear energy conversion with stacks of graphene nanocapacitors". Complexity. 18 (3): 24–27. Bibcode:2013Cmplx..18c..24S. doi:10.1002/cplx.21427. S2CID 35742708.

[5]. Elishakoff,I., D. Pentaras, K. Dujat, C. Versaci, G. Muscolino, J. Storch, S. Bucas, N. Challamel, T. Natsuki, Y.Y. Zhang, C.M. Wang and G. Ghyselinck, Carbon Nanotubes and Nano Sensors: Vibrations, Buckling, and Ballistic Impact, ISTE-Wiley, London, 2012, XIII+pp.421; ISBN 978-1-84821-345-6.

[6]. Lyon, David; et., al. (2013). "Gap size dependence of the dielectric strength in nano vacuum gaps". IEEE Transactions on Dielectrics and Electrical Insulation. 20 (4): 1467–1471. doi:10.1109/TDEI.2013.6571470. S2CID 709782.

[7]. Saini, Rajiv; Saini, Santosh; Sharma, Sugandha (2010). "Nanotechnology: The Future Medicine". Journal of Cutaneous and Aesthetic Surgery. 3 (1): 32–33. doi:10.4103/0974-2077.63301. PMC 2890134. PMID 20606992.

[8]. Belkin, A.; et., al. (2015). "Self-Assembled Wiggling Nano-Structures and the Principle of Maximum Entropy Production". Sci. Rep. 5: 8323. Bibcode:2015NatSR...5E8323B. doi:10.1038/srep08323. PMC 4321171. PMID 25662746.

[9]. Buzea, C.; Pacheco, I. I.; Robbie, K. (2007). "Nanomaterials and nanoparticles: Sources and toxicity". Biointerphases. 2 (4): MR17–MR71. arXiv:0801.3280. doi:10.1116/1.2815690. PMID 20419892. S2CID 35457219.

[10]. Binnig, G.; Rohrer, H. (1986). "Scanning tunneling microscopy". IBM Journal of Research and Development. 30 (4): 355–69.

[11]. "Press Release: the 1986 Nobel Prize in Physics". Nobelprize.org. 15 October 1986. Archived from the original on 5 June 2011. Retrieved 12 May 2011.

[12]. Kroto, H. W.; Heath, J. R.; O'Brien, S. C.; Curl, R. F.; Smalley, R. E. (1985). "C60: Buckminsterfullerene". Nature. 318 (6042): 162–163. Bibcode:1985Natur.318..162K. doi:10.1038/318162a0. S2CID 4314237.

[13]. Adams, W. W.; Baughman, R. H. (2005). "RETROSPECTIVE: Richard E. Smalley (1943-2005)". Science. 310 (5756): 1916. doi:10.1126/science.1122120. PMID 16373566.

[14]. Monthioux, Marc; Kuznetsov, V (2006). "Who should be given the credit for the discovery of carbon nanotubes?" (PDF). Carbon. 44 (9): 1621–1623. doi:10.1016/j.carbon.2006.03.019.

[15]. Pasa, André Avelino (2010). "Chapter 13: Metal Nanolayer-Base Transistor". Handbook of Nanophysics: Nanoelectronics and Nanophotonics. CRC Press. pp. 13–1, 13–4. ISBN 9781420075519.

[16]. Tsu-Jae King, Liu (June 11, 2012). "FinFET: History, Fundamentals and Future". University of California, Berkeley. Symposium on VLSI Technology Short Course. Retrieved 9 July 2019.

[17]. Jump up to:a b "Nanoscience and nanotechnologies: opportunities and uncertainties". Royal Society and Royal Academy of Engineering. July 2004. Archived from the original on 26 May 2011. Retrieved 13 May 2011.

[18]. "Nanotechnology: Drexler and Smalley make the case for and against 'molecular assemblers'". Chemical & Engineering News. 81 (48): 37–42. 1 December 2003. doi:10.1021/cen-v081n036.p037. Retrieved 9 May 2010.

[19]. ^ Jump up to:a b "Nanotechnology Information Center: Properties, Applications, Research, and Safety Guidelines". American Elements. Archived from the original on 26 December 2014. Retrieved 13 May 2011.

[20]. Jump up to:a b "Analysis: This is the first publicly available on-line inventory of nanotechnology-based consumer products". The Project on Emerging Nanotechnologies. 2008. Archived from the original on 5 May 2011. Retrieved 13 May 2011.

[21]. "Productive Nanosystems Technology Roadmap" (PDF). Archived (PDF) from the original on 2013-09-08.

[22]. "NASA Draft Nanotechnology Roadmap" (PDF). Archived (PDF) from the original on 2013-01-22.

[23]. "Still Room at the Bottom (nanometer transistor developed by Yang-kyu Choi from the Korea Advanced Institute of Science and Technology)", Nanoparticle News, 1 April 2006, archived from the original on 6 November 2012

[24]. Lee, Hyunjin; et al. (2006), "Sub-5nm All-Around Gate FinFET for Ultimate Scaling", Symposium on VLSI Technology, 2006: 58–59, doi:10.1109/VLSIT.2006.1705215, hdl:10203/698, ISBN 978-1-4244-0005-8, S2CID 26482358

[25]. Jump up to:a b c d World Intellectual Property Report: Breakthrough Innovation and Economic Growth (PDF). World Intellectual Property Organization. 2015. pp. 112–4. Retrieved 9 July 2019.

[26]. Allhoff, Fritz; Lin, Patrick; Moore, Daniel (2010). What is nanotechnology and why does it matter?: from science to ethics. John Wiley and Sons. pp. 3–5. ISBN 978-1-4051-7545-6.

[27]. ^ Prasad, S. K. (2008). Modern Concepts in Nanotechnology. Discovery Publishing House. pp. 31–32. ISBN 978-81-8356-296-6.

[28]. Jump up to:a b Kahn, Jennifer (2006). "Nanotechnology". National Geographic. 2006 (June): 98–119.

[29]. Jump up to:a b Kralj, Slavko; Makovec, Darko (27 October 2015). "Magnetic Assembly of Superparamagnetic Iron Oxide Nanoparticle Clusters into Nanochains and Nanobundles". ACS Nano. 9 (10): 9700–9707. doi:10.1021/acsnano.5b02328. PMID 26394039.

[30]. Rodgers, P. (2006). "Nanoelectronics: Single file". Nature Nanotechnology. doi:10.1038/nnano.2006.5.

[31]. Lubick N; Betts, Kellyn (2008). "Silver socks have cloudy lining". Environ Sci Technol. 42(11): 3910. Bibcode:2008EnST...42.3910L. doi:10.1021/es0871199. PMID 18589943.

[32]. Phoenix, Chris (March 2005) Nanotechnology: Developing Molecular ManufacturingArchived 2005-09-01 at the Wayback Machine. crnano.org

[33]. "Some papers by K. Eric Drexler". imm.org. Archived from the original on 2006-04-11.

[34]. Carlo Montemagno, Ph.D. Archived 2011-09-17 at the Wayback Machine California NanoSystems Institute

[35]. "Cover Story – Nanotechnology". Chemical and Engineering News. 81 (48): 37–42. December 1, 2003.

[36]. Regan, BC; Aloni, S; Jensen, K; Ritchie, RO; Zettl, A (2005). "Nanocrystal-powered nanomotor" (PDF). Nano Letters. 5 (9): 1730–3. Bibcode:2005NanoL...5.1730R. doi:10.1021/nl0510659. OSTI 1017464. PMID 16159214. Archived from the original (PDF) on 2006-05-10.

[37]. Regan, B. C.; Aloni, S.; Jensen, K.; Zettl, A. (2005). "Surface-tension-driven nanoelectromechanical relaxation oscillator" (PDF). Applied Physics Letters. 86 (12): 123119. Bibcode:2005ApPhL..86l3119R. doi:10.1063/1.1887827. Archived (PDF)from the original on 2006-05-26.

[38]. Goodman, R.P.; Schaap, I.A.T.; Tardin, C.F.; Erben, C.M.; Berry, R.M.; Schmidt, C.F.; Turberfield, A.J. (9 December 2005). "Rapid chiral assembly of rigid DNA building blocks for molecular nanofabrication". Science. 310 (5754): 1661–1665. Bibcode:2005Sci...310.1661G. doi:10.1126/science.1120367. PMID 16339440. S2CID 13678773.

International Virtual Conference on Materials and Nanotechnology
In Association with International Journal of Scientific Research in Science and Technology
Volume 9 | Issue 4 | Print ISSN: 2395-6011 | Online ISSN: 2395-602X (www.ijsrst.com)

Structural, Morphological, Dielectric and Magnetic Behaviour of Rare Earth Substituted Cobalt Ferrite Nanoparticles - A Brief Review

Y. S. Bopche*[1], M. S. Bisen[2], A. M. Shahare[1], D. S. Choudhary[3]

*[1]Assistant Professor, Department of Physics, D. B. Science College, Gondia, Maharashtra, India

[2]Assistant Professor, Department of Physics, Y. C. Arts, Commerce and Science College, Lakhandur, Maharashtra, India

[3]Professor, Department of Physics, D. B. Science College, Gondia, Maharashtra, India

ABSTRACT

Cobalt ferrite proposes an excellent platform for solid state crystallography and structural chemistry point of view. The partial substitution of rare earth (RE) ion, such as Sm, Ce, Er, Dy, La and Nd for Fe3+ leads to structural bend in spinel structure which in turn induces strain and considerably modifies electrical and dielectric properties. The chemical as well as physical nature of the dopant into Cobalt Ferrite Oxide (CFO) matrix allows tuning of structural, magnetic and electrical characteristics. In the field of engineering, doping of advanced and efficient ferrite materials with different RE/TM-ions is a well-adopted, straightforward and flexible way to tune the structural properties. Depending on the ionic size and concentration, assimilation of RE/TM-ions in spinel ferrite results in upgraded dielectric constant, rise in resistivity and reductions in dielectric and magnetic losses. Such a detailed understanding of RE incorporation might allow further opportunities to tailor the CFO-based materials' behavior for selective applications, where thermal and chemical constancy becomes important. The amalgamation of rare earths elements into CFO would be more attractive for future applications, such as advanced sensors and photo-catalysis. Thus, a better understanding of the combined structural, magnetic, dielectric and transport properties of CFMO is highly beneficial to tune the properties for desired electronic and electromagnetic applications. The objective of present review article is to derive a precise understanding of the rare earth elements, substitution effects on the crystal structure, morphology, magnetic behavior, and dielectric properties of CFO.

Keywords : Rare earth elements (RE), Cobalt ferrite oxide (CFO), EDAX, VSM, SEM, TEM

I. INTRODUCTION

The cobalt ferrite ($CoFe_2O_4$) has got special attention due to its interesting and notable properties. A unit cell of cubic closed packed structure of spinel ferrite is composed of total 96 number of interstitialcies by O^{2-} anions, out of which 64 are at tetrahedral (A) site and remaining 32 are at octahedral (B) site. From 64 A-site 8 and from 32 B-site 16 voids are occupied by

metal cations, which lead to free drift of cations between octahedral and tetrahedral sites.

Cobalt ferrite materials have engrossed a prodigious attention in the field of fundamental and applied research because of its high thermal stability, mechanical hardness, large coercive field, high magnetostriction coefficient and anisotropy constant. Due to which we can use cobalt ferrites in a wide-ranging applications from medicine (e.g. MRI contrast agents, DNA isolation, magnetically activated drug delivery) to electronics (e.g. magnetostrictive and gas sensors, optoelectronics, microwave frequency devices, storage media). Cobalt ferrite is considered as a possible alternative for magneto-optical (MO) devices which are included not only in magnetic recording but also in light modulators and deflectors. The infrared emissivity of cobalt ferrites can also be enhanced by varying the dissemination and nature of the cations by doping rare earth elements into cobalt based spinel ferrites.

The physical and chemical properties of cobalt ferrite nanoparticles can be designed for numerous applications by substituting rare-earth metal (RE) ions such as La^{3+}, Ce^{3+}, Gd^{3+}, Sm^{3+}, Y^{3+}, Er^{3+} etc for host Fe^{3+} induces large strain as well as surface area increases by reducing the particle size. Small doping of rare earth metal ions in ferrites greatly affects electric and magnetic properties of ferrite nanoparticles due to higher ionic radius and various different oxidation states with different magnetic moment values of RE metal. Substitutions of rare earth elements show large impact upon the magnetic anisotropy of the system making the spinel ferrite an excellent option instead of hexa ferrites or garnets. Thus by choosing the proper rare earth cation, we can change electrical and magnetic properties of ferrites. Magnetic properties of the ferrites such as magnetization, coercivity (H_C), remanent magnetization (M_r) prominently depend on the quantity of doped rare earth ions in which 4f electrons are magnetism carriers.

The influence of microstructural and magnetic properties of substituted ferrite is related to the occupancy of the 4f electron shell with their magnetic moments which is a core interest in substitutions of rare earth element. Thus the structural, electrical, spectral and magnetic properties of spinel ferrites can vary with the addition of RE ions into spinel ferrite lattice. RE ions possess unpaired 4f electrons, moderate elastic constants as well as the strong spin-orbit coupling and display large magnetostrictions effect. Hence the substitution of RE ions is felicitous a proficient way of ameliorating the structural and electric-magnetic properties. This review paper represents the structural, magnetic and dielectric properties of pure and RE (Ce, Sm, Gd, Eu and Yb) doped cobalt ferrite bulk materials.

II. LITERATURE REVIEW & DISCUSSIONS

Fractional substitution of Fe^{3+} by rare earth ion, such as Er, Dy, La, Nd, Ho, leads to structural distortion in spinel structure which induces strain and considerably modifies the electrical and dielectric properties. Ferrites [1], doping with different RE/TM-ions is a well-accepted, straightforward and flexible way to tune the structure and properties. An improved dielectric constant with resistivity and a decrease in dielectric loss with magnetic losses can be achieved by incorporation of RE/TM-ions in spinel ferrite depending ionic size and concentration. When we substitute the rare earth elements of large ionic radii with the smaller ionic radii of cobalt ferrites, an internal stress will generate and as a result there is a change in cell symmetry and hence the structural properties will change. Thus in addition with structural properties of the material dielectric, magnetic and magnetostrictive properties of substituted materials will also change.

The impact of rare earth ion substitution on magnetic properties of the ferrite materials have been widely studied by many investigators [2], for the different

applications such as MO-recording, MO-sensors and hyperthermia treatment. The substitutions of RE ions in Co-Fe ferrite leads to lattice strain and structural disorder which permits to modify the electrical and dielectric properties. Thus the doping of parent spinel ferrite with rare earth ions (Y^{3+}, Gd^{3+}, Ho^{3+}, Sm^{3+}, Nd^{3+}) leads to increasing in the electrical and magnetic parameters. The properties of ferrites are mostly dependent on synthesis methods which affect the distribution of cations of tetrahedral and octahedral sites, particle size and surface area. Rare earth ions are stated to lower the Curie temperature and enhance the magneto-optical response when substitute in ferrite structures while decrease the grain size, which is an important factor in low noise media.

The substitutions of rare-earth elements in CoFe2O4 are fruitful for magneto-optical recording applications because they are efficacious in reducing the Curie temperature (T_c) as equated to pure ferrite. Saturation magnetization and coercivity values changes abruptly by the substitution of rare-earths in the cobalt ferrite materials and reduces the grain size. Hydrothermal and co-precipitation methods shows decreased value of saturation magnetization and coercivity for a series of RE (Sm^{3+}, Pr^{3+}, Tb^{3+}, Ho^{3+}, Gd^{3+}, Dy^{3+}, Yb^{3+}) substituted cobalt ferrite also shows large differences in their observed and calculated magnetic moments values [3,4].

R. N. Panda et al [5] synthesize nano-crystalline $CoM_xFe_{2-x}O_4$ (where M=Gd and Pr) powders by a citrate precursor technique and found that the crystallite sizes of the materials are within the range of 6.8 nm to 87.5 nm. Formation of the single phase spinel ferrite phase at 2201^c was observed through TG and XRD analysis. Decrease in saturation magnetization at room temperature with reduction in size of the sample was observed which attributes to the presence of super paramagnetic fractions in the materials and spin canting at the surface of nanoparticles. Compared to pure cobalt ferrite materials the substitutions of rare-earth in the crystal lattice inhibit the grain growth of the materials in a systematic manner and improve coercivity.

The structural and magnetic properties of Sm and Ce co-substituted nanocrystalline cobalt ferrite, $CoFe_{2-x-y}Sm_xCe_yO_4$ (x = y = 0.00, 0.5, 0.1, 0.12 and 0.25) through sol-gel combustion method have been studied by Syed Ismail Ahmad et al [6] and observed spinel structure with a secondary phase of RE_2O_3 for higher molar concentration of rare earth ions by XRD method. As we increase Sm and Ce concentrations specific surface area and strain will increase while crystallite size decrease. SEM micrographs displays inhomogeneous grain distributions with some agglomerates and average grain size of 0.15 mm. Energy dispersive x-ray spectroscopy (EDAX) define the stoichiometry of the samples. Surface morphology studies (TEM) substantiate the occurrence of agglomerations in the sample. FTIR spectroscopy confirmed the spinel phase by pointing two frequency bands, y_1 in higher frequency range 580-559 cm^{-1} and lower frequency band y_2 at 392-372 cm^{-1}. The force constant for octahedral site was found to be less than that of tetrahedral position. M_s and H_c was found to decrease with increase in concentration of rare earth ions due to weakening of AB interaction. VSM technique at room temperature reflects the decrease in particle size and surface effect. Thus by increasing the rare earth concentrations the Yafet-Kittle (YeK) angle was also found to increase.

Tahar et al. [7] have examined the effect of Sm^{3+} and Gd^{3+} on the magnetic properties of cobalt ferrite synthesized by forced hydrolysis method and stated that particle size increased slightly with rare earth substitution. Several research groups consecutively explained the increase in saturation magnetization in substituted ferrites on the concept of Neel's two sub-lattice model. Hence a systematic study on the impact of rare earth doping in cobalt ferrite has a well-defined significance.

III. COMPARATIVE OBSERVATIONS

The different rare earth cation substitutions and their significant effects on the characteristics (structural, dielectric, magnetic, microstructural) of the cobalt ferrites have been intensively studied. In particular, the effect of partial interstitial substitution of the rare earth cation like, Ce^{3+}, Gd^{3+}, Sm^{3+}, Yb^{3+}, Eu^{3+} etc.

A. Sm substitutions

Sheena Xavier et al [8] synthesized a series of samarium-substituted cobalt ferrites ($CoFe_{2-x}Sm_xO_4$) by sol-gel technique and confirm the formation of single-phase cubic spinel structure in all the compositions by XRD analysis without any secondary phase. Increase in samarium concentration observed the expansion of unit cell due to increase in lattice parameter. Average crystallite size and low value of lattice strain induced in the sample with increase in crystallinity are also observed. TEM analysis evident the spherical morphology of the prepared sample. EDS analysis confirms the stoichiometry of the sample and absorption bands in FTIR spectra of all the samples are found in the expected range. The occupancy of Sm^{3+} ions on the octahedral sites was revealed by decrease in band frequencies with increase in samarium content. Resultant magnetic moment decreases due to substitution of nonmagnetic ion in the octahedral site leading to decrease in saturation magnetization. The variation of coercivity of nanoparticles in the multidomain system is also observed. Substitution of samarium strongly influences the magnetic properties and hence the properties of the cobalt ferrite nanoparticles substituted with samarium ions can be tailored for suitable applications. Rashad et al. [9] specified the change in the magnetic properties of samarium substituted $CoFe_2O_4$ synthesized by citrate precursor method and the results shown the decrease in saturation magnetization and coercivity with the addition of Sm^{3+} ions.

B. Yb substitutions

Y^{3+}- doped cobalt ferrite nanoparticles, $CoY_xFe_{2-x}O_4$, were synthesized by S. S. Satpute et al [10] using the sol-gel method and observed the formation of pure with single-phase cubic spinel structure by the X-ray diffraction technique. The increased lattice parameter was found with the increase of Y^{3+} content in the cobalt ferrite due to the alteration in ionic radii of Fe^{3+} and Y^{3+} ions. SEM images showed the preparation of samples with distinct crystalline nanoparticles of spherical shape with small accumulation with the decrease of grain size with the yttrium substitution. EDAX results showed good agreement with the specific composition. The reduction in saturation magnetization (M_s), remanent magnetization (M_r) and coercivity (H_c) by Y^{3+} substitution was observed by vibrating sample magnetometer. The dielectric constant decreases and the dielectric loss tangent increases with the substitution of yttrium in the cobalt ferrite composition which shows the natural behavior of the ferrite material with increasing frequency. The decrease in dielectric constant with yttrium content was also reported by Jacobo and Bercoff et al [11]. Hence addition of non-magnetic Y^{3+} ion in cobalt ferrite intensely affects the magnetic properties. Also, yttrium ion moves in the octahedral site of the lattice which again increases the inversion parameter of cobalt ferrite.

C. Gd substitutions

A series of Gd^{3+} doped Co-ferrites $CoGd_xFe_{2-x}O_4$ (x =0.0 to 0.1) has prepared by sol-gel auto combustion method by Erum Pervaiz et al [12]. Formation of pure cubic spinel phase without any impurity was observed and crystal strain increases with increase in doping concentration. Due to large ionic radii (0.94nm) of Gd^{3+} replacing Fe^{3+} (0.64nm) the lattice constant (a) and crystallite size D (311) increases. Spherical morphology with uniform size distribution was also shown by SEM. DC electrical resistivity at room

temperature decreases (~106) up to x=0.025 then increases up to x=0.1 ~ ($4.5x10^7$). All prepared samples show a semi-conducting behavior as permittivity and tangent loss (tanδ) decreases with the substitution of Gd^{3+} in parent crystal structure. Magnetization (Ms) decreases with increase in Gd^{3+} concentration from 63 emu/gm to 27.26 emu/gm due to influence on A-B exchange interactions. Coercivity (H_c) first decreases for x=0.025, after which it increases to 2308 Oe for *x*=0.1. Magnetic anisotropy of Co-ferrites reduces with increase in Gd^{3+} concentration (*x*). B. Ravi et al [13], K.K. Bharathia et al [14] and A. Rana et al [15] have proved the effect of Gd substitution on dielectric properties of cobalt ferrite. Peng et al [16] have described an increase in crystallite size of cobalt ferrite nanoparticles by the doping of gadolinium. Addition of Gd^{3+} ions in cobalt ferrite decreases the saturation magnetization and retentivity due to migration of cations. Thus the rare earth (Gd^{3+}) doped Co-ferrites found a great application in high frequency devices and power supply field due to of its high resistivity and low losses.

D. Ce substitutions

Syed I. A. et al [17] synthesized Cerium substituted cobalt ferrite nanoparticles with composition $CoFe_{2-x}Ce_xO_4$ (x = 0.00, 0.075) by Sol-gel route method and studied structural, morphological, dielectric and magnetic properties. An increase in lattice parameter with specific surface area and decrease in crystallite were observed with increasing cerium concentrations. Normal dielectric dispersion of ferrites was shown by the dielectric study that is dielectric constant, dielectric loss at room temperature found decreased with increasing frequency. Fading of A-B interaction was revealed by decreasing value of M_S and H_C due to substitution of cerium ions. Thus the samples have uniaxial anisotropy with decreased H_C and anisotropic constant. Hence M_S and H_C can be tailored for the application of nano cobalt ferrite particles in high density recording media.

E. Eu substitutions

Europium (Eu) doped spinel cobalt ferrites with composition $CoEu_xFe_{2-x}O_4$ were made-up by co-precipitation route method by Aiman Zubair et al [18] and found to constitute a face centered cubic (FCC) spinel structure belonging to Fd3m space group with some traces of ortho and hematite phases. SEM confirms the nanocrystalline grains with spherical shape of the prepared sample. Energy dispersive X-ray spectra give the composition of the sample without any impurity. Saturation magnetization (M_s) of maximum value 65 emu/g and coercivity (H_c) of 966 Oe exhibited by the hysteresis study at room temperature. With the substitution of Eu^{3+} overall coercivity was increases and magnetization was decreases. Hence magnetic behavior is highly depend on Eu substitution and anisotropy becomes constant with change in coercivity.

I. CONCLUSION

In the present paper, the different rare earth cation substitutions like Sm3+, Ce3+, Yb3+, Gd3+ and Eu3+ etc. in cobalt spinel ferrite and their significant effects on structural, dielectric and magnetic properties of the ferrites have been intensively studied by the researchers. It seems that the XRD technique confirms the formation of pure and simple cubic spinel structure. Surface morphology reveals the formation of nanocrystalline grains with spherical shape. An increase in lattice parameter with specific surface area and decrease in crystallite are observed with increasing rare earth concentrations. The substitution of rare earth cations into the cobalt ferrites toughly impacts the magnetic and dielectric properties of the rare earth doped cobalt ferrites. It is seen that the enhancement in these properties depends on the dopant concentration, the type of dopant, sintering temperature and also on the method of preparation of the sample.

II. REFERENCES

[1]. C. Orozco1, A. Melendez, S. Manadhar, S. R. Singamaneni, Kongara M. Reddy, K. Gandha, I. C. Niebedim, and C. V. Ramana, Ames Laboratory Accepted Manuscripts, 161 (2017) 25463-25471.

[2]. G. Bulai, L. Diamandescu, I. Dumitru, S. Gurlui, M. Feder, O. F. Caltun; Journal of Magnetism and Magnetic Materials, 390 (2015) 123-131.

[3]. Constantin Virlan, Georgiana Bulai, Ovidiu Florin Caltun, Rolf Hempelmann, Aurel Pui, Ceramics International, 42 (2016) 11958-11965.

[4]. Xiaofei Wu, Zui Ding, Ningning Song, Lin Li, WeiWang; Ceramics International, 42 (2016) 4246-4255.

[5]. R. N. Pandaa, J. C. Shihb, T. S. Chin; Journal of Magnetism and Magnetic Materials, 257 (2003) 79-86.

[6]. Syed Ismail Ahmad, Shakeel Ahmed Ansari, D. Ravi Kumar, Materials Chemistry and Physics, 208 (2018) 248-257.

[7]. L. B. Tahar, L. S. Smiri, M. Artus, Materials Research Bulletin, 42 (2007)1888–1896.

[8]. Sheena Xavier, Smitha Thankachan, Binu P. Jacob, and E. M. Mohammed, Journal of Nanoscience, 524380 (2013) 1-7.

[9]. M. M. Rashad, R. M. Mohamed, and H. El-Shall; Journal of Materials Processing Technology, 198 (2008) 139–146.

[10]. S. S. Satpute, S. R. Wadgane, K. Desai, D. R. Mane, R. H. Kadam; Ceramica 66 (2020) 43-49.

[11]. S. E. Jacobo, P. G. Bercoff, Ceramics International, 42 (2016) 7664.

[12]. Erum Pervaiz, I H Gul, Journal of physics, 439 (2013) 012015.

[13]. Kumar B R, Ravinder D, Materials Letters, 53 (2002) 441-445.

[14]. Bharathi K K, Chelvane J A, Markandeyulu G, Journal of Magnetism and Magnetic Materials, 32 (2009) 3677-3680.

[15]. Rana A, Thakur O P, Kumar V, Materials Letters, 65 (2011) 3191–3192.

[16]. Peng J, Hojamberdiev M, Xu Y, Cao B, Wang J, Wu H, Journal of Magnetism and Magnetic Materials, 323 (2011) 133-138.

[17]. Syed Ismail Ahmad, Madireddy Buchi Suresh, D. Ravi Kumar; AIP Conference Proceedings, 2162 (2019) 020085.

[18]. Aiman Zubair, Zahoor Ahmad, Azhar Mahmood, Weng-Chon Cheong, Irshad Ali, Muhammad Azhar Khan, Adeel Hussain Chughtai, Muhammad Naeem Ashiq, Results in Physics, 7 (2017) 3203–3208.

International Virtual Conference on Materials and Nanotechnology
In Association with International Journal of Scientific Research in Science and Technology
Volume 9 | Issue 4 | Print ISSN: 2395-6011 | Online ISSN: 2395-602X (www.ijsrst.com)

Ultrasonic Study of "Molecular Interaction of 2- Substituted 4, 5-Diphenyl Imidazole with Ethanol at Different Temperature"

T.M.Bhagat[1], Kalyani K. Kumbhare[1], Pradip B.Rathod[2]

[1]P.G, Department of Chemistry, G. S. Gawande College Umarkhed, Dist –Yavatmal, Maharashtra, India

[2]Department of Chemistry, S.P.M. Science and Gilani Arts, Commerce College, Ghatanji, Maharashtra, India

ABSTRACT

Ultrasonic studies provided a wealth of information in understanding the molecular behaviour and intermolecular interaction of aqueous solution of ethanol. Attempts were made to measure ultrasonic velocity, density and viscosity for the solute solvent mixture at different concentration and temperature. Using crystal controlled ultrasonic interferometer, specific gravity bottle and Ostwald viscometer, respectively. The acoustic parameter adiabatic compressibility (β_s), intermolecular free path length (L_f) ,acoustic independence (z), relaxation time (τ),Ultrasonic attenuation (α/f^2),relative association (R_A) have been estimated using experimental data with well-known technique. The variation of this acoustic parameter is explained in term of solute – solvent molecular interaction in a solution.

Keywords : Ultrasonic Velocity, Density, Viscosity, Adiabatic Compressibility, Apparent Molar Volume, Viscosity Relaxation Time.

I. INTRODUCTION

The ultrasonic technique is powerful and effective tool for investigation of the measurement of ultrasonic speed in liquid mixture enables accurate determination of some useful acoustical and thermo dynamical parameters are highly sensitive to molecular interaction in their mixture. Acoustic and thermodynamic parameter have been used to understand different kinds of association the molecular packing , molecular motion and various type of intermolecular interaction and their strength influenced by the size in pure components and in the mixture. Ultrasonic studies in solution have drawn the attention of many researchers in the recent year[1-4]

Study of molecular interaction between solute molecule and solvent media has got great important in many field of science including medicinal chemistry, industrial process, biochemistry etc. The solute-solvent and solvent-solvent interaction can be studied by the measurement of relative viscosity and ultrasonic velocity of an electrolyte in solution. This type of study helps us to understand the structure making and breaking properties of solute [6]

In our experimental investigation, we used the ultrasonic technique to find the acoustic parameters such as adiabatic compressibility(β_s), intermolecular free path length (L_f) ,acoustic independence (z), relaxation time (τ),Ultrasonic attenuation (α/f^2),relative association(R_A)

II. MATERIAL AND METHOD

2.1. Preparation of 2- substituted 4,5-diphenyl imidazole by using P-chlorobenzaldehyde

In a round bottom flask take Benzil (2.1gm), P-chlorobenzaldehyde (1.4gm) and ammonium acetate (4.62gm) in glacial acetic acid (20 ml) then reflux the content for 3-5 hrs. After refluxing the reaction mixture the content was kept overnight. Then content was poured in crushed ice. The obtained solid product was filtered and recrystallised by using ethanol. Yield of compound is 2.17gm and M.P.228^{0}C.

Physical Measurement:

Solutions of varying concentration were prepared on molarity basis from 0.04 stock solution of each complex sample with double distilled water. All the measurements were carried out at 303.15K, 308.15K, 313.15K, and. Density measurements were carried out for different solutions at 303.15K, 308.15K, 313.15K, and using a open capillary density bottle. The ultrasonic velocity in the solutions was measured using an ultrasonic interferometer at a frequency of 2 MHz with an accuracy of ±0.05 %. The relative viscosity was measured using a pre-calibrated Ostwald viscometer.

Methods of calculation:

The data of density (ρ), ultrasonic velocity (u) and viscosity (η) has been used to evaluate many acoustical parameters by using the following standard expressions for understanding solute-solvent, solvent-solvent interaction and structural changes.

(i) Adiabatic compressibility:-

$$\beta_s = \frac{1}{\rho_s u_s^2} \text{-------(1)}$$

Where ρ_s = density of solution,

u_s = sound velocity solution.

(ii) Intermolecular free length (L_f) :-

$$L_f = K\sqrt{\beta_s} \text{------(2)}$$

Where 'K' is a temperature dependent constant known as Jacobson constant [(m)].

(iii) Specific acoustic impedance (Z):-

$$Z = u_s \rho_s \text{--------(3)}$$

(iv) Molar sound velocity or Rao's constant (R) :-

$$R = \left(\frac{M}{\rho_s}\right) \cdot u_s \, 1/3 \text{--------(4)}$$

Where 'M'molar mass of the solution.

(v) Relative association (R_A):-

$$R_A = \left(\frac{d_s}{d_o}\right)\left(\frac{u_o}{u_s}\right)^{1/3} \text{------(5)}$$

Where ρ_o = density of solvent,

u_o = velocity of solvent

(vi) Apparent molar volume (Φ_V):-

$$\Phi_V = \left(\frac{1000}{m\rho\rho_o}\right)(\rho_o - \rho) + \left(\frac{M}{\rho_0}\right) \text{----(6)}$$

Where 'm' molarity of solution.

(vii) Apparent molar compressibility(Φ_β):

$$\Phi_\beta = \left(\frac{1000}{m\rho\rho_o}\right) - (\rho_o\beta - \rho\beta_0) + \left(\frac{\beta_0 M}{\rho_0}\right) \text{---(7)}$$

(viii) Viscosity relaxation time :-

$$\Gamma = \frac{4\eta}{3\rho.u^2} \text{----------(8)}$$

(ix) Ultrasonic attenuation :

$$(a/f2) = \frac{8\pi^2\eta}{\rho \times u^2} \text{------(9)}$$

(x) Relative viscosity(η):-

$$\eta_r = \left[\frac{d_s.t_s}{d_w t_w}\right]\eta_w \text{----------(10)}$$

The units of –Density (ρ): kg cm^{-3}, Viscosity(η): cp , Ultrasonic velocity (U) : ms^{-1}

Adiabatic compressibility (β_s): cm^2dyne^{-1}, Apparent molar volume (Qv):$cm^{-3}mol^{-1}$, Apparent molar compressibility (Q k): $cm^{-3}mol^{-1}bar^{-1}$,
Acoustical Impedance (Z): kg. $m^{-2}s^{-1}$ Intermolecular free length (L_f): m, Viscosity relaxation time (τ): s

Compound In Ethanol

Table 1: Density (ρ), ultrasonic velocity (u), Viscosity (η), adiabatic compressibility (β_s), apparent molar compressibility (ϕ_β), apparent molar volume (ϕ_V) for Compound IN ethanol at different temperatures.

Conc	ρ g/ml	u m s^{-1}	η Ns/m^{-2} 10^{-4}	β_s m^2N^{-1}	Φ_V m^3 mol^{-1} 10^2	Φ_β m^2n^{-1} 10^3
T=303.15K						
0.04	0.4885	1194.4	8.354	2.9203	4.8857	2.9202
0.02	0.4874	1139.6	8.293	2.6645	4.8743	2.6644
0.01	0.4872	1138.2	8.231	2.6590	4.8721	2.6589
0.005	0.4869	1136.8	8.130	2.6541	4.8690	2.6540
T=308.15K						
0.04	0.4861	1127.5	8.059	2.6152	4.8617	2.6151
0.02	0.4857	1125.3	8.048	2.6071	4.8573	2.6070
0.01	0.4853	1123.4	7.993	2.6005	4.8531	2.6004
0.005	0.4849	1121.9	7.980	2.5957	4.8490	2.5956
T=313.15K						
0.04	0.4843	1102.8	7.261	2.5111	4.8437	2.5110
0.02	0.4838	1102.1	7.211	2.5105	4.8383	2.5104
0.01	0.4828	1100.5	7.168	2.5084	4.8281	2.5083
0.005	0.4812	1098.1	7.057	2.5058	4.8120	2.5057

Table 2:.Acoustical Impedance (Z), Intermolecular free length (L_f), viscosity relaxation time (τ), Ultrasonic attenuation (α/f^2) Rao's constant (R), relative association (R_A),

Conc.	z Ns/m^3 10^1	L_f M 10^2	τ s 10^{-1}	α/f^2 10^2	R	R_A
T=303.15K						
0.04	5.834	5.1776	7.7624	2.2984	805.63	1.1350
0.02	5.554	4.9458	6.9990	1.9862	770.41	1.1863
0.01	5.545	4.9407	6.9268	1.9649	769.78	1.1855
0.005	5.535	4.9361	6.8208	1.9348	769.30	1.1856
T=308.15K						
0.04	5.480	4.9806	6.6401	1.8743	764.26	1.3210
0.02	5.465	4.9729	6.5998	1.8624	763.40	1.2068
0.01	5.451	4.9668	6.5272	1.8418	762.74	1.2072
0.005	5.440	4.9621	6.4938	1.8330	762.35	1.2067

T=313.15K						
0.04	5.340	4.9597	5.7022	1.5860	750.30	1.2436
0.02	5.331	4.9591	5.6499	1.5737	750.60	1.2376
0.01	5.313	4.9569	5.5883	1.5608	751.06	1.2361
0.005	5.284	4.9544	5.4596	1.5316	751.92	1.2290

III. RESULT AND DISCUSION

Density decrease and ultrasonic velocity and viscosity are also decrease with decrease in concentration of solute. The linear behavior with decrease in velocity with concentration indicates the interaction between unlike molecule, which suggests weak solute-solvent (dipole-dipole) interaction between the component molecules. As density decreases the number of solute particles in the given region decreases [7]. It shows reverse trends in ultrasonic velocity and density with increase in temperature show molecular forces are weakening at high temperature. The increase in ultrasonic velocity is structure making type.

Decrease in concentration of 2- substituted 4,5-diphenyl imidazole results the linearly decreases in adiabatic compressibility and free length. This trend supports weak solute-solvent interaction and suggests aggregation of solvent molecules around solute molecules[8,9]. The magnitude of adiabatic compressibility and free length decreases with increase in temperature, it clearly reveal that interaction become stronger at higher temperature[10]. The specific acoustic impedance is the parameter related to the elastic properties of the medium. The specific acoustic impedance is the impedance offered to the sound wave by the components of the mixture. In present investigation, specific acoustic impedance decrease with decrease in concentration. This trend further supports that there was no possibility of molecular interaction due to H-bonding between solute-solvents and solvent-solvent molecules which restrict the free flow of sound waves [11]. The specific acoustic impedance is directly proportional to density, ultrasonic velocity and inversely proportional adiabatic compressibility[12].

Molar sound velocity (Rao's constant) nonlinearly increase or decrease with decrease in concentration which indicates that the magnitude of molecular interaction is enhanced in the system, which indicate interaction between solute-solvent molecule decrease. This leads to tight packing of the medium by decrease the molecular interactions [13].

Relative association is the measure of extent of association of components in the medium. The relative association is depends on either breaking up of the solvent molecules on addition of solute to it or the solvation of present ions. The relative association non-linearly decreases with decrease in concentration.

The apparent molar compressibility and apparent molar volume decreases with decrease in concentration which indicates interaction between solute-solvent molecules enhanced.

Values are positive due to the compressibility of solvent due to the weak electrostatic force in the vicinity of ions. This trend supports that the availability of more number of components in a given regions of space. This leads to tight packing of the medium and there by increases the interactions [14].
The viscosity relaxation time is the time required for the excitation energy to appear as translational energy. In present work viscosity relaxation time non-linearly

decreases with decrease in molar concentration and decreases with increases in temperature. Where, with increase in temperature, it shows the instantaneous conversion of excitation energy to translational energy. This indicates strong molecular interaction between the solute and solvent molecules, where it show the instantaneous conversion of excitation energy to translational energy[15]. Absorption coefficient decreases with decrease in concentration and this trend suggest that the extent of complexity decreases with decrease in concentration[16].

IV. CONCLUSION

From the present investigation experimental values of density, ultrasonic velocity, viscosity and related acoustic parameter values indicate that thermodynamic parameters are sensitive to molecular interactions for ternary liquid mixtures at different concentrations and at varying temperatures. Thus it's concluding that in mixture of studied compound, solute-solvent interaction is existed. Some parameters specially, free length and adiabatic compressibility indicate strong interaction between solute-solvent molecules in the studied systems.

V. REFERENCES

[1]. K. Sreekanth, M.Kondaiah, D. Sravana Kumar and D. Krishna Rao, Journal of Solution Chemistry, vol.41,no 7 pp. 1088-1102, 2012.

[2]. M.K.Praharaj, A.Satapathy, P.Mishra,and S.Mishra, Journal of Theoretical and Applied Physics, vol.7, article 23,6 pages 2013.

[3]. B. Nagarjun, A.V.Sarma,G.V.Rama Rao,and C.Rambabu, Journal of Thermodynamics,vol.2013, Article ID 285796, 9 pages ,2013.

[4]. D.R.Godhani , P.B.Dobariya, A.M.Sanghani, and J.P.Mehta, Arabian Journal of Chemistry,2012.

[5]. F.M.Sannaningannavar,B.S.Navati,and N.H.Ayachit, Polymer Bulletin, vol 70,no 2,pp.603-618,2013.

[6]. S.D.Deosarkar and M. L. Narwade RASAYAN J.Chem Vol.3, No. 1 (2010) 55-59 ISSN: 0974-1496 CODEN : RJCABP.

[7]. A. N .Kannapan, Thirumaran, Palanichammy, J. Physical sci, vol. 20 (2), (2009) 97-108.

[8]. H. Eyrin, J.F. Kincad, J. Chem. Phys, 6 (1938) 620-629.

[9]. K.C. Patil and V.D. Umare, Int. J. Resh. in Pure app. Phys,2(4);(2012) 25-27.

[10]. A. Pal, H. Kumar, R. Mann, H. K. Sharma, J. Chem. Eng. Data 58 (2013) 3190-200.

[11]. R. K. Bachu, M. K. Patwari, S. Boodida, S. J. Tangeda, S. Nallani, Ind. J. Chem. 47A (2008) 1026.

[12]. S. J. Kharat, Physics Chemistry liqs. 51 (2013) 1-10.

[13]. S.Padma, Rasayan J. Chem 6 (2) (2013) 111.

[14]. R. Mohanty and R. Paikaray, Res. J. of Chem. Sci. 3(5) (2013) 71-73

[15]. S. Nithiyanantham and Palaniappan chem. sci. Trans., 2(1) (2013) 35-40.

[16]. ZareenaBegaum, et. al., J. Mol. Liqs, 178 (2013) 99-112.

International Virtual Conference on Materials and Nanotechnology
In Association with International Journal of Scientific Research in Science and Technology
Volume 9 | Issue 4 | Print ISSN: 2395-6011 | Online ISSN: 2395-602X (www.ijsrst.com)

Band gap of $Bi_2Al_4O_9$

S.G.Revankar[1], K.A.Gedekar[2], S.P.Puppulwar[1], S.P.Wankhede[2], P.D.Belsare[3], S.V.Moharil[4]

[1]Department of Physics, Kamla Nehru Mahavidyalaya, Nagpur, 440009, Maharashtra, India

[2]Department of Physics, K.D.K. College of Engineering, Nagpur, Maharashtra, India

[3]Department of Physics, Shri Ramdeobaba College of Engineering and Management, Nagpur, 440013, Maharashtra, India

[4]Department of Physics, RTM Nagpur University, Nagpur, 440033, Maharashtra, India

ABSTRACT

In the system Al_2O_3-Bi_2O_3 two compounds, viz. $BiAlO_3$ and $Bi_2Al_4O_9$ are well known. $Bi_2Al_4O_9$ is useful for several applications such as photo catalysis, dye degradation, scintillation, ratio metric thermometry, etc. However, literature data on the optical and electronic properties of this compound are confusing. Some researchers have mentioned $Bi_2Al_4O_9$ to be colourless, with optical absorption in deep ultraviolet, while some relatively recent literature mentions $Bi_2Al_4O_9$ powders to be yellow coloured. The band gap had been stated as 2.84 eV. These discrepancies are investigated. $Bi_2Al_4O_9$ is freshly prepared and the band gap was calculated from diffused reflectance measurements as 4.5 eV. Yellow colour was attributed to the lattice defects and thus the inconsistencies in the literatures results explained.

Keywords : Aluminate, $Bi_2Al_4O_9$, band gap, tauc plot

I. INTRODUCTION

In the system Al_2O_3-Bi_2O_3 two compounds, viz. $BiAlO_3$ and $Bi_2Al_4O_9$ are well known. $Bi_2Al_4O_9$ is useful for several applications such as photo catalysis, dye degradation, scintillation, ratio metric thermometry, etc. However, literature data on the optical and electronic properties of this compound are confusing. In the early literature, optical absorption of this compound is shown to have an absorption edge around 290 nm[i]. The powders samples are mentioned to be white and single crystals colourless. UV absorption around 285 nm had been assigned to $^1S_o \rightarrow {}^3P_1$ transition of the Bi^{3+} ion by some researchers [ii] . Absorption spectrum of the single crystal showed bands at 270 and 233 nm[iii]. On the other hand, relatively recent literature mentions $Bi_2Al_4O_9$ powders to be yellow coloured with band gap of 2.71 eV[iv]. Considering these inconsistencies, we decided to reinvestigate the band gap of this compound and obtain an explanation for the differences in the literature data.

II. METHODS AND MATERIAL

$Bi_2Al_4O_9$ phosphors were prepared by combustion synthesis. “Aluminium nitrate has exothermic reaction with urea. Reagent grade (Indian Rare Earths, Ltd.) Lanthanide/Chromium oxides were converted to the corresponding nitrates by dissolving in minimum amount of nitric acid. The nitrates were dried by prolonged, gentle warming. Stoichiometric amounts of hydrated nitrates of bismuth and aluminium were thoroughly mixed with urea or urea/glycine mixture.

The oxidizer (metal nitrates) to fuel ratios were calculated by the method described earlier [v vi]. Due to the presence of large water of crystallization in aluminium nitrate, a thick paste was formed. A china dish containing the paste was inserted in a furnace preheated to 500 ^{0}C. With urea/glycine mixture as a fuel, within minutes the paste foamed and a flame was produced which lasted for several seconds. No foam was formed with urea alone. The china dish was immediately removed from the furnace. Reflectance spectra at room temperature were studied using a Hitachi F-7000 spectrofluorimeter, with 1 nm spectral slit width. $BaSO_4$ was used as a white standard.".

III. RESULTS AND DISCUSSION

Fig.1. shows a photograph of as-combusted, foamy powders of $Bi_2Al_4O_9$. Yellow body colour is apparent. Fig.2 shows reflectance spectra of $Bi_2Al_4O_9$. It can be seen that reflectance drops below 450 nm. To get better idea about the absorption, Kubelka-Munk functions are also plotted in Fig.2. Absorption bands are observed around 450 and 360 nm. There are two more absorption structures around 270 and 230 nm in UV region. Literature results on optical properties of $Bi_2Al_4O_9$ are not consistent. Brixner [1] mentions the absorption edge of this material at about 290 nm. Timmermans and Blasse also obtained similar results.[vii] These researchers obtained white coloured powders. On the other hand, we have obtained products with yellow body colour. Several other articles mention this colour which is consistent with the band gap 2.84 eV.

Using the reflectance data, band gap was obtained using Tauc plot[viii]. The band gaps of the compounds can be estimated using the equation-"$[F(R)h\nu]^n = A(h\nu - Eg)$ where hv is the photon energy, A is a constant, Eg is the band gap, n = 2 for a direct transition and 1/2 for an indirect".

Tauc plot for $Bi_2Al_4O_9$ is shown in Fig.3. From the Tauc plot, a direct band gap 4.5 eV is obtained for $Bi_2Al_4O_9$. Other absorption bands indicated in the reflectance spectra around 360 and 450 nm and which are responsible for the body colour are due to defects

Figure 1 As-combusted $Bi_2Al_4O_9$ powder.

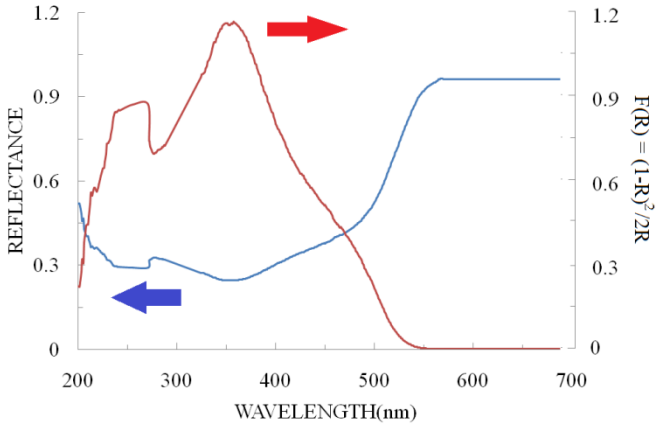

Figure 2 Reflectance Spectra of Bi2Al4O9 powder.

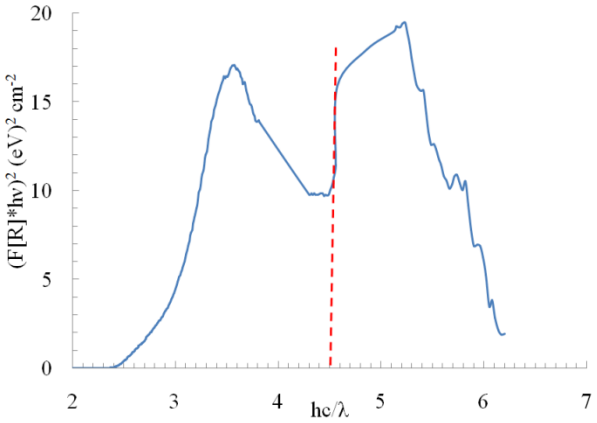

Figure 3 Tauc plot for $Bi_2Al_4O_9$

IV. CONCLUSION

Inconsistencies regarding the optical properties and bandgap of Bi2Al4O9 are thus resolved. Optical absorption in the visible region is responsible for the yellow body colour. However, this absorption is not due to band to band transition as interepreted by previous researchers. The visible absorption is due to lattice defects. Bi2Al4O9 has a direct band gap of 4.5 eV activated.

V. REFERENCES

[1]. L. H. Brixner," Fluorescence And X-Ray Data Of Bi2Al409 And Bi2Ga409," Mat. Res. Bull. Vol. 13 (1978) 563-566

[2]. G.Blasse and O. B. Ho. "On the Luminescence of Bismuth Aluminate (Bi2Al4O9)," J. Lumin. 21 (1980) 165-168

[3]. V. V.Volkov and A. V. Egorysheva.. "Photoluminescence in Fast-Response Bi2Al4O9 and Bi2Ga4O9 Oxide Scintillators," Opt. Mater. 5 (1996) 273-277

[4]. E.Zahedi, B. Xiao and M. Shayestefar. . "First-Principles Investigations of the Structure, Electronic, and Optical Properties of Mullite-Type Orthorhombic Bi2M4O9 (M = Al3+, Ga3+)." Inorg. Chem. 55 (10) (2016) 4824-4835.

[5]. J.J. Kingsley, K. Suresh and K.C. Patil, Combustion synthesis of fine-particle metal aluminates, J. Mater. Sci. 25 (1990) 1305-1312

[6]. J.J. Kingsley, N. Manickam and K.C. Patil, Combustion synthesis and properties of fine particle fluorescent aluminous oxides, Bull. Mater. Sci. 13 (1990) 179-189

[7]. C. W. M. Timmermans and G. Blasse, The Luminescence of Some Oxidic Bismuth and Lead Compounds, J. Solid State Chem. 52 (1984) 222-232

[8]. J. Tauc, R. Grigorovici, A. Vancu, Optical properties and electronic structure of amorphous germanium, Phys. Status Solidi. 15 (1966) 627-637.

International Virtual Conference on Materials and Nanotechnology
In Association with International Journal of Scientific Research in Science and Technology
Volume 9 | Issue 4 | Print ISSN: 2395-6011 | Online ISSN: 2395-602X (www.ijsrst.com)

Synthesis, Structural and Magnetic Study of Nickel Substituted Magnesium Spinel Ferrites

Pranali K. Tembhurne*[1], Nomdeov M. Gahane[2], Kishor G. Rewatkar[3], Sanjay J. Dhoble[4]

*[1]Assistant Professor, Department of Physics, Gramgeeta Mahavidyalaya, Chimur, Maharashtra, India

[2]Assistant Professor, Department of Physics, Hislope College, Nagpur, Maharashtra, India

[3]Professor, Department of Physics, Dr. Ambedakar College, Nagpur, Maharashtra, India

[4]Asssociate Professor, Department of Physics, Nagpur University, Maharashtra, India

ABSTRACT

In our present investigation, Nickel doped Magnesium ferrite nanoparticles having the basic composition NixMg1-xFe2O4 (x=0.1, 0.3, 0.5) were synthesized by the Sol-gel auto combustion method. The structural and magnetic properties of samples were investigated by XRD, SEM, TEM, and VSM. The single-phase face-cantered cubic structured nanoparticles were confirmed by the XRD pattern. The structural parameter like Particle size, X-ray density, Bulk density, Lattice constant from X-RD data was calculated by the various formulas. The surface agglomerated morphology of the samples has been investigated using FESEM. The Coercivity (Hc), a remnant (Mr), and Saturation magnetization (Ms) show variation with every sample is confirmed by VSM.

Keyword: - Ferrites, Sol-gel Method, X-RD, SEM, HR-TEM, VSM

I. INTRODUCTION

Nano sized magnetic spinel ferrites with chemical formula MFe2O4 are isotropic with mineral spinel MgAl2O4.Spinel ferrites due to their unique, remarkable, and interesting properties of the electric insulator and magnetic conductor attracted several researchers, scientists, and technologists. Because of their fascinating properties, Nano sized spinel ferrites have a wide range of applications in medical diagnosis such as targeted drug delivery, magnetic hyperthermia, contrast agents for magnetic resonance imaging (MRI), bio separation, and microwave and storage device system etc.[1-4]. Spinel ferrites can be normal spinel, mixed spinel, and inverse spinel structures. Among all spinel ferrites Nickel ferrite (NiFe2O4) is inverse spinels and it is interesting due to the distribution of cations among interstitial sites such as tetrahedral (A) sites are occupied by ferric ions, and the octahedral (B) sites are occupied by Ni ions. Nickel ferrite, as a p-type semiconducting oxide [5-6]. Magnesium ferrite (MgFe2O4) is a partially inverse spinel with a soft magnetic and n-type semiconducting material. In this ferrites random distribution of cations over the available tetrahedral (A) and octahedral [B] sites. The various properties of ferrites depend on the synthesis methods, sintering temperature, and the kind of substituting ions. In all

the spinel ferrites, NiMgFe2O4 is a very interesting spinel ferrite. several researchers have reported the synthesis of Ni-Mg ferrites, by substitution of Ni ions in Magnesium ferrites or Mg ions in Nickel ferrites leads to the modification of the structural, electrical and magnetic properties using different techniques like citrate gel[7],Solid-state reaction [8],hydrothermal [9], combustion [10], co-precipitation[11], reverse-micelle process [12],spark plasma sintering [13], micro emulsion etc.

II. METHODOLOGY AND EXPERIMENTATION

The samples of Ni substituted Mg ferrites with the composition NixMg1-xFe2O4 (x=0.1, 0.2, 0.3) were prepared by the Sol-Gel auto combustion method. The sol-gel auto combustion method requires less time and low temperature for synthesis produces homogenous and Nano-size samples. The method is low cost and chemically stable [14].

[1]. The sol-gel auto combustion method

In the case of sol-gel auto combustion method AR grade nitrates like magnesium nitrate Mg (NO3)2.6H2O], Nickel nitrates [Ni (NO3)2.3H2O] and iron (III) nitrate [Fe (NO3)3.9H2O], and urea was used as fuel for the auto combustion reaction. These nitrates were accurately weighed on an electronic balance and mixed and dissolved together according to stoichiometric proportions in deionized water. The mixture of the nitrates is then stirred continuously at 700 rpm and heated to a temperature of 800C while it is being stirred continuously sol is formed. Due to the heating of the sol, its water content gets evaporated and the sol gets converted into a viscous gel. after the formation of gel, it kept in a microwave for few minutes until the gel burns out within few minutes leaving the loose voluminous ferrite powder behind The as-prepared ferrite powder is then ground for about 3h and sintered at 8000C for 4 h in a programmable furnace and then cooled slowly to room temperature. Finally, the sintered powder was used for characterization and the measurement of structural and magnetic properties.

[2]. Characterization

To analyse the crystalline phase and the structural parameters, The XRD pattern was recorded at room temperature using Cu-Kα λ=1.5406 Å radiation. The crystal structure, lattice parameter, crystallite size, X-ray density, bulk density, and porosity were determined from the XRD pattern. The shape, size, and morphology of the particles were examined by scanning electron microscope (SEM) and transmission electron microscopy (TEM). The elemental composition was confirmed with the help of energy dispersive X-ray analysis. Magnetic characterization i.e. Hysteresis loops of the samples was carried out by vibrating sample magnetometer at room temperature with a maximum applied field of 20 kOe.

III. RESULTS AND DISCUSSION

1. XRD Analysis

The single-phase cubic spinel structure of the prepared NixMg1–xFe2O4 (x = 0.1, 0.2, 0.3) ferrite was confirmed by X-Ray diffraction technique in the 2θ range of 100to 800. Fig.1 shows X-ray diffraction pattern indicating (h k l) values for Ni substituted magnesium ferrite. The diffraction peaks corresponding to planes (220), (311), (400), (422), (511), and (440) provide clear evidence for the formation of the spinel structure of the ferrite. By using Debye - Scherrer formula the average crystallite sizes of all the samples were calculated from the XRD peak. The values of the lattice parameter ‘a’ are calculated from the most prominent peak in the XRD[15]. It is observed that the lattice constant decreases from 8.3933 to 8.3840 Å with an increase of Ni2+ ion content in ferrites; this is due to the difference in ionic radii of the Mg2+ and Ni2+ ions.

The ionic radii of Mg2+ ions (0.072 nm) are slightly greater than Ni2+ (0.069 nm) and Fe3+ ions (0.0645 nm)[16].

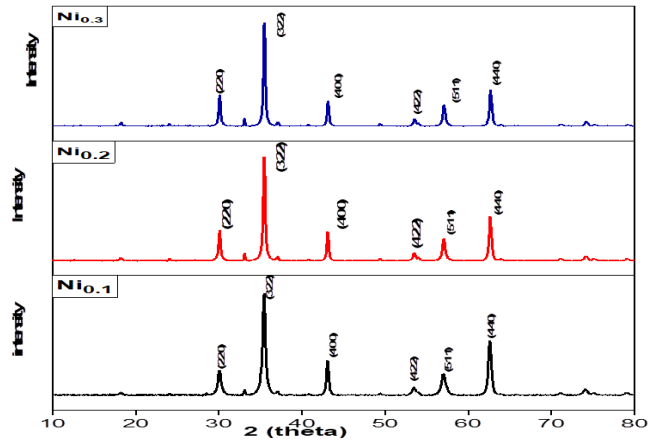

Fig. 1 X-RD pattern of Nix Mg 1-x Fe204 (x = 0.1, 0.2, 0.3)

From X-RD data different parameters obtained such as lattice constant (a), particle size (D), cell volume (a3), Porosity (P) is listed in tables.

Table1: Structural parameters from XRD data for NixMg1-xFe2O4 (x=0.1, 0.2, 0.3) of different composition

Composition	Lattice Parameter (a) (Å)	Volume "a3" (Å)³	Bulk Density "Db"(gm/cm3)	X-ray Density "Dx"(gm/cm3)	Porosity "P"(%)	Particle Size(nm)
Ni0.1Mg0.9Fe2O4	8.3933	591.286	4.10	4.569	10.3	23.26
Ni0.2Mg0.8Fe2O4	8.3897	590.52	3.89	4.653	16	26.94
Ni0.3Mg0.7Fe2O4	8.3840	589.32	3.90	4.740	17.7	31.10

It is observed that the crystallite size increases with increase in Ni content; it varies from 23.26 nm to 31.10 nm. The particle size is calculated using the Scherrer equation.

$D = 0.9\lambda/\beta\cos\theta$ ……(1)

The X-ray density and bulk density also calculated by using the formula

$Dx = 8M/Na3$……2)

$Db = M/(\pi r^2 h)$……...(3)

Ni has larger molar mass compared with Mg ferrites due to X-ry density increases with the substitution of Ni2+ in magnesium ferrites. Cell Volume and magnitude of Bulk density decreases with Ni constant as shown in table [17].

2. SEM and EDAX Analysis

Fig.2 shows the Field emission scanning electron microscopic (FE-SEM) image of the synthesized Ni-doped MgFe2O4 nanoparticles. The SEM images indicate agglomerated nanoparticles because of magnetic interaction between the nanoparticles. The SEM image reveals that there were irregular grains. The particles are lumped and become compact. Aggregation of smaller grains observed with the formation of lesser pores.

The fig.2 shows the energy dispersive X-ray analysis (EDAX) spectrum for Ni Mg ferrites. Regarding the EDX analysis, the nickel doped magnesium ferrite is roughly high in the concentration of oxygen.

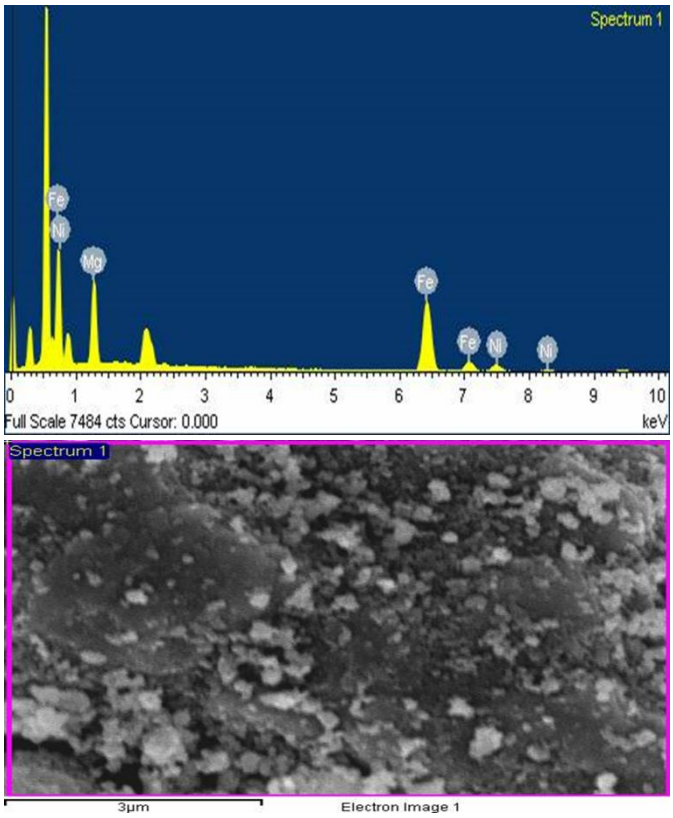

Fig.2 SEM image and EDAX Spectrum of Ni0.2Mg0.8Fe2O4

It is apparent that the presence of nickel causing oxygen removal from the surface part, which is assumed due to the bonding formation between nickel and oxygen.

The results confirmed the presence of the required elements in the prepared composition with almost all the peaks associated with elements. Suggesting the formation of pure Ni-Mg spinel ferrites.

3. TEM Studies

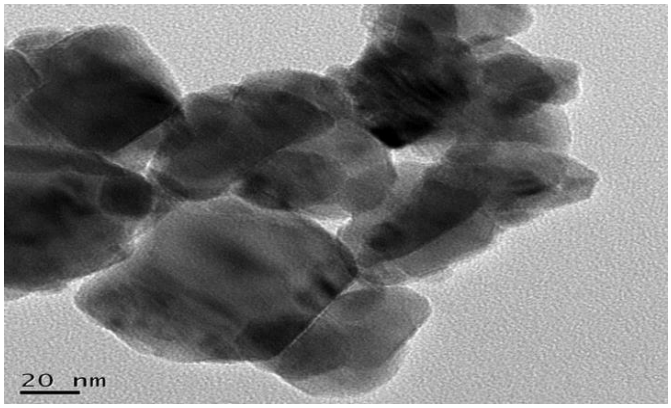

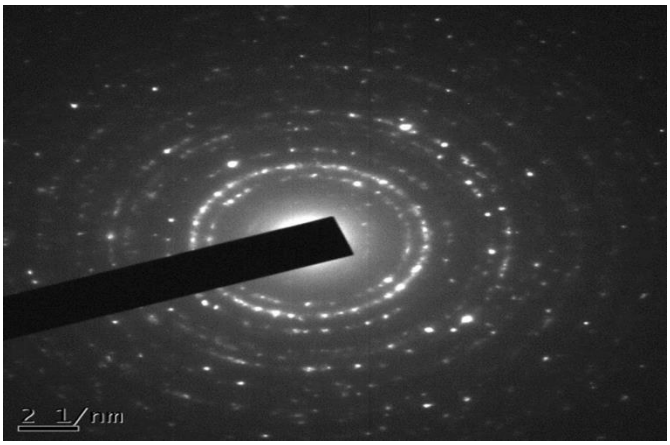

Fig 3. TEM and SAED image of x=0.2

Fig.3 shows the transmission electron micrograph of the sample for x=0.2. The micrograph indicates the agglomerated, well-defined particle with inhomogeneous grain size distribution. The average values of particle size is 20 nm estimated from the TEM studies are in good agreement with those values obtained from XRD. The rings of selected area electron diffraction (SAED) (Fig. 3) clearly show the diffraction planes belonging to spinel ferrite. The SAED patterns indicate that Ni substituted MgFe2O4. ferrite nanoparticles were found in well- defined crystalline nature.

4. Magnetic Properties

The magnetic properties of spinel ferrites are strongly dependent on the distribution of the different cations among (A) and (B) sites. The synthesized nickel ferrite (NiFe2O4) and magnesium ferrite (MgFe2O4) have inverse spinel structure in which half of the Fe3+ ions spatially fill the tetrahedral sites and the rest occupy the octahedral sites. Magnetic characterisations of the samples were carried out by vibration sample magnetometer at room temperature with a maximum applied field of 20 kOe.

The saturation magnetisation (Ms), coercivity (Hc) and remanence (Mr) of the samples are shown in Table 2. coercivity (Hc) of a magnetic material is a measure of magneto-crystalline anisotropy of samples. The coercivity (Hc) of the synthesized nanoferrites

sample has been obtained from Fig4. Note that the Hc values of all prepared nanocrystals are close to zero, which is considered to be a typical superparamagnetic behavior at room temperature[18]. The value of saturation magnetization depends on the grain size and preparation temperature . The coercivity and magnetic remanence values of samples are also small.

Table2. Magnetization measurements of the compounds NixMg1-xFe2o4 (x=0.1,0.2,0.3)

Conc. (x)	Saturation Magnetization(Ms) (emu/g)	Retentivity (Mr)(emu/g)	Coercivity (Hc) (Gauss)	Bohr magneton (μB)	SQRRatio Mr/Ms
0.1	0.1653	0.021	165	0.04	0.13
0.2	0.4109	0.075	167	0.11	0.18
0.3	0.3005	0.066	171	0.08	0.22

The saturation magnetization of sample shows large variation with every concentration of x. The variation in magnetization can be due to a rearrangement of cations i.e., a change in distribution of Ni2+ and Mg2+on the octahedral and tetrahedral sites [19].

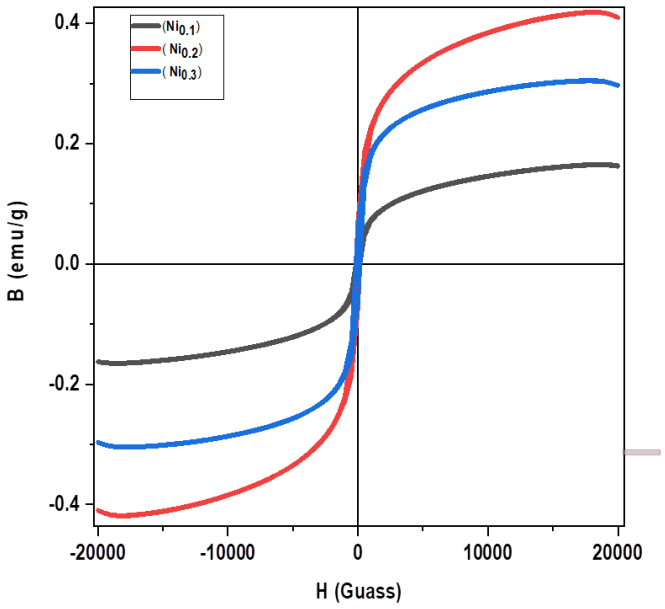

Fig.4 shows the Hysteresis loops for NixMg1-xFe2O4 (x=0.1, 0.2, 0.3) Nano ferrites

IV. CONCLUSION

Ni substituted magnesium ferrites NixMg1-x Fe2O4 (x=0.1,0.2,0.3) were synthesized by sol-gel auto combustion method which confirmed the existence of single-phase cubic spinel structure of ferrites with the help of X-ray diffraction measurement. The mean crystallite sizes of synthesized nanoparticles were calculated using the Debye Sherrer formula which are 23nm, 26nm, and 31nm. Magnetic measurements showed that all synthesized samples have Smaller values of coercivity revealed that the prepared nanomaterials have soft magnetic nature. i.e. exhibit superparamagnetic behavior. The saturation magnetization of the sample shows a large variation with every concentration of 'x', this is due to the cationic distribution at tetrahedral and octahedral sites. The FESEM and HR-TEM results reveal that the morphology of the Ni+2doped MgFe2O4 nano-particles are the same in morphological shape and show nearly comparable crystalline size which is shown by XRD. The pure phase and structure of the ferrite samples were confirmed by Energy Dispersive Spectrometer (EDS) analysis.

V. REFERENCES

[1]. Mohammed L., Gomaa H. G., Ragab D., Zhu J. Magnetic nanoparticles for environmental and biomedical applications: A review, Particuology, V. 30 (2017) 1-14.

[2]. Tatarchuk T., Bououdina M., Judith Vijaya J., John Kennedy L. Spinel Ferrite Nanoparticles: Synthesis, Crystal Structure, Properties, and Perspective Applications. In: Fesenko O.,Yatsenko L. (eds) Nanophysics, Nanomaterials, Interface Studies, and Applications. Springer Proceedings in Physics, 195 (2017) 305-325.

[3]. Matsui I. Nanoparticles for Electronic Device Applications: A Brief Review, Journal of chemical engineering of Japan, V. 38 (2005) 535-546.

[4]. Koh I., Josephson L. Magnetic Nanoparticle Sensors, Sensors, V. 9 (2009) 8130-8145.

[5]. G. F. Goya, H. R. Rechenbury, J. L. Jiang J. Appl. Phys. 84 (1998) 1101.

[6]. S. Marup, J. Z. Jiang, F. Bodker, A Harsewell, Euro physlett. 56 (2001) 441.

[7]. S. E. Jacobo, S. Duhalde and H. R. Bertorello, "Rare Earth Influence on the Structural and Magnetic Properties of NiZn Ferrites," Journal of Magnetism and Magnetic Materials, Vol. 272-276, No. 3, 2004, pp. 2253-2254.

[8]. S. D. Shenoy, P. A. Joy and M. R. Anantharaman, "Effect of Mechanical Milling on the Structural, Magnetic and Dielectric Properties of Coprecipitated Ultrafine Zinc Fer- rite," Journal of Magnetism and Magnetic Materials, Vol. 269, No. 2, 2004, pp. 217-226.

[9]. S. A. Morrison, C. L. Cahill, E. E. Carpenter, S. Calvin, R. Swaminathan, M. E. McHenry and V. G. Harris, "Mag-netic and Structural Properties of Nickel Zinc Ferrite Na- noparticles Synthesized at Room Temperature," Journal of Applied Physics, Vol. 95, 2004, pp. 6392-6395.

[10]. J. J. Sun, J. B. Li, G. L. Sun and W. G. Qu, "Synthesis of Dense NiZn Ferrites by Spark Plasma sintering," Ceramics International, Vol. 28, No. 8, 2002, pp. 855-858.

[11]. A. Verma, T. C. Goel, R. G. Mendiratta and M. I. Alam, "Dielectric Properties of NiZn Ferrites Prepared by the Citrate Precursor Method," Materials Science and Engin- eering: B, Vol. 60, No. 2, 1999, pp. 156-162.

[12]. G. P. Lópeza, S. P. Silvetti, S. E. Urreta and E. D. Cabanil-las, "Magnetic Interactions in High-Energy Ball-Milled NiZnFe2O4/SiO2 Composites," Physica B: Condensed Mat- ter, Vol. 398, No. 2, 2007, pp. 241-244.

[13]. C. Upadhyay, D. Mishra, H. C. Verma, S. Anand and R. P. Das, "Effect of Preparation Conditions on Formation of Nanophase Ni-Zn Ferrites through Hydrothermal Te- chnique," Journal of Magnetism and Magnetic Materials, Vol. 260, No. 1-2, 2003, pp. 188-194.

[14]. M. Atif, M. Nadeem, R. Grössinger, R.S. Turtelli, Studies on the magnetic, magnetostrictive and electrical properties of sol–gel synthesized Zn doped nickel ferrite, J. Alloy. Compd. 509 (2011) 5720–5724.

[15]. H. Moradmard, S. Farjami Shayesteh, P. Tohidi, Z. Abbas, M. Khaleghi, Structural, magnetic and dielectric properties of magnesium doped nickel ferrite nanoparticles,J. Alloy. Compd. 650 (2015) 116–122

[16]. L.R. Pradeep Chavan, P.B. Naik, Belavi, C.K. Geeta Chavan, Ramesha, R. Kotnala, Studies on electrical and magnetic properties of Mg-substituted nickel ferrites, J.Electron. Mater. 46 (2017) 188–198.

[17]. K. Rama Krishna, K. Vijaya Kumar, Dachepalli Ravinder, Structural and electrical conductivity studies in nickel-zinc ferrite, Adv. Mater. Phys. Chem. 2 (2012) 185–191.

[18]. A. Manikandan, J. Judith Vijaya, M. Sundararajan, C. Meganathan, L. JohnKennedy, M. Bououdina, Optical and magnetic properties of Mg-doped ZnFe2O4nanoparticles prepared by rapid microwave combustion method, Superlattices Microstruct. 64 (2013) 118–131.

International Virtual Conference on Materials and Nanotechnology
In Association with International Journal of Scientific Research in Science and Technology
Volume 9 | Issue 4 | Print ISSN: 2395-6011 | Online ISSN: 2395-602X (www.ijsrst.com)

Literature Survey on Aspect Based Sentiment Analysis for Products on E-Commerce Business Platform

Shraddha H. Ingle[1], Prof. Mayur S. Burange[2], Dr. Ajay B. Gadicha[3]

[1]Department of Computer Science and Engineering, P. R. Patil College of Engineering and Technology, Amravati, Maharashtra, India

[2]Department of Computer Science and Engineering, P. R. Pote(Patil)College of Engineering and Technology, Amravati, Maharashtra, India

[3]Head Of Department , Department of Computer Science and Engineering, P.R. Pote(Patil) College of Engineering and Technology, Amravati, Maharashtra, India

ABSTRACT

Now a days with the tremendous development in technology made many things possible for business as well as for customers and manufacturers to buy and sell online and know about those products from opinions, comments provided by previous user on various platforms like social media, forums, e-commerce sites. The opinions of customers which can also called as reviews can be present in any form like structured or unstructured. The collection of these reviews create large amount of data for producers to know more about their product .Sentiment analysis can help to know what customers want to tell from these positive or negative reviews to producers by doing analysis on that data .At the same time only to know about sentiment will not be sufficient so Aspect based sentiment analysis will help to do some feature based sentiment analysis .This survey paper will present how aspect based sentiment analysis will help customers to know about feature based analysis and for producers to know about improvisation in products from the reviews on E-commerce platform. With the use of some machine learning algorithms and using natural language processing we will be able to do this sentiment analysis.

Keywords : Sentiment Analysis, Aspects/Features, Business Intelligence, E-Commerce, Machine Learning, Natural Language Processing (NLP)

I. INTRODUCTION

In the present time there are large number of people uses social media and online platform for various purposes like some people uses it for online purchasing, while some uses it to comment or give review on some product, while some people just check those reviews before purchasing particular product as customer is unable to touch or look at quality, user friendliness of the product , so most of the customer depend on reviews .So large amount of data is available online for customers as well as for producers regarding their product. So to get useful information from this data and using it for well development of business is the need of today's business. To help those customers and producers Sentiment analysis in the most useful way to know

more about product from reviews provided by previous users of the product.

When an individual wants to make a decision about buying a product or using a service, they have access to a huge number of user reviews, but reading and analysing all of them is a tedious task. Also when an organization wants to benefit by obtaining the public opinion or to market its products, even to identify new opportunities, predict sales trends, or manage its reputation, it needs to deal with an overwhelming number of available customer comments. With sentiment analysis techniques, it is possible to analyse a large amount of available data, and extract opinions from them that may help both customers and organization to achieve their goals.[1]

II. RELATED WORK

The development of technology along with the demand of analyzing opinionated information has led to a new research topic in natural language processing and data mining named "opinion mining and sentiment analysis". Studies on this problem started from the 2000[3] Just 101 articles on this subject were published in 2005, while almost 5,699 were published in 2015. This means that over a decade sentiment analysis has increased almost 50 times, making it one of the most quickly expanding fields of study in previous years.[4]

The consumer can compare products according to the people's reviews on these products. So, for making this more successful they have produced supervised techniques for the consumer reviews. There are two types of methods are mentioned that is, association rules techniques and naïve Bayes classifiers to categorize the features of the products that according to the needs of consumers. This analysis is not only based on the ratings, but the important character also is, and this sentimental analysis compares and identifies the preferred products which make comfortable for the consumer.[4]

Li et al. proposed the Sentiment-LDA model and Dependency-Sentiment-LDA. Unlike the previous models making assumption that the sentiments of the words in the document are all independent, this model views the sentiments of words as a Markov chain. Zhao et al. proposed a MaxEnt-LDA hybrid model to jointly discover both aspects and aspect-specific opinion words. They show that with a relatively small amount of training data, Max- Ent-LDA hybrid model can effectively identify aspect and opinion words simultaneously.[6]

III. SENTIMENT ANALYSIS

Sentiment analysis is a type of data mining that aims to determine the polarity of people's opinions about someone or something.[2] Sentiment Analysis is also known as opinion extraction, opinion mining, effect analysis, sentiment mining, emotion analysis, review mining, etc. [7] Sentimental Analysis is necessary for producing companies to evaluate various reviews automatically provided by customer regarding product. The use of the classification of sentimental analysis as an efficient way of analysing textual data from different online platforms. Opinion mining offers an accurate and dynamic view of customers in real-time and may have a huge impact on business decision-making. They also recognized potential areas for further research from the Business Intelligence research pond.[4] For processing the textual information Sentiment Analysis adapts the approaches of NLP (Natural language processing), AI (Artificial Intelligence) and ML (Machine Learning). [9]

Sentiment Classifications are as follows

Document-level:

The Document-level uses the entire documents to categorize it into a positive or negative class as a simple information category [4]

Sentence level:

In the Sentence level, the sentiment classification categorize any sentence as subjective or objective, and then it categorize into a positive, negative, or common class.[4] Consider an example someone brought chair online and posted comment, "Brought chair online but the leather of chair is not very good quality", this type of sentence shows negative sentiment.

Aspect or Feature level:

This type of sentiment classification discusses the identification and extraction of item features from source data. [4] If some customer brought some shirt from E-commerce site and he put review that "color of the shirt is not same ,but quality of cloth is good" for this kind of mix sentiments aspect level will work better as compared to document level or sentiment level.

Natural Language Processing (NLP)

NLP is the set of methodologies and techniques which allows computer to make sense of human speech as it is spoken. Common NLP tasks in machine learning include: sentence segmentation, parts of speech tagging, parsing text results, deep analytics and named entity extraction [1]

Aspect-Based Sentiment Analysis

Aspect-based sentiment analysis is a special type of sentiment analysis, its task is to identify the different aspects of entities in textual reviews and to determine the sentiments associated with these aspects [2]. Aspect-based sentiment analysis involves predicting the aspects of a predefined object and the associated sentiments like positive or negative assigned to each aspect in a certain context .[2] Aspect Level Sentiment Analysis aims to notify the shortcomings of document and sentence levels of Sentiment Analysis.

IV. MACHINE LEARNING

Machine learning field is a subfield from the broad field of artificial intelligence, this aims to make machines able to learn like human. Learning here means understood, observe and represent information about some statistical phenomenon.[8] Machine learning techniques in the classification of sentiment depends on the use of well-known machine learning technology on text data. The classification of the sentiment based on machine learning can be categorized primarily into supervised and unsupervised methods of learning [4].

There are various machine learning algorithms can be used to perform sentimental analysis of huge data like Naive Bayes, Support vector machine, and Maximum entropy classifier algorithms using these techniques, a large amount of data can be utilized to get optimized results and helpful for decision-making capability.
Most Frequently used classification Algorithms for Sentiment Analysis are as follows

Naive Bayes:

This method is based on the theorem of Bayes used by increasingly sophisticated classification methods. It is a classification technique. It learns how an entity with certain characteristics belonging to a certain category or class is possible [4] Naïve Bayes is considered as baseline algorithm for research in decision level classification problems. It directly considers the probability of positivity and negativity of the text with respect to that class to which it belongs.[1]

Support vector machine:

A Binary Classifier (BC) is a Support Vector Machine (SVM). On the n-dimensional point, row data is drawn. In this, a hyper plane separating the data sets is drawn. This enhanced separation maximizes the training data margin [4].

KNN:

This technique is used for classification and regression. This is one of the simple machine learning algorithms. It saves the cases and searches most k-neighbours it resembles for new data. It saves the cases. With a testing dataset, KNN makes clear predictions.[4]

K-means Clustering:

It is an unsupervised algorithm for learning to reach the cap. The initial partition is achieved by Euclidean distance for grouping the datasets into clusters.[4]

Random Forest:

It is the category of the supervised algorithm. In a random forest algorithm, i.e. set of many classification trees, is generated by many decision trees taken together. This can be used for both regression and classification. The Decision Tree algorithm has rules for the given training data set with targets and features. [4]

V. CONCLUSION

After studying various research presentenced by different people on sentiment analysis and aspect based sentimental analysis we come to conclude that using sentimental analysis most hectic work for customers and producers can be eased. In this work we have studied various sentimental analysis classifications and technique based on machine learning. One commerce platforms where the reviews can be structured or unstructured provided by user can be categories to make it further useful in future to build good business intelligence.

VI. REFERENCES

[1]. D. Mali, M. Abhyankar, P. Bhavarathi, K. Gaidhar, M.Bangare International Journal of Management and Applied Science, ISSN: 2394-7926 Volume-2, Issue-1, Jan.-2016

[2]. Duc-HongPham, Anh-CuongLe, 2018 International Journal of Approximate Reasoning (2018)

[3]. Duc-Hong Pham , Anh-Cuong Le, 2018, Data & Knowledge Engineering(2018)

[4]. Anvar Shathik J. & Krishna Prasad K. ,2020,International Journal of Applied Engineering and Management Letters (IJAEML), ISSN: 2581-7000, Vol. 4, No. 2, August 2020.

[5]. Wenhao Zhang, Hua Xu , Wei Wan ,2012Expert Systems with Applications 39 (2012)

[6]. Fu Xianghua , Liu Guo, Guo Yanyan, Wang Zhiqiang, ,2013,Knowledge-Based Systems 37 (2013)

[7]. Raktim Kumar Dey, Debabrata Sarddar, Indranil Sarkar, Rajesh Bose, Sandip Roy,2020, International Journal Of Scientific & Technology Research Volume 9, Issue 05, May 2020 ISSN 2277-8616

[8]. W.A. Awad and S.M. ELseuofi, 2011, International Journal of Computer Science & Information Technology (IJCSIT), Vol 3, No 1, Feb 2011

[9]. Hemamalini, Dr.S. Perumal, 2020, International Journal Of Scientific & Technology Research Volume 9 ,Issue 04, April 2020 ISSN 2277-8616

International Virtual Conference on Materials and Nanotechnology
In Association with International Journal of Scientific Research in Science and Technology
Volume 9 | Issue 4 | Print ISSN: 2395-6011 | Online ISSN: 2395-602X (www.ijsrst.com)

A Prominent Overlapping of Red Phosphor Emission with the Absorption Spectra of Green Plants Useful for Artificial LED Plant Lighting

P. J. Yadav*[1], N. D. Meshram[2], S. V. Moharil[3]

*[1]Jawaharlal Nehru Aluminium Research Development and Design Centre, Wadi, Amravati road, Nagpur, Maharashtra, India

[2]Shri. Mathuradas Mohota College of Science, Sakkardara Square, Nagpur, Maharashtra, India

[3]Department of Physics, R.T.M. Nagpur University campus, Nagpur, Maharashtra, India

ABSTRACT

Horticultural lighting allows for year-round cultivation of vegetable crops independent of weather conditions or season of the year. Certain living organisms, such as plants and algae, cannot directly process the energy gathered from solar radiation. Instead, it has to be first converted into chemical energy. This process is called photosynthesis and it is one of the oldest, most abundant and perhaps most important biochemical processes on Earth. During photosynthesis, the incident solar energy is converted into chemical energy used for the growth and development of plants.

Artificial light sources were used to grow plants before the invention of incandescent lamp, with some of the earliest reports in the year 1861. The use and usefulness of incandescent lamps in horticultural lighting has been limited. The reasons are the low electrical efficiency, low light emission, unbalanced spectrum (reduced emission in the blue region) and short lifetime.

Conventional light sources cannot be spectrally controlled without the inefficient and limited utilization of additional filters. The LED does not suffer from these limitations. LEDs have emerged as a potentially energy-efficient, viable and promising technology for use in horticultural lighting. The use of LEDs in plant production applications offers completely novel opportunities for optimization of plant growth and development that can be achieved through more versatile and appropriate control of the quantity, periodicity and spectrum of the light provided. This optimization can be tailored to the specific needs of each crop species and their production conditions.

In this paper we reported the red emitting phosphor CaS: $Eu2^{+}$ with good overlapping in the photosynthetic and photo morphogenetic receptors absorption spectra of green plants. It can be a promising candidate for coating on the 410 nm LEDs to get emission in the range 300-400 and 600-700 nm.

Keywords : Horticulture lighting, LEDs, absorption spectra, plant growth.

I. INTRODUCTION

It is well known that light is one of most important influence factors for plant growth because it plays an important role in normal growth and development of plants [1]. The natural rhythms of the plant can be controlled by light because light is acted as rapid and reversible molecular switches. The blue light (400-

500 nm) is responsible for plant bud and the red and deep-red light (620-710 nm) is helpful for plant bud, photosynthesis, phytochromes, and flower [2,3]. Thus, the light in these two bands is called "light fertilizer" for plant growth [4,5]. To meet human needs, the modern greenhouse industry has been developed widely in agriculture and horticulture. The illuminants are used to control the light environment for plant growth (e.g., the intensity and spectral composition). According to the above-mentioned, the designed plant-growth light-emitting diodes (LEDs) have been recognized as the light source and investigated extensively owing to the long lifetime, power-economical, low radiant heat output, and environmental friendly [6,7]. The spectral composition and intensity of phosphor-converted LEDs with the mature preparation techniques are easily tunable by adjusting phosphors and the LEDs are considered to be the most appropriate for plant-growth. Here, the present research is to develop a deep red emitting phosphor for plant growth LEDs. Sulfide based phosphors have been studied for more than 100 years [8]. Most of the prototype luminescent devices used sulfide phosphors though in later developments these have been usually replaced by more suitable luminophors. Sulfide phosphors suffer from the drawback of degradation, but when mixed with epoxy in LED coating they remain consistently luminescent.

II. METHODS AND MATERIAL

Conventionally, host sulfides are prepared by methods like carbothermal reduction. Doping is then done by solid state diffusion under inert/reducing atmosphere at temperatures around 1000° C. We attempted a different approach. In the first step, $CaSO_4$ doped with the desired activators was prepared by Yamashita's method. This was then reduced to sulfide by double crucible method at 850° C temperatures.

III. RESULTS AND DISCUSSION

Figure 1, shows XRD pattern of CaS so prepared. It is seen that the pattern matches excellently with ICDD file. There are some weak lines present corresponding to $CaSO_3$.

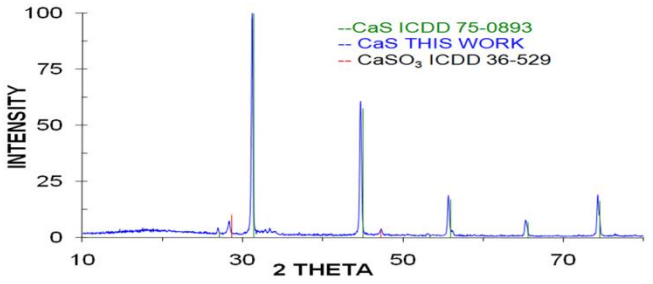

Figure 1: XRD pattern comparison for CaS compound compared with standard ICDD file.

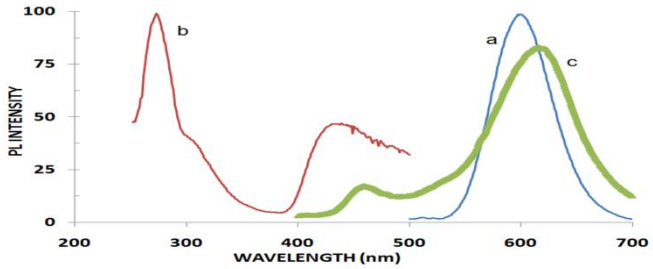

Figure 2: a> PL emission of CaS:Eu for 460 nm excitation, b> PL excitation of CaS:Eu for 605 nm emission, c> LED spectrum for CaS:Eu deposited on blue chip

The PL spectra for Eu^{2+} activator are shown in Figure 2, Eu^{2+} exhibits intense red emission with a maximum at 630 nm, for 460 nm excitation. This originates in transition from the lowest state of $4f^6 5d^1$ configuration to the $^8S_{7/2}$ state of $4f^7$ configuration. It is thus seen that efficient CaS based phosphors can be prepared by the procedure described here. The phosphor can be useful for plant lighting

The phosphor (3 wt %) was dispersed in a transparent silicone resin (Wells Electronic Materials Company, 5012-2A and 5012-2B), and LED was then fabricated by coating the blue LED chip (CREE 458 nm, 300 micron) with the epoxy resin. The electroluminescence (EL) spectra, CIE chromaticity

coordinates, and lumen output at room temperature were measured using a 300 mm integrating sphere and lumen meter (Hangzhou Zhongwei Photoelectricity Company ZVision ZW 3900). The measurements were carried out at 3.2 V, 20 mA. The colour co-ordiates are 0.383, 0.233 and output was 50 lumen/Watt. Emission spectrum is shown in Figure 2, (curve c).

IV. CONCLUSION

From the above results of the PL and EL emission spectra it is clear that the Cas:Eu phosphor is a good candidate to be used as the red emitting candidate in the plant lighting LEDs. As the red band is useful for Chlorophyll b, photo receptors in the green plants, the present study will definitely help to increase the crop plant cultivation.

V. REFERENCES

[1]. Z. Zhou, J. Zheng, R. Shi, N. Zhang, J. Chen, R. Zhang, H. Suo, E.M. Goldys, C. Guo, Ab initio site occupancy and far-red emission of Mn4þ in cubic-phase La(MgTi)1/2O3 for plant cultivation, ACS Appl. Mater. Interfaces 9 (7) (2017) 6177e6185.

[2]. R. Cao, Z. Shi, G. Quan, T. Chen, S. Guo, Z. Hu, P. Liu, Preparation and luminescence properties of Li2MgZrO4:Mn4þ red phosphor for plant growth, J. Lumin. 188 (2017) 577e581.

[3]. J. Xiang, J. Chen, N. Zhang, H. Yao, C. Guo, Far red and near infrared double wavelength emitting phosphor Gd2ZnTiO6:Mn4þ, Yb3þ for plant cultivation LEDs, Dyes Pigments 154 (2018) 257e262.

[4]. X. Huang, H. Guo, Finding a novel highly efficient Mn4þ-activated Ca3La2W2O12 far-red emitting phosphor with excellent responsiveness to phytochrome PFR: towards indoor plant cultivation application, Dyes Pigments 152 (2018) 36e42.

[5]. R.M. Metallo, D.A. Kopsell, C.E. Sams, N.R. Bumgarner, Influence of blue/red vs. white LED light treatments on biomass, shoot morphology, and quality parameters of hydroponically grown kale, Sci. Hortic. 235 (2018) 189e197.

[6]. J.Y. Chen, C.F. Guo, Z. Yang, T. Li, J. Zhao, Li2SrSiO4:Ce3þ, Pr3þ phosphor with blue, red, and near-infrared emissions used for plant growth LED, J. Am.Ceram. Soc. 99 (2016) 218e225.

[7]. A. Agarwal, S.D. Gupta, Impact of light-emitting diodes (LEDs) and its potential on plant growth and development in controlled-environment plant production system, Curr. Biotechnol. 5 (2016) 28e43

[8]. R. P. Rao J.Mat.Sci. 21, 4117 (1986)

International Virtual Conference on Materials and Nanotechnology
In Association with International Journal of Scientific Research in Science and Technology
Volume 9 | Issue 4 | Print ISSN: 2395-6011 | Online ISSN: 2395-602X (www.ijsrst.com)

Study on Optical Properties of CDS Annealed Thin Films by Spray Pyrolysis

Dr. L. M. Shanware[1], Dr. R. S. Meshram[2], Dr. R. M. Thombre[3]
[1]N. S. College, Mulchera, Dist. Gadchiroli, Maharashtra, India
[2]N. H. College, Bramhapuri, Dist. Chandrapur, Maharashtra, India
[3]M. G. Arts & Science College, Armori, Dist .Gadchiroli, Maharashtra, India

ABSTRACT

The CdS shows the direct band gap 2.4 eV and indirect band gap 2.35 eV CdS thin films were deposited by spray pyrolysis technique on glass substrate of different thicknesses. CdS thin films were annealed in air from 1000C about 3 hours.. Rhe XRD reveled that the films were polycrystalline in nature and with hexagonal phase. The crysternality of the films was improved by annealing in air at 1000 C. The optical transmittances, reflectance's and absorption of annealed CdS thin films are studied and found to be different thickness and the refractive index varies from 2.15 to 2.85

Keywords : CdS, Spray pyrolysis, XRD, Optical and thin film

I. INTRODUCTION

Cadmium sulphide belongs to II-VI compound semiconductor materials The spray pyrolysis [1] is one of the most popular techniques At present CdS thin films area widely used as the window material in several CdS based thin films solar cells. CdS[2]and [3]. The chemical prepared CdS[2] films is more ideal window material solar cells. The optical energy band gap is 2.24 to 2.40 eV[4]. Particularly in case of chalcopurite there are several published works on different properties of CdS films prepared by using techniques like sputtering[5];[6]; evaporation Shibata [7]:[8] electrolilytic deposition [9]. But the films prepared by using spray paralysis are quite few in number [10]. In the present work, optical properties of CdS thin films annealed and unannealed of various thicknesses is studied.

II. EXPERIMENTAL DETAILS

The CdS films were deposited by spray pyrolysis on heated glass substrage by spraying an aqeous solution of cadmium chlroried (0.01 M) and thiourea (0.01M) in 1:1 ratio 1) [11] on microscopic cleaned glass substrate maintained By using the spray nozzle, adjusting the airflow rate and the required temperature could be achieved by supplying suitable power through variac, the thin films are prepared. The thickness of films was determined by weighing method. The annealing of the sample was carried out in air for about 3 hours at 1000C.

The absorption and transmission spectra of annealed samples were recorded using Elico SL 159 UV-VIS spectrophotometer. The XRD patterns of annealed and unannealed CdS thin films were recorded with Phillips X-ray diffractometer.

III. RESULT & DISCUSSION

The CdS films were deposit using pyrolysis method containing various thickness. The film deposited by eqimolar concentration of cadmium chloride and thiourea found to have uniformity and adhesion characteristic and the film thickness depends on amount of solutions sprayed.

The films fabricated at low temperature have low transmission and those prepared at higher temp have higher transmission as shown in fig. (4). It can be observed that in increase in substrate temp. Improve the transmission. This improvement can be attribute to either the decrease in thickness or the improvement in the perfection and stoichemetry of the film. The semiconductor band gap Eg was determined by analysis the optical
data with the expression for the optical absorption and photon energy his using relation

$$\alpha = \frac{A}{h\nu}(h\nu - Eg)^{1/2} \quad \ldots\ldots\ldots\ldots\ldots\ldots(1)$$

where A is constant , ν is incident photon energy, h is the Plank's constant and Eg is band gap.

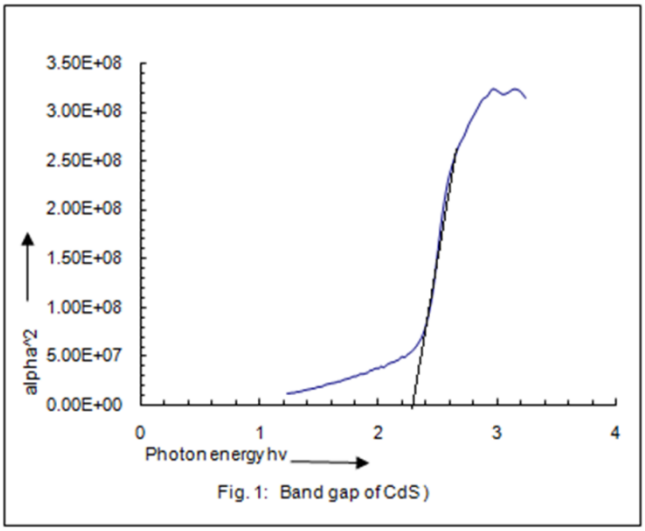

Fig. 1: Band gap of CdS)

A plot of $(\alpha h\nu)^2$ Vs $(h\nu)$ in shown in fig. (1) for different thickness gives fairly good straight line. The band gap Eg was 2.54 eV. This is fairly good agreement with Chavhan(20040[13].

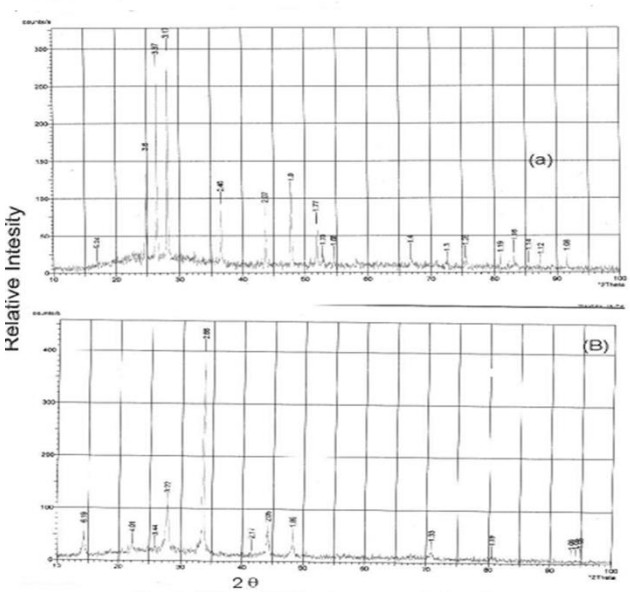

Fig. 2: XRD of CdS a) auannealed and b) annealed

Fig. (2) shows XRD, XRD was used to confirm the crystal structure of CdS thin film annealed for about 3 hours in air

IV. CONCLUSION

Optical and structural properties of films were studied as a function of substrate tempreture, molarity of solution and thickness. The range of band gap is 2.35 – 2.4 eV. The CdS thin film prepared by pyrolisis have good adherence and thickness uniformityafter annealed. The film is polycrystalline in nature The crystanality incases with annealing[23] of CdS thin film. From this study it in clear that film have good optical and physical qualities. Hence these films are best suited for solar cell applications.

V. REFERENCES

[1]. Chamberlin RR and Skaraman J.S. J. Electrochemical Society 86,133(1966)

[2]. Basal BM, Kapur VK and Halani A 1991 Cong. Records of 22nd photovoltaic specialist conference. Las Vegas, NV, USA P 893.

[3]. AritaT, HAnafusa H, Kitamura S and Takakura H 1991 conf. Records of 22nd Photovoltaic

Specialist conference. Las Vegas, NV, USA, P. 946 (1991)

[4]. Volyommana A.G. Nethew S. Vijarkumar K.P. & Purushottam C. 13 all. Mater . Sci. 16,55(1993)

[5]. Takeuchi M, Sakagawa Y and Nagasaka H Thin solld films 33, 89 (1976)

[6]. Clarke J.R. and green JE J, Vac sci. & Technol. 18, 382 (1981)

[7]. Shibata H. J. Vac. Soc Japan 20, 358 (1977)

[8]. Bhide VG, Jatar S and Rastogi AG Prama – J. Phy 10,477 (1978)

[9]. Krupa R and Wrzesinka A Acta Physics Pol A-53,67 (1978)

[10]. Gupta B.K. Agnihotri, OP and Ahmar Raja Thin solid film 48,153 (1978)

[11]. Vijaykumar KP Bull. Mater. Sci 14, 57 (1991)

[12]. Chandra S. Photoelectrical solarcell, Newyork Vol 5 (1985)

[13]. Chavhan S.D., Bagul SV, Patil AR, Sharma RP Indian J. Engineering and Mater. Sci. 11,130(2004)

[14]. Valyomenana A.G. Vijarkumar K.P. and Purushottam C J. mater Sci letter 9, 1025 (1990)

[15]. Narayana K.L, Vijaykumar Kp, Nair KGM & Rao CV, Bull mater. Sci 20, 287 (1997)

[16]. Kale S.S. Jadhav US. & Lokhande CD. Indian J. Pure & Appl. Phys 34, 324 (1996)

[17]. Mane R.S. & Lokhande C.D. Mater chem.. Phys 1 ,65 (2000)

[18]. S.D. Chavhan S.V. Bagul, AR Patic & R.P. Sharma Indian J. of Engg. & Mater. Sci 11, 130 (2004)

[19]. P.P. Karve, A.K. Khasbag. S.P.Kolhe As Nigwekar & S.K. Kulkarni a. Indian J. Pure & App. Phys 23, 174 (1985)

[20]. M.D. Uplane & S.H. Pawar Solid State Commun, 46, 947(1993)

[21]. Su B and Choy KL, Thin Solid film 160,359 (2000)

[22]. A. Ashour Turk J. Phys 27, 551(2003)

[23]. K.Senthil Applied Surface Science Volumes 169–170, 15 January 2001, Pages 476-479

International Virtual Conference on Materials and Nanotechnology
In Association with International Journal of Scientific Research in Science and Technology
Volume 9 | Issue 4 | Print ISSN: 2395-6011 | Online ISSN: 2395-602X (www.ijsrst.com)

A Review on Mn_3O_4 and Its Composite Nano materials of Different Morphologies as an Electrode Material in Super capacitors

Tanaji S. Patil[1], Satish A. Gangawane[2], Mansing Takale[3]

[1]Bhogawati Mahavidyalaya, Kurukali, Tal – Karveer, Dist. – Kolhapur, Maharashtra, India

[2]Dhoodhsakhar Mahavidyalaya, Bidri, Tal – Kagal, Dist. – Kolhapur, Maharashtra, India

[3]Department of Physics, Shivaji University, Kolhapur, Maharashtra, India

ABSTRACT

Mn3O4 and its composite nanomaterials have become promising candidate as an electrode for supercapacitor devices, because of its low cost, non-toxicity, large abundance, high porosity and high capacitance values in aqueous electrolyte. Here, we systematically summarized the impact of different morphologies of Mn3O4 and its composite nanomaterials on supercapacitive performance. Different researchers synthesized various Mn3O4 and its composite nanomaterials of exceptional properties and different morphologies for energy storage. This article reviews recent efforts and developments in synthesis methods Mn3O4 and its composite nanomaterials as an electrode material in supercapacitors.

I. INTRODUCTION

Due to vital scientific significance and wide applications arises because of their tunable properties, nanomaterials having at least one dimension is less than 100 nm, have attracted great attention of many researchers. In addition, nanomaterials have phase, size and morphology dependent physical and chemical properties and applications; therefore, many efforts made to govern the phase, shape, size and morphologies of nanomaterials. The nanomaterials can be synthesized using variety of reagents and tactics with extensive range of reaction circumstances [1]. The electrodes of nanomaterials Manganese oxide have enormous applications in electrochemistry, due to their exceptional electrochemical properties such as high capacitance, huge surface area, and small current densities [2]. Water purification, catalysis, sensors, supercapacitors, and alkaline and rechargeable batteries were some fascinating applications of Manganese oxide having different phases such as MnO, MnO_2, and Mn_3O_4, and their composite materials. Particularly, the Mn_3O_4 electrode replaced the toxic RuO_2 electrode in electrochemical charge storage devices due to the its parameters like low cost, non-toxicity, large abundance, high porosity and high capacitance values in aqueous electrolyte [3]. The proper dopant can perturb the growth process of the Mn_3O_4 electrode, during chemical reaction and it can modify the morphology of nanostructure. So selecting proper dopant, there is possibility to change morphology of Mn_3O_4 nanostructured electrode. [4]. There are numerous synthesis techniques have been reported by various researchers to prepare Manganese oxide nanomaterials of several morphologies and distinct

properties, such as Electrodeposition, Sol-gel, Hydrothermal, Chemical bath deposition, SILAR, Spray pyrolysis etc. [5]. In last decade, many efforts executed to inspect the different properties and applications of Mn_3O_4 nanostructured electrode, for example, Y. Kong et al. reported the synthesis of octahedron-like Mn_3O_4 nanocrystals by single-step hydrothermal reduction method and reported that it is the most promising element in assemble lithium-ion batteries [6]. X. Zhang et al successfully synthesized Mn_3O_4 nanowires of diameter 15 nm and a length of the order of several micrometers hydrothermally, without any use of surfactants [7]. H. Shah and coworkers prepared square-shaped nanostructures by hydrothermal-growth method and reported that it has potential applications in supercapacitors and Li ion batteries [8]. Thus, to keep the readers up-to-date of the rapid development, it is essential to review the advancement of Mn_3O_4 nanomaterials. In this article, we review the different Mn_3O_4 nanomaterials of various morphologies and their supercapacitive application.

II. SYNTHESIS OF MN_3O_4 NANOMATERIALS

At room temperature, Mn_3O_4 has a tetragonal structure and due to Jahn–Teller distortion along c axis at the Mn^{3+} sites, it has a distorted spinel structure. Manganese ions lodge the octahedral site (Mn^{3+}) and tetrahedral site (Mn^{2+}) corresponds to a normal spinel structure. There are 32 oxygens and 24 cations in the unit cell. Generally, the ionic formula of Mn_3O_4 is Mn^{2+} [Mn_2^{3+}] O_4. At 33 K, the chemical and magnetic unit cells become identical with rearrangement of moments and it is ferromagnetic up to 43 K. Therefore, its study gains importance as it has wide applications [9].

A. Ullah et al. via a gel formation route reduced the $KMnO_4$ with glycerol at 80 °C in aqueous media to synthesize Mn_3O_4 nanoparticles. They observed temperature dependent phase transformation of Mn_3O_4 into Mn_5O_8 and Mn_2O_3 with distinct surface morphologies viz., spherical, rod and cube shape respectively through heat treatment [10]. Using the precipitation method, in presence of CTAB, H. Dhaouadi et al. synthesized Mn_3O_4 nanoparticles of tetragonal structure with crystallite size ranges from 20 nm to 80 nm. They observed that temperature dependence of dielectric properties of Mn_3O_4 nanoparticles at higher frequency [11]. Y. Tan successfully fabricated 1D single-crystalline Mn_3O_4 nanostructures under solvothermal conditions. They easily tuned the diameter and length of nanostructures by altering the concentration of the precursor [12]. W. Wang did decomposition the precursor $MnCO_3$ nanoparticles in NaCl flux to synthesize nanowires of Mn_3O_4 with diameters 30 -60 nm [13]. Using co-precipitation, sol-gel and hydrothermal methods, B. Jhansi Rani et al synthesized different nanostructures of Hausmannite (Mn3O4) plate like nano-grains, coin like nano-sphere and nano-petals and they studied the structural, morphological, optical, electrochemical and magnetic properties of nanostructured materials [14]. A. U. Ubale et al employed simple and economic SILAR method for deposit nanostructured thin films on glass surface at room temperature [15]. Using $MnCl_2 \cdot 4H_2O$ and KOH precursors, A.M. Toufiq and coworkers grown self-assembled 3D coins-like nanostructures having single-crystalline tetragonal Mn_3O_4 nanoparticles of average diameter 95 nm and thickness 35 nm [16]. H. K. Yang et al. to fabricated homogeneous micro-spherical particles having porous structure of Mn_3O_4 carbon composite material using ultrasonic spray pyrolysis technique with the help of surfactants TX 114, P123, F127. They elaborated particles of smaller size and high surface area using TX 114 surfactant with active bi-functional catalyst [17]. H. L. Fei and coworkers explained the synthesis of microflowers of Mn_3O_4 made up of super thin nano sheets by solvothermal method using CTABr surfactant. They reported the morphology dependence of Mn_3O_4 on solvent [18]. Low

temperature chemical bath deposition technique was used to prepare Mn_3O_4 thin films of smooth surface made up of the crystalline nanograins by H. Y. Xu.et al [19]. J. K. Sharma et al. reported the low budget green synthesis, using the reducing agent, a leaf extract of A. Indica (Neem) plant, synthesize uniform Mn_3O_4 nanoparticles for chemical sensor application [20].

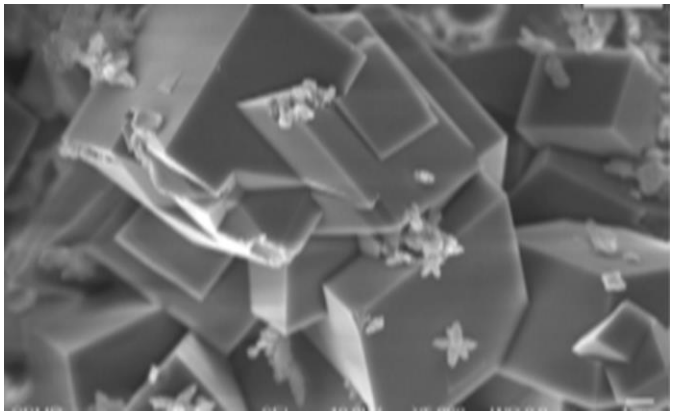

The SEM images of Mn_3O_4 thin film at (a) ×2000 and (b) ×5000 magnifications (interlocked cubes) [21]

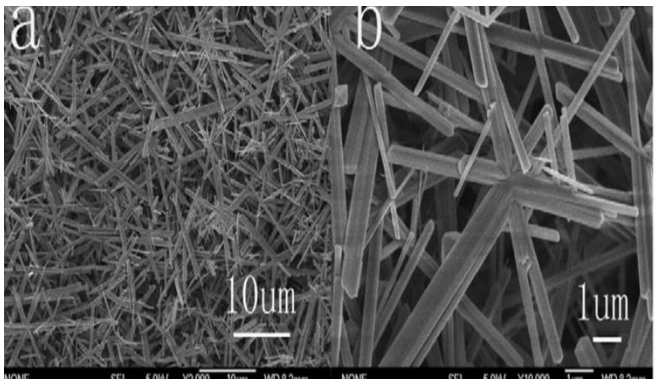

Low (a) and (b) high magnification FESEM images of Mn3O4 nanorods [22].

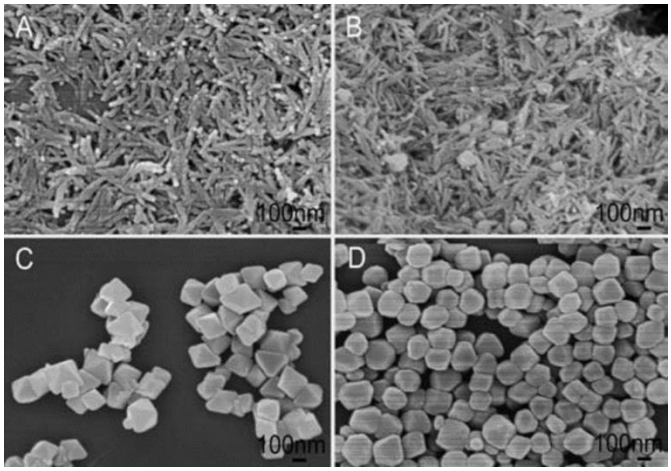

FESEM images of the Mn_3O_4 nano-octahedrons for various reaction times: (A) 1.5 h; (B) 2 h; (C) 3 h; (D) 8 h [33].

III. THE MN_3O_4 NANOMATERIALS FOR SUPER CAPACITOR APPLICATION

Super capacitors have the ability to charge and discharge quickly, high power density and outstanding cyclic stability, but their small energy density dragged them back in several such applications. Depending on mechanisms, that governing capacitance the super capacitors are classified into two types. First type is electrical double layer capacitor (EDLC) in which double layer of charges at the interface of electrode and electrolyte is responsible for capacitance and in second type pseudo or redox capacitor where capacitance arises due to oxidation-reduction reactions. Researchers are trying to search many novel materials and processes to improve energy density values by manufacturing new electrode materials, electrolytes and device designing [23]. Among many metal oxides, Mn_3O_4 and its composites have attracted more attentions due its large advantageous parameters and special properties.

Y. Luo and coworkers synthesized interlocked Mn_3O_4 cubes by mixing 1.9791g $MnCl_2$.$4H_2O$ and ethyl alcohol with constant stirring for 30 min. at room temperature. Then they dried the solution in an oven at 100 °C for eight hours with final calcination at 500 °C for two hours. They observed that it could be a promising candidate as electrode material for super capacitors showing excellent specific capacitance in terms of fast charge–discharge rate, high specific power and long life span [24]. Microwave-assisted reflux synthesis method used by K. V. Sankar Mn_3O_4 nanoparticles of size 50 nm having tetragonal structure. Low internal resistance, high capacitance (94 F g^{-1}) in 6M KOH with long stability reveals Mn_3O_4 electrode is suitable for supercapacitor application [25]. J.W. Lee Mn_3O_4 nanorods of 100 nm

to one μm length dispersed on graphene sheets using ethylene glycol as a reducing agent by simple template-free hydrothermal reaction of $KMnO_4$. The composite of Graphene/Mn_3O_4 showed better supercapacitive performance than free Mn_3O_4 nanorods [26]. D. Li et al. employed one-step hydrothermal method for synthesize Mn_3O_4 nanorods on Ni foam using aqueous solutions of Mn $(NO_3)_2$ and $C_6H_{12}N_4$. Due to porous Ni foam fast charge transfer takes place, high surface area and conductivity, this composite has shown better supercapacitor performance [27]. R. Aswathy anchored the surface of oxidized graphite paper by Mn3O4 nanoparticles using hydrothermal method. They calculated the high specific capacitance value 471Fg^{-1} at 1 mA cm^{-2} current density in 1 M Na_2SO_4 solution [28]. By heavily distributing, the Mn_3O_4 particles of size 10 nm graphene nanosheets, B. Wang et al. observed that the functional groups of Mn_3O_4 attached to the nanosheet and increased surface area plays a key role in improving the electrochemical performance. A specific capacitance value for these Mn_3O_4/graphene nanocomposites was 256 F g^{-1} that was almost double that of the pure graphene nanosheets [29].

H. U. Shah and coworkers have successfully synthesized exceptional spongy Mn3O4 nanoparticles, through hydrothermal method. They observed high specific capacitance value 380 Fg^{-1}, which is quite larger than previously synthesized Mn_3O_4 nanoparticles. [30]. H. Jiang fabricated octahedron of Mn_3O_4 of base length 160 nm with smooth surface by a simple EDTA-2Na assisted hydrothermal method, and he reported that it shows excellent electrochemical performance [31]. Doping with different transition-metal ions, size controlled synthesis of Mn_3O_4 octahedrons were synthesized by R. Dong et al. and reported improvement in the capacitive properties Mn_3O_4 by doping transition metals signifying a doping effect for the growth and electrochemical performance [32].

List of pure and composite materials based on Mn3O4 reported recently.

Sr. No.	Compound	Method	Morphology	Electrolyte	Specific Capacitance Fg^{-1}	Ref.
1.	Pure	Hydrothermal	Nanoparticles	0.5 M Li_2SO_4	198	33
2.	Graphene/Mn_3O_4	CBD	Nanoparticles	1 M Na_2SO_4	193	34
3.	Graphene/Mn_3O_4	Hydrothermal	Nano rods	1 M Na_2SO_4	121	26
4.	Pure	chemical precipitation	Nanoparticles	1 M Na_2SO_4	322	35
5.	Pure	CBD	Thin film	1 M Na_2SO_4	321	36
6.	Pure	Hydrothermal	Nano octahedron	1 M Na_2SO_4	153	37
7.	Ni-Mn_3O_4	Chemical oxidation	Nano composite	0.5 M Na_2SO_4	230	38
8.	Mn_3O_4/multi-walled carbon nanotube	CBD	Nano composite	1 M Na_2SO_4	257	39
9.	Graphene/Mn_3O_4	Arc discharge	Nano composite	1 M Na_2SO_4	38	40
10.	rGO–Mn_3O_4	microwave hydrothermal	Nano composite	1 M Na_2SO_4	153	41
11	rGO-Mn3O4	Electrodeposition	Nano composite	1 M Na_2SO_4	364	42
12	Pure	Electrodeposition	Nanostructure	3 M Na_2SO_4	210	43

13	Pure	Hydrothermal	Square-shaped nanostructures	1 M KOH	355.5	8
14	Mn3O4-Activated Carbon	Sonication-assisted mechanical-stirring method	Nano composite	1 M Li_2SO_4	106	44
15	Cr- Mn_3O_4	Hydrothermal	Nanocrystal	1 M Na_2SO_4	272	32
16	Pure	SILAR	Thin film	1 M Na_2SO_4	314	45
17	Pure	Hydrothermal	Nano sheet	1 M Na_2SO_4	1014	46
18	Pure	Hydrothermal	Nano octahedron	1 M Na_2SO_4	322	31
19	Mn3O4/rGO	Solution thermal decomposition	Nano sheet	0.1 M Na_2SO_4	342	47
20	Ni-Mn3O4	Spray pyrolysis	Thin film	1 M Na_2SO_4	705	48
21	Co - Mn3O4	Co-precipitation	Nano granules	6 M KOH	2701	49
22	Pure	Spray pyrolysis	Nanoparticles	1 M Na_2SO_4	187	50
23	RuO2-Mn3O4	Electrospinning	nanofiber	1 M Na_2SO_4	293	51
24	Pure	spray pyrolysis	Thin film	1M Na2SO4	394	52
25	Pure	Ultrasonic irradiation assisted co precipitation	Nanoparticles	1M Na2SO4	296	53
26	Pure	Hydrothermal	Nanoparticles	1M Na2SO4	435	54
27	Mn_2O_3 and Mn_3O_4	co precipitation	Nanoparticles	1M H_2SO_4	305	55
28	Mn_3O_4- CNT	chemical reflux method	Nanoparticles	PVP: Na_2SO_4	499	56
29	Mn_3O_4-$Li_4Mn_5O_{12}$	Electrochemical deposition	Nanofibers	Li_2SO_4	527	57
30	Mn_3O_4@carbon Foam	Hydrothermal	Nanoparticles	1M Na2SO4	212.8	58

IV. CONCLUSION

In summary, we have reviewed recent development of Mn3O4 nanomaterials. We discussed about simple and effective methods to synthesize Mn3O4 nanomaterials of high surface area, unique morphologies and showing outstanding supercapacitive performance. In short, we expect that this paper will not only show the recent advances in Mn3O4 nanomaterials but also give the readers some motivation to discover novel techniques for the synthesis of Mn3O4 nanomaterials of excellent supercapacitive properties.

V. REFERENCES

[1]. X. Liu et al, Journal of Nanomaterials, Volume 2013, Article ID 736375.

[2]. K. Zhang et al, Chemical Society Reviews, CS-REV-06-2014-000218.R1.

[3]. W.Wei et al, Chem. Soc. Rev., 2011, 40, 1697–1721.

[4]. Z. sun et al, Sci China Mater 2017, 60(1): 1–24.

[5]. A. Sukhdev et al, Heliyon 6 (2020) e03245.
[6]. Y. Kong et al, Nanomaterials 2020, 10, 367.
[7]. X. Zhang et al, CrystEngComm, 2012, 14, 1485.
[8]. H. U. Shah et al, Int. J. Electrochem. Sci., 11 (2016) 8155 – 8162.
[9]. T. Ahmad et al, J. Mater. Chem.,2004, 14 3406 - 3410.
[10]. A. Ullah et al, Journal of Saudi Chemical Society (2017).
[11]. H. Dhaouadi et al, ISRN Spectroscopy, Volume 2012, Article ID 706398.
[12]. Y. Tan et al, Chem. Commun., 2011, 47, 1172–1174.
[13]. W. Wang et al, Crystal Growth & Design, 2008 Vol. 8, No. 1, 358–362.
[14]. B. Jhansi Rani et al, Surfaces and Interfaces, 2018.
[15]. A. Ubale et al, Materials Chemistry and Physics 136 (2012) 1067 – 1072.
[16]. A. M. Toufiq et al, Mater. Express, 2014, Vol. 4, No. 3.
[17]. H.K. Yang et al,, Nanomaterials 2016, 6, 203.
[18]. H. L. Fei et al, JMSRR, 1(1): 1-10, 2018; Article no. JMSRR.43347.
[19]. H. Y. Xu et al, Applied Surface Science 252, (2006) 4091–4096.
[20]. J. K. Sharma et al, Journal of Colloid and Interface Science (2016).
[21]. D. P. Dubal et al, Journal of Alloys and Compounds 484 (2009) 218–221.
[22]. J. Du et al, Nanotechnology, 17 (2006) 4923–4928.
[23]. Z. Yu et al, Energy Environ. Sci., 2015, 8, 702.
[24]. Y. Luo et al, Materials Letters, 178(2016), 171–174.
[25]. K. V. sankar et al, J Appl. Electrochem (2012) 42:463–470.
[26]. J. W. Lee et al, Chem. Mater. 2012, 24, 1158–1164.
[27]. D. Lee et al, Nanoscale Research Letters 2013, 8:535.
[28]. R. Aswathy et al, Journal of Alloys and Compounds, 2018.
[29]. B. Wang et al, Electrochimica Acta 55 (2010) 6812–6817.
[30]. H. U. Shah et al, J. Nanosci. Nanotechnol., 2018, Vol. 18, No. 1.
[31]. H. Jiang et al, Nanoscale, 2010, 2, 2195–2198.
[32]. R. Dong et al, ACS Appl. Mater. Interfaces 2013, 5, 9508–9516.
[33]. D.P. Shaik et.al, Materials Today: Proceedings 3, 2016, 64 – 73.
[34]. Qu Jiangying et al, Nanoscale, RSC publishing, 2013.
[35]. B.G.S. Raj et al, Journal of Alloys and Compounds, 2015.
[36]. D.P. Dubal et al, Journal of Alloys and Compounds 497 (2010) 166–170.
[37]. Y. Xing et al, Mater Sci: Mater Electron, 2017.
[38]. G-r. Xu et al, Journal of Alloys and Compounds 2015.
[39]. K. Jang et al, Bull. Korean Chem. Soc. 2014, Vol. 35, No. 10.
[40]. M. Zhu et al, Advanced Composites Letters, 2017, Vol. 26, Iss.1.
[41]. Li Li et al, Electrochimica Acta, 2013, 87801-808.
[42]. M. Aghazadeh et al, Anal. Bioanal. Electrochem., Vol. 10, No. 8, 2018, 961-973.
[43]. Zhenjun Qi et al, Nano-Micro Lett., 2015.
[44]. Chaofeng Liu et al, Nano Research 2015, 8(10): 3372–3383.
[45]. D.P. Dubal et al, Journal of Electroanalytical Chemistry 647 (2010) 60–65.
[46]. P. A. Shinde et al, International Journal of Engineering Research and Technology, 2017, ISSN 0974-3154 Volume 10, Number 1.
[47]. Y. Zhou et al, Materials 2018, 11, 881.
[48]. A.G. Naiknaware, Journal of Alloys and Compounds, 2018.
[49]. Tian et al. Nanoscale Research Letters, 2017 12:214.
[50]. S. Kulkarni et al, Electrochimica Acta 231, 2017, 460–467.

[51]. Doo-Young Youn et al, Journal of The Electrochemical Society, 158 (8) A970-A975, 2011.
[52]. Abhijit A.Yadav et al, Electrochimica Acta, 2016.
[53]. R. Tholkappiyan et al, Journal of Taibah University for Science, 2018.
[54]. Dadamiah PMD Shaik et al, Ceramics International, 2018.
[55]. M. S. Yadav et al, Journal of Energy Storage, 2020.
[56]. R. Ranjithkumar et al, Superlattices and Microstructures, 2020.
[57]. Nan Zhao et al, Nano Energy, 2020.
[58]. Y. Zhu et al, Energy Fuels, 2020.

International Virtual Conference on Materials and Nanotechnology
In Association with International Journal of Scientific Research in Science and Technology
Volume 9 | Issue 4 | Print ISSN: 2395-6011 | Online ISSN: 2395-602X (www.ijsrst.com)

Low Temperature Photoluminescence Analysis of CDS Nano Crystals

Nilesh Pote
Department of Physics, K. J. Somaiya College, Kopargaon, Maharashtra, India

ABSTRACT

Spherical CdS Nano crystals of 4.8 nm diameter are synthesized by colloidal synthesis. Their structural, optical and electrical properties are studied. By photoluminescence measurements photoluminescence quantum yield of Nano crystals found about 10%. From low temperature photoluminescence measurements band edge energy level was attributed to transitions of ground state energy levels 1S3/2 → 1S. Low temperature analysis of band edge peak and defect peak shows increase in HOMO-LUMO gap with decreasing temperature. Also at low temperature there is reduction in thermal line broadening of energy levels with decreasing surface trap states.

Keywords : Nano crystals, CdS Nano crystals, Energy levels, Low temperature energy evolution.

I. INTRODUCTION

In semiconductor nanocrystals (NCs), quantum confinement effects observed when one or more dimensions of the NCs approach the size of bulk Bohr exaction radius (a_B) given by equation.1 [1]:

$$a_B = \frac{4\pi\epsilon_\infty \hbar^2}{m_0 e^2}\left(\frac{1}{m_e^*} + \frac{1}{m_h^*}\right)$$

----- (1)

Here, ε_∞ is the high frequency relative dielectric constant of the medium, m_e^* and m_h^* are effective masses of the electron and hole, respectively (both in units of m_0), and m_0 is rest mass of the electron. For CdS NCs exciton Bohr radius is 2.92nm. Quantum confinement effect can be understood by considering a relationship between free and confined particles [2,3]. For a free particle in a periodic potential the energy and the crystal momentum 'ħk' may both be precisely defined, while the position is not. When the radius of a particle approaches the size of the Bohr exaction radius, electrons and hole is confined. Thus in case of confined particles (localized) the uncertainty in position decreases, so that momentum is no longer well defined. The wider range of momentum translates to a higher average energy. As a result the electron of a confined particle has higher energy compared to that in a bulk solid. Due to the spatial confinement of the charge carriers, the valence and conduction bands split into discrete, quantized, electronic energy levels. The spacing of the electronic energy levels and the band gap increases with decreasing particle size. This is because the electron hole pairs are now much closer together and the Coulomb interaction between them can no longer be neglected giving overall higher kinetic energy. The increase in band gap can be observed experimentally by the blue-shift in the absorption spectrum. Sometimes, even visually one can observe change in colour of sample with size of

NCs. Theoretical models, such as the effective mass approximation (EMA) [4,5], empirical tight-binding method (ETBM)[6,7], effective bond orbital model (EBOM)[8] and empirical pseudo-potential method (EPM)[9-11] have been proposed to explain quantum size effects.

The simplest model to explain quantum size effects is EMA. As a first approximation the masses of the electron and hole are taken to be the effective masses of electron and hole in the bulk semiconductor. According to EMA, the quantum-size effects can be described by a "particle in a box" model, in which the electron motion is restricted in all three dimensions by impenetrable walls [12-14]. An exciton (electron-hole pair) created by absorption of photon is considered as particle in a rigid sphere of radius R. This model was first developed by Efros *et al.* [12] using an infinite potential well and excluding coulomb interaction. Brus *et al.* [14] included the coulomb interactions and in addition considered the effect of the matrix's dielectric constant on exciton binding energies. In EMA, the valence band and the conduction band are taken to be parabolic at their extrema, i.e. near k = 0. The E-k curves are parabolic (of the form $E = \hbar^2k^2/2m$). But ask increases, the shape of the E-k curve becomes complex and depends on the direction of electron transport with respect to the principal crystal directions. Away from k = 0, E-k curve, can still be described by a parabolic relation $E = \hbar^2k^2/2m^*$ where m is replaced by m*. Here m* is the effective mass of the electron given by,

$$m^* = \frac{\hbar^2}{\frac{\partial^2 E}{\partial k^2}} \quad \text{-----(2)}$$

Eigen value of the lowest excited state is given by [14],

$$E(R) = E_g + \frac{\hbar^2}{2}\left(\frac{1}{m_e^*} + \frac{1}{m_h^*}\right)\frac{\pi^2}{R^2} - 1.786\frac{e^2}{\epsilon R} - 0.248E_{Ry}^* \quad \text{----- (3)}$$

Where, R is the cluster radius and E_{Ry}^* is the effective Rydberg energy given by,

$$E_{Ry}^* = \frac{e^4}{2\varepsilon^2\hbar^2\left(\frac{1}{m_e}+\frac{1}{m_h}\right)} \quad \text{----- (4)}$$

The first term in eigenvalue equation, represents the band gap of the bulk semiconductor. The second term represents a particle in a box type eigenvalue and has $1/R^2$ dependence, which is the increase in the kinetic energy due to the localization of the exciton in the rigid sphere. The third term is the Coulomb energy term with 1/R dependence. It comes into picture because the electron and hole interact via Coulomb attraction. The last term is a result of the spatial correlation effect and gives a measure of the correlation between electron and hole. Equation 5 represents the last term in which energy is inversely proportional to square of the permittivity of material hence become significant for semiconductors with small dielectric constant and this term is independent of size of a NCs. In the early time, Ekimov *et al.* [10] reported the absorption spectra of CdS NCs ranging in size from 30 to 800 Å. The optical absorption spectra of NCs have revealed that exciton energies are blue shifted compared to the value in bulk materials, and it can be understood in terms of quantum confinement of the exciton. Wang *et al.* [11] have experimentally investigated the dependence of the lowest exciton energy of CdS NCs on the cluster size.

In the present work CdS NCs with sizes 4.8 nm were synthesized with oleic acid capping agent.. The synthesized nanocrystals were highly crystalline. Size and energy gap of nanocrystals calculated by absorption spectroscopy. Quantum efficiency measurements performed using photoluminescence excitation spectroscopy which shows that CdS nanocrystals have quantum yield of 10 %. The study of low temperature photoluminescence was performed on CdS NCs from room temperature to 10 K.

II. EXPERIMENTAL SECTION

2.1. Chemicals:

Cadmium oxide (99.99%), sulphur powder (99.98%) was purchased from Aldrich. Oleic acid (OA, tech. 90%), 1-octadecene (ODE, tech. 90%) (ACS,

98.0101.0%). All organic solvents were purchased from EM Sciences. All chemicals were used directly without any further purification unless otherwise stated

2.2. Synthesis Procedure:

Synthesis of CdS NCs performed by reported method with slight modification [15]. Briefly a mixture of CdO (0.0256 g, 0.2 mmol), oleic acid (0.3 mL), and octadecene [ODE (6 g)] was heated to 260 ^{0}C in a three-neck round-bottom reaction flask under argon. When the solution turned clear, 1 mL of sulfur solution (0.1 mol/l) in ODE was swiftly injected into this hot solution, and the reaction mixture was allowed to cool down to 240 ^{0}C for 5 minutes. The reaction was stopped and cooled down to 50 ^{0}C when the CdS core reached a desired size. An in situ purification procedure was performed as described below. An excess of methanol (~10 mL), an extraction solvent, was added to the flask with stirring at 50 ^{0}C. When ODE layer and methanol layer were separated, the upper methanol layer was taken by syringe to remove un-reacted precursors and side products. The purification procedure was repeated three times. Linear optical absorption studies were performed using Perkin Elmer Lambda 950 spectrophotometer to estimate the gap between the highest occupied molecular orbital (HOMO) and the lowest unoccupied molecular orbital (LUMO). Photoluminescence measurements were carried out with Jobin-Yvon PL spectrometer.

III. RESULT AND DISCUSSION

In order to obtain CdS NCs, oleic acid (OA) which acts as a capping ligand concentration is taken to 0.3 mL keeping all other reaction parameters same during synthesis. It is observed that the amount of OA determines the size of CdS NCs. Optical absorption measurements are used to estimate NC size with the aid of empirical formula [15, 16],

$$D = (-6.6521 \times 10^{-8})\lambda^3 + (1.9557 \times 10^{-4})\lambda^2 - (9.2352 \times 10^{-2})\lambda + 13.29 \quad \text{----(5)}$$

In the above equations, D (nm) is the size of a given nanocrystal sample, and λ (nm) is the wavelength of the first excitonic absorption peak of the corresponding sample. Using value of λ, which is 416 nm, size of nanocrystals 4.8 nm was estimated and room temperature absorption and photoluminescence spectra are shown in figure 1. The narrow absorption features of CdS NCs in absorption spectra near bandedge indicate focusing of size distribution of the particles in sample. Photoluminescence spectra clearly show bandedge peak at 420 nm and defect peak at 560 nm.

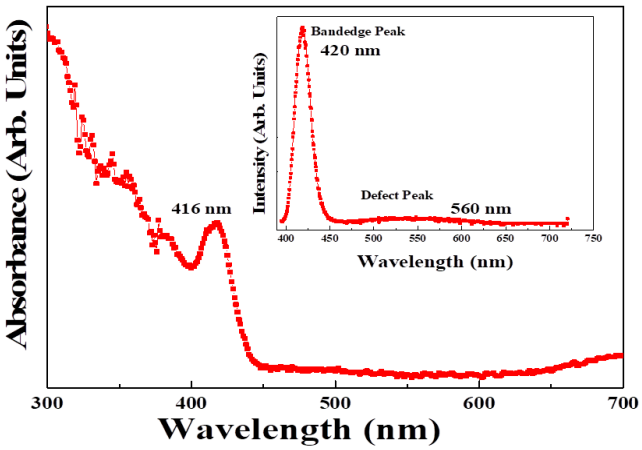

Fig.1 Absorption and photoluminescence spectra (Inset) of CdS nanocrystals having sizes CdS (2.3nm) radius.

Photoluminescence (PL) emission spectra of CdS nanocrystals depicted in figure 1 recorded at excitation wavelength of 375 nm at room temperature. Photoluminescence efficiency (QE) is also measured found to around 10 %. The PL peaks observed in figure 1 have Gaussian nature with low full width at half maximum which again suggest focusing of particle size. There is also defect level emission observed in all CdS nanocrystals around 560 nm this may be due to surface dangling bonds and surface trap states which also limits quantum efficiency of nanocrystals [17-23]. Low temperature

photoluminescence spectra recorded at room temperature (RT), 250 K, 200 K, 150K, 100K, 50K and 10K shown in figure 2. With decreasing temperature intensity of band edge luminescence enhances with decreasing defect level peak. There is no any shift in peak position was observed at low temperature. FWHM of bandedge luminescence also goes on decreasing. For detailed study of evolution of bandegdge and defect peak position further analysis of results was performed.

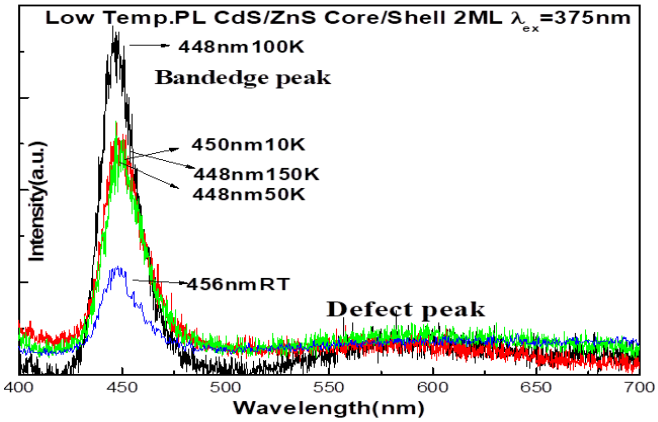

Fig.2 Low temperature photoluminescence spectra of CdS Nanocrystals having sizes CdS (2.3nm) radius.

Figure 3 depict variation of bandedge luminescence with temperature of CdS NCs. As temperature decreasing from room temperature to l0 K there is exponential decay in bandedge peak position as expected due to decrease in bandgap of NCs [17-23]. Bandedge peak position red shift with temperature. Since bandedge luminescence is observed by electron and hole recombination at low temperature thermal agitation of electron and hole de Broglie dispersion was reduced by increasing bandgap [17-23].

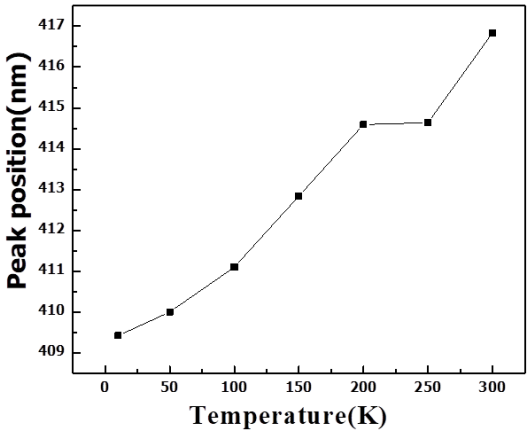

Fig.3 Variation of bandedge peak postion with temperature of CdS NCs.

Figure 3 depict variation defect peak position of luminescence with temperature of CdS NCs. As temperature decreasing from room temperature to l0 K there is reduction in defect peak position. Defect peak in photoluminescence spectra was obtained because of surface trap states [17-23]. Defect level energy levels was situated between HOMO-LUMO gap of NCs. As temperature decrease there is redistribution of defect energy levels and blue shift with decreasing temperature [17-23].

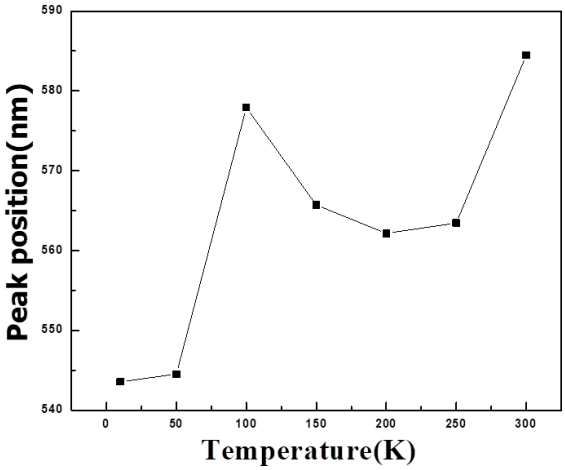

Fig.4 Variation of defect peak postion with temperature of CdS NCs.

Figure 5 show variation of full width at half maximum (FWHM) of bandedge peak and defect peak of luminescence with temperature of CdS NCs. As

temperature decreasing from room temperature to l0 K there is about 5 nm decrease FWHM. Bandedge luminescence shows Gaussian nature at all temperature as observed in figure 1. FWHM of NCs was due to line broadening obtained by temperature, size etc. [17-23]. At low temperature broadening due to thermal effects was reduced significantly but there is still broadening due to size distribution. The defect peak is broader compared to bandedge peak. The FWHM of defect peak is decreasing with increasing tempearature.

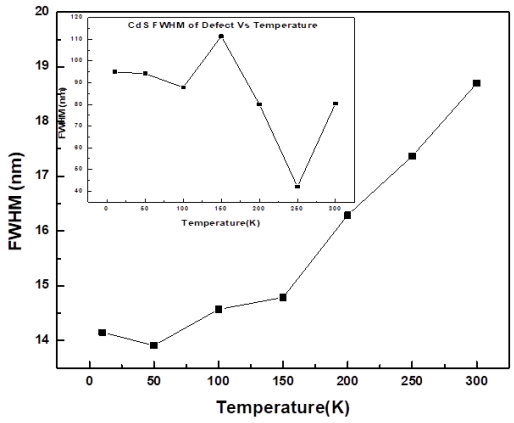

Fig.5 Variation of FWHM of bandedge and defect peak positions (Inset) with temperature of CdS NCs.

Figure 6 shows variation of ratio of intensity of bandedge to intensity of defect peak for CdS NCs. As temperature reduces the intensity of defect peak is decreasing while enhancement of bandedge peak was observed. The trap states from defect energy level are reducing with decreasing temperature and this increases probability of electron hole wavefunction overlap enhancing bandedge luminescence [17-23].

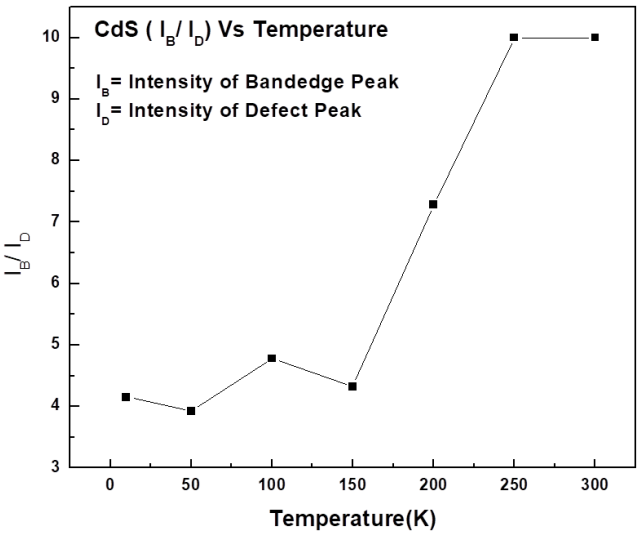

Fig. 6 Variation of ratio of intensity of bandedge to and intensity of defect peak with temperature of CdS NCs.

IV. CONCLUSION

CdS nanocrystals with 4.8 nm size were synthesized by colloidal synthesis. The optical absorption spectroscopy was used to find size and HOMO-LUMO gap of NCs. The photoluminescence quantum yield of NCs is around 10%. From low temperature photoluminescence measurements bandedge energy level was attributed to transitions of energy level 1S3/2 → 1S of ground state. Both bandedge peak and defect peak are blue shifted with decreasing temperature suggesting redistribution of energy levels of CdS NCs at low temperature. Also at low temperature FWHM of bandedge peak was reduced suggesting reduced thermal line broadening of energy levels at low temperature. At low temperature intensity of bandedge peak also enhanced due to decrease in trap states of defect energy levels of CdS NCs.

V. REFERENCES

[1]. S. V. Gaponenko, Optical Properties of Semiconductor Nanocrystals, 1st ed. Cambridge University Press, 1998, pp. 30-35.

[2]. V. I. Klimov, Semiconductor and Metal Nanocrystals, 1st ed. Marcel Dekker New York, 2004, pp. 65-99.

[3]. U. Woggon, Optical Properties of Semiconductor Quantum Dots, 1st ed. Springer, 1997, pp. 43-101.

[4]. Al. L. Efros and A. L. Efros, "Interband absorption of light in a semiconductor sphere," Soviet Phys. Semicond. vol. 16, pp. 772-775, Jan 1982.

[5]. L. E. Brus, "A simple model for the ionization potential, electron affinity, and aqueous redox potentials of small semiconductor crystallites," J. Chem. Phys. Vol. 79, pp. 5566-5571, Dec. 1983.

[6]. L. E. Brus, "Electron–electron and electron-hole interactions in small semiconductor crystallites: The size dependence of the lowest excited electronic state," J. Chem. Phys. Vol. 80, pp. 4403-4409, May 1984.

[7]. S. V. Nair, L. M. Ramaniah, and K. C. Rustagi, "Electron states in a quantum dot in an effective-bond-orbital model," Phys. Rev. B, vol. 45, pp. 5969, Mar. 1992.

[8]. N. A. Hill and K. B. Whaley, "Electronic structure of semiconductor nanoclusters: A time dependent theoretical approach," J. Chem. Phys. Vol. 99, pp. 3707-3715, Sep. 1993.

[9]. N. A. Hill and K. B. Whaley, "Two-particle calculation of excitonic effects in semiconductor nanocrystals," Chem. Phys. Vol. 210, pp. 117-133, Oct. 1996.

[10]. J. P. Conde and A. K. Bhattacharjee, "Exciton states and optical properties of CdSe nanocrystals," Phys. Rev. B, vol. 63, pp. 245318, Jun. 2001.

[11]. J. G. Diaz and J. Planelles, "Theoretical characterization of triangular CdS nanocrystals: a tight-binding approach," Langmuir, vol. 20, pp. 11278-11284, Dec. 2004.

[12]. G. W. Bryant and W. Jaskolski, "Tight-binding theory of quantum-dot quantum wells: Single-particle effects and near-band-edge structure," Phys. Rev. B, vol. 67, pp. 205320, May 2003.

[13]. G. T. Einevoll and Y. C. Chang, "Effective bond-orbital model for acceptor states in semiconductors and quantum dots," Phys. Rev. B, vol. 94, pp. 9683-9697, Nov. 1989.

[14]. L. W. Wang and A. Zunger, "Pseudopotential calculations of nanoscale CdSe quantum dots," Phys. Rev. B, vol. 53, pp. 9579, Apr. 1996.

[15]. D. Chen, F. Zhao, H. Qi, M. Rutherford, and X. Peng, "Bright and stable purple/blue emitting CdS/ZnS core/shell nanocrystals grown by thermal cycling using a single-source precursor," Chem. Mater. Vol. 22, pp. 1437-1444, Jan. 2010.

[16]. W. W. Yu, L. Qu, W. Guo, and X. Peng, "Experimental determination of the extinction coefficient of CdTe, CdSe, and CdS nanocrystals." Chem. Mater. Vol. 15, pp. 2854-2860, July 2003.

[17]. M. Tanaka, J. Qi, and Y. Masumoto, "Optical properties of undoped and Mn 2+-doped CdS nanocrystals in polymer," Journal of Crystal Growth, vol. 214, pp. 410-414, June 2000.

[18]. J. G. Diaz, J. Planelles, G. W. Bryant, and J. Aizpurua, "Tight-binding method and multiband effective mass theory applied to CdS nanocrystals: Single-particle effects and optical spectra fine structure," J. Phys. Chem. B, vol. 108, pp. 17800-17804, Nov. 2004.

[19]. Z. Yu, J. Li, D. B. O'Connor, L. Wang, and P. F. Barbara, "Large resonant stokes shift in CdS nanocrystals," J. Phys. Chem. B, vol. 107, pp. 5670-5674, May 2003.

[20]. N. Pote, C. Phadnis, K. Sonawane, V. Sudarsan, S. Mahamunia, "The impact of lattice strain on

optical properties of CdS nanocrystals," Solid state communications, vol. 192, pp. 6-9, August 2014.

[21]. W. Chen, Y. Xu, Z. Lin, Z. Wang and L. Lin, "Formation, structure and fluorescence of CdS clusters in a mesoporous zeolite," Solid State Communications, vol. 105, pp. 129-134, Jan. 1998.

[22]. J. Li, J. B. Xia, "Hole levels and exciton states in CdS nanocrystals," Phys. Rev. B, vol. 62, pp. 12613 – 12616, Nov. 2000.

[23]. Low temperature photoluminescence study of Cds nanocrystals, Journal Eng. Science, vol. 11 4 pp. 1305-1909 Apr. 2020.

International Virtual Conference on Materials and Nanotechnology
In Association with International Journal of Scientific Research in Science and Technology
Volume 9 | Issue 4 | Print ISSN: 2395-6011 | Online ISSN: 2395-602X (www.ijsrst.com)

Stability Constants and Thermodynamic Parameters of Lanthanides (III) Complexes with 5-Bromo, Ortho Hydroxy Acetophenone – N – (4'– Methyl Phenyl) Imine at 250C

S.B. Maulage[1], S V Gayakwad[1], R G Machale[1], S V Kshirsagar[1]
[1]Mrs. K.S.K. College, Beed, Maharashtra, India

ABSTRACT

Stability constants of some trivalent lanthanides (La, Ce, Pr, Nd, Sm, Gd, Tb, Dy, Yb and Ho) complexes with Schiff base 5-bromo, Ortho hydroxy Acetophenone – N – (4'– methyl phenyl) imine (R_1), have been determined in 50 % (v/v) ethanol-water medium at 25^{0}C and μ = 0.1 M ($NaClO_4$) ionic strength by Irving – Rossotti method. The log K^H and log K values are used to discuss the effect of substituents and atomic size of the trivalent lanthanides. The thermodynamic parameters for the formation of 1:1 and 1:2 complexes have been calculated.

Keywords : Stability Constants, Thermodynamic Parameters, Lanthanides, Schiff Base.

I. INTRODUCTION

Literature survey has revealed that there not enough systematic study has been recorded so far on the trivalent lanthanide complexes of Schiff base derived from 5-bromo, ortho hydroxy acetophenone – N – (4'– methyl phenyl) imine. The objective of the present investigation is to ascertain the coordination behavior of this Schiff base towards lanthanides (III) ions in 50 % (v/v) alcohol-water medium. The observed values of stability constants of these complexes have been explained on the basis of ionic size of the metals, basicity of ligand, gadolinium break and tetrad effect. The changes in thermodynamic parameters are used to explain the stability of these complexes.

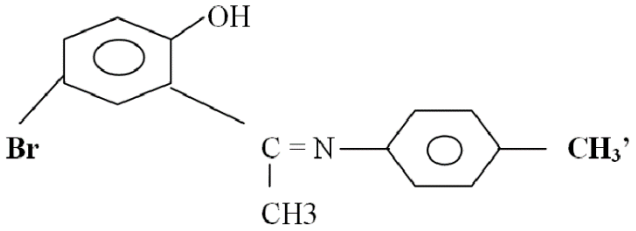

II. EXPERIMENTAL

All the chemicals used for the synthesis of bidentate ligand and their complexes were AR grade. The Schiff base 5-bromo, ortho hydroxy acetophenone – N – (4'– methyl phenyl) imine was synthesized by reported method.[3] The solutions of lanthanide complexes were prepared in the double distilled water and standardized.[4] The initial ionic strength of all the solutions was maintained at 0.1 M by $NaClO_4$. An Elico LI – 120 P^H meter in conjunction with a combined electrode was used. The measurements

were made at 25⁰ C (±0.01º) and μ = 0.01M $NaCLO_4$ in 50 % aqueous ethanol. The log K^H and log K values were computed by half – integral method, point wise calculations and also by the method of least squares. The average log K values were used to calculate ΔG from the Van't Hoff's isotherm. The ΔH and ΔS values were calculated from the Van't Hoff's isochore and the equation ΔG = ΔH - TΔS, respectively. The data are listed in Table – 2.

The pK_1 and pK_2 values of synthesized Schiff base 5-bromo, ortho hydroxy acetophenone – N – (4'– methyl phenyl) imine which represent the de-protonation of NH group at azomethine nitrogen atom and phenolic OH group were determined at n_A = 1.5 and 0.5 respectively. The values were further checked from the plots of log $[(2-n_A)\sqrt{(n_A-1)}]$ vs B and log $n_A/(1-n_A)$ vs B (B = pH meter reading) and are given in Table -1. The pK_1 value of ligand is lower since it is having bromo substituent at *para* position to amino group. This can be attributed on the basis of domination nature of -M effect of bromide group.

Table – 1: Complex formation of lanthanides (III) with 5-bromo, ortho hydroxy acetophenone – N – (4'– methyl phenyl) imine

Temp ⟶		**25 ºC**
Ligand	pK_1	4.66
	pK_2	9.74

III. RESULTS AND DISCUSSIONS

Table – 2: Stability constants and thermodynamic parameters of lanthanides (III) complexes of bidentate Schiff base 5-bromo, ortho hydroxy acetophenone – N – (4'– methyl phenyl) imine at 25° C ± 0.02° C and 0.1 M $NaClO_4$.

Complexes	log K_1	log K_2	$-\Delta G_1$ KJ Mol^{-1}	$-\Delta G_2$ KJ Mol^{-1}	$-\Delta H_1$ KJ Mol^{-1}	$-\Delta H_2$ KJ Mol^{-1}	ΔS_1 KJ Mol^{-1}	ΔS_2 KJ Mol^{-1}
La (III)	5.99	4.46	34.179	25.449	18.731	16.412	51.839	30.324
Ce (III)	6.13	4.66	34.978	26.590	13.791	17.552	71.099	30.329
Pr (III)	6.33	5.14	36.119	29.329	15.231	12.765	70.095	55.584
Nd (III)	6.39	5.23	36.462	29.843	15.414	17.036	70.631	42.976
Sm (III)	6.45	5.32	36.804	30.356	16.455	13.677	68.286	55.971
Eu (III)	6.58	5.59	37.546	31.897	11.584	17.682	87.120	47.700
Gd (III)	6.17	5.26	35.206	30.014	14.913	19.973	68.099	33.694
Tb (III)	6.28	5.38	35.834	30.699	12.067	15.018	79.756	52.621
Dy (III)	6.62	5.87	37.774	33.495	15.956	12.644	73.214	69.967
Ho (III)	6.25	5.36	35.663	30.584	13.962	18.530	72.823	40.451

*Standard deviation for log K_1 and log K_2 are ± 0.019 and ± 0.035 respectively.

The shielding of the *4f* –electrons is exhibited in the stability constants of the present rare earth complexes, which shows very little difference in these values with the increase in atomic number. In these complexes the rare earth metal ions bind predominantly to oxygen and weakly to nitrogen of the Schiff bases.[2] These complexes show a regular increase of stability constants from La (III) to Eu (III) with a discontinuity of Gd (III) and Tb (III) which is commonly known as gadolinium break. After Tb (III), stability constant increases up to Dy (III) and then decreases for Ho (III) as shown in Table – 2. This shows occasional maxima and minima after gadolinium break. In all cases, Gd (III) and Eu (III)

chelates have lower value of log K_1 in relation to those of Dy (III) to Ho (III) chelates.

The change in free energy is directly related to log K values. The stability constants of trivalent La, Ce, Pr, Nd, Sm, Eu, Gd, Tb, Dy, and Ho complexes with 5-bromo, ortho hydroxy acetophenone – N – (4'–methyl phenyl) imine follows the order Dy > Eu > Sm > Nd > Pr > Tb > Ho > Gd > Ce ≥ La. These stabilities are similar to the observations made by number of workers. [7-10] and are accordance with Irving – Williams orer.[11] The thermodynamic parameters for lanthanide complexes with Schiff base were obtained from log K_1 and log K_2 at 25^{0}C temperature. It seems that the log K_1 and log K_2 values decrease with increase in temperature, indicating that the high temperature does not favour the formation of stable complexes. The ΔH_1 and ΔH_2 values are all negative, while ΔS_1 and ΔS_2 are all positive. The resulting ΔG_1 and ΔG_2 values are all negative. The more negative values of ΔG_1 and ΔG_2 indicate that the 1:1 and 1:2 complex formation is thermodynamically favored. The negative values of ΔH_1 and ΔH_2 also lead to the same inference. The entropy effect is found to be predominant over the enthalpy effect which is indicated by the high positive values of entropy.

IV. REFERENCES

[1]. S. M. Irving and H.S. Rossotti, J. Chem. Soc.,2904 (1954).

[2]. V. Mishra and M. C. Jain. Indian Chem. Soc., 1988. 65. 380.

[3]. T.K. Chondhekar and D.D. Khanolkar, Indian J. Chem., Sect. A. 1986,25, 868.

[4]. H. Flaschka, Microchim. Acta, 1955, 55.

[5]. A Syamal, Coord, Chem, Rev., 16, 309 (1985).

[6]. M.S. Mayadeo, S.S. Purohit and S.H. Hussain, J. Indian Chem. Soc., 1982, 59, 894.

[7]. H.L. Kalara, K.E. Jabalpurwala and K.A. Venkatchalam., Inorg. Nucl. Chem. Lett., 26, 1027 (1964).

[8]. R. G.Pearson and F. Basolo, Mechanism of Inorganic reactions:study of complexesin solution, John Wiley, New York, Vol 9, p.16 (1958).

[9]. K.T.Kendre, N.R.Manjaramkar and Y.H. Deshpande, J.Indian Chem. Soc.,63, 615 (1986).

[10]. D.V.Jahagirdar and D. D. Khanolkar, Indian J. Chem., 13,168 (1975).

[11]. H. Irving and R.J.P. Williams, Nature (London), 162,746 (1948).

International Virtual Conference on Materials and Nanotechnology
In Association with International Journal of Scientific Research in Science and Technology
Volume 9 | Issue 4 | Print ISSN: 2395-6011 | Online ISSN: 2395-602X (www.ijsrst.com)

Synthesis and Reactivity of 2-Imino-3-(6-Methyl-1, 3-Benzothiazol-2-Yl)-1, 3-Thiazolidin-4-One

T. M. Bhagat
P.G, Department of Chemistry, G. S. Gawande College, Umarkhed, Dist-Yeotmal, Maharashtra, India

ABSTRACT

4-thiazolidinone has been prepared by the series of reactions. We have synthesized 2-amino-6-methyl benzothiazole from p-toluidine (1) which is then treated with chloro acetyl chloride to form 2-chloro-N-(6-methyl-1,3-benzothiazol-2-yl) acetamide (2). Compound (2) on thiocynation and refluxation with DMF, 2-imino-3-(6-methyl-1,3-benzothiazol-2-yl)-1,3-thiazolidin-4-one is obtained as product(4). This 4-thiazoidinone compound (4) treated with benzaldehyde, 4-methoxy benzaldehyde, 4-chloro benzaldehyde, 2-nitro benzaldehyde and 4-dimethyl amino benzaldehyde in presence of acetic acid and sodium acetate to form corresponding 5-substituted product (5a-5h). The newly synthesized compounds are characterized by spectral analysis.

Keywords : Benzothiazole, Thiazolidinone

I. INTRODUCTION

A survey of literature reveals that large work has been carried out on the synthesis of 4-thiazolidinone and known to exhibits various biological activities as antitubercular[1], antiallergic[2]. 4-thiazolidinone compound are reported to possess different biological activities, such as antimicrobial, anti-inflammatory, antiviral, antiparasitic and antituberculosis[3-9].

4-thiazolidinones are good pharmacological properties[10] and known to exhibits antitubercular[11], antibacterial[12], anticonvulsant[13], antifungal activity[14]. Large work has been carried out on 4-thiazolidinone but very less information is available about 3 and 5-substituted 4-thiazolidinone

The starting compound were prepared by the reaction of 2-amino-6-methyl benzothiazole and chloro acetyl chloride to form 2-chloro-*N*-(6-methyl-1,3-benzothiazol-2-yl) acetamide which on treatment with potassium thiocynate and DMF, 2-imino-3-(6-methyl-1,3-benzothiazol-2-yl)-1,3-thiazolidin-4-one obtained as a product. This thiazolidinone treated with substituted aromatic aldehyde to obtained corresponding 5-substituted 4-thiazolidinone

II. EXPERIMENTAL

All the melting points were determined in open capillary tube and may be uncorrected. The purity of compound was checked by TLC on silica gel coated glass plate. Infra-red spectra were monitored in KBr palates on Bomen 104 FT infra-red spectrophotometer.

H1 NMR spectra were obtained on a Gemani 200 Mz spectrometer with tetra methyl silane as an internal standard. Elemental analysis was performed on a Heraeus CHN-O rapid analyzer

2-chloro-N-(6-methyl-1,3-benzothiazol-2-yl)acetamide (2)

2-amino 6-methyl benzothiazole (5gm, 0.01M) and100ml of dry benzene is taken in a round bottom flask. 15ml of chloro acetyl chloride added drop wise fashion maintaining temperature 0-5 ^{0}C in a reaction mixture. Then reflux the reaction mixture on water bath for 5 hours. The solvent was removed by distillation, the solid product is obtained. The completion of the reaction was monitored by TLC. The solid was recrystallized by using ethanol.

Yield: 5.3 gm,(72%) M.P: 172 °C I.R. (KBr) : 3420 cm^{-1} (Asymmetric stretching of -NH), 3320 cm^{-1} (N-H Symmetrical stretching of -NH), 3052 cm^{-1} (Ar-H stretching), 1630 cm^{-1} (-C=N stretching), 1750 cm^{-1} (-C=O stretching); PMR ($CDCl_3$) δ 2.5 (singlet, 1H, NH), δ 6.8 (singlet, 1H, Ar-H), δ 7.0-7.5 (two doublet, 2H, Ar-H) [Found : C: 49.5 %, H : 3.50%, Cl : 14.5% N : 11.0%, O : 6.5% S: 13.0 %.$C_{10}H_9ClN_2OS$ required : C: 49.90 %, H : 3.77 %, Cl : 14.73% N : 11.64%, O : 6.65% S: 13.32 %.]

2-[(6-methyl-1,3-benzothiazol-2-yl)amino]-2-oxoethyl thiocyanate 9 (3)

3.8gm (0.015M) of compound (2) and 2gm (0.02M) KSCN taken in a round bottom flask. Then 40ml dry acetone was added and refluxed on water bath for 4 hours. The resulting mixture was cooled, excess of acetone was removed by distillation & residue poured into crushed ice, thus solid residue obtained was filtered, washed with cold water, dried & recrystalised from ethanol.

Yield: 3.5 gm, (80%) M.P: 172 °C I.R. (KBr) : 3420 cm^{-1} (Asymmetric stretching of -NH), 3320 cm^{-1} (N-H Symmetrical stretching of -NH), 3052 cm^{-1} (Ar-H stretching), 1630 cm^{-1} (-C=N stretching), 1750 cm^{-1} (-C=O stretching) 2230 cm^{-1} (-C≡N stretching in cyanide) ; PMR ($CDCl_3$) δ 2.4 (singlet, 1H, NH), δ 6.8 (singlet, 1H, Ar-H), δ 7.0-7.5 (two doublet, 2H, Ar-H) [Found : C: 49.5 %, H : 3.50%, N : 15.5%, O : 6.0% S: 24.0 %.$C_{11}H_9N_3OS_2$ required : C: 50.17 %, H : 3.44 %, N : 15.96%, O : 6.08% S: 24.35 %.] .

2-imino-3-(6-methyl-1,3-benzothiazol-2-yl)-1,3-thiazolidin-4-one (4)

2.63gm (0.01M) of compound (3) in a round bottom flask was refluxed in 30ml DMF (Dimethyl Formamide) in an oil bath by maintaining temperature of 150-160 ^{0}C for 6 hours. The solvent removed by distillation under vaccume & the crude product obtained is recrystallized from ethanol. The completion of reaction was monitored by TCL.

Yield: 2.6 gm, (74%) M.P: 162 °C I.R. (KBr) : 3420 cm^{-1} (Asymmetric stretching of -NH), 3320 cm^{-1} (N-H Symmetrical stretching of -NH), 3052 cm^{-1} (Ar-H stretching), 1630 cm^{-1} (-C=N stretching), 1750 cm^{-1} (-C=O stretching) ; PMR ($CDCl_3$) δ 2.6 (singlet, 1H, NH), δ 6.8 (singlet, 1H, Ar-H), δ 7.0-7.5 (two doublet, 2H, Ar-H) [Found : C: 49.5 %, H : 3.50%, N : 15.5%, O : 6.0% S: 24.0 %.$C_{11}H_9N_3OS_2$ required : C: 50.17 %, H : 3.44 %, N : 15.96%, O : 6.08% S: 24.35 %.]

5-substituted-2-imino-3-(6-methyl-1,3-benzothiazol-2-yl)-1,3-thiazolidin-4-one (5a-5f)

1.3 gm (0.005M) of compound (4) and 0.4 gm (0.005M) of sodium acetate was taken in a 50 ml round bottom flask. Then aromatic aldehyde (a-f) & 10 ml of acetic acid was added, refluxed for 5 hours and allow to cool. This reaction mixture pours on crushed ice. Precipitate once formed. Filtered & washed with cold water & recrystallized from proper solvent.

5a. Yield: 0.8 gm, M.P: 128 °C I.R. (KBr): 3420 cm^{-1} (Asymmetric stretching of -NH), 3320 cm^{-1} (N-H Symmetrical stretching of -NH), 3052 cm^{-1} (Ar-H stretching), 1630 cm^{-1} (-C=N stretching), 1750 cm^{-1} (-C=O stretching); [Found C: 61.5 %, H : 3.5 %, N : 11.5%, O : 4.5% S: 18.0 % M.F.-$C_{18}H_{13}N_3OS_2$

required : C: 61.52 %, H : 3.73 %, N : 11.96%, O : 4.55% S: 18.25 %.]

5b. Yield: 0.6 gm, M.P: 122 °C I.R. (KBr) : 3410 cm^{-1} (Asymmetric stretching of -NH), 3325 cm^{-1} (N-H Symmetrical stretching of -NH), 3050 cm^{-1} (Ar-H stretching), 1620 cm^{-1} (-C=N stretching), 1760 cm^{-1} (-C=O stretching); [Found C: 63.5 %, H : 3.8 %, N : 11.0%, O : 4.1% S: 16.80 % M.F.-$C_{20}H_{15}N_3OS_2$ required : C: 63.64 %, H : 4.0 %, N : 11.13%, O : 4.24% S: 17.0 %.]

5c. Yield: 0.6 gm, M.P: 108 °C I.R. (KBr) : 3430 cm^{-1} (stretching of -NH), 3050 cm^{-1} (Ar-H stretching), 1620 cm^{-1} (-C=N stretching), 1760 cm^{-1} (-C=O stretching); [Found C: 59.7 %, H : 3.8 %, N : 11.0%, O : 8.2% S: 16.5 % M.F.-$C_{19}H_{15}N_3OS_2$ required : C: 59.82 %, H : 3.96 %, N : 11.02%, O : 8.39% S: 16.81 %.]

5d. Yield: 0.6 gm, M.P: 130 °C I.R. (KBr) : 3400 cm^{-1} (stretching of -NH), 3070 cm^{-1} (Ar-H stretching), 1620 cm^{-1} (-C=N stretching), 1720 cm^{-1} (-C=O stretching); [Found C: 55.8 %, H : 3.1 %, Cl : 9.1 %, N : 11.8%, O : 4.1% S: 16.5 %; M.F.-$C_{18}H_{12}ClN_3OS_2$ required : C: 56.02 %, H : 3.13 %, Cl : 9.19 %, N : 11.89%, O : 4.15% S: 16.62 %.]

5e. Yield: 0.7 gm, M.P: 115 °C I.R. (KBr) : 3430 cm^{-1} (stretching of -NH), 3020 cm^{-1} (Ar-H stretching), 1630 cm^{-1} (-C=N stretching), 1730 cm^{-1} (-C=O stretching); [Found C: 54.5 %, H : 3.0 %, N : 14.1%, O : 12.1% S: 16.1 %.; M.F.-$C_{18}H_{12}N_4O_3S_2$ required : C: 54.53 %, H : 3.05 %, N : 14.13%, O : 12.11% S: 16.18 %.]

5f. Yield: 0.6 gm, M.P: 125 °C I.R. (KBr) : 3440 cm^{-1} (stretching of -NH), 3050 cm^{-1} (Ar-H stretching), 1620 cm^{-1} (-C=N stretching), 1740 cm^{-1} (-C=O stretching); [Found C: 60.6 %, H : 4.5 %, N : 14.1%, O : 4.0% S: 16.2 %.; M.F.-$C_{20}H_{18}N_4OS_2$ required : C: 60.89 %, H : 4.60 %, N : 14.20%, O : 4.06% S: 16.26 %.]

Scheme

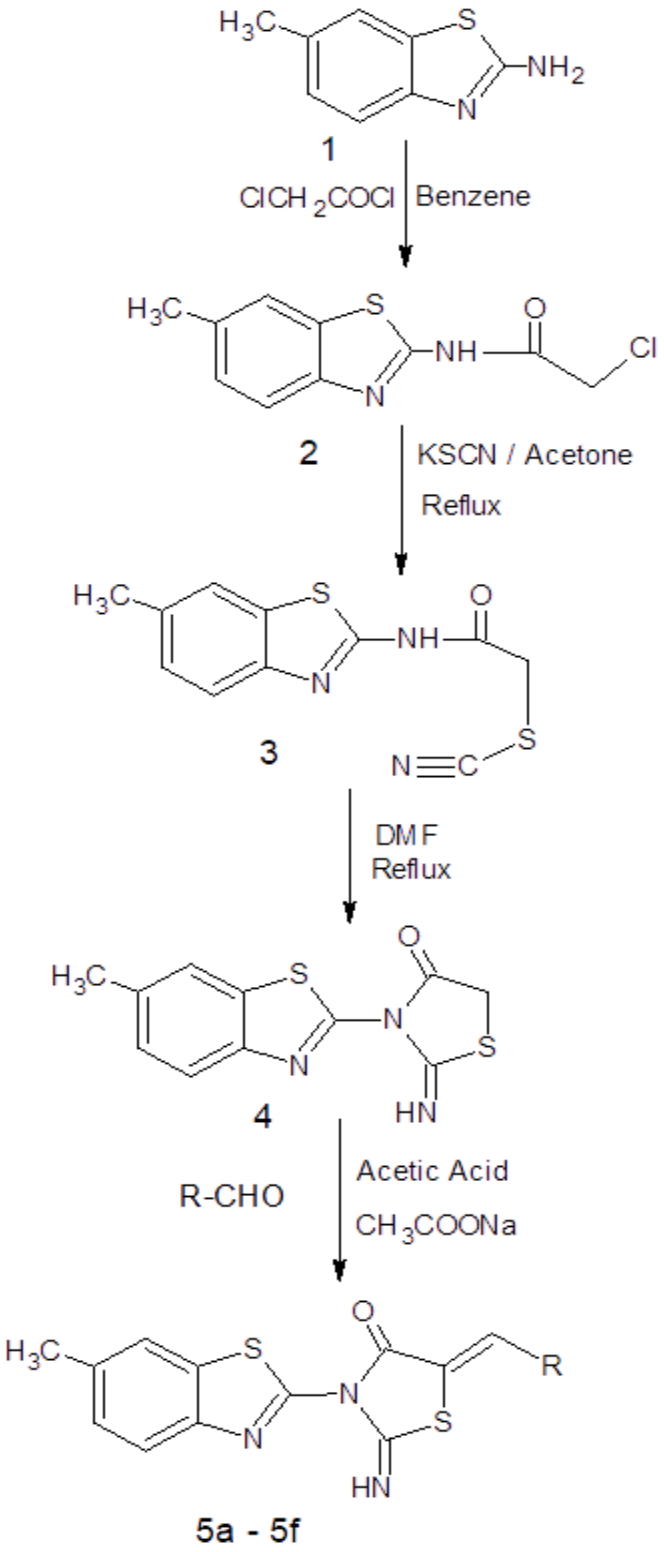

Where

R-

a 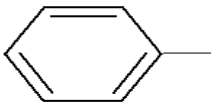

b 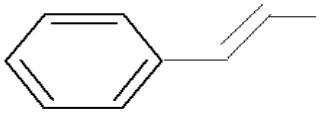

c 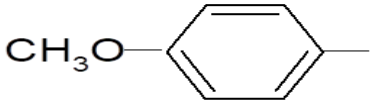

d 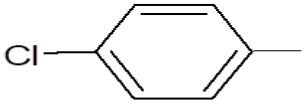

e 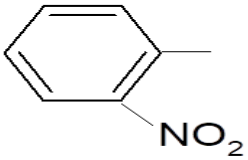

f 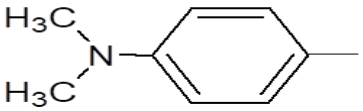

III. RESULT AND DISCUSION

The structures of these 3 and 5-substituted thiazolidinone (5a- 5f) were assigned on the basis of their elemental analysis and spectral data

2-chloro-N-(6-methyl-1,3-benzothiazol-2-yl)acetamide showed stretching absorption bands in IR spectra in the region 3320 cm^{-1} due to N-H stretching. The presence of broad singlet in their PMR spectra in the region δ 2.5 to δ 4.5 confirmed the presence of -NH proton. The signal at 1750 cm^{-1} in IR spectra indicates the presence of carbonyl group.

The I. R. spectra of Compound (3) shows absorption signal in the region 2230 cm^{-1} indicates the presence of cyano grop. While the IR spectra of compound (4) observed the absence of strong bands in the region 2230cm^{-1} due to –C-N stretching of cyano group , confirms the formation of cyclised product.

IV. REFERENCES

[1]. Kasel W, Dolezal M, Sidoova E,Odlerova Z and Drasata, J. Chem. Abstr.,1989,110,128063e.

[2]. Ronssel U and Jpn Kokai Tokkyo, Chem. Ast.r, 1987, 106, 156494G.

[3]. Capan, G., Ulusoy N., Ergenc N., Kiraz M. Monatshefte fur Chemie 1999, 130, 1399.

[4]. Vigorita, M. G., Ottana R., Monforte F., Maccari R., Trivato A., Monforte M. T., Zaviano M. F. Bioorg. Med. Chem. Lett. 2001, 11, 2791.

[5]. Rawal, R. K.; Prabhakar, Y. S.; Katti, S. B.; Clercq, E. Bioorg. Med. Chem. 2005, 13, 6771.

[6]. Babaoglu, K.; Page, M. A.; Jones, V. C.; McNeil, M. R.; Dong, C.; Naismith, J. H.; Lee, R. E. Bioorg. Med. Chem. Lett. 2003, 13, 3227.

[7]. Alves, A. J.; Ramos, S. V. V.; Silva, M. J.; Fulcrand, P.; Artis, A. M.; Quero, A. M. Rev. Farm. Bioquı´m. Univ. Sao Paulo 1998, 34, 77.

[8]. Alves, A. J.; Leite, A. C. L.; Santana, D. P.; Beltrao, T. M.; Coelho, M. R. D. IL Farmaco 1993, 48, 1167.

[9]. N. C. Desai, H. K Shukla, R. R. Astik and K. A. Thakar, J. Indian Chem. Soc., 61, 238, (1984).

[10]. L.I. Petlichna, M. M. Turekevich and V. M. Vaedenski, Ukvkhim. Zh., 29, 170, (1963)

[11]. Raj Singh. J. Indian chem. Soc., 53, 595, (1976).

[12]. E. Schropal and R. Pohloudek- Febini, Pharmazie, 23, 638, (1968)

[13]. M. Pargel. K. Popov. Pargel and N. Kobillarov, Synthesis, 11, 190, (1976).

[14]. J. M. Decazes, J. L. Luche, H. B. Kagam, R. Parthsarathy and J. Ohrt, Tetrahedron Lett. 3633, (1972)

International Virtual Conference on Materials and Nanotechnology
In Association with International Journal of Scientific Research in Science and Technology
Volume 9 | Issue 4 | Print ISSN: 2395-6011 | Online ISSN: 2395-602X (www.ijsrst.com)

State of The Art : Phase Change Material as Means of Thermal Energy Storage

Punam Mehta*

*Department of Physics, Government PG College Narsinghgarh, Rajgarh, Madhya Pradesh, India

ABSTRACT

With the rapid increase in energy demand, focusing on renewable sources of energy have been increased rapidly. As fossil fuels are created in hundreds of years and will be exploited soon, if other sources of energy are not employed then the world may enter in dark age .So there is a paradigm shift in searches for sources of energy from non-renewable to renewable sources. Solar energy, Wind energy, Hydro energy, Tidal energy, Geothermal energy, Biomass energy are getting the attention of the entire scientific community being renewable sources of energy. There are different materials which are used to store thermal energy. Phase Change Material has proved its significant role in thermal energy storage. This article provides a comprehensive view of Phase change material, it's working principle, it's types and application in different fields. As such, this paper summarizes the investigations made on the recent researches in the field of phase change material for thermal energy storage. This paper will benefit the researcher in conducting further research on thermal energy storage.

Keywords : Phase Change Material, Thermal Energy Storage, Latent Heat, Renewable And Sustainable Energy.

I. INTRODUCTION

These days Countries are facing energy demand and supply mismatch due to the rapid growth of population, modernization and increased industrial dependence. Thus a lot of new fields have emerged in the last few decades for meeting the energy demands of the world .Renewable sources are getting more attention and researchers are searching new ,effective and economic ways to generate, store and distribute the electricity, although all these are still in an infancy. According to the International Energy Agency IEA 2019, coal contributed 45%, petroleum and other liquid contributed 26%, traditional biomass and waste contributed about 20% in India's total energy consumption. Primary energy consumption reached 916 million tonnes of oil equivalent by 2018.[1] Renewable sources have contributed little in primary energy consumption of India.[2] India's crude oil imports reached a new hike in the current scenario. India's dry natural gas production remained flat at about 1.1 trillion cubic feet (Tcf) between 2015 and 2019. [3] Such figures force the scientific community to search for new ways for generating and storing thermal energy to fulfil the needs of people.[4] Thus it is found that Energy storage is a

very appealing field to study as excess energy stored properly can be used for future purposes . So countries worldwide increased their focus on alternative sources of energy. Direct sun radiation has been considered as a prospective source of energy .To overcome the mismatch between energy generation and utilisation, thermal energy storage (TES) has emerged as a powerful energy storage concept. For thermal energy storage, Phases Change Materials (PCM) are very useful as it's working is based on the latent heat concept.[5] For example ,when 0^0C of ice changes its phase and converts into water of 0^0C , it stores latent heat which can be released later during solidification process. Thus latent heat stored or released during phase change could be a great source of thermal energy storage. Phase Change Materials like paraffin, salt hydrates and fatty acids and eutectics of organic and non-organic compounds have been widely studied in order to minimize the greenhouse effect and to minimize dependence of the country on foreign oil imports which costs the economy millions of rupees every year.

II. THERMAL ENERGY STORAGE (TES)

Thermal energy storage are used to hold thermal energy for a certain period of time (in the form of heat or cold) in a suitable media and suitable form when it is surplus, and extracting the same at a later time when needed .[6]

Different modes of heat transfer used for storing thermal energy-

Temperature profile of phase change material (PCM) can be divided into different regions like the sensible heat, the latent heat and the thermo chemical energy. [7] These regions of temperature profile represent the mode of heat transfer for storing thermal energy. In The region of latent heat, the temperature remains constant while changing the phase of material. In this region the phase change is influenced by intermolecular forces while in the sensible region translational, rotational and irrational motions of the atoms and molecules plays a vital role. The energy stored in the chemical bonds between atoms is responsible for the thermo chemical component. (Source: Said Al-Hallaj & Riza Kizilel)

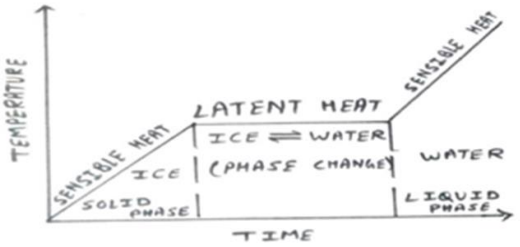

Figure 1-Temperature Profile of a PCM. [8]

Advantages of thermal energy storage (TES) are as follows

- TES helps to achieve a better and efficient use of energy.
- TES reduces greenhouse gas emission and lower pollution. Thus it helps in preserving the environment.
- TES improves system performance and reliability .Thus leads to sustainable energy storage.
- TES reduces the capital and Operational cost so TES are economical in Nature.

Phase Change Material (PCM)

Phase Change Material (PCM) are those materials which absorb or release large amounts of heat on melting or solidifying as it has the high latent heat of fusion. During the phase change process, heat conduction and heat convection takes place in PCM. Using proper heat transfer techniques in PCM, heat conduction can be increased and heat convection can be decreased. Potential of PCM can be realized in TES because of negligible temperature variations and

remarkable energy storage density.[**9**]PCM works as heat accumulating material. PCM stores heat in the form of latent heat of fusion which is about 100 times more than the sensible heat. For example, latent heat of fusion of water is about 334 kJ/kg whereas sensible heat at 25° Celsius (77°F) is about 4.18 kJ/kg. Two widely used PCMs are water and wax. Water requires a significant amount of energy when it changes from solid phase to liquid phase at 0°C (32°F) or Wax extends the burning time of a candle.

Working principle of PCM-

Phase change process of a PCM can be explained as follows (Source: Said Al-Hallaj & Riza Kizile) in the melting process PCM (Solid State) converted to PCM (Liquid State). Here energy is stored in PCM. It is also known as the charging process. In the freezing process PCM in Liquid State converts into PCM in Solid State. Here energy is released in process. So this process is known as discharging process. This cycle of the melting and solidification of phase change material can be repeated many times.[8]

Criteria for selection of the phase change material (PCM) as TES-

While designing a thermal storage system following criteria should meet:

1. PCM should have a suitable phase transition temperature
2. IT should have high heat conductivity
3. It should have high latent heat of transportation
4. The melting temperature should lie in the range of the operation
5. It should be chemically stable
6. It should be low in cost,
7. It should be non-corrosive
8. It should be nontoxic.[**8**]

Types of PCM

PCM may be classified on the basis of phase transition like solid-liquid, solid-gas, solid-solid, and liquid-gas. (Source: Said Al-Hallaj & Riza Kizilel)

1. Organics PCMs (e.g. Paraffin, Fatty Acids, PEG)

Merits-Available in a large temperature range, No super cooling, compatible with other materials, No separation, Chemically PCMs are stable, safe to use, Non-reactive in nature, recyclable

Limitations-Low thermal conductivity, Relative large volume changes, Flammable, Expensive except technical grade paraffin wax

2. Inorganic PCMs (e.g. salt hydrates, Nitrates, Metalics)

Merits-High volumetric latent heat, less expensive, easily available, Thermal conductivity is higher, Lower volumetric variation, Non- flammable

Limitations-Changed volume is remarkably high, Super cooling, Corrosiveness

3. Eutectics- Eutectics are homogenous mixture of two or more substances (organic / inorganic) in a specific proportion. Melting point of eutectic is generally lower than the melting point of individual components. Also it melts with no phase segregation which is the most important characteristics of eutectics. Example of eutectic are Mg-Zn eutectic metal alloy (P. Blanco-Rodriguez et.al, 2015), Mg-Zn-Al Eutectic alloy (E. Risueñoet.al, 2015), Al-Si Alloy (N. Gokon et.al 2015)

Merits-The melting points of eutectics are sharp. It possesses high volumetric storage density.

Limitations-Data on Thermo physical properties of eutectic are not available properly.

PCMs Composite-

Phase change materials are encapsulated in a polymer matrix to make composite. Composites are mainly employed in case of PCM with low melting temperature such as paraffin waxes. PCMs composite incorporate the structural functionality with Thermal energy storage. Sheo Peng and others studied the solid–liquid latent heat effect of the Polymeric phase change composites for thermal energy storage .Room temperature cured bisphenol-A epoxy and styrene–ethylene–butylene–styrene (SEBS) polymers are chosen as matrix materials because of their excellent chemical and mechanical properties.[10] Moussa Aadmi and others have used the Phase change materials based on epoxy resin paraffin wax with the melting point 27 °C as a new energy storage system.[11]

Heat transfer enhancement techniques for PCM-

Active heat transfer enhancement techniques and Passive heat transfer enhancement techniques.

When external power is supplied then the Heat transfer techniques are known as active heat transfer enhancement techniques while when external power is not supplied then the Heat transfer techniques are known as passive techniques .The passive techniques are more valuable than the active techniques because it can be easily employed in an existing heat exchanger.[12] This combination of techniques is referred to as hybrid heat transfer enhancement which can be used for improving PCM based system performance.

Properties of PCMs

a. Thermo physical Properties of PCMs are Latent heat, Suitable heat releasing temperature, Small or no sub cooling, High change of enthalpy at temperature of use, Effective heat releasing time, crystallite size, and Thermal stability during heating and cooling cycles. Phase change temperature useful for application
b. Chemical Properties of PCMs are Stability, Comparability of container Material, Non toxic, Non flammable, Non polluting, No phase separation
c. Economic Properties are Cheap and abundant

PCM Characterization –

The most widely used technique for determining thermo physical properties like - enthalpy, heat capacity, thermal conductivity, thermal diffusivity and density is Differential Scanning Calorimetry (DSC). According to the Japanese Industrial Standard, DSC is of two types-Heat Flux DSC and Power Compensation DSC.Temperature of the sample unit (made up by sample and reference material) is varied with the help of specific program and difference in temperature of sample and reference material is measured as a function of temperature in case of Heat Flux DSCs, while difference in thermal energy applied per unit time to. Sample and reference material is measured as a function of temperature in case of Power Compensation DSC. [13] Other useful techniques are Differential thermal analysis (DTA), Thermo gravimetric analysis (TGA),T-history

Application of PCM

Night Ventilation-Night ventilation (NV) is a productive passive cooling technique which demonstrates a high potential for reducing cooling loads and improving thermal comfort. PCMs can be used as efficient lightweight thermal energy storage for NV. [14]

Cooling System of buildings-PCM can be used in the cooling system of buildings. The cooling strategy of PCM is based on thermal balance concept that it absorbs heat energy at charging period and releases back at discharging period. [15]

Heat storage material-The PCMs used as storage media (for medium-high temperature solar applications as concentrated solar thermal power, CSP) are in general molten salts.

Solar Water Heater-Kulkarni and others found that solar water heater with PCM helps to reduce cooling rate of water, reduces tank size and cost also. Thus it leads to maximum utilization of solar energy.[16]

Helmets-Helmet cooling system using PCM can provide motorcycle riders a comfortable cooling experience. In 2006, Tana and Fok designed a helmet cooling system using PCM. In such a system the heat from the users' bodies is conducted to the PCM pouch which is in contact with users. As PCMs change phase at constant temperature employing latent heat, cooling comfort is provided to the user till PCM completely melts. Heat stored in PCM then discharged by immersing it in water, which again solidifies PCMs. [17]

Heating Pad- Heat packs are made of poly vinyl chloride (PVC), low density polyethylene (LDPE), high density polyethylene (HDPE) etc. packaging materials and contain aqueous solution of sodium acetate trihydrate PCM and metallic triggering device. Akanksha Mishra et.al. found that in these heat packs, PCM remains in a metastable supercooled liquid state, far below its solidification temperature. This property helps in storing the thermal energy as the latent heat of PCM, even at low ambient temperature (~0 °C) for very long time. [18]

Telecom Shelter-Being temperature sensitive Instruments in the telecom sector necessitates to be maintained below 35^0 C. PCMs help in this regard. Ramesh Rathod et. al. found that PCMs absorb heat in case of power shortage or black out thus maintaining the device temperature below 35^0C and get re-charged on availability of power source Thus, PCM store energy using a cheap source of power and release it when that cheap source of power is not available [19]

Memory Application- Cold storage-for improvement of thermal performance of cold storage PCM can be used. Studies shows that application of polyethylene glycol 400 (PEG 400) as a Phase change material (PCM) reduced the rise in the temperature of air inside the cold space in the situations like frequent door openings and electrical power failures.[20]

Hybrid Cooling System-It combines both passive (PCM) and active (fins and fans) cooling solutions. It can be used in telecom base station power amplifiers, where the power is proportional to the traffic load [21]

PCM-based heat sink –It can be used for cooling of mobile electronic devices like notebook, personal digital assistants (PDAs).[22]

Fighter Protective Clothing- Thermal protection of the multi-layered fabrics can be increased using PCM fabrics. The time to reach a second degree burn was largely reduced. [23]

Refrigerated Trucks-PCM can be used in lowering peak heat transfer rates and total heat flows into a refrigerated trailer. Ahmed et. al. worked on paraffin based PCM in the refrigerated truck trailer . They found an average reduction in peak heat transfer rate of 29.1 % for all walls and 11.3 - 43.8 % for individual walls have been observed.[24]

Room Cooling Application-Energy consumption of air conditioning systems can be reduced by using the phase change material (PCM) as thermal energy storage. Temperature difference between day and night is utilised in PCMs to store and release thermal energy. [25]

Boiler -PCM embedded heat exchanger (PCM-HEX) is used for recovering the waste heat from the exhaust

of a gas-fired combi-boiler to heat the domestic water is placed at the top of the combi-boiler and connected with the exhaust of flue gas. In the charging mode, PCM turns into liquid phase by storing thermal energy, while in discharging mode PCM turns into solid phase releasing energy when demand arises. . [26]

PCM textile-To improve athletes' performance, the textile industry is employing advanced manufacturing technology in sports wear by using PCM in fabrics. In this technology PCM microcapsules are incorporated in fabrics, and the property of PCM to change phase within a temperature range that is just above and just below human body temperature to store body heat and then release it when needed. [27][28]

Therapeutic Applications-Rohitash Kumar et .al experimentally demonstrate that addition of ethylene glycol (EG) in aqueous sodium acetate trihydrate (SAT) enhanced the softness of SAT crystallite, enhance the degree of supercooling and increase the heat releasing time by ~10%.EG-SAT composite phase change materials can be used in low ambient temperature to get rid of cold and for the therapeutic application as it has high thermal energy storage density and suitable heat releasing temperature.[29]

Commercial Status of PCMs as thermal energy storage

According to EPRI, thermal energy storage systems like Steam accumulator are in commercial stage, two tank direct and indirect thermal energy storage are in pre commercial proto type stage, while PCMs are still in developmental stage. (Source: EPRI, 2009) [30] Wide Spectrum of PCMs applications includes solar pumps, solar heater, solar cooker, thermal comfort in building, refrigerated trucks (freight at specific temperatures),hybrid vehicles using Li-ion batteries with PCM ,telecom sector, PCM based heat sinks for cooling electronics etc. But all these are not suitable for field applications.

Research Gaps in Literature Review & Future Research Directions

Despite profound contributions by research scholars and academicians in the use of PCM as solar thermal energy storage, still there are wide range of research gap, which has to be addressed in the future research Author proposed following research topics after rigorous literature Review: Anusuiah Vasu and others (2017) in their work studied the corrosion behaviour of PCMs, especially salt hydrates with container materials. Stainless steel has been found to be a more compatible material for making containers in TES than Aluminium. Condition is more serious in case of large scale solar power production. Research is required in the field of Anti corrosive compatible container Material that can be used with PCMs so that the potential of solar energy to harnessed completely .[31] For high temperature thermal energy storage, Attention of the scientific community must be drawn to draw out the utilities of PCMs Composite. Different composite PCMs must be analysed. With respect to their performance curve to know best Composite PCMs for thermal energy storage. Multifunctional storage units which work on both sensible and latent heat need to be developed. Other properties besides thermal properties like chemical, mechanical need to be addressed properly.

III.CONCLUSION

According to California Public Utilities Commission (CPUC, 2010) PCM can be used as storage media for storing the excess wind and off peak energy so that it can be used later when needed. Thus it can be concluded that Phase change materials need of hour .These materials have proved its efficiency in thermal energy storage. With proper utilisation of PCM ,industries can enjoy the advantage of day-night temperature difference .It has covered a vast area in the recent years due to its latent heat properties , large heat storage capacity and isothermal behaviour during the charging and discharging

processes. PCMs help in developing alternative renewable, reusable and cost effective heating sources .PCMs help in storing available thermal energy (solar energy, waste energy etc.) at high temperature, retain it at lower ambient temperature and release the latent heat later when needed. But it has low thermal conductivity which reduces its practicability. To enhance the commercial acceptability of TES applications employed with PCM, such systems should be made economical. So some additives are used with base fluid to increase the thermal conductivity of PCM. Such PCMs are now known as nano enhanced phase change material (NEPCM). Hence to harness the efficacy of PCMs , for any latent heat thermal storage (LHTS) applications, extensive research must be carried out in the field of Nanoparticles (NPs) inclusion in PCMs so that the world can be freed from energy mismatch and can moved towards a better and sustainable tomorrow. Thus it can be concluded that phase change material has started a new era in thermal energy storage.

IV. REFERENCES

[1]. International Energy Agency(IEA), World Energy Outlook 2019, page 734.

[2]. The Economic Times, "India's plan to raise natural gas share in energy basket to 15% looks increasingly ambitious: WoodMac," February 8, 2019; International Energy Agency, Gas 2019, page 31.

[3]. https://www.eia.gov/international/analysis/country/IND

[4]. The Times of India, "Power distribution plan soon to ensure 24X7 electricity supply for all," July 16, 2019; Live Mint, "Govt's 100-day plan aims to re-energize India's power sector," June 12, 2019.

[5]. Murat Kenisarin Khamid Mahkamov Solar energy storage using phase change materials Renewable and Sustainable Energy Reviews Volume 11, Issue 9, December 2007, Pages 1913-1965

[6]. Zalba B, Marín JM, and Cabeza L F, et al. Review on thermal energy storage with phase change: materials, heat transfer analysis and applications. Applied Thermal Engineering. 2003; 23(3); 251–283.

[7]. Tatsidjodoung P, Le Pierrès N, Luo L. A review of potential materials for thermal energy storage in building applications. Renewable and Sustainable Energy Reviews. 2013;18:327–349.

[8]. Said Al-Hallaj,Riza Kizilel (2012) Applications of Phase Change Materials for Sustainable Energy in Tim Theis and Jonathan Tomkin(Ed.) , Sustainability: A Comprehensive Foundation

[9]. RVSR Vera, RV Seeniraj, B Hafner, Christian Faber, Clemens Schwarzer Heat transfer enhancement in a latent heat storage system Solar energy 65 (3), 171-180, 1999 Retrieved from www.sciencedirect.com

[10]. Shuo Peng,Alan Fuchs,RA Wirtz Polymeric phase change composites for thermal energy storage August 2004 Journal of Applied Polymer Science 93(3):1240 – 1251 DOI: 10.1002/app.20578 Retrieved from https://www.researchgate.net/publication/227737305_Polymeric_phase_change_composites_for_thermal_energy_storage

[11]. Aadmi, Moussa Karkri, Mustapha ,El Hammouti, MimounI DEAS Heat transfer characteristics of thermal energy storage for PCM (phase change material) melting in horizontal tube: Numerical and experimental investigations retrieved from https://ideas.repec.org/a/eee/energy/v85y2015icp339-352.html

[12]. Lin, Y.; Alva, G.; Fang, G. Review on thermal performances and applications of thermal energy storage systems with inorganic phase change materials. Energy 2018, 165, 685–708.

[13]. Principle of Differential Scanning Calorimetry (DSC) HITACHI inspire the next retrieved from https://www.hitachi-

hightech.com/global/products/science/tech/ana/thermal/descriptions/dsc.html?gclid=CjwKCAiAg8OBBhA8EiwAlKw3khjrbZQ_Uw_RSOmn-VPhGBWDI5g2oouHfehTM8eUYZTOZqbCs11U9RoCIFwQAvD_BwE

[14]. Ebrahim Solgia Henry Skatesa A parametric study of phase change material behaviour when used with night ventilation in different climatic zones Building and Environment Volume 147, January 2019, Pages 327-336

[15]. A Jurists and S Wonorahardjo A Review on The Application of Phase Change Material for Indoor Temperature Management in Tropical Area IOP Conference Series: Earth and Environmental Science

[16]. M.V. Kulkarni, D. S Deshmukh Improving Efficiency Of Solar Water Heater Using Phase Change Materials , Resonance june2015,PRATIBHA: International Journal Of Science, Spirituality, Business and Technology (IJSSBT), Vol. 3, No. 1, Dec 2014 ISSN (Print) 2277—7261 Retrieved from www.ijssbt.org

[17]. F.L.Tana ,S.C.Fok Cooling of helmet with phase change material Applied Thermal Engineering Volume 26, Issues 17–18, December 2006, Pages 2067-2072

[18]. Mishra A.,Shukla A., and Sharma A. Latent Heat Storage Through Phase Change Materials Resonance volume 20, page 532–541(2015) Retrieved from https://link.springer.com/article/10.1007/s12045-015-0212-5

[19]. Rathod R. , Ingle P., Shaikh F. , Sharma N., Naiknaware K. Phase Change Material and its Selection Criteria-An Overview IJERT,volume 09, issue 09 (September 2020)

[20]. Vivek Raj, Goswami TK Use of phase change material (PCM) for the improvement of thermal performance of cold storage March 29, 2018 Retrieved from https://medcraveonline.com/MOJCRR/use-of-phase-change-material-pcm-for-the-improvement-of-thermal-performance-of-cold-storage.html

[21]. G Casano and S Piva A Further Contribution to the Parametric Analysis of a PCM Energy Storage System Journal of Physics: Conference Series, Volume 796, 34th UIT Heat Transfer Conference 2016 4–6 July 2016, Ferrara, Italy

[22]. Xiang-Qi Wang Arun S.Mujumdar,A parametric study of phase change material (PCM)-based heat sinks International Journal of Thermal Sciences Volume 47, Issue 8, August 2008, Pages 1055-1068

[23]. Mengmeng Zhao The usage of phase change materials in firefighter protective clothing: its effect on thermal protection IOP Conference Series: Materials Science and Engineering, Volume 274, 1st International Conference on Frontiers of Materials Synthesis and Processing (FMSP 2017) 28–29 October 2017, Changsha, China

[24]. Ahmed, M., Meade, O., & Medina, M. A. (2010, March). Reducing heat transfer across the insulated walls of refrigerated truck trailers by the application of phase change materials. Energy Conversion and Management, 51, 383-392. doi: 10.1016/j.enconman.2009.09.003

[25]. M. Irsyad and Harmen Heat transfer characteristics of coconut oil as phase change material to room cooling application IOP Conference Series: Earth and Environmental Science, Volume 60, 1st International Symposium on Green Technology for Value Chains 2016 3–5 October 2016, Tangerang, Indonesia

[26]. Ozan M Balci , Mehmet A Ezan ,Kutbettin Z Turhan A heat recovery unit with phase change material for combi-boilers 29 July 2019 Energy Storage Volume 1, Issue 5 ee81 https://doi.org/10.1002/est2.81 Retrieved from https://onlinelibrary.wiley.com/doi/full/10.1002/est2.81

[27]. Dong Mao Ye Research on PCM Textiles with Material Properties in Sports Wear Application Advanced Materials Research March, 2014 Retrieved from www.scientific.net/AMR.910.450
[28]. https://www.textileworld.com/textile-world/features/2004/03/phase-change-materials/
[29]. Rohitash Kumar,Vyas S.,Ravindra Kumar ,Dixit A. Development of sodium acetate trihydrate-ethylene glycol composite phase change materials with enhanced thermophysical properties for thermal comfort and therapeutic applications Scientific Reports volume 7, Article number: 5203 (2017) Retrieved from https://www.nature.com/articles/s41598-017-05310-3
[30]. Phase change materials for thermal energy storage Climate technology Centre and network CTCN Retrieved from https://www.ctc-n.org/technologies/phase-change-materials-thermal-energy-storage
[31]. Vasu, Anusuiah ,Hagos, Ftwi Y.,Noor, M.M.,Mamat, R.,Azmi, W.H.,Abdullah, Abdul A.,Ibrahim, Thamir Corrosion effect of phase change materials in solar thermal energy storage application September 2017 Renewable and Sustainable Energy Reviews 76:19-33 Retrieved from https://ideas.repec.org/a/eee/rensus/v76y2017icp19-33.html
[32]. P. Blanco-Rodríguez, J. Rodríguez-Aseguinolaza,A. Gil,E. Risueño,B. D'Aguanno,I. Loroño,L. Martín Experiments on a lab scale TES unit using eutectic metal alloy as PCM Materials engineering,2015 Retrieved from https://cyberleninka.org/article/n/535963/viewer
[33]. E. Risueño,A. Faik, J.Rodríguez - Aseguinolaza,P.Blanco-Rodríguez, A. Gil,M. Tello,B. D'Aguanno, Mg-Zn-Al eutectic alloys as phase change material for latent Heat thermal energy storage Materials engineering,2015 Retrieved from https://cyberleninka.org/article/n/535963
[34]. N. Gokon,S.Nakamura, T.Yamaguchi ,T. Kodama Cyclic properties of thermal storage /discharge for Al-Si alloy in vacuum for solar thermochemical fuel production Materials engineering ,2015 Retrieved from https://cyberleninka.org/article/n/528391

International Virtual Conference on Materials and Nanotechnology
In Association with International Journal of Scientific Research in Science and Technology
Volume 9 | Issue 4 | Print ISSN: 2395-6011 | Online ISSN: 2395-602X (www.ijsrst.com)

A Floristic Survey of Dicotyledonous Plants from Guru Nanak College of Science, Ballarpur Campus Dist. Chandrapur (Maharashtra) India

S. S. Dudhe*, P. D. Khirade, N. S. Dudhe
Department of Botany, Guru Nanak College of Science Ballarpur, District Chandrapur- 442701, Maharashtra, India

ABSTRACT

Plant taxonomy dominates the field of botanical activity. Today the plant taxonomist is interested in the problem associated with the distribution of the plants. Knowledge of plant distribution is relevant to the determination of geographic areas. Accurate and timely information on the floristic composition is of importance in judging status of the forest and availability of plant resources. In present investigation floristic survey of dicotyledonous plants from Guru Nanak College of Science, Ballarpur campus in various seasons time to time was carried out. During exploration about 2.5 hectors of college campus was surveyed. Total 184 dicotyledonous flowering plant species were documented which include 31 trees, 104 herbs, 32 shrubs, 03 aquatic herb, 13 climbers and 01 parasite belonging to 51 families. Such survey would be of great help to students for making inventory of useful species, habitat, characteristics, and identification of potential species for various dissertation works of post graduate students of the college.

Keywords : Floristic Survey, Dicotyledonous Plants, Diversity, Ballarpur, Chandrapur

I. INTRODUCTION

Human plants associations seem to have had its origin way back in the history of human's civilization. Human life is intricately linked with species of plants and animals. Our foods, cloths, buildings and shelter materials, medicines etc. are all derived from it. Biodiversity is functionally important as it provides insurance against large changes in ecosystem processes and may enhance the efficiency of resource utilization. The addition and deletion of species from an ecosystem will change both the species richness and evenness (Pielou, 1975). Biodiversity loss is carried out due to various anthropogenic activities and by nature in the form of high rainfall, low rainfall and lightening. So it is urgent need to conserve plants by planning and management of natural resources. Before going to conserve one must have an idea about the threats to biodiversity. The main threats are degradation, fragmentation and habitat loss of indigenous plants, spreading of invasive/alien species, unsustainable use and misuse of natural resources, global climate change etc. (Joseph Wanjui, 2009). Floristic diversity is of fundamental importance for human society, adverse consequences of biodiversity loss to ecosystem possess have led ecologist and society to appreciate the need of maintaining diversity. Taxonomy is a dynamic science correlated with numerous wings of life sciences which deals with the study of the plants in regards with collection,

identification, classification of the taxa. Survey and collection of the plants from the area under investigation was done by the standard method like collection of the flowering plants with least flowering or fruiting which will be helpful for easy identification and comparing the taxa with available floras.

Before understanding the relation between ecology and biodiversity, it is importance to learn about taxonomic plant diversity, the documenting of plant diversity of country, state and city. Keeping this view in mind we have embarked on the task of compiling and documenting the diversity of college campus time to time and season to season in the former sense that is individual species in the area. In this survey we have focused only on dicotyledonous flowering plants of the campus. Although the lower group of plants like algae, bryophyta, pteridophyta and from the higher group gymnosperm form a important part of vegetation and contribute significantly to the floristic diversity, they have been excluded in the present discussion.

II. STUDY AREA

The present investigation was conducted in Guru Nanak College of Science, Ballarpur campus Ballarpur district Chandrapur of Maharashtra state (Map 1 & 2). It is situated at 19^{0}50'N and 79^{0}21'E. The area comes under the sub-tropical climatic condition with sufficient rain fall in the monsoon, summer is comparatively dry and hot, maximum temperature exceed 46^0 C and lows during the winter season are around 27 to 30^{0}C.

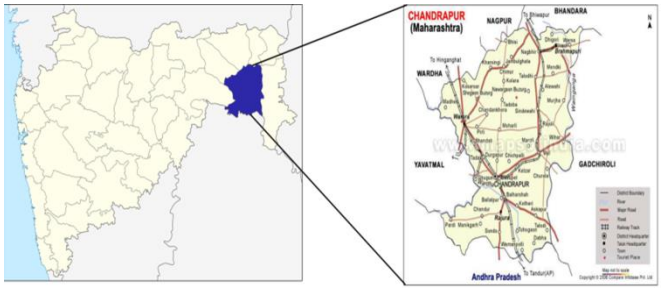

Map 1: Chandrapur a district in the state of Maharashtra

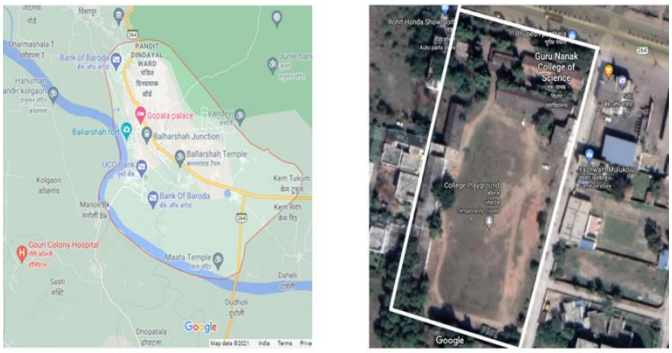

Map 2: Ballarpur City and G. N. College campus

III. MATERIAL AND METHODS

The present study was undertaken at college campus area of Guru Nanak College of Science in Ballarpur tahsil of Chandrapur district. The town is served by Ballarshah junction railway station and the city has a good number of migratory populations resulting in a rich diversity of vascular plants. The college is located on east side of the city which is famous for quality education having well equipped laboratories, sufficient playground, gardens situated over the 2.5 hectors of a piece of land. (Ballarpur city Wikipedia, 2013, http://en.m.wikipedia.org/wiki/ballarpur)

Plants were observed during all season of the year. Data of plant specimens entered into the computer and field diary record was based on plant specimens collected from their natural habitat. Collected specimen was processed using usual taxonomic methods of drying and mounting.

After identification of specimen with the help of floras and available literature, list of species was prepared by referring like Flora of Maharashtra, vol. I - IV (Almeida, 1998-2003), Flora of Chandrapur and Gadchiroli district (Moghe, 1992), Flora of Maharashtra State Vol. I (Singh & Kartikeyan, 2000), Flora of Maharashtra State vol. II (Singh et al., 2001) and Digital database of some dicot plants of Chandrapur district (Dudhe, 2017). Processed plants specimens have been preserved in the herbarium at Department of Botany, Guru Nanak College of Science Ballarpur.

IV. RESULT AND DISCUSSION

Floristic diversity of the college campus area is the total of the dicotyledonous herbs, shrubs and trees plant species within it (Table 1). Total 184 dicotyledonous plant species belonging to different 51 families were recorded in which 31 were trees, 104 herbs, 32 shrubs, 03 aquatic herb, 13 climbers and 01 parasite (Fig.1).

Euphorbiaceae was found as dominating family with 18 species, Asteraceae represented by 17 species with second largest number. Followed by Fabaceae 14 species, 10 species of Acanthaceae and 7 species each from Mimosaceae and Caesalpiniaceae family were recorded.

Table 1: Species of Guru Nanak College of Science Ballarpur campus area

Sr. No.	Name of the species	Family	Habit
1	Annona squamosa L.	Annonaceae	Tree
2	Polyalthia longifolia (Sonner.) Thw.	Annonaceae	Tree
3	Cocculus hirsutus (L.) Diels.	Menispermaceae	Climber
4	Tinospora glabra Brum. f.	Menispermaceae	Climber
5	Nymphaea nauchali Burm.f.	Nympheaceae	Aquatic herb
6	Nymphaea pubescens Willd.	Nympheaceae	Aquatic herb
7	Argemone mexicana L.	Papaveraceae	Herb
8	Brassica juncea L.	Brassicaceae	Herb
9	Cleome viscosa L.	Cleomaceae	Herb
10	Hybanthus enneasperma (L.)Muell	Violaceae	Herb
11	• Polygala arvensis Willd.	Polygalaceae	Herb
12	Dianthus chinensis L.	Caryophyllaceae	Herb
13	Portulaca oleracea L.	Portulaceae	Herb
14	Abutilon indicum (L.) Sweet.	Malvaceae	Herb
15	Hibiscus rosa-sinensis L.	Malvaceae	Herb
16	Malachra capitata L.	Malvaceae	Herb
17	Malvastrum coromandelianum L.	Malvaceae	Herb
18	Sida acuta Burm.f.	Malvaceae	Herb
19	Sida cordata (Burm.f.) Borss.	Malvaceae	Herb
20	Sida cordifolia L.	Malvaceae	Herb
21	Sida rhombifolia L. var. retusa(Linn.)	Malvaceae	Herb
22	Thespetia populnea (L.) Soland. ex Corr.	Malvaceae	Tree
23	Melochia corchorifolia L.	Sterculiaceae	Herb
24	Corchorus aestuans L.	Tiliaceae	Herb
25	Triumfetta pentandra A.Rich.	Tiliaceae	Herb
26	Biophytum sensitivum (L.) DC.	Oxalidaceae	Herb
27	Oxalis corniculata L.	Oxalidaceae	Herb
28	Impatiens balsamina L. var.balsamina	Balsaminaceae	Herb
29	Citrus aurantifolia (Christ.) Swingle.	Rutaceae	Shrub
30	Murraya koenigii (L.) Spreng.	Rutaceae	Shrub
31	Murrya paniculata (L.) Jack.	Rutaceae	Shrub

32	Azadirachta indica Juss.	Meliaceae	Tree
33	Melia azedarach L.	Meliaceae	Tree
34	Ziziphus mauritiana Lamk.	Rhamnaceae	Tree
35	Cayratia trifolia (L.) Domin	Vitaceae	Climber
36	Abrus precatorius.L.	Fabaceae	Climber
37	Butea monosperma (Lamk.) Taub.	Fabaceae	Tree
38	Crotalaria prostrata Willd.	Fabaceae	Herb
39	Crotalaria verrucosa L.	Fabaceae	Shrub
40	Dalbergia sisoo Roxb.ex DC.	Fabaceae	Tree
41	Derris indica (Lamk.)Bennett	Fabaceae	Tree
42	Desmodium triflorum (Linn.) DC.	Fabaceae	Herb
43	Goniogyna hirta (Willd.) Ali.	Fabaceae	Herb
44	Indigofera linifolia (Linn.f.) Retz.var.linifolia	Fabaceae	Herb
45	Indigofera linifolia Retz.var. campbellii Wight ex Baker	Fabaceae	Herb
46	Tephrosia purpurea (Linn.) Pers.	Fabaceae	Herb
47	Tephrosia villosa (Linn.) Pers.	Fabaceae	Herb
48	Teramnus labialis (Linn.f.)Spreng.	Fabaceae	Climber
49	Vigna trilobata (Linn.) Verdcourt	Fabaceae	Climber
50	Cassia alata Linn.	Caesalpiniaceae	Shrub
51	Cassia occidentalis Linn.	Caesalpiniaceae	Shrub
52	Cassia siamea Lamk.	Caesalpiniaceae	Tree
53	Cassia tora L.	Caesalpiniaceae	Herb
54	Cassia uniflora Mill.	Caesalpiniaceae	Herb
55	Delonix regia (Boj.) Raf.	Caesalpiniaceae	Tree
5661	Peltophorum pterocarpum Baker.	Caesalpiniaceae	Tree
57	Acacia nilotica var.indica Benth.	Mimosaceae	Tree
58	Leucaena leucocephala (Lamk.) De Wit.	Mimosaceae	Tree
59	Neptunia triquetra Benth.	Mimosaceae	Herb
60	Pithecellobium dulce (Roxb.) Benth.	Mimosaceae	Tree
61	Prosopis chilensis (Molina.)Stunz.	Mimosaceae	Shrub
62	Samanea saman (Jacq.) Merrill	Mimosaceae	Tree
63	Quisqualis indica L.	Combretaceae	Climber
64	Terminalia catappa LInn.	Combretaceae	Tree
65	Callistemon citrinus (Curtis) Skeels	Myrtaceae	Tree
66	Eucalyptus citriodora Hook.f.	Myrtaceae	Tree
67	Psidium guajava Linn.	Myrtaceae	Tree
68	Syzygium cumini (Linn.) Skeels.	Myrtaceae	Tree
69	Ammania baccifera L.	Lytheraceae	Herb
70	Ammania baccifera L.var. aegyptiaca (Willd.) Koehne.	Lytheraceae	Herb
71	Lawsonia inermis Linn.	Lytheraceae	Shrub
72	Ludwigia hyssopifolia G.Don	Onagraceae	Herb

73	Ludwigia perennis Linn.	Onagraceae	Herb
74	Turneria ulmifolia var.ulmifolia Linn.	Turneraceae	Herb
75	Carica papaya Linn.,	Caricaceae	Tree
76	Benincasa hispida (Thunb.) Cogn.	Cucurbitaceae	Climber
77	Lagenaria siceraria (Molina) Standl.	Cucurbitaceae	Climber
78	Mukia maderaspatana (Linn) Roem.	Cucurbitaceae	Climber
79	Trichosanthes cucumerina Linn.	Cucurbitaceae	Climber
80	Glinus oppositifolia (L.) DC.	Molluginaceae	Herb
81	Mollugo nudicaulis Lamk.	Molluginaceae	Herb
82	Mollugo pentaphyla Linn.	Molluginaceae	Herb
83	Triathema portulacastrum L.	Aizoaceae	Herb
84	Borreria articularis (Linn.)Will.	Rubiaceae	Herb
85	Borreria pusilla (Wall.) DC.	Rubiaceae	Herb
86	Ixora coccinea Linn.	Rubiaceae	Shrub
87	Oldenlandia corymbosa Linn.	Rubiaceae	Herb
88	Blumea lacera (Burm.f.) DC.	Asteraceae	Herb
89	Blumea eriantha DC.	Asteraceae	Herb
90	Caesulia axillaria Roxb.	Asteraceae	Herb
91	Cosmos artemisifolia (Jacq.) Almeida (comb.nov.)	Asteraceae	Herb
92	Lagascea mollis Cav.	Asteraceae	Herb
93	Launea sarmentosa (Willd.) Sch.-Bip. ex O.Kuntze	Asteraceae	Herb
94	Pentanema indicum (Linn.) Ling	Asteraceae	Herb
95	Parthenium hysterophorus Linn.	Asteraceae	Herb
96	Sphaeranthus indicus Linn.	Asteraceae	Herb
97	Spilanthes paniculata DC.	Asteraceae	Herb
98	Synedrella nodiflora (Linn.) Gaertn.	Asteraceae	Herb
99	Synedrella vialis (Less.) Gray.	Asteraceae	Herb
100	Tagetus erecta Linn.	Asteraceae	Shrub
101	Tagetes patula L.	Asteraceae	Shrub
102	Tagetes tenuifolia Cav.	Asteraceae	Shrub
103	Tridax procumbens L.	Asteraceae	Herb
104	Xanthium strumarium L.	Asteraceae	Shrub
105	Mimusops elengi Linn.	Sapotaceae	Tree
106	Jasminum hirsutum Linn.	Oleaceae	Shrub
107	Alstonia scholaris (Linn.) R.Br.	Apocynaceae	Tree
108	Catharanthus roseus (Linn.) G. Don.	Apocynaceae	Herb
109	Nerium indicum Mill.	Apocynaceae	Shrub
110	Rauwolfia tetraphylla Linn.	Apocynaceae	Herb
111	Thevetia peruviana Pers	Apocynaceae	Shrub
112	Calotropis gigantea Willd.	Asclepiadaceae	Shrub
113	Calotropis procera Willd.	Asclepiadaceae	Shrub

114	Dregea volubilis (Linn.f.) Benth. ex Hook.f.	Asclepiadaceae	Climber
115	Heliotropium indicum L.	Boraginaceae	Herb
116	Heliotropium ovalifolium Forsk.	Boraginaceae	Herb
117	Trichodesma indicum (Linn.) Lehm.	Boraginaceae	Herb
118	Trichodesma zeylanicum (Jacq.) R.Br.	Boraginaceae	Herb
119	Cuscuta chinensis Lamk.	Cuscutaceae	Parasite
120	Evolvulus alsinoides Linn.	Convolvulaceae	Herb
121	Evolvulus nummularius Linn.	Convolvulaceae	Herb
122	Ipomoea fistulosa Mart.ex Choisy	Convolvulaceae	Shrub
123	Ipomoea hederifolia Linn.	Convolvulaceae	Climber
124	Ipomoea obscura L.	Convolvulaceae	Climber
125	Merremia hederacea (Burm.f.) Hall. f.	Convolvulaceae	Climber
126	Datura inoxia Mill.	Solanaceae	Shrub
127	Withania somnifera (Linn.) Dunal	Solanaceae	Shrub
128	Lindernia ciliata (Colsm.) Penn.	Scrophulariaceae	Herb
129	Lindernia crustacea (L.) F.V.Muell.	Scrophulariaceae	Herb
130	Mecardonia procumbens (Miller.) Small	Scrophulariaceae	Herb
131	Scoparia dulcis Linn.	Scrophulariaceae	Herb
132	Sopubia delphinifolia (Linn.)G.Don.	Scrophulariaceae	Herb
133	Stemodia viscosa Roxb.	Scrophulariaceae	Herb
134	Striga angustifolia (D.Dan)Saldanha.	Scrophulariaceae	Herb
135	Oroxylum indicum (Linn.)Vent.	Bignoniaceae	Tree
136	Tecoma stans (L.) Juss.	Bignoniaceae	Tree
137	Andrographis paniculata (Burm.f.) Wall.	Acanthaceae	Herb
138	Asystasia gangetica (Linn.) T.Anders.	Acanthaceae	Herb
139	Erianthera echioides (L.)Almeida	Acanthaceae	Herb
140	Hygrophila schulli (Buch.Ham.) Almeida & Almeida	Acanthaceae	Herb
141	Justicia adhatoda Linn.	Acanthaceae	Shrub
142	Lepidagathis trinervia Wall.	Acanthaceae	Herb
143	Peristrophe paniculata (Forsk.) Brummitt.	Acanthaceae	Shrub
144	Ruellia tuberosa Linn.	Acanthaceae	Herb
145	Rungia pectinata (Linn.) Nees,	Acanthaceae	Herb
146	Rungia repens (Linn.) Nees.	Acanthaceae	Herb
147	Duranta erecta L.	Verbenaceae	Shrub
148	Gmelina asiatica L.	Verbenaceae	Shrub
149	Lantana indica Roxb.	Verbenaceae	Shrub
150	Phyla nodiflora Linn.	Verbenaceae	Herb
151	Tectona grandis L.f.	Verbenaceae	Tree
152	Hyptis suaveolens L.	Lamiaceae	Herb
153	Leucas aspera (Willd.) Link	Lamiaceae	Herb
154	Leucas cephalotes Spreng.	Lamiaceae	Herb

155	Ocimum americanum auct.	Lamiaceae	Herb
156	Ocimum tenuiflorum Linn.	Lamiaceae	Herb
157	Boerhaavia diffusa Linn.	Nyctaginaceae	Herb
158	Bougainvillea spectabilis Willd.	Nyctaginaceae	Shrub
159	Achyranthes aspera Linn.	Amaranthaceae	Herb
160	Aerva lanata (Linn.) Juss.	Amaranthaceae	Herb
161	Amaranthus spinosus Linn.	Amaranthaceae	Herb
162	Acalypha fruticosa Forsk.	Euphorbiaceae	Herb
163	Acalypha indica Linn.	Euphorbiaceae	Herb
164	Acalypha lanceolata Willd.	Euphorbiaceae	Herb
165	Croton bonaplandianus Baill.	Euphorbiaceae	Herb
166	Euphorbia chamaesyce L.	Euphorbiaceae	Herb
167	Euphorbia erythroclada Boiss. in DC.,	Euphorbiaceae	Herb
168	Euphorbia hirta Linn.	Euphorbiaceae	Herb
169	Euphorbia thymifolia Linn.	Euphorbiaceae	Herb
170	Jatropha gossypifolia Linn.	Euphorbiaceae	Shrub
171	Jatropha panduraefolia Andrew.	Euphorbiaceae	Shrub
172	Jatropha podagrica Hook.	Euphorbiaceae	Shrub
173	Kirganelia reticulata Baill.	Euphorbiaceae	Shrub
174	Phyllanthus emblica L.	Euphorbiaceae	Tree
175	Phyllanthus fraternus Webster.	Euphorbiaceae	Herb
176	Phyllanthus maderaspatensis Linn.	Euphorbiaceae	Herb
177	Phyllanthus urinaria L.	Euphorbiaceae	Herb
178	Phyllanthus virgatus Forst.	Euphorbiaceae	Herb
179	Ricinus communis Linn.	Euphorbiaceae	Shrub
180	Artocarpus hetrophyllus Lamk.	Moraceae	Tree
181	Ficus hispida Linn.f.	Moraceae	Shrub
182	Ficus racemosa Linn.	Moraceae	Tree
183	Ficus religiosa Linn.	Moraceae	Tree
184	Pilea microphylla (Linn.) Liebm.	Urticaceae	Herb

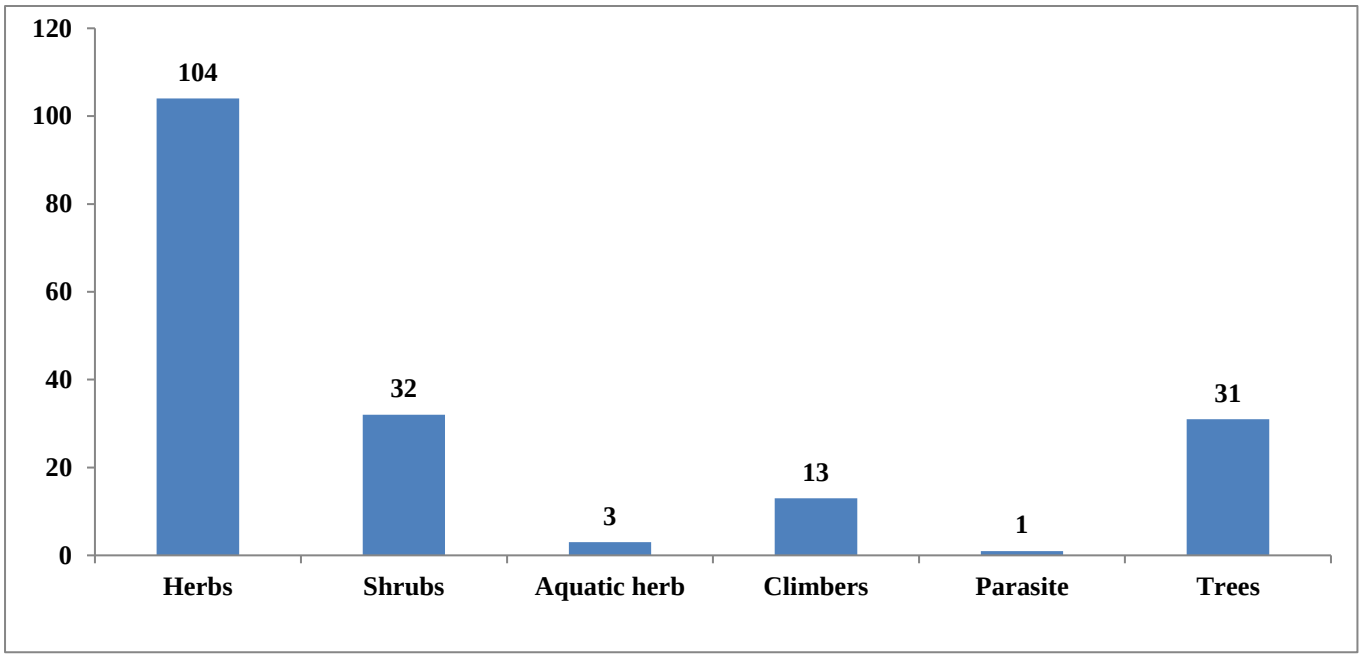

Fig. 1 Life forms of plants of study area

V. ACKNOWLEDGEMENT

The authors are thankful to Management and Principal of Guru Nanak college of Science Ballarpur for providing necessary facilities to carry out the work.

VI. REFERENCES

[1]. Almeida, M. R. 1990. Flora of Sawantwadi, Maharashtra, India. J. Econ. Tax. Bot. Addli. Ser. 22 Vol.

[2]. Almeida, M. R. 1996. Flora of Maharashtra. Vol. I, Orient Press, Mumbai.

[3]. Almeida, M. R. 1998. Flora of Maharashtra. Vol. II, Orient Press, Mumbai.

[4]. Almeida, M. R. 2001. Flora of Maharashtra. Vol.III A-B, Orient Press, Mumbai.

[5]. Almeida, M. R. 2003. Flora of Maharashtra. Vol.IV, Orient Press, Mumbai.

[6]. Ballarpur city Wikipedia, 2013, http://en.m.wikipedia.org/wiki/ballarpur.

[7]. Cooke, T. 1958. The Flora of the Presidency of Bombay, Vol. I-II, Taylor Francis, London; reprinted edition, BSI, Calcutta.

[8]. Dudhe, N. S. 2017. Electronic Herbarium and Digital Database of some Dicot Plants of Chandrapur district. Ph.D. Thesis, Nagpur University,Nagpur.

[9]. Joseph Wanjui 2009, My Native Roots – A Family Story , Colourprint Limited,Nairobi, 299p.

[10]. Moghe, R. P. 1993. Dicot Flora of Chandrapur Forest Division of Vidarbha Region of Maharashtra State. Ph.D. Thesis, Nagpur University, Nagpur.

[11]. Pielou, E.C. 1975 , Ecological Diversity – John Wiley and Sons, New York, 165p.

[12]. Singh, N.P.,Lakshminarasimhan,P.,Karthikeyan,S.and Prasanna, P.V. 2001. Flora of Maharashtra State: Dicotyledons. Vol.2, BSI, Calcutta.

[13]. Singh,N.P. and Karthikeyan,S. 2000. Flora of Maharashtra State:Dicotyledons. Vol.1. BSI, Calcutta.

International Virtual Conference on Materials and Nanotechnology
In Association with International Journal of Scientific Research in Science and Technology
Volume 9 | Issue 4 | Print ISSN: 2395-6011 | Online ISSN: 2395-602X (www.ijsrst.com)

The Cloud-Based Health Tracking and Monitoring System with AWS

Vaishnavi Raosaheb Thoke*1, Prof. Prachi V. Kale*2
*1Department of Computer Science & Engineering, P. R. Pote (Patil) College of Engineering & Management, Amravati-444605, Maharashtra, India
2Professor, Department of Computer Science & Engineering, P. R. Pote (Patil) College of Engineering & Management, Amravati-444605, Maharashtra, India

ABSTRACT

Medical care has a basic situation in living souls particularly for the individuals who have some medical conditions and need a down to earth answer for a superior life. As of late, there is a quick ascent in e-wellbeing advances, for example, Electronic Health Records (EHRs) and some crisis location and reaction strategies for that used AWS cloud for storing and retrieving managing records. One of the advances that can deal with a portion of the difficulties of shrewd medical care as far as security, sharing, files for avoid data leakages and illegal access help of encryption and description algorithm addition security are digital signature. The motivation behind this article is to feature the estimation of inescapable processing, particularly cloud-based frameworks in medical services area. We survey the importance and chances of AWS Services in inescapable medical services.

Keywords : Cloud Computing, Smart Healthcare, E-health, multi-key search, AWS, DES3.

I. INTRODUCTION

Data innovation can assume a principal part in medical care administrations as far as electronic wellbeing. Late advances in e-wellbeing can be predominantly characterized as the use of data and correspondence innovations in medical services frameworks [1]. Utilizing web for putting away, getting to and changing medical services data and digitizing a ton of cycles and assignments that are important strides for realizing e-wellbeing, is a certain interaction. For this situation, we have the benefits of e-wellbeing, for example, improvement in the nature of administrations in maturing social orders; decrease in expense and in clinical blunders and the straight forwardness by which information can be moved to the perfect spot. All things considered, digitizing paper-based records, gathering and putting away clinical data just as absence of appropriate innovation for preventive consideration can turn out to be somewhat testing. For that used as an AWS (Amazon Web Services) is a subsidiary of Amazon providing on-demand cloud computing platforms and APIs to individuals as well as companies.

COVID-19 affects different people in different ways. Most infected people will develop mild to moderate illness and recover without hospitalization. The first

known infections from SARS-CoV-2 were discovered in Wuhan, China and within year its get spread all over glob these is because many factor but among those are not proper medicinal treatment. Experts believe the virus that causes COVID-19 spreads mainly from person to person for avoid that scenario that patient and doctor without getting physical involved to get best treatment and with proper time span is "Smart healthcare systems on improving the efficiency of healthcare services".

The Cloud market is growing rapidly and has accepted AWS to a great extent in recent years. AWS package has been turned as a huge revenue earner for Amazon as it is being used by most of the companies worldwide for migrating applications over cloud. For Assibilate and security as well many aspect cloud (AWS) is best solution:

- AWS is an Ease of Use, Incredibly Diverse Array of Tools, Unlimited Server Capacity, and Reliable Encryption & Security.
- To provide the Hospital (patient need-preference), e-Blood Bank and Patient Profile(file, daily report) applications to hospitals
- To provide online patient portal for delivery of citizen centric services like online appointment booking, access to lab reports online and blood availability status.

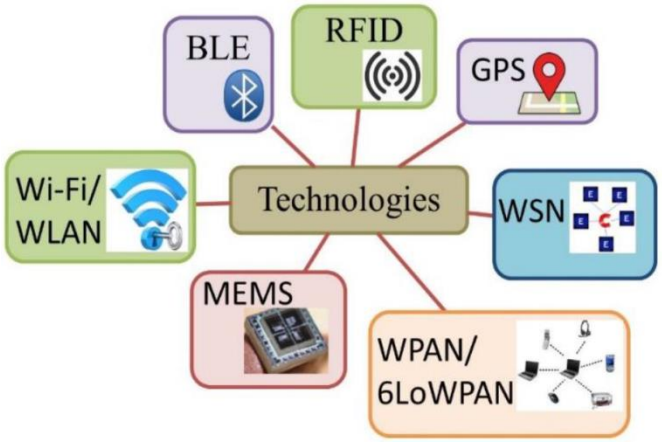

FIGURE 1. Different Technologies used to Deploy Smart Healthcare

Cloud-based healthcare system is build a consumer-focused integrated primary health care system; Improve access and reduce inequity; Increase the focus on health promotion and prevention. In health care System we design Cloud and Admin Module screening that maintain Doctor and Patient record information and other some operation to achieve quality, safety, performance and accountability. For example the heart disease core reasons are many but most affective are physical fitness; low or high cholesterol level vary blood pressure that not affect daily routine but cause major problem after average time such as heart attack, to avoid such scenarios that uses cloud computing to treat, manage and control patients. The systems are supported and consisted of different algorithms such as Authentication Algorithms (the process or action of verifying the identity of a patient or process.)For patient record safety and cloud infrastructures (AWS) for store patient data/record, smart devices, and sensors and initiate different service types according to their context and environment.

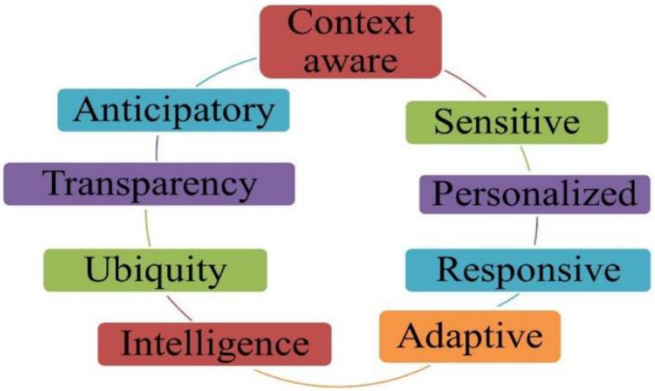

FIGURE 2: Characteristics of Smart Healthcare.

II. LITERATURE SURVEY

A. Cloud Computing (CC)

There are many recent new technologies including mobile computing [1] [2], Cloud Computing, and wireless communications changed people lives

everywhere the world and made it easier [3][4]. The concept of Cloud Computing (CC) relies on a network-based resource sharing to extend resource availability and reduce financial and management costs [5].

There are several examples for emerging Cloud computing infrastructures/ platforms like Microsoft Azure, Amazon EC2, Google App Engine, and Aneka [6]. Cloud Computing utilizes a good range of various computing technologies, and involves distributed systems, virtualization, storage, networking, security, management and automation, service oriented architecture (SOA), and service-level agreement (SLA). Furthermore, CC helps companies improve the IT services, develop applications to realize unlimited scalability and automaticity on demand services of the IT infrastructure, and increase their revenues.

There are many advantages for adopting the cloud environment like [5]: Storage, Backup and Recovery: Location Flexibility: Time Efficiency and price saving.

B. Mobile Cloud Computing

The development and therefore the spread of mobile devices allow the users to profit from wide selection of useful services and mobile applications at any time and from anywhere within the world. People use mobile devices to accomplish sort of daily tasks like online shopping, business management, educating and also health monitoring.

Mobile Cloud Computing (MCC) integrates mobile devices to utilize the cloud unlimited service and to enable information access for mobile devices users [7]. The Cloud Computing depends on network-connected resources pooled to maximise their utilization leading to reduced management and capital costs. Many sectors can enjoy MCC including the cloud-healthcare system. As an example, there's a MCC healthcare system that was built to watch and analyse real time biomedical signals (such as ECG) for users in multiple locations. A customized healthcare application is installed on the mobile device, and health data are being synchronized into the healthcare cloud computing service to be stored and analysed [8].

There are many limitations facing portable mobile device that prevent taking advantage of their portability feature in many sectors including the healthcare. First, portable devices are restricted by their short battery lifetime, computational and storage capacity, which prevents them from performing complicated tasks, computation-intensive applications, and image processing, in social networking and organize meeting. Second, portable devices are operated on heterogeneous wireless networks, which cause the difference of network bandwidth capacity and communication quality; device mobility further affects the network connectivity and cloud resource availability [9]. In other words, MCC increases the capabilities of the mobile devices and overcomes their limitations, therefore the users won't worry about the specified CPU power and memory size to run intensive tasks.

To mitigate the requirements of mobile devices in computing capacity and resources, the mobile cloud computing (MCC) paradigm allows the computing, data storage and mass information science be offloaded to the cloud platform for enhancing the reliability and availability of services while minimizing the energy and computational requirements in mobile devices [10].

There are other challenges associated with storing data on the cloud, essentially is about data privacy and deny unauthorized access and malicious attacks. The supply of the owners' data in the least times for any request is challenge. Also, the integrity of the info and stop alternation or modification on the info by intruders is another issue. These information security concerns might be solved by using cryptographic techniques [11].

Although all the good features of the MCC, the MCC faces some challenges like the delay between the mobile device request and cloud service response especially when there's a far distance between the

cloud and therefore the mobile device. Also, there are inherited challenges of wireless network like variable data rates and fewer throughputs.

A cloudlet may be a recent concept that would be considered an answer for a few of the challenges facing the normal mobile cloud computing model. A cloudlet is little resource rich equipped cloud to be placed between the enterprise cloud and therefore the mobile device, to scale back the connection latencies and mobile power consumption [12]. The subsequent section highlights the cloudlet concept.

C. Cloudlet

The cloudlet's concept may be a closer cloud with many advantages and capabilities to avoid several limitations of the remote cloud. It's believed that the cloudlet scheme which is taken into account as a middle stage between the enterprise cloud and therefore the mobile device has a superb chance to beat the challenges related to MCC like power consumption and latencies [8].

But, in some cases, the mobile user has got to connect on to the EC even when it's connected to the cloudlet. This happens when:

The mobile device must update files stored within the Enterprise Cloud. So, the mobile device sends the request for the precise file, then the file is going to be downloaded from the EC to the Cloudlet, and therefore the mobile device can process it.

Requesting specific services that aren't available within the Cloudlet. Motivated by the cloudlet concept, the authors in [12] proposed a mobile cloud system for university applications.

Their system uses different sensors to hold out many tasks. They introduced and implemented two main applications in traffic management and fire detection inside a university whereas the info from sensors is processed within the mobile cloud system.

In the same context, the researcher in [8] introduced an efficient cloudlet MCC model during which the mobile users communicate on to the cloudlet rather than the enterprise cloud. Their model is applicable in many environments including hospitals were saving and processing big amounts of knowledge. There's a replacement concept of massive Data that's associated with the large amounts of stored/obtained data thanks to the advances in several technologies including cloud computing, social media, and wireless communication [13].

On the opposite hand, processing of massive amount of knowledge might be offline or real-time operation of some applications like healthcare applications where the info analysis and extracting the proper decisions make a difference between patient's life and death [14]. Figure 2 shows a general plot for the thought of using Mobile cloud computing for healthcare big data applications [15]. During this MCC model, the cloudlets are placed nearby the hospital and canopy a neighbourhood which will be accessed by authorized people that can access the patients' information and monitor their status remotely.

D. Cloud-based Healthcare Systems

The healthcare sector and usually many other areas like transportation, finance industry, etc. have skilled a rapid climb recently thanks to the exponential growth in ICT.

The increasing role and benefits of ICT in healthcare are getting visible within the enhancement and emergence of technologies like health informatics, epidemiology, bioengineering and Healthcare Information Systems (HIS). we will now imagine a near future where healthcare providers can port powerful analytics and decision support tools to mobile computing devices (smartphones, tablets, laptops, etc.) aiding clinicians at the purpose of care helping them with synthesis of knowledge from multiple sources, optimization of clinical workflows, and context-aware deciding . the gang sourcing technologies also are coming to healthcare augmenting people in their deciding processes for his

or her wellbeing though the complexity of such a setting in healthcare domain, including appropriate models (reimbursement, who holds the liability), are posing challenges [16].

Aminian and Naji (2013) [17] propose a hospital healthcare monitoring system supported wireless sensor networks. Specifically, the monitoring system monitors physiological parameters from multiple patient bodies through a coordinator node attached to the patient's body that collects the signals from the wireless sensors and sends them to the bottom station. A presented mobile healthcare application in [18] to manage patient health records and medical images. The mobile application is developed using Android OS. The Amazon's S3 cloud service is employed during this mobile application. Authors in [19] discussed networked healthcare and the way mobile cloud computing could enable it. They presented the motivation and development of networked healthcare applications with the adoption of cloud computing. They described a usable cloudlet-based mobile cloud-computing infrastructure for dedicated healthcare applications. They utilized the cloud model in building fall detection system for elderly people.

In [20], the authors discussed EHR sharing and integration in healthcare clouds and related concepts. They analyzed the critical security and privacy issues in EHRs accessing and managing. An EHR security reference model was described to manage healthcare cloud security issues. They presented HER security reference model through a use-case scenario and described the corresponding security countermeasures and state of the art of applicable security techniques which will be primary security guards.

As an infrastructure for assistive healthcare, the Mobile Cloud for Assistive Healthcare (MoCAsH) is proposed in [21]. MoCAsH deployed intelligent mobile agents, context-aware middleware, and collaborative protocol for efficient resource sharing. MoCAsH deployed P2P paradigm to federate cloud to manage security issues like data protecting and data ownership preserving.

Authors in [22] proposed a framework for secure health data system supported big data analytics in mobile cloud computing environment. This framework provides a high level of integration, availability, interoperability, and sharing of healthcare data among healthcare stakeholders. Thanks to the huge size of healthcare data and therefore the complexity of healthcare data types, the proposed framework employs big data analytics to assist physicians take critical decision at the proper time.

The authors in [23] proposed a Real-time face recognition acceleration architecture that integrates mobile devices, cloudlets, and cloud servers. They utilized the features of cloudlet-mobile cloud model and developed Cloud-Vision system to reinforce the vision related operations. Their results showed improvements in real-time face recognition by reducing the reaction time during face recognition process.

The authors in [24] proposed a Cloudlet based MCC system getting to reduce the facility consumption and therefore the network delay while using MCC. The MCC concepts are merged with the proposed Cloudlet framework and propose a replacement framework for the MCC model. The author of [25] presented an efficient software based mobile cloud computing which will be utilized in many useful different applications including: education and healthcare.

A Scalable Cloudlet-based Mobile Computing Model is proposed in [26]. The model utilizes the scalability feature where the number of deployed cloudlets can be adjusted based on the design requirements and the number of users in the region to be covered. The authors in [27] proposed a solution to automate patients' vital data collection by using sensors attached to existing medical equipment. These data are transformed to cloud for processing. The authors

in [28] proposed a framework for the unified middleware over heterogeneous networks.

III.CONCLUSION

There are also a lack of research on the various issues of this area as in recent studies showed. Generally speaking, cloud-based pervasive healthcare is a new paradigm in healthcare sector and has many potential and beneficial features, but there are still several problems and challenges that need to be addressed by researchers in the future. These can be summarized into the following open research directions that should be focused upon in the future:

- As we described above, there are various service types in healthcare sector, such as monitoring, daily life assistance, medical assistance, pervasive access, emergency management and smart hospital. Designing a functional healthcare system for managing emergency situations or assisting medical cares is very important.
- Access to private context types like patient medical information by illegal persons should be banned. Security and privacy for sharing health records and access rights for both patients and professionals are other essential issues.

IV. REFERENCES

[1]. Susmit Paul, Asmita Sharma, "Concept of Wireless Sensor AD-HOC Network Focusing on Mobile Computing," ISTP Journal of Research in Electrical and Electronics Engineering (ISTP-JREEE) 1st International Conference on Research in Science, Engineering & Management (IOCRSEM 2014), 2014, pp. 137-147.

[2]. Amit Kumar, Dr. Yunfei Liu, Dr. Jyotsna Sengupta, Divya." Evolution of Mobile Wireless Communication Networks: 1G to 4G," International Journal of Electronics & Communication Technology, 2010, pp.68-72. Doi: 0910/101/124.

[3]. Zimmerman, James B., "Mobile Computing: Characteristics, Business benefits, and the mobile framework,"University of Maryland European Division-Bowie State 10, 1999.

[4]. N. D. Lane, E. Miluzzo, H. Lu, D. Peebles, and A. T. Campbell, "A survey of mobile phone sensing'' IEEE Commun. Mag., vol. 48, no. 9, pp. 140_150, Sep. 2010.

[5]. P. Mell and T. Grance, "The NIST Definition of Cloud Computing" Recommendations of the National Institute of Standards and Technology (Technical Report No. Gaithersburg, MD, USA: NIST, 2011.

[6]. Copeland, Marshall, Julian Soh, Anthony Puca, Mike Manning, and David Gollob. "Microsoft azure and cloud computing." In Microsoft Azure, pp. 3-26. Apress, Berkeley, CA, 2015.

[7]. Bahwaireth, Khadijah, and Lo'ai Tawalbeh. "Cooperative models in cloud and mobile cloud computing." InTelecommunications (ICT), 2016 23rd International Conference on, pp. 1-4. IEEE, 2016.

[8]. Lo'ai, A. Tawalbeh, Waseem Bakhader, Rashid Mehmood, and Houbing Song. "Cloudlet-based mobile cloud computing for healthcare 2016 IEEE, pp. 1-6. IEEE, 2016.

[9]. Tawalbeh, Lo'ai, Norah Alassaf, Waseem Bakheder, and Alaa Tawalbeh. "Resilience Mobile Cloud Computing: Features, Applications and Challenges." In e-Learning (econf), 2015 Fifth International Conference on, pp. 280-284. IEEE, 2015.

[10]. Qi, Han, and Abdullah Gani, "Research on mobile cloud computing: Review, trend and perspectives," Digital Information and Communication Technology and it's Applications (DICTAP) 2012 Second International Conference on, Bangkok, 2012, pp. 195-202.

[11]. L. A. Tawalbeh, N. Darwazeh, R. Al-Qassas, F. Dosari, " A Secure Cloud Computing Model based on Data Classification". In the Int.

Workshop on Mobile Cloud Computing Systems, Management, and Security (MCSMS-2015). Procedia Computer Science, Vol.52, pp 1153–1158, UK. June 2015.

[12]. Lo'ai, A. Tawalbeh, and Waseem Bakhader. "A mobile cloud system for different useful applications." In Future Internet of Things and Cloud Workshops (FiCloudW), IEEE International Conference on, pp. 295-298. IEEE, 2016.

[13]. A. Zaslavsky, C. Perera, and D. Georgakopoulos. (2013). ``Sensing as a service and big data.'' [Online]. Available: https://arxiv.org/abs/1301.0159 <Last accessed 18/6/2017>

[14]. M. Chen, S. Mao, and Y. Liu, "Big data: A survey,'' Mobile Netw. Appl., vol. 19, no. 2, pp. 171_209, Apr. 2014.

[15]. L. A. Tawalbeh, W. Bakheder, and H. Song, ``A mobile cloud computing model using the cloudlet scheme for big data applications,'' in Proc. IEEE 1st Int. Conf. Connected Health, Appl., Syst. Eng. Technol. (CHASE), Jun. 2016, pp. 73_77.

[16]. D. Fluckinger, "Pulse Strategic insight for health IT leaders," TechTarget Inc, 2014.

[17]. M. Aminian, "A Hospital Healthcare Monitoring System Using Wireless Sensor Networks," J. Health Med. Inform., vol. 04, no. 02, 2013.

[18]. C. Doukas, T. Pliakas, & I. Maglogiannis "Mobile healthcare information management utilizing Cloud Computing and Android OS". In Engineering in Medicine and Biology Society (EMBC), 2010 Annual International Conference of the IEEE (pp. 1037-1040). IEEE.

[19]. F. Muheidat, Lo'ai Tawalbeh, and H. Tyrer. "Context-Aware, Accurate, and Real Time Fall Detection System for Elderly People". In the proceedings of the 12th IEEE International Conference on Semantic Computing, Jan 31st 2018,Laguna Hills, CA,USA

[20]. Zhang, Rui, and Ling Liu. "Security models and requirements for healthcare application clouds." In Cloud Computing (CLOUD), 2010 IEEE 3rd International Conf. on, pp. 268-275. IEEE, 2010.

[21]. Hoang, Doan B., and Lingfeng Chen. "Mobile cloud for assistive healthcare (MoCAsH)." In Services Computing Conference (APSCC), 2010 IEEE Asia-Pacific, pp. 325-332. IEEE, 2010.

[22]. L. A. Tawalbeh, R. Mehmood, E. Benkhelifa, and H. Song. "Mobile Cloud Computing Model and Big Data Analysis for Healthcare Applications." IEEE Access Journal., Vol 4, pp 6171-6180, Sept 2016.

[23]. T. Soyata, R. Muraleedharan, C. Funai, M. Kwon, and W. Heinzelman, "Cloud-Vision: Real-time face recognition using a mobile-cloudlet cloud acceleration architecture," in 2012 IEEE Symposium on Computers and Communications (ISCC), 2012, pp. 59–66.

[24]. Y. Jararweh, L. Tawalbeh, F. Ababneh, and F. Dosari, "Resource Efficient Mobile Computing Using Cloudlet Infrastructure," in 2013 IEEE Ninth International Conference on Mobile Ad-hoc and Sensor Networks (MSN), 2013, pp. 373–377.

[25]. F. Macias and G. Thomas, "Cloud Computing Advantages in the Public Sector: How Today's Government, Education, and Healthcare Organizations Are Benefiting from Cloud Computing Environments," Cisco Systems, Inc., White Paper, 2011.

[26]. Y. Jararweh, L. Tawalbeh, F. Ababneh, A. Khreishah, and F. Dosari, "Scalable Cloudlet-based Mobile Computing Model," Procedia Comp. Sci.,(34), pp. 434–441, 2014

[27]. C. O. Rolim, , F. L. Koch, C. B. Westphall, J. Werner, A. Fracalossi , & G. S. Salvador. (2010, February). A cloud computing solution for patient's data collection in health care institutions. In eHealth, Telemedicine, and Social Medicine, 2010. ETELEMED'10. Second International Conference on (pp. 95-99). IEEE.

[28]. A. Soomro and R. Schmitt, “A framework for mobile healthcare applications over heterogeneous networks,” in 2011 13th IEEE International Conference on e-Health Networking Applications and Services (Healthcom), 2011, pp. 70–73.

[29]. Bahwaireth, Khadijah, and Lo'ai Tawalbeh. "Cooperative models in cloud and mobile cloud computing." In Telecommunications (ICT), 2016 23rd International Conference on, pp. 1-4. IEEE, 2016.

[30]. King Faisal Specialist Hospital and Research Center. [Online].<Last Accessed: 1/8/2018> Available: http://www.kfshrc.edu.sa

[31]. N. Saquib, and at al. , “Chronic disease prevalence among elderly Saudi men,” International Journal of Health Sciences, vol. 11, no. 5, pp. 11–16, 2017.

[32]. Z. A. Memish and at.al, “Obesity and associated factors – kingdom of saudi arabia, 2013,” Preventing Chronic Disease, vol. 11, p. E174, Oct. 2014.

[33]. M. N. Koukias, and D. K. Lymberopoulos, Biomedical Engineering. Available from: InTech, 2009, ch. Requirements and Solutions for Advanced Telemedicine Applications, pp. 645–658.

[34]. Alesanco and J. GarcÃ a, “Clinical assessment of wireless ECG transmission in real-time cardiac telemonitoring,” IEEE Transactions on Information Technology in Biomedicine, vol. 14, no. 5, pp. 1144–1152, Sept 2010.

[35]. Sensor and data transmission needs and technologies for patient monitoring in the operating room and intensive care unit,” in 2005 IEEE Engineering in Medicine and Biology 27th Annual Conference, Jan 2005, pp. 5182– 5185.

[36]. K. Kumar and Y. H. Lu, “Cloud computing for mobile users: Can offloading computation save energy?” Computer, vol. 43, no. 4, pp. 51–56, April 2010.

[37]. T. Muhammed and R. A. Shaikh, “An analysis of fault detection strategiesin wireless sensor networks,” Journal of Network and Computer Applications, vol. 78, pp. 267 – 287, Jan. 2017.

[38]. J. Sametinger, J. Rozenblit, R. Lysecky, and P. Ott, “Security challenges for medical devices,” Commun. ACM, vol. 58, no. 4, pp. 74–82, March, 2015.

International Virtual Conference on Materials and Nanotechnology
In Association with International Journal of Scientific Research in Science and Technology
Volume 9 | Issue 4 | Print ISSN: 2395-6011 | Online ISSN: 2395-602X (www.ijsrst.com)

Applications of Nanotechnology in Diabetes - A Review

A. D. Suryawanshi[1], V. B. Sanap[2], D. D. Suryawanshi[3], B. H. Pawar[4]
[1]Department of Physics, B. J. College, Ale, Pune, Maharashtra, India
[2]Department of Physics Y.C.College, Sillod, Aurangabad, Maharashtra, India
[3]Department of Chemistry, S.C.S. College, Omerga, Osmanabad, Maharashtra, India
[4]Ex.Head, Department of Physics S.G.B. Amravati University, Amravati, Maharashtra, India

ABSTRACT

Nanotechnology is an advanced scientific technique that provides more accurate and timely medical information for diagnosing disease. Diabetes mellitus (DM) is a commonly seen chronic disease, which seriously threatens the health of human beings. About 150 million people suffer from diabetes in the world and it has been predicted that this number will be doubled within 15 years. Nanotechnology is a focal point in diabetes research, where nanoparticles in particular are showing great promise in improving the treatment and management of the disease. Nanotechnology can now offers new implantable or wearable sensing technologies that provide continuous and extremely accurate medical information. The purpose of this is to throw more light on the recent advances and impact of nanotechnology on biomedical sciences to cure diabetes. Nano medicine, the application of nanotechnology to medicine, has already offered some new solutions, and many pharmaceutical companies are trying to develop targeted drug delivery using nanotechnology and already existing drugs. Nanotechnology offers some new solutions in treating diabetes mellitus. This review concluded that nanotechnology will be effective therapy in diabetes.

Keywords : Nanotechnology, Diabetes, Nanoparticles, Nanomedicine, Nanospheres.

I. INTRODUCTION

Diabetes mellitus, often simply referred to as diabetes—is a group of metabolic diseases in which a person has high blood sugar, either because the body does not produce enough insulin, or because cells do not respond to the insulin that is produced. This high blood sugar produces the classical symptoms of polyuria (frequent urination), polydipsia (increased thirst) and polyphagia (increased hunger)[1] ¬ . There are three main types of diabetes:

- Type 1 diabetes: results from the body's failure to produce insulin, and presently requires the person to inject insulin
- Type 2 diabetes: results from insulin¬ resistance, a condition in which cells fail to use insulin properly, sometimes combined with an absolute insulin deficiency.

Gestational diabetes: is when pregnant¬ women, who have never had diabetes before, have a high blood glucose level during pregnancy. It may precede development of type 2 DM. Other forms of diabetes mellitus include congenital diabetes, which is due to

genetic defects of insulin secretion, cystic fibrosis-related diabetes, steroid diabetes induced by high doses of glucocorticoids, and several forms of monogenic diabetes. All forms of diabetes have been treatable since insulin became available in 1921, and type 2 diabetes may be controlled with medications. Both type 1 and 2 are chronic conditions that usually cannot be cured. Pancreas transplants have been tried with limited success in type 1 DM; gastric bypass surgery has been successful in many with morbid obesity and type 2 DM [2] . Gestational diabetes usually resolves after delivery. Diabetes without proper treatments can cause many complications. Acute complications include hypoglycemia, diabetic ketoacidosis, or nonketotic hyperosmolar coma. Serious long-term complications include cardiovascular disease, chronic renal failure, retinal damage. Adequate treatment of diabetes is thus important, as well as blood pressure control and lifestyle factors such as smoking cessation and maintaining a healthy body weight [3]

II. USE OF NANOTECHNOLOGY IN THE DETECTION OF INSULIN AND BLOOD SUGAR

A new method that uses nanotechnology to rapidly measure minute amounts of insulin and blood sugar level is a major step toward developing the ability to assess the health of the body's insulin-producing cells. It can be achieved by following ways.

BY MICROPHYSIOMETER:

The microphysiometer is built from multiwalled carbon nanotubes, which are like several flat sheets of carbon atoms stacked and rolled into very small tubes. The nanotubes are electrically conductive and the concentration of insulin in the chamber can be directly related to the current at the electrode and the nanotubes operate reliably at pH levels characteristic of living cells. Current detection methods measure insulin production at intervals by periodically collecting small samples and measuring their insulin levels. The new sensor detects insulin levels continuously by measuring the transfer of electrons produced when insulin molecules oxidize in the presence of glucose. When the cells produce more insulin molecules, the current in the sensor increases and vice versa, allowing monitoring insulin concentrations in real time [4].

BY IMPLANTABLE SENSOR :

Use of polyethylene glycol beads coated with fluorescent molecules to monitor diabetes blood sugar levels is very effective in this method the beads are injected under the skin and stay in the interstitial fluid. When glucose in the interstitial fluid drops to dangerous levels, glucose displaces the fluorescent molecules and creates a glow. This glow is seen on a tattoo placed on the arm. Sensor microchips are also being developed to continuously monitor key body parameters including pulse, temperature and blood glucose. A chip would be implanted under the skin and transmit a signal that could be monitored continuously.

III. USE OF NANOTECHNOLOGY IN THE TREATMENT OF DIABETES

Diabetes is considered to be one of the major afflictions of modern western society. To date, diabetic patients control their blood-sugar levels via insulin introduced directly into the bloodstream using injections. This unpleasant method is required since stomach acid destroys protein-based substances such as Insulin, making oral insulin consumption useless. The new system is based on inhaling the insulin (instead of injecting it) and on a controlled release of insulin into the bloodstream (instead of manually controlling the amount of insulin injected) [5]. The treatment of diabetes includes the proper delivery of insulin in the blood stream which can be achieved by nanotechnology in the following ways:

DEVELOPMENT OF ORAL INSULIN:

Production of pharmaceutically active proteins, such as insulin, in large quantities has become feasible [6, 7]. The oral route is considered to be the most convenient and comfortable means for administration of insulin for less invasive and painless diabetes management, leading to a higher patient compliance [8]. Nevertheless, the intestinal epithelium is a major barrier to the absorption of hydrophilic drugs, as they cannot diffuse across epithelial cells through lipid-bilayer cell membranes to the bloodstream [9]. Therefore, attention has been given to improving the Para cellular transport of hydrophilic drugs [10, 11]. A variety of intestinal permeation enhancers including chitosan (CS) have been used for the assistance of the absorption of hydrophilic macromolecules [12]. Therefore, a carrier system is needed to protect protein drugs from the harsh environment in the stomach and small intestine, if given orally [13]. Additionally, CS nanoparticles (NPs) enhanced the intestinal absorption of protein molecules to a greater extent than aqueous solutions of CS in vivo [14]. The insulin loaded NPs coated with mucoadhesive CS may prolong their residence in the small intestine, infiltrate into the mucus layer and subsequently mediate transiently opening the tight junctions between epithelial cells while becoming unstable and broken apart due to their pH sensitivity and/or degradability. The insulin released from the broken-apart NPs could then permeate through the Para cellular pathway to the bloodstream, its ultimate destination.

MICROSPHERE FOR ORAL INSULIN PRODUCTION:

The most promising strategy to achieve oral insulin is the use of a microsphere system which is inherently a combination strategy. Microspheres act both as protease inhibitors by protecting the encapsulated insulin from enzymatic degradation within its matrix and as permeation enhancers by effectively crossing the epithelial layer after oral administration [15].

ARTIFICIAL PANCREAS:

Development of artificial pancreas could be the permanent solution for diabetic patients. The original idea was first described in 1974. The concept of its work is simple: a sensor electrode repeatedly measures the level of blood glucose; this information feeds into a small computer that energizes an infusion pump, and the needed units of insulin enter the bloodstream from a small reservoir [16]. Another way to restore body glucose is the use of a tiny silicon box that contains pancreatic beta cells taken from animals. The box is surrounded by a material with a very specific nanopore size (about 20 nanometers in diameter). These pores are big enough to allow for glucose and insulin to pass through them, but small enough to impede the passage of much larger immune system molecules. These boxes can be implanted under the skin of diabetes patients. This could temporarily restore the body's delicate glucose control feedback loop without the need of powerful immunosuppressant that can leave the patient at a serious risk of infection [17].

THE NANOPUMP:

The Nano pump is a powerful device and has many possible applications in the medical field. The first application of the pump, introduced by DE biotech, is Insulin delivery. The pump injects Insulin to the patient's body in a constant rate, balancing the amount of sugars in his or her blood. The pump can also administer small drug doses over a long period of time [18]

IV. CONCLUSION

Nanotechnology can be defined as the monitoring, repairing, construction and control of human biological systems at the cellular level by using

materials and structures engineered at the molecular level. It is useful in detection of insulin and blood sugar by the help of microphysiometer and implantable sensors. By using nanotechnology the nanoparticles were formed and these nanoparticles are also useful in treatment of diabetes. Hopefully, the new kind of treatment may help in making the everyday lives of millions of diabetes patients more tolerable.

V. REFERENCES

[1]. Wild S, Roglic G, et al. "Global prevalence of diabetes: estimates for 2000 and projections for 2030". Diabetes Care 27 (5): 2004; 1047–53.

[2]. Agabegi D Elizabeth; Agabegi, Steven S. Step-Up to Medicine (Step-Up Series). Hagerstwon, MD: Lippincott Williams & Wilkins. ISBN 2008; 0-7817-7153-6.

[3]. Lambert P. "What is Type 1 Diabetes?". Medicine 30: 2002; 1–5.

[4]. Microphysiometer using multiwall carbon nanotubes enable constant realtime monitoring of microliters of insulin [electronic resource] [accessed 2008 Apr 18]. Available from: URL: http://nextbigfuture.com/2008/04/microphysiometer-using-multiwall carbon.html

[5]. Insulin Nanodrug under Development; [electronic resource] [accessed 2007 Oct 02]. Available from: URL: http://thefutureofthings.com/news/1014/insulin-nanodrug-under- development.html

[6]. Liang H F, Hong M H, Ho R M, Chung C K, Lin Y H, Chen C H and Sung H W. Novel method using a temperature-sensitive polymer (methylcellulose) to thermally gel aqueous alginate as a pH-sensitive hydrogel Biomacromolecules 5, 1917– 25(2004).

[7]. Smyth S and Heron A. Diabetes and obesity: the twin epidemics Nat. Med. 12, 75– 80 (2006)

[8]. Krauland A H, Guggi D and Bernkop-Schn¨urch A . Oral insulin delivery: the potential of thiolated chitosan-insulin tablets on non-diabetic rats J. Control. Release 95, 547–55(2004)

[9]. Borchard G, Lueßen H L, de Boer A G, Verhoef J C, Lehr C M and Junginger H E. The potential of mucoadhesive polymers in enhancing intestinal peptide drug absorption. III: Effects of chitosan-glutamate and carbomer on epithelial tight junctions in vitro J. Control. Release 39, 131–8(1996).

[10]. Kotz´e A F, Lueßen H L, de Leeuw B J, de Boer (A)B G, Verhoef J C and Junginger H E . Comparison of the effect of different chitosan salts and N-trimethyl chitosan chloride on the permeability of intestinal epithelial cells (Caco-2) J. Control. Release 51, 35– 46(1998). 225

[11]. Lamprecht A, Koenig P, Ubrich N, Maincent P and Neumann D. Low molecular weight heparin nanoparticles: mucoadhesion and behaviour in Caco-2 cells Nanotechnology 17, 3673– 80(2006).

[12]. Ward P D, Tippin T K and Thakker D R . Enhancing paracellular permeability by modulating epithelial tight junctions Pharm. Sci. Technol. Today 3, 346– 58(2000).

[13]. Ramadas M, Paul W, Dileep K J, Anitha Y and Sharma C P. Lipoinsulin encapsulated alginate-chitosan capsules: Intestinal delivery in diabetic rats J. Microencapsul 17, 405– 11 (2000).

[14]. Agnihotri S A, Mallikarjuna N N and Aminabhavi T M. Recent advances on chitosan-based micro-and nanoparticles in drug delivery J. Control. Release 100,5– 28(2004).

[15]. Gerardo P. Carino, Edith Mathiowitz. Oral insulin delivery; Advanced Drug Delivery Reviews 35,249–257(1999).

[16]. Hanazaki K, Nose Y, Brunicardi FCh. Artificial endocrine pancreas. J Am Coll Surg [electronic resource] [accessed 2006 Jan 20]. Available from: URL: http://www.sciencedirect.com/science?_ob=Article

[17]. Freitas RA. Current status of Nanomedicine and Medical Nanorobotics [electronic resource] [accessed 2006 Jan 20]. Available from: URL:http://www.nanomedicine.com/Papers/NMRevMar05.pdf

[18]. Insulin Nanopump for Accurate Drug Delivery.[electronic resource][accessed 2008Aug 15]. Available from: http://thefutureofthings.com/news/1286/insulin-nanopump-for-accurate-drug-delivery.html.

International Virtual Conference on Materials and Nanotechnology
In Association with International Journal of Scientific Research in Science and Technology
Volume 9 | Issue 4 | Print ISSN: 2395-6011 | Online ISSN: 2395-602X (www.ijsrst.com)

Structural and Morphological Properties of Spray Deposited Lead Telluride Thin Films

Syed Ghause Ibrahim*[1], S. A.Waghuley[2], M. M. Hasan Farooqi[3], A.V. Kadu[4]

*[1]Department of Engineering Physics, Prof. Ram Meghe College of Engineering & Management, Badnera-444701, Maharashtra, India

[2]Department of Physics, Sant Gadge Baba Amravati University, Amravati-444602, Maharashtra, India

[3]Department of Applied Science and Humanities, Jamia Millia Islamia, New Delhi 110025, India

[4]Department of Engineering Chemistry, Prof. Ram Meghe College of Engineering & Management, Badnera-444701, Maharashtra, India

ABSTRACT

The present research work reports on the deposition of lead telluride (PbTe) thin films onto the glass substrates by economical spray pyrolysis technique at 473K. The deposited lead telluride films are nanocrystalline in nature with cubic lattice and having preferred orientation along (200) and exhibit a direct bandgap of 1.27eV. The electrical resistivity of the as-deposited films was found to be $1.80\times10^{-2}\Omega$cm.Thermo-emf studies confirm that the films possess n-type conductivity.

Keywords : Nanostructured thin films, Scanning electron microscopy, X-ray diffractometry.

I. INTRODUCTION

In the field of science and technology, thin film research has been widely expanded due to the increasing demands for microelectronics and microstructural components manufacturing. Since last few decades lead telluride (PbTe), a metal chalcogenide semiconductor in the IV-VI group gained a remarkable attention due to its unique properties, which includes a narrow band gap of about 0.27 eV, high absorption coefficient, high dielectric constant and free carrier mobilities which may be utilized for numerous applications such as infrared (IR) detectors, light-emitting devices, photovoltaic converters, thermoelectric power generators and more recently as infrared laser in fibre optics and thermoelectric devices [1-5]. There are different methods which has been utilized by different researchers for the deposition of lead telluride (PbTe) thin films such as thermal evaporation [1], hot-wall epitaxy [6], RF magnetron sputtering [7], pulsed laser evaporation [8], flash evaporation [9], electrodeposition [10], solvothermal method [11], chemical bath deposition [12], drop casting [13] and spray pyrolysis method [14]. However, not much work has been reported by spray deposited deposition method. So it was plan to deposit lead telluride thin films on the glass substrates by economical spray pyrolysis technique and study its structural and morphological properties.

II. EXPERIMENTAL DETAILS

The spray deposition method was used to deposit the lead telluride thin films onto glass substrate. For the deposition of the film, solutions of lead acetate trihydrate (0.1 M) in deionized water and sodium tellurite in methanol were prepared. These precursor solutions were amalgamated separately and then these solutions were mixed together into another beaker and stirred for 20 minutes to obtain a solution of stable phase. Further this solution was sprayed using compressed air as a carrier gas onto hot glass substrates kept at 473 ± 5K temperature. Several trials were conducted [15] to optimize the different deposition parameters such as substrate temperature, spray rate, concentrations of cationic and anionic sources etc. The average thickness of the as deposited lead telluride thin film was measured by the gravimetric method. The structural studies were carried out using Philips PW 1710 diffractometer with Cu-Kα radiation of wavelength 1.5405Å and the surface morphological studies were carried out using JEOL 6380A scanning electron microscope.

III. RESULTS AND DISCUSSION

Structural Analysis

X-rays diffraction was used to evaluate the structural properties of lead telluride thin films. XRD of the as deposited thin film samples were characterized by using Philips PW 1710 diffractometer with Cu-Kα radiation of wavelength 1.5405 Å. The XRD pattern shows that lead telluride thin films are nanocrystalline in nature with cubic lattice and having well defined (200), (220), (400), (420) and (422) peaks with preferred orientation along (200) plane which is as listed by Kungumadevi et al., [1]. Comparison of observed and standard X-rays diffraction data of lead telluride thin films is shown in table.

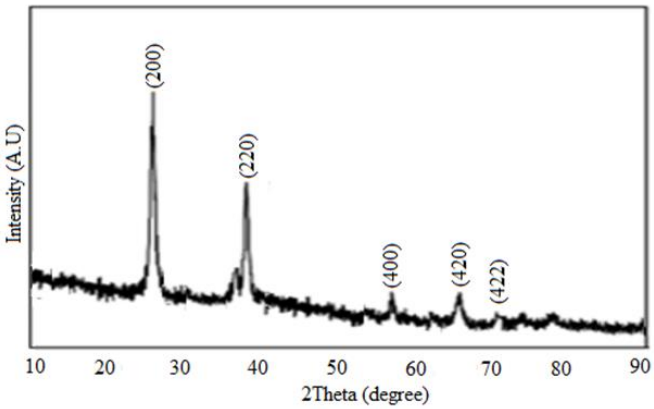

Figure 1 : XRD image of lead telluride thin film

Table1. Comparison of observed and standard XRD data of lead telluride thin films (JCPDS - 078-1905)

Film	Observed data		Standard data		h k l	Phase
	2θ (degree)	d (Å)	2θ (degree)	d (Å)		
PbTe	27.619	3.227	27.720	3.201	2 0 0	Cubic
	39.458	2.281	39.398	2.293	2 2 0	Cubic
	57.031	1.613	57.121	1.601	4 0 0	Cubic
	64.518	1.443	64.530	1.439	4 2 0	Cubic
	71.562	1.317	71.578	1.315	4 2 2	Cubic

Morphology

The morphology of the lead telluride thin films was studied by scanning electron microscopy. Typical SEM images of the as-deposited thin films are presented in Figure 2. It was found that the films were well-covered, homogeneous, dense, continuous and compact with no cracks on the surfaces.

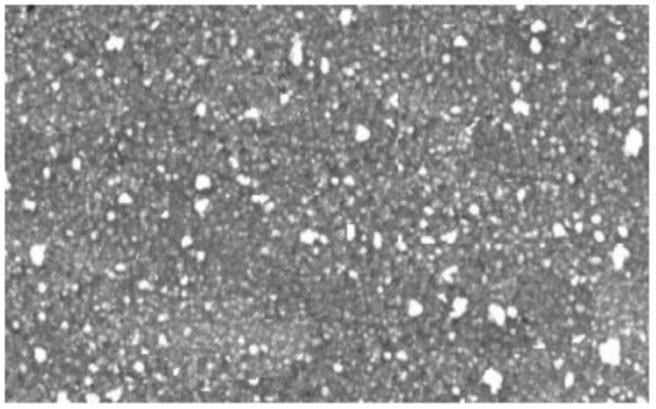

Figure 2 : SEM image of lead telluride thin film

IV. CONCLUSION

In the present paper, structural and morphological properties of spray deposited nanocrystalline lead telluride thin films have been reported. Deposited films are nanocrystalline in nature with Cubic phase. Scanning electron micrographs shows that the deposited film were well-covered, homogeneous, dense, continuous and compact with no cracks neither voids. The optical absorption analysis showed that, the film exhibits direct band gap of the order of 1.27eV.

V. REFERENCES

[1]. Kungumadevi, L., Sathyamoorthy, R., & Subbarayan, A. (2010). AC conductivity and dielectric properties of thermally evaporated PbTe thin films. Solid-State Electronics, 54(1), 58–62. DOI:10.1016/j.sse.2009.09.023

[2]. Böhm, M. L., Jellicoe, T. C., Tabachnyk, M., Davis, N. J. L. K., Wisnivesky-Rocca-Rivarola, F., Ducati, C.,.. Greenham, N. C. (2015). Lead Telluride Quantum Dot Solar Cells Displaying External Quantum Efficiencies Exceeding 120%. Nano Letters, 15(12), 7987–7993. DOI:10.1021/acs.nanolett.5b03161

[3]. Zogg, H., Alchalabi, K., Zimin, D., Kellermann, K., & Buttler, W. (2003). Two-dimensional monolithic lead chalcogenide infrared sensor array on silicon read-out chip. Nuclear Instruments and Methods in Physics Research Section A: Accelerators, Spectrometers, Detectors and Associated Equipment, 512(1-2), 440–444. DOI:10.1016/s0168-9002(03)01924-7

[4]. Dughaish, Z. H. (2002). Lead telluride as a thermoelectric material for thermoelectric power generation. Physica B: Condensed Matter, 322(1-2), 205–223. DOI:10.1016/s0921-4526(02)01187-0

[5]. Pei, Y., LaLonde, A., Iwanaga, S., & Snyder, G. J. (2011). High thermoelectric figure of merit in heavy hole dominated PbTe. Energy&EnvironmentalScience,4(6),2085. DOI:10.1039/c0ee00456a

[6]. Teichert, C., Jamnig, B., Oswald, J. (2000). Pattern formation in PbTe multilayer films. Surface Science, 454-456, 823–826. DOI:10.1016/s0039-6028(00)00256-9

[7]. Jdanov, A., Pelleg, J., Dashevsky, Z., Shneck, R (2004). Growth and characterization of PbTe films by magnetron sputtering, Materials Science and Engineering B, 106(10), 89–94

[8]. Baleva, M., Surtehev, M (2003). Structural and optical characterization of laser-deposited PbTe films on silicon substrates, Vaccum, 69(1–3), 419–423

[9]. Kungumadevi, L., & Sathyamoorthy, R. (2012). Structural, Electrical, and Optical Properties of PbTe Thin Films Prepared by Simple Flash Evaporation Method, Advances in Condensed Matter Physics,1–5 DOI:10.1155/2012/763209

[10]. Saloniemi, H., Kanniainen, T., Ritala, M., Leskela, M (1998). Electrodeposition of PbTe thin films, Thin Solid Films, 326(1-2), 78–82

[11]. Ahuome, B.A., Adamu, I., Adamu, M.A., Baba-Kutigi, A.N (2019). Growth and Characterization of PbTe Thin-film through Solvo Thermal Method, Int. J. Phys. Sci. 22(2),1-5.

[12]. Chávez Urbiola, I. R., Bernal Martínez, J. A., Makhniy, V. P., Ramírez Bon, R., & Vorobiev, Y. V. (2014).Preparation of II–VI and IV–VI semiconductor films for solar cells by the isovalent substitution technique with a CBD-made substrate. Inorganic Materials, 50(6), 546–550. DOI:10.1134/s002016851406003x

[13]. Wang, Z., Ma, Y., Vartak, P. B., & Wang, R. Y. (2018). Precursors for PbTe, PbSe, SnTe, and SnSe synthesized using diphenyl dichalcogenides. Chemical Communications, 54(65), 9055–9058. DOI:10.1039/c8cc03869d

[14]. Krataitong, C., Srichai, K., Tubtimtae, A (2020). Structural and optical properties of undoped and antimony-doped lead telluride thin films, Materials Letters https://doi.org/10.1016/j.matlet.2020.129085

[15]. Ibrahim, S.G., Ubale, A.U (2015) Structural, electrical and optical properties of nanocrystalline Cd1–xFexSe thin films deposited by chemical spray technique, J. Saudi Chem. Soc. (19), 667–675

International Virtual Conference on Materials and Nanotechnology
In Association with International Journal of Scientific Research in Science and Technology
Volume 9 | Issue 4 | Print ISSN: 2395-6011 | Online ISSN: 2395-602X (www.ijsrst.com)

Determination of Macronutrients in Soil Samples at Tiwasa Region

N. A. Kalambe
Department of Chemistry, Shri Shivaji Science College, Amravati, Maharashtra, India

ABSTRACT

Tiwasa Taluka is situated in Amravati district. The soils in the area were analyzed for selected macronutrients. Macronutrients analyzed included potassium, sulphur and phosphates. The techniques employed were PUSA STFR Meter. The results indicate generally that macronutrient level of phosphates below the required minimum required levels for normal plant. Micronutrients were within the limits for normal plant growth.

Keywords : Soil characteristics, macronutrients, Pusa STFR Meter

I. INTRODUCTION

Phosphorus (P) and potassium (K) are essential nutrients required in rather large amounts by crops. The application of fertilizers is often required to meet the crop's demand, with the application rate depending on the availability of nutrients in the soil. Insufficient application rates result in lower yields and may reduce soil fertility over time as the availability of nutrients decreases. In contrast, the application of excess nutrients increases production costs and may cause environmental problems.

Soil testing is one of the most cost effective nutrient management tools available to growers and crop advisers. It can guide fertilization decisions for individual fields, and it can assess whether a soil is likely to respond to fertilization Soils differ in their capacity to supply nutrients to crops.

Soil fertility is the amount of plant nutrients available in soil while soil stability is the ability of soil to resist erosion mostly determined by soil texture, structure consistency and hardness of layers[1]. Mineral nutrients are divided into two types: macronutrients and micronutrients. Macronutrients are further divided into primary and secondary. Primary nutrients are used in large quantities by plants and they include nitrogen, phosphorus and potassium. Secondary nutrients include calcium, magnesium and sulphur. Micronutrients are needed in very small amounts and they include boron, copper, iron, manganese and zinc[2]. Having the right amount of nutrients is essential for normal plant growth and reproduction. As nutrient ions are removed from soil solution by plant absorption they are replenished from several sources. Seldom is the rate of renewal for all essential elements from untreated soil fast enough to achieve maximum crop production. To augment this removal fertilizers are usually applied[3].

The methods are laborious, expensive and prone to inaccuracies due to the possibility of contamination from the chemical reagents used. Moreover, digestion often involves heating which may lead to loss of volatile analytes. More innovative analytical techniques are thus required for soil quality (SQ) analysis[4]. The soil samples analyzed for macronutrients were taken from two research field stations in Kenya, i.e. Katumani (Eastern Kenya) and Kitale (Western Kenya). The soils were of ferrosol

type but under different cultivation and climatic conditions. Elemental analyses of the soils had been done using the 'Mehlich' method[5] (for determining macronutrients P, Mg, Na), the Walkley–Black procedure[6] (for determining organic C) and the 'Kjeldahl after Bremner' method[7] Soil testing for P and K has value in nutrient management for annual crops[8]. Available macro nutrients (N, P, K and S) in the soils of Chiraigaon block of district Varanasi (U.P.) in relation to soil characteristics[9]. Determination of selected micro and macronutrients in sugarcane growing soils at Kakamega North District, Kenya[10].

II. METHODS AND MATERIAL

PUSA STFR Meter:

A) INSTRUMENTATION

STFR meter is a low cost, user friendly digital embedded system instrument which can quantitatively estimate available nutrients in soil such as organic carbon, phosphorus, potassium.

The available nutrients in the soil are extracted with an extractant and a colour is developed in the extract with another reagent. The colour intensity which is proportional to the amount of nutrients extracted measured by this STFR meter. Fertilizer doses item of the menu gives fertilizer doses for N, P and K from soil test value of organic phosphorus, potassium for a selected crop. So the STFR meter used for following test of soil –

Phosphorus, Potassium, Sulphur, iron, Zinc, Copper and recommendation for crop specific fertilizer and micronutrients.

Description of the Instrument:

The instrument has sixteen key and the function of which are as follow

ENT Key: This key is used to enter into program mode and parameter.

INC key: This key is used to go into next parameter in increment order.

DEC key: This key is used to go into next parameter in decrement order.

ESC key: This key is used to exit fromcurrent parameter.

RST key: This key is used to rest instrument.

(0 – 9) Numeric key: This key are used to enter numeric value.

Beside there are two electrode assemble. Assemblies for measurement of electrical conductivity and pH.

Cuvette:

Cuvette is a small tube like container with straight side and a circular or square cross section. It is sealed at one end and made of a clear transparent material such as plastic, glass or fused quartz. Proper cuvette is very important . proper cleaning of your cuvettes will increase their useful life and provide more constituents result .Handle the cuvette carefully to avoid breakage. Avoid contact with clear side of cuvette with any hard surface while filling the cuvette, avoid spillage of the solution on the outside of the cuvette.

In associated with Indian Agriculture Research Institute (IARI) Technosurge have brought out a programmable portable low cost equipment named PUSA soil test Fertilizer recommendation meter STFR Kit, that bring soil testing and fertilizer recommendation of farmer doorstep. This not only test soil parameters but also gives crop. Specific fertilizer recommendation and suggests ameliorants for problem soil. STFR meter consist of :-

1. Digital STFR meter
2. Reagent Kit
3. Lab ware kit
4. Mini shaker
5. Self-explanatory usage meter.

For Estimation of Component of Macro nutrients:-

For the phosphorus determination PHX 40 g, PH1 125 ml, PH3 60 ml, and charcoal 25 g plastic bottle and potassium determination PSX , PSX1 60 g, PSX2 30 ml plastic bottle and PT3 vials. B2 vials and also

determination of sulphur SW 45ml, S1 70 ml, S2 25g plastic bottle. PUSA STFR Meter kit help in determining the available nutrients in the soil. Help in determining the correct dosage of fertilizers according to the crop save money of farmer and nation by optimal usage of fertilizer. Prevents soil deterioration and maintain soil fertility.

Increase crop yield and hence farmer have more income. Soil test can be done within a short time flame testing can be done at a centre near a village or panchayat. PUSA meter gives accurate and reliable digital result and easily portable to any region.

PUSA STFR METER

Sample Collection:

For making composite sample collect small portions of soil up to the desired depth by means of sampling tools like tube augher, spade or khurpi from 15 to 20 well distributed spots. Moving in a zigzag manner from each individual sampling, site after scrapping off the surface litter if any, without removing soil from field having standing crops in row draw samples in between the rows. mix together the soil collected from all the spots within one field very thoroughly by hand on a clean piece of cloth or polythene sheet reduce the bulk to about 500 g by quartering process. for this spread the entire soil mass, divided into four quarters discard two opposite ones and remix the remaining two repeat the process until about 500 g soil is left.

Sample Processing:

Air dry the soil sample in shade discard the plant residues, gravels and other materials, if present. Crush the soil clods lightly and grind with the help of wooden pestle and mortars. Pass the entire quantity of sieved soil thoroughly and preserve for analysis.

Preparation of Blank Solution for Macro Nutrients:

Macronutrients

1. Phosphorus:

Take 2.ml PHX in 10 ml test tube add 5 drops of PH1 add 2ml PH2, 1ml PH3 and dilute the solution upto 10 ml with distilled water and then rest the test tube for 15 min.

PHX: 4.2 g of PHX dilute with 100ml distilled water in volumetric flask.

2. Sulphur:

Take 2.5 ml PSX in 10 ml test tube add 2 drops of S3, 0.15 g S2 powder and 25 time up down. Then add 10 drops of S1 rest the test tube for 10-15 min.

S3: Take 9 ml SW in test tube add 4 drops of S4 and 20 drops of S1.

PSX: Take 7.5 g PSX1 add 3.8 ml pSX2 and dilute with 120 ml distilled water and store the reagent bottle.

3. Potassium:

Take 1ml PSX in 10 ml test tube add 10 drops of PT-1, 6 drops of PT2, 3drops of PT3 and add 0.5 ml PS2 and dilute with distilled water up to the 5 ml and rest the test tube for 5min.

PT3: take 1 PT3 vial dissolved in 10 ml distilled water.

Preparation of Sample Solution for Macro Nutrients

I. Macronutrients

1. Phosphorus:

Extract Solution: - 0.6 g soil sample add 12 ml PHX and small quantity of charcoal. Then shaking the mixture up to 20 min. then filter the mixture with the help to funnel and filter paper. Take 2ml extract solution in 10 ml test tube add 5drops of PH1, 2ml PH2 , 1 ml PH3 and

dilute the solution with distilled water up to 10 ml.

Extract Solution for Potassium and Sulphur are same.

Extract Solution: Take 3 g of soil sample in shaking bottle and add 15ml PSX solution, small quantity of charcoal then shaking the mixture up to 15 to 20 min. then filter the mixture with the help to funnel and filter paper.

2. Potassium:

Take 1ml PSX in 10 ml test tube add 1ml extract solution , 20 drops of PT1, 10 drops PT2, 5 drops of PT3 and ad 1ml PS2 solution dilute the solution with distilled water up to 10 ml then rest the solution for 5 min.

3. Sulphur:

Take 5 ml extract solution in 10 ml test tube add 4 drops of S3, 0.3 g S2 and 40to 45 time up down and then add 20 drops of S1

For determination of various component by PUSA STFR METER following

Procedure work adapted

Procedure:

Before taking reading by STFR Meter one should be ready with color development of blank and sample solution of a particular nutrients of the five sample followed by other nutrients. Put on the STFR Meter the display will be "PUSA STFR METER" keep it at this state for 10 min. for warming up. Then press ENTER button to see the opening menu comprising pH, Electrical Conductivity Macronutrient, Micronutrients, fertilizer, SMS each of which can be accessed by pass in DOWN or UP button. here, first starting with macronutrients go to organic carbon menu by ENTER the screen will show OC%.

Press ENTER the screen will display "BLANK" then put blank solution in the 5 ml measuring tube (cuvette) and keep in the sample holder of the meter. in a particular orientation by matching a mark on the measuring a tube with mark on the meter near the sample holder.

This is require to avoid possion error and press ENTER the screen will show a reading Blank..... and then ENTER. This process may be repeated till a more or less constant reading comes.

Sample reading - Press DOWN button and meter show "Sampler" put first sample solution in the 5 ml measuring tube. The press ENTER, the screen will display enter sample NO. In XXX form at enter the tree digit soil sample no. and press ENTER. The screen will show the soil test result in term of actual value and in the category of low, medium, high and very high after noting the first sample value put the second sample and follow the procedure. Same way after completion of one nutrient, go to pressing ESC button till the opening menu come the press down, when the next item or nutrient come on screen the press enter and follow these step again to get reading.

III. RESULTS AND DISCUSSION:

Observation Tables:

PUSA STFR METRY:

Room temp __29____℃

Macronutrients in soil sample

Sr.No	Macronutrients	Reference Value	Soil Sample No	Observation	
				Blank Soln.	Sample Soln.
1	Phosphorus Kg/Ha	350-400 Kg/Ha	1	368.3	59.5
			2	367.0	44.1
			3	367.0	23.8
			4	367.1	66.7
			5	366.8	77.2
2	Potassium Kg/Ha	300-400 Kg/Ha	1	244.4	663.4
			2	244.9	611.6
			3	244.8	586.5
			4	244.6	627.6
			5	245.2	703.3
3	Sulphur Kg/Ha	1Kg/Ha	1	298.7	3.87
			2	300.7	11.16
			3	300.6	12.00
			4	300.9	6.83
			5	292.0	15.83

Soil analysis is a set of various chemical processes that determine the amount of available plant nutrients in

the soil, but also the chemical, physical and biological soil properties important for the plant nutrition or soil health, chemical soil analysis determine the nutrients present in the soil.

The Macronutrients are analyzed from the soil by PUSA STFR METRY. The Macronutrients are phosphorus, potassium and sulphur. I analyzed the nutrients from the soil, the macronutrients are potassium, phosphorus and sulphur. The soil contains large amounts of nutrients, the most need of crop is, how much quantity of nutrients present in the soil. In the Amravati district the soil contains large quantity of nutrients present in the soil. Macronutrients play a very important role in plant growth and development. Their functions range from being structural units to redox-sensitive agents. Generally, application of **macronutrient** increases yield, growth, and quality of crops.

IV. CONCLUSION

The predictions and suggestions are made based on past records and present input. It also makes use of feedback from the user to improve the prediction. The network of moisture sensors provides real time irrigation and minimizes the load of watering. This helps save water and also prevents over saturation of soil. FARM-IT is therefore an efficient and important tool for a regular farmer that can help him in his day-to-day agricultural activities and also help improve his farming habits.

V. REFERENCES

[1]. O. B Harry and N. C Brady, The Nature and Properties of Soils, 7th ed 1969, pp 20-33

[2]. C.T Simpson, E Whittemore and W Henderson, Handbook in Agriculture, 2nd ed, 1981, pp54

[3]. K.D.W. Shepherd, G. Markus, Soil Sci. Soc. Am. J. 66 (3) (2002) 988–998.

[4]. A. Mehlich, Commun. Soil Sci. Plant Anal. 9 (6) (1978) 477–492.

[5]. M. Diaz-Zorita, Commun. Soil Sci. Plant Anal. 30 (5–6) (1999) 739–745.

[6]. J.M. Bremner, C.S. Mulvaney, Methods Soil Anal. Agron. (1982) 595–625.

[7]. Daniel Geisseler and Gene Miyao, Sept 2016, Journal California Agriculture, 70(3) ISSN 0008-0845 DOI 10.3733/ca.2016a0007 pp 152-159.

[8]. Singh, R.P., and S.K. Mishra. Indian Journal of Scientific Research, 2012, p. 97.

[9]. Preston Akenga, Ali Salim, Anam Onditi, Amir Yusuf, Walyambillah Waudo IOSR Journal of Applied Chemistry (IOSR-JAC) e-ISSN: 2278-5736.Volume 7, Issue 7 Ver. I. (July. 2014), PP 34-41

International Virtual Conference on Materials and Nanotechnology
In Association with International Journal of Scientific Research in Science and Technology
Volume 9 | Issue 4 | Print ISSN: 2395-6011 | Online ISSN: 2395-602X (www.ijsrst.com)

Determination of Nitrogen in Soil Samples of Tiwasa Region in Amravati District

N. A. Kalambe
Department of Chemistry, Shri Shivaji Science College, Amravati, Maharashtra, India

ABSTRACT

Soil fertility evaluation of an area or region is an important aspect in context of sustainable agricultural production. The Tiwasa Region of district Amravati was selected for the study. Five representative villages were chosen and different number of surface soil samples collected and analysed for available Nitrogen status. It will stimulate above ground growth, and produces the rich green colour that is the characteristic of healthy plants, because of this Nitrogen is essential for plant. A method for the determination of total (Kjeldahl) nitrogen in soil is presented. The Kjeldahl method permits the available nitrogen to be precisely determined in the plant and in the soil. The method of determination involves three successive phases which are, Digestion of the organic material to convert nitrogen into HNO3.Distillation of the released Ammonia into an absorbing surface or medium.

Keywords : Soil Samples, Kjeldahl Method

I. INTRODUCTION

Soil fertility is an important factor, which determines the growth of plant. Soil fertility is determined by the presence or absence of nutrients i.e., macro and micronutrients4. Macronutrients such as nitrogen (N), phosphorus (P) and potassium (K) together make up the trio known as NPK. All these nutrients are accumulated by the plants in their bodies in different concentrations. However, these nutrients are usually lacking from the soil because plants use them in large amounts for growth and survival. Hence, these nutrients are known to govern the fertility of the soils, control the yields of the crops and hence have agronomic importance. Assessment of Soil Macronutrient Status of Some Threatened Medicinal Plants of Kashmir Himalaya, India1. - Methods of Analysis of Soils, Plants, Waters and Fertilizers2. Determination of nitrogen in soil by the Kjeldhal method3. Soil samples were found low in organic carbon, available nitrogen and phosphorus while medium in potassium. About 62 % of samples were found deficient in available sulphur. Significant positive correlations were found to exist between organic carbon and available N, P, K and S status of soil under study. Available macro nutrients (N, P, K and S) in the soils of Chiraigaon block of district Varanasi (U.P.) in relation to soil characteristics4. Estimation of Soil Organic Matter, Total Nitrogen and Total Carbon in Sustainable Coastal Wetlands5. Nitrogen is the most important limiting nutrient in wetland soils and a sensitive indicator for measuring the soil nutrient levels in wetlands6. Estimating of soil total nitrogen concentration based on hyperspectral remote sensing data in Minjiang River estuarine wetland7. Total Nitrogen Analysis of Soil

and Plant Tissues8. Kjeldahl digestion, which converts nitrogen to ammonium, is probably the most common method of analyzing substances for nitrogen 9-11.

II. METHOD AND MATERIAL

Sample Collection:

For making composite sample collect small portions of soil up to the desired depth by means of sampling tools like tube augher, spade or khurpi from 15 to 20 well distributed spots. moving in a zigzag manner from each individual sampling, site after scrapping off the surface litter if any, without removing soil from field having standing crops in row draw samples in between the rows. Mix together the soil collected from all the spots within one field very thoroughly by hand on a clean piece of cloth or polythene sheet reduce the bulk to about 500 g by quartering process. for this spread the entire soil mass, divided into four quarters discard two opposite ones and remix the remaining two repeat the process until about 500 g soil is left.

Sample Processing:

Air dry the soil sample in shade discard the plant residues, gravels and other materials, if present. Crush the soil clods lightly and grind with the help of wooden pestle and mortars. Pass the entire quantity of sieved soil thoroughly and preserve for analysis.

KJELDAHL FLASK / APPARATUS:

INSTRUMENTATION:

VELP Scientific has developed the widest range of Kjeldahl apparatus consisting of digestion units, Such instruments respond to the different need in QC, QA, laboratories. Today, The traditional Kjeldahl apparatus for digestion consists in a 250 ml flask capacity. Macro Kjeldahl flask started to appear for volume from 400-800 ml, suggested for soil, grain or protein samples with a very low amount of nitrogen and handle relatively big sample sizes, Micro Kjeldahl apparatus consisting 30-180 ml volume, commonly used with low sample amount. The typical Kjeldahl apparatus for distillation is designed to accept straight digestion tubes directly from the block digester. Steam distillation is much more rapid than classical kjeldahl distillation.

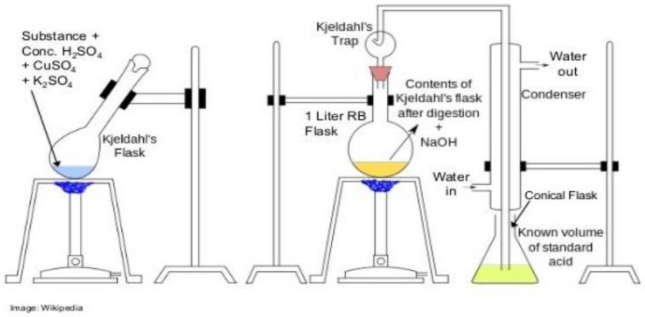

USES / APPLICATIONS

Kjeldahl flask is a round bottom flask with a long wide neck that is used in determination of nitrogen by kjeldahl method.

- The kjeldahl flasks are used in small digestion up in processes.
- Kjeldahl method is used for determination of total nitrogen in a sample.
- Distillation on the basis of kjeldahl method.
- Kjeldahl flasks are round bottom flasks with long wide neck that are used in kjeldahl method for quantitive determination of sample nitrogen content.

Kjeldahl flasks are typically manufactured from borosilicate glass, which is resistant to heat and chemicals. Flasks are available in a wide range of capacities with or without tooled necks or reinforced bead at the top.

METHODOLOGY:

Determination of Nitrogen on soil by the KJELDAHL METHOD.

As it was not convenient or practical to employed to kjeldahl methods tested modifications of these methods were employed that permitted the use of smaller amounts of reagents and of soil.

REAGENTS / PREPARATION OF REAGENTS

Ferrous Sulphate (0.5M=0.5N) – Dissolve FeSO4.7H2O in about 800ml water and add 100 ml to 1 liter in volumetric flask.

Diphenylamine indicator - Dissolve 0.5gm in a mixture of 20 ml water and 100 ml of conc. H2SO4.

Sulphuric Acid- Concentration not less than 96%. If high amount of chloride is present in the samples and silver sulphate (Ag2SO4) at the rate of g/lit. to the acid.

Ortho-phosphoric acid (85%) /Sodium fluoride chemically pure.

Liquid paraffin (extra pure)

Sulphuric acid 0.02 (N/50)

Mixed indicator – Dissolve 0.07g methyl red with 0.1g bromocresol green in 100ml of 95% ethanol.

Boric acid indicator solution- Dissolve 20g of pure boric acid (H3BO3) in about 700 ml of hot water. Transfer the cooled solution to a 1 litre volumetric flask containing 20 ml ethanol and 20 ml of mixed indicator solution. After mixing the contents of the flask add approx. 0.05 NaOH continuously until the colour is reddish purple. Then dilute the solution to volume with water and mix it thoroughly.

KJEIDAHL DIGESTION

Digestion was performed in 500ml Pyrex Kjeldahl flask. Accurately 1g of soil and was placed it into this flask. The Pyrex Kjeldahl flask using the gas heated six-flask digestion stand as the vapour tubes provided with these stands. The top plate of each stand was covered with a sheet of asbestos drilled with holes. At full heat of the burners on the stand brought 200 ml distilled water. It includes two blanks to standardize FeSO4 solution.

Potassium dichromate solution (10 ml) was poured in the flask, Swirl the flask gently and keeps it on an asbestos sheet.

Conc. H2SO4 (20 ml) was mixed in the flask by directing stream into the suspension. Then again swirl flask for 2-3 times.

The flask was allowed to stand on the asbestos sheet for 30 min. Then after there was addition of water (10 ml), 10 ml phosphoric acid and 1 ml diphenylamine indicator .

The content of the flask was titrated with ferrous ammonium sulphate till the colour flashes from blue violet to green.

If burette reading was 0.4 ml then repeated with less soil. If it was 17 ml or higher repeated it with more soil. As in this process kjeldahl flask to a rolling boiled in approximately 3-5 min.

Digestion were generally performed using the full heat of the burners so that sulphuric acid about one-third of the way up the neck of the flask.

KJELDAHL DISTILLATION AND TITRATION

Kjeldahl flask containing two glass beads (to reduce bumping). 20g soil was introduced in 800 ml dry kjeldahl flask. Two drops or 1ml of liquid paraffin added, as to prevent frothing bumping, respectively during distillation and 20 ml water was added and then swirled it. After that 100ml of each 0.32% KMnO4 and 2.5% NaOH solution were mixed in the flask. The flask was connected to the distillation apparatus and its contents were made alkaline, mixed and distilled.

Heat was regulated so that the rate of distillation was about ml/min, the distillate was collected in (250 ml) flask containing 20ml of boric acid solution with mixed indicator. With the absorption of ammonia the pink colour of boric acid solution turned to green. Nearby 100 ml of distillate to be collected in about 30 minutes. Later on, the contents of the flask were titrated with 0.02% H2SO4 to the original shade (pink). Blank titration (without soil) reaction was to be made for the final calculations.

III. RESULT AND DISCUSSION

KJELDHAL DIGESTION

OBSERVATION TABLES:

BLANK TITRATION:

Sr. No.	Vol. Of K2Cr2O7	Water	Phosphoric Acid	Concentrated H2SO4	Vol. Of EDTA added	Mean
1.	0.5 ml	5 ml	100 ml	5 ml	4.1 ml	3.75 ml
2	0.5 ml	5 ml	100 ml	5 ml	3.4ml	

MAIN TITRATION

Soil Sample No. 1

Sr. No.	Soil Sample No.1	Vol. Of K2Cr2O7	Water	Phosphoric Acid	Concentrated H2SO4	Vol. Of EDTA	Mean
1.	5 gm	5 ml	100 ml	5 ml	10 ml	3.5 ml	3.35 ml
2	5 gm	5 ml	100 ml	5 ml	10 ml	3.2 ml	

Soil Sample No. 2

Sr. No.	Soil Sample No.2	Vol. Of K2Cr2O7	Water	Phosphoric Acid	Concentrated H2SO4	Vol. Of EDTA	Mean
1.	5 gm	5 ml	100 ml	5 ml	10 ml	3.1 ml	2.75 ml
2	5 gm	5 ml	100 ml	5 ml	10 ml	2.4 ml	

Soil Sample No. 3

Sr. No.	Soil Sample No.3	Vol. Of K2Cr2O7	Water	Phosphoric Acid	Concentrated H2SO4	Vol. Of EDTA	Mean
1.	5 gm	5 ml	100 ml	5 ml	10 ml	4.2 ml	4.05 ml
2	5 gm	5 ml	100 ml	5 ml	10 ml	3.9 ml	

Soil Sample No. 4

Sr. No.	Soil Sample No.4	Vol. Of K2Cr2O7	Water	Phosphoric Acid	Concentrated H2SO4	Vol. Of EDTA	Mean
1.	5 gm	5 ml	100 ml	5 ml	10 ml	3.4 ml	3.15 ml
2	5 gm	5 ml	100 ml	5 ml	10 ml	2.9 ml	

Soil Sample No. 5

Sr. No.	Soil Sample No.5	Vol. Of K2Cr2O7	Water	Phosphoric Acid	Concentrated H2SO4	Vol. Of EDTA	Mean
1.	5 gm	5 ml	100 ml	5 ml	10 ml	4.5 ml	4.2 ml
2	5 gm	5 ml	100 ml	5 ml	10 ml	3.9 ml	

CALCULATIONS:

(For Blank solution):

1. Organic carbon % =10 (B-T)/B × 0.003 ×100/Wt. of soil =10 (3.35–3.2)/3.35× 0.003 ×100/0.5
= 0.26%

B – Blank titration
B-T = Blank titration reading 1 – Blank titration reading 2

2. Actual organic carbon (%) = (% × 1.3)
= 0.26 × 1.3
= 0.33%

3. Organic matter (%) = Actual % × 1.724
= 0.33 × 1.724
= 0.56%

For soil sample 1:

4. Organic carbon % =10 (B-T)/B × 0.003 ×100/Wt. of soil
=10 (3.75–3.4)/3.75× 0.003 ×100/0.5
= 0.55%

B – Blank titration
B-T = Blank titration reading 1 – Blank titration reading 2
5. Actual organic carbon (%) = (% × 1.3)
= 0.55×1.3
= 0.71%

6. Organic matter (%) = Actual % × 1.724
= 0.71×1.724
= 1.23%
For soil sample 2:
7. Organic carbon % =10 (B-T)/B × 0.003 ×100/Wt. of soil
=10 (2.75–2.4)/2.75× 0.003 ×100/0.5
= 0.76%
B – Blank titration
B-T = Blank titration reading 1 – Blank titration reading 2

8. Actual organic carbon (%) = (% × 1.3)
= 0.76×1.3
= 0.98%

9. Organic matter (%) = Actual % × 1.724
= 0.98×1.724
= 1.68%

For soil sample 3:

10. Organic carbon % =10 (B-T)/B × 0.003 ×100/Wt. of soil
=10 (4.05–3.9)/4.05× 0.003 ×100/0.5
= 0.22%

B – Blank titration
B-T = Blank titration reading 1 – Blank titration reading 2
11. Actual organic carbon (%) = (% × 1.3)
= 0.22×1.3
= 0.28%

12. Organic matter (%) = Actual % × 1.724
= 0.28×1.724
= 0.48%

For soil sample 4:
13. Organic carbon % =10 (B-T)/B × 0.003 ×100/Wt. of soil
=10 (3.15–2.9)/3.15× 0.003 ×100/0.5
= 0.47%

B – Blank titration
B-T = Blank titration reading 1 – Blank titration reading 2

14. Actual organic carbon (%) = (% × 1.3)

= 0.47×1.3
= 0.61%

15. Organic matter (%) = Actual % × 1.724
= 0.61×1.724
= 1.05%

For soil sample 5:

16. Organic carbon % =10 (B-T)/B × 0.003 ×100/Wt. of soil
=10 (4.2–3.9)/4.2× 0.003 ×100/0.5
= 0.42%

B-T = Blank titration reading 1 – Blank titration reading 2

17. Actual organic carbon (%) = (% × 1.3)
= 0.42×1.3
= 0.54%

18. Organic matter (%) = Actual % × 1.724
= 0.54×1.724
= 0.93%

KJELDAHL DISTILLATION

OBSERVATION TABLE:

B – Blank titration

BLANK TITRATION

Sr. No.	Boric Acid Indicator	Distillate added	Vol. Of 0.02 N concentrated H2SO4	Mean
1.	20 ml	80 ml	1.9 ml	1.65 ml
2	20 ml	80 ml	1.4ml	

MAIN TITRATION

Soil Sample No. 1

Sr. No.	Soil sample added	Boric Acid Indicator	Distillate added	Vol. Of 0.02 N conc. H2SO4	Mean
1.	0.5 gm	20 ml	80 ml	0.5 ml	0.35 ml
2	0.5 gm	20 ml	80 ml	0.2 ml	

Soil Sample No. 2

Sr. No.	Soil sample added	Boric Acid Indicator	Distillate	Vol. Of 0.02 N H2SO4	Mean
1.	0.5 gm	20 ml	80 ml	0.8 ml	0.6 ml
2	0.5 gm	20 ml	80 ml	0.4ml	

Soil Sample No. 3

Sr. No.	Soil sample added	Boric Acid Indicator	Distillate	Vol. Of 0.02 N H2SO4	Mean
1.	0.5 gm	20 ml	80 ml	0.6 ml	0.75 ml
2	0.5 gm	20 ml	80 ml	0.3 ml	

Soil Sample No. 4

Sr. No.	Soil sample added	Boric Acid Indicator	Distillate added	Vol. Of 0.02 N conc. H2SO4	Mean
1.	0.5 gm	20 ml	80 ml	1.6 ml	1.45 ml
2	0.5gm	20 ml	80 ml	1.3 ml	

Soil Sample No. 5

Sr. No.	Soil sample added	Boric Acid Indicator	Distillate added	Vol. Of 0.02 N conc. H2SO4	Mean
1.	0.5 gm	20 ml	80 ml	1.5 ml	1.3 ml
2	0.5 gm	20 ml	80 ml	1.1 ml	

CALCULATIONS:

Mineralizable N (kg/ha) = R × 31.36 (for each soil sample)

Where R = Volume of 0.02N H2SO4 in ml requires for Titration.

For blank solution:

Mineralizable N (kg/ha) = R × 31.36

= 1.65 × 31.36

= 51.7%

For soil sample 1:

Mineralizable N (kg/ha) = R × 31.36

= 0.35 × 31.36

= 10.97%

For soil sample 2:

Mineralizable N (kg/ha) = R × 31.36

= 0.6 × 31.36

= 18.81%

For soil sample 3:

Mineralizable N (kg/ha) = R × 31.36

= 0.75 × 31.36

= 23.52%

For soil sample 4:

Mineralizable N (kg/ha) = R × 31.36

= 1.45 × 31.36

= 45.47%

For soil sample 5:

Mineralizable N (kg/ha) = R × 31.36

= 1.3 × 31.36

= 40.76%

The Determination of total Nitrogen from the soil by Kjeldahl Method by digestion and distillation process. By Digestion, the total nitrogen is obtained from each soil is 1.23%, 1.68%, 0.48%, 1.05%, 0.93%. By Distillation, the total nitrogen is obtained from each soil is 10.97%, 18.81%, 23.52%, 45.47%, 40.76%. The rate of plant growth is proportional to the rate of nitrogen supply. If the soil is deficient in Nitrogen, the plants become stunted and pale. However, an excess of Nitrogen can damage the plants just as over-fertilizing the lawn can burn and damage the grass. Nitrogen is essential for plant development, since it plays a fundamental role in energy metabolism and protein synthesis. Soil analysis is a set of various chemical processes that determine the amount of available plant nutrients in the soil, but also the chemical, physical and biological soil properties important for the plant nutrition or soil health, chemical soil analysis determine the nutrients present in the soil. The soil contains large amounts of nutrients, the most need of crop is, how much quantity of nutrients present in the soil. In the Amravati district the soil contains large quantity of nutrients present in the soil.

IV. CONCLUSION

The network of moisture sensors provides real time irrigation and minimizes the load of watering. This helps save water and also prevents over saturation of

soil. FARM-IT is therefore an efficient and important tool for a regular farmer that can help him in his day-to-day agricultural activities and also help improve his farming habits. The results described in this paper should encourage other worker s who wish to analyze nitrogen while living under field conditions. The equipment we used was portable, reliable, and relatively inexpensive. The methods quickly produced accurate estimates of total nitrogen. This rapid feedback improved our study immensely and allowed us to constructively modify our research in situ.

V. REFERENCES

[1]. Parvaiz Ahmad Lone, Ajay Kumar Bhardwaj, Kunwar Wajahat Shah and Fayaz Ahmad Bahar, 2016. Assessment of Soil Macronutrient Status of Some Threatened Medicinal Plants of Kashmir Himalaya, India. Research Journal of Botany, 11: 18-24. DOI: 10.3923/rjb.2016.18.24

[2]. H.L.S Tandon - Methods Of Analysis Of Soils, Plants, Waters and Fertilizers 1st Edition (1993)

[3]. J. M. Bremner - International Journal for Research in Determination of nitrogen in soil by the Kjeldhal method , J.Agric.Sci. (1960), 55,

[4]. Singh, R.P. and S.K. Mishra, 2012. Available macro nutrients (N, P, K and S) in the soils of chiraigaon block of district Varanasi (U.P.) in relation to soil characteristics. Indian J. Scient. Res., 3: 97-100.

[5]. Sen Zhang, Xia Lu, Yuanzhi Zhang, Gege Nie and Yurong Li- Estimation of Soil Organic Matter, Total Nitrogen and Total Carbon in Sustainable Coastal Wetlands Sustainability 2019, 11, 667; doi:10.3390/su11030667 pp 1-18

[6]. Ma, K.; Zhang, Y.; Tang, S.X.; Liu, G. Characteristics of spatial distribution of soil total nitrogen in Zoigen alpine wetland. Chin. J. Ecol. 2016, 35, 1988–1995.

[7]. Gao, D.Z.; Zeng, C.S.; Zhang, W.L.; Liu, Q.Q.; Wang, Z.P.; Chen, Y.T. Estimating of soil total nitrogen concentration based on hyperspectral remote sensing data in Minjiang River estuarine wetland. Chin. J. Ecol. 2016, 35, 952–959

[8]. Darrell W Nelson, Lee E Sommers, Total Nitrogen Analysis of Soil and Plant Tissues, Journal of Association of Official Analytical Chemists, Volume 63, Issue 4, 1 July 1980, Pages770-778, https://doi.org/10.1093/jaoac/63.4.770

[9]. Bremner, J. M. and C. S. Mulvaney. 1982. Nitrogen-Total, pp 595-624. IN: A. L. Page (ed.) Methods of Soil Analysis, part 2. Madison, WI: Am. Soc. Agron. Mon. No. 9. 2nd Edition.

[10]. Morries, P. 1983. A century of Kjeldahl (1883-1983). J. Assoc. Pub. Anal. 21:53-58.

[11]. Jones, Jr., J. B. 1987. Kjeldahl nitrogen determination - J. Plant Nutr. 10:1675-1682

International Virtual Conference on Materials and Nanotechnology
In Association with International Journal of Scientific Research in Science and Technology
Volume 9 | Issue 4 | Print ISSN: 2395-6011 | Online ISSN: 2395-602X (www.ijsrst.com)

The Different Phases of Lithium Sulphate and Its Transition at Different Temperature

N R Thakare[1], A.V Nande[2], A D Bhoyar[1], S A Patil[1]
[1]Department of Physics, PRPCEM, Amravati, Maharashtra, India
[2]Department of Physics, G S College, Ballarpur Dist. Chandrapur, Maharashtra, India

ABSTRACT

The present review is focused on Li_2SO_4 salt and its different temperature phases. The enhancement in the conductivity with addition of different compounds in it has been observed by many researchers. Lithium sulphate is a material that has received quite a bit of attention in recent years. It is an ionic salt, presenting a reversible solid-solid phase transition (monoclinic ± FCC) at a relatively high temperature (578^0C). The high temperature form of lithium sulfate is a plastic (rotator) phase, presenting an unusually high ionic conductivity, deserving therefore the name of solid electrolyte. From the practical point of view its importance may rest on its application as an electrolyte for high-energy batteries, or as a stable nontoxic material for thermal energy storage.

Keywords : Lithium Sulfate, Phase Transition.

I. INTRODUCTION

The literature survey shows that the lithium sulphate is uniquely interesting among the all types of solid electrolytes system. It has special structural and physical properties which assert high ionic conductivity to this alkali metal sulphate. The FCC phase of the lithium sulphate has very high ionic conductivity about 3 Scm^{-1} close to its melting point with activation energy 0.41 eV, which also shows that it has high mobility of lithium ion [1]. The monoclinic phase of lithium sulphate has low ionic conductivity around 10^{-10} Scm^{-1} at 100^0C with activation energy 1.4 eV [2]. The high lithium ion mobility in the FCC phase is due to the sulphate ion which forms the translationally fixed lattice associated with the volume change and large value of latent heat near transition temperature. This leads to considerable orientational disordering of sulphate groups in the cubic phase [3, 4].

The heat capacity measurement at transition temperature [5] suggested that the existence of pre-melting phenomenon [6] gives the evidence of plastic phase, disordered with respect to Li^+ positions and SO_4^{2-} tetrahedra in the α-phase (FCC) are matrix isolated[7].

Though the high temperature phase of lithium sulphate is superionically conducting it is practically impossible to use it in lithium batteries. It is therefore always thought to stabilize α-phase of lithium sulphate at ambient temperature as reported by Balaya M.J.Verkerk et al. [8].

The high latent heat near transition for this salt has provoked the author to add the salts which has high heat content at ambient temperature. This can possibly affect the transition temperature of lithium sulphate by maintaining the disorder in Li^+ and matrix isolation of SO_4-terahedra.The various salts which are added to achieve the goal are given in the chapter-3. The different measurements carried on the prepared samples are also given in the same chapter.

II. X-RAY DIFFRACTION RESULTS SERIES: Li_2S0_4 _ (Li_2O:B_2O_3) _ZrO_2

The room temperature x-ray pattern of samples prepared in this series is shown in figures. 1,3,5,7 and respective h k l planes are shown in fig.2,4,6,8.

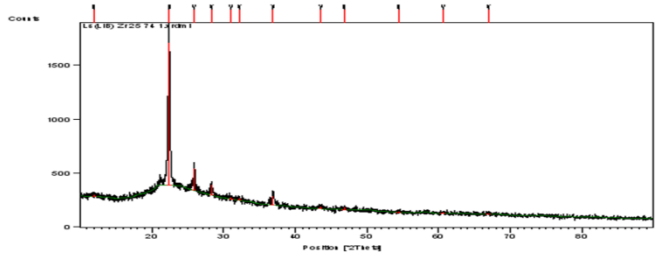

Fig.1.LS_ (LO: BO) _Zr :(25_74_1)

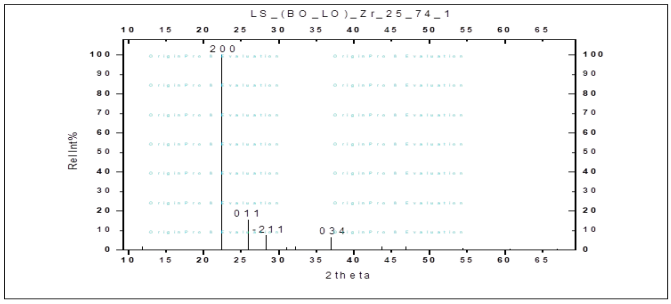

FIG.2.h k l values: LS_(LO:BO)_Zr:(25_74_1)

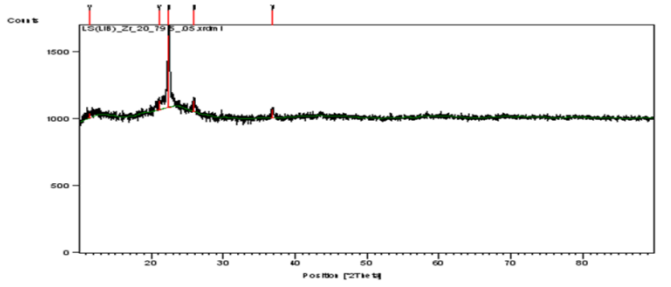

FIG.3. LS_(LO:BO)_ZrO2:(20_79.5_0.5)

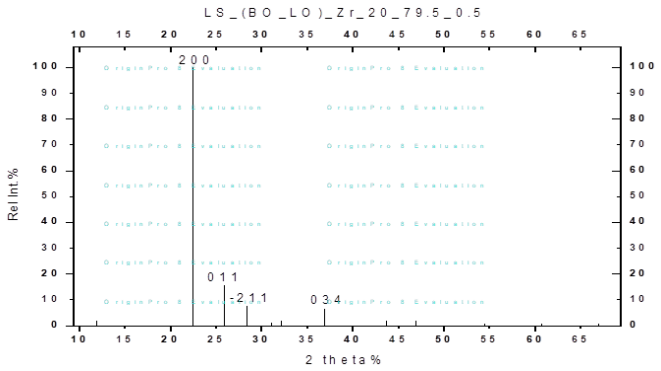

FIG.4..LS_(LO:BO)_ZrO2:(20_79.5_0.5)

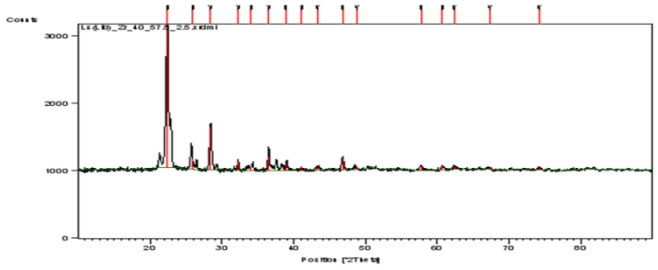

FIG.5. LS_(LO:BO)_ZrO_2:(40_57.5_2.5)

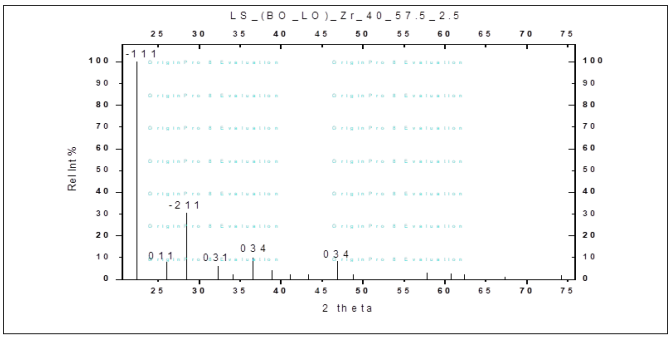

FIG.6.h k l Values: LS_(LO:BO)_ZrO_2:(40_57.5_2.5)

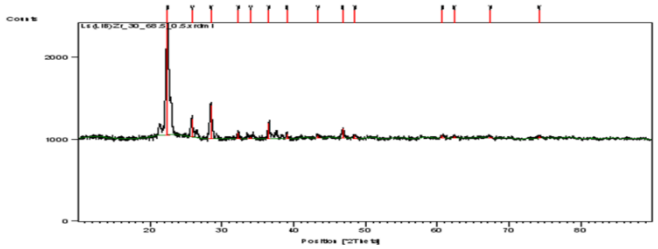

FIG.7. LS_(LO:BO)_ZrO_2:(30_68.5_1.5)

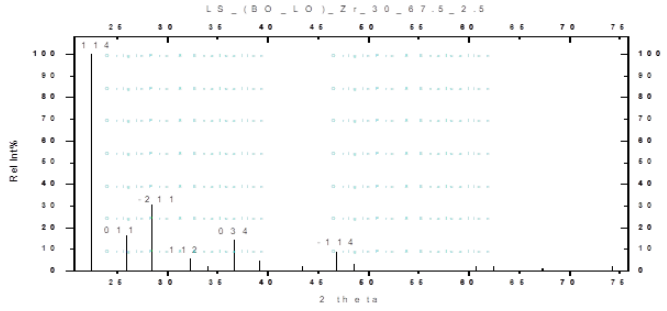

FIG.8. LS_(LO:BO)_ZrO_2:(30_68.5_1.5)

SERIES Li_2S0_4_(Li_2O:B_2O_3)_ZrO_2:

COMPOSITION	d values from XRD with intensity	d values ICCD	Components
Li_2S0_4_(Li_2O:B_2O_3)_ZrO_2 (20%_79.5%_0.5%)	3.96 100 3.43276 15.60 4.21974 12.41 2.43537 11.63	3.96 3.43 4.22 2.43	ZrSO4(O) Li HDROXIDE BORATE(A) Zr(OH)SO4(O) ZrO2(R)
Li_2S0_4_(LI2O:B2O3)_ZrO_2 (25%_74%_1%)	3.96073 100.00 3.44423 15.19 3.15656 21.67 2.43 6.17	3.96 3.44 3.15 2.43	ZrSO4(O) Li HDROXIDE BORATE(A) Zr O2(M) ZrO2(R)
Li_2S0_4_(Li2O:B2O3)_ZrO_2 (30%_68.5%_1.5%)	3.96244 100.00 3.13410 30.07 2.45432 14.51	3.96 3.13 2.45	ZrSO4(O) LI BORATE HYDRATE(M) ZrO2(R)
Li_2S0_4_(Li_2O:B_2O_3)_ZrO_2 (40%_57.5%_2.5%)	3.97069 100.00 3.13978 30.50 2.46279 9.95 1.94160 8.23	3.97 3.13 2.46 1.94	Li-BORATE HYDRATE(X) LIB5O6(M) Zr(H) Li BORATE HYDOXIDE(T)

Table 1

III. DIFFERENTIAL SCANNING CALORIMETRY

The DSC curve for lithium sulphate salt revealed the phase transition as an endothermic peak at 575°C, as shown in figure 9. Moreover no peak for dehydration has been observed in quenched lithium sulphate salt. The figures show the DSC curves for all series prepared in the present work.

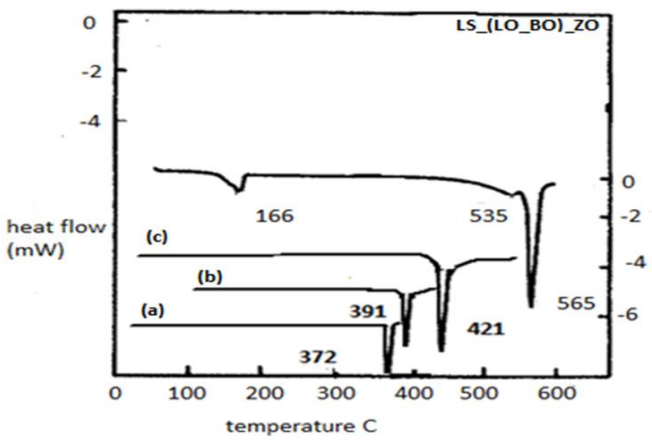

Fig 9

Series	Composition	Eg	Transition temp
	PURE Li2SO4	0.6348eV	574 C
LS_(LO_BO)_ZrO	83%_7%_10% 85%_5%_10% 80%_10%_10%	0.617eV o.44eV 0.566eV	441 C 393 C 490 C

Table 2

IV. CONCLUSION

The series- Li_2S0_4_$(Li_2O:B_2O_3)$_ZrO_2 is with composition, lithium borate glass and ZrO_2 added lithium sulphate, The minimum transition temperature is 372°C obtained for sample containing 25 mol% of lithium sulphate. The figure 9 shows the Endotherm for different mol % Li_2O-B_2O_3+ZrO_2 added in lithium sulphate also the inset shows the variation in endotherm temperature with Li_2O-B_2O_3+ZrO_2. This variation in endotherm temperature is also given in table 2. It is observed that the increase in the glassy phase due to addition ZrO_2 increases the viscosity of the melt as observed during synthesis, this may restrict the moment of SO_4 ion to support FCC structure of lithium sulphate to get stabilized at lower temperature as observed in earlier series.

V. REFERENCES

[1]. Bashir M.Suleiman, Arnold Lunden, Ernest karawaski, solid-state Ionics 136- 137(2000) 325-330.
[2]. A.Lunden, J.Thomas in: T.Takahashi (Ed) High conductivity solid Ionics Conductors, world science,Singapore, 1989,45.
[3]. T.Forland, J.Krogh-Moe, Acta.chem.Scand11 (1957) 565.
[4]. R.Tarneberg, A.Luden, Solid State Ionics 90(1996) 209.
[5]. A.Lunden in: Scrosati A.Magistris, C.M.Mari, G Mariotto (Eds) Fast Ion Transport in solids, NATO ASI series E: 250,Kluwer Dordrecht (1993), 181.
[6]. A.Lunden, Z.Naturforsch, 50a (1995), 1067.
[7]. Xin Guo, wilfried sigle, Jurgen Fleig, Joachim Maier, Solid State Ionics 154-155(2002), 555-561.
[8]. M.J.Verkerk, B.J.Middelhuis, A.J.Burggraaf, Solid state Ionics 6(1982), 159

International Virtual Conference on Materials and Nanotechnology
In Association with International Journal of Scientific Research in Science and Technology
Volume 9 | Issue 4 | Print ISSN: 2395-6011 | Online ISSN: 2395-602X (www.ijsrst.com)

Synthesis, Spectral and Thermal Degradation Kinetics Studies of Copolymer Resin

Jyotsana Khobragade[1], W. B. Gurnule[2]
[1]Department of Chemistry, Gurunanak Science College, Ballarpur, Maharashtra, India
[2]Department of Chemistry, Kamla Nehru Mahavidyalaya, Nagpur-440024, Maharashtra, India

ABSTRACT

Terpolymer (PTFM-II) has been synthesized by using the three monomers pthalic acid, melamine and formaldehyde in 2:1:4 molar proportions. The structure of PTFM-II copolymer has been elucidated on the basis of elemental analysis and various physicochemical techniques, i.e. UV–Visible, FT-IR and H^1-NMR spectroscopy. Thermal degradation study of the new copolymer has been carried out for its thermal stability. The activation energy (*Ea*) and thermal stability calculated by using the Sharp-Wentworth and Freeman-Carroll methods. Thermodynamic parameters such as entropy change (ΔS), apparent entropy change (S^*) and frequency factor (*z*) have also been evaluated on the basis of the data of Freeman-Carroll method.

Keywords : PTMF-II, copolymer; Synthesis; characterization; Sharp–Wentworth method; Freeman–Carroll method, Thermal degradation.

I. INTRODUCTION

Copolymers, very special class of polymer, are known for their versatile uses and are found to be amorphous, crystalline or resinous in nature. Due to their exciting features such as high thermal stability of copolymer resin which is considerable attention has been paid in the past two decades. The study of thermal behavior of polymers in air at different temperature provides an important information about its practical applicability. The thermal stability of the synthesized compounds was determined by thermogravimetric analysis [1]. Thermogravimetric analysis (TGA) has been proved to be a useful and efficient technique for the estimation of lifetimes of polymers. Phenol-formaldehyde resins were the first synthetic polymers to be commercialized. Phenolics are still very important industrial polymers, though their most common use today is in adhesives for the bonding of plywood and other structural wood products.

Melamine-formaldehyde resin is hard, thermosetting and water soluble resin. These are formed by the polymerization of melamine with formaldehyde.

In more than 70% of all wood-based materials in use today, adhesives and the physicochemical phenomenon of adhesion play an important role [2, 3]. This adhesives also used in paper products, paints, and finishes. The forest products industry have been used natural adhesives derived from starch, soybeans, animal waste, and byproducts of the meat processing, tanning industries, casein from skim milk [4]. In

many respects, the chemistry of the formation of melamine-based resins is very similar to that of UF resins.

MF resins have versatile applications such as in preparing kitchen utensil, table ware, furniture, automotive industry, clutch facing, brake pads, friction materials, for clutch and break, coated abrasive, grinding wheels, laminated paper and cloth, wood panel industry, composite wood panels, electrical molding, binder for leather tanning. Melamine resin is often used in kitchen utensils and plates. MF resins (also known as amino resins) are water soluble and, hence, find use as sizing agents and textiles-finishing resins. They are also used in paper industry, plywood industry and as adhesives. A considerable attention has been paid in the past two decades to the synthesis of copolymer resin due to their exciting features such as high thermal stability. Sami Ullah and coworker studied the thermal decomposition kinetics study of melamine-formaldehyde resin [5]. A. B. Zade and coworker studied the thermal degradation of copolymer resin (*p*-NP-4,4′-MDA-F) from p-nitrophenol (*p*-NP) and 4,4′-methylene dianiline (4,4′-MDA) with formaldehyde (F)[6] .

R. N. Singaru and coworker synthesis, characterization, and thermal degradation studies of copolymer resin derived from p-cresol, melamine, and formaldehyde[7]. Synthesis, characterisation and thermal degradation studies of copolymer resin by Wasudeo B. Gurnule and Vaishali R. Bisen Synthesised by monomers 2,4-dihydroxybenzoic acid, phenyl hydrazine and formaldehyde[8]

The objective of this work is synthesis and characterization of PTMF-II resins at 2:1:4 molar ratios of pthalic acid, melamine and formaldehyde and determination of the morphology, molecular weight synthesized resin samples. The synthesised resin samples were characterized by using molecular weight determination by conductoetric titration, and thermogravimetric analysis (TGA). The elemental analysis has been carried out to ascertain the molecular formula and the spectral studies have been used to characterize the complete structure of the PTMF-II resins. After treating the thermal degradation data with Sharp–Wentworth (S-W) and Freeman–Carroll (F-C) methods, activation energy and kinetic parameters such as ΔS, z, S^* and n (order of reaction) have been evaluated [9].

II. MATERIALS AND METHOD

Materials and samples

All the chemicals used were of analytical grade. Pthalic acid, melamine and formaldehyde which are purchased from Merck Chemicals, India. Solvents like N-,Ndimethylformamide and dimethylsulphoxide purchased from SD Fine Ltd, Mumbai, India, were used after distillation.

Synthesis of PTMF-II copolymer resin

The PTMF-II copolymer was synthesized by condensing pthalic acid (0.2 mol) – melamine (0.1 mol) – formaldehyde (0.4 mol) (PTMF) copolymers in the presence glacial acetic acid (200 ml) as a reaction medium at 126 ± 2°C in oil bath for 5 hours [10-11].

The resinous product so obtained was repeatedly washed with cold distilled water, dried in air and powdered with the help of mortar and pestle. The powdered sample was washed many times with boiling water and methanol to remove unreacted monomers. The air dried powdered then extracted with diethyl ether and then with petroleum ether to remove melamine formaldehyde copolymer which might be present along with PTMF copolymer resin. It was further purified by dissolving in 8% NaOH solution, filtered and reprecipitated by gradual drop wise addition of ice cold 1:1 (v/v) concentrated HCl/distill water with constant and rapid stirring to avoid lump formation. The process of reprecipitation was repeated thrice. The resulting polymer sample was filtered, washed several time with boiling water, dried in air, powdered and kept in vacuum over silica

gel. The yield of these copolymer resins found to be 85%. The reaction is shown as follows.

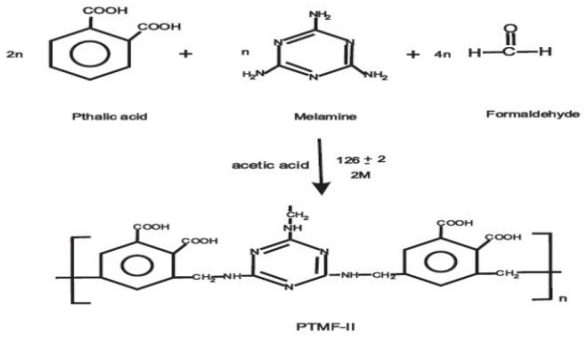

Fig.1 Synthesis of PTMF-II Terpolymer Resin

Analytical and physicochemical studies

The elemental analysis was carried out on a Perkin Elmer 2400 Elemental Analyzer instrument. The UV–Visible studies were out carried using Scimadzu UV-1800 Spectrophotometer in the range 200-800 nm. The Infrared spectrum was recorded in the region of 500–4000 cm-1 on Shimadzu Affinity-1 FTIR Spectrophotometer at Department of Chemistry, Kamla Nehru Mahavidyalaya, Nagpur. 1H-NMR studied using Bruker Avance-II FT-NMR Spectrometer in DMSO-d6 solvent. All the analytical and spectral studies for the newly synthesized copolymer were carried out at Sophisticated Testing Instrumentation Centre (STIC), Kochi.

Instrumentation

The nonisothermal thermogravimetric analysis was performed in air atmosphere with heating rate of 10 ^{0}C. min-1 using 5 - 6 mg of samples in platinum crucible from temperature of 40 ^{0}C to 800 ^{0}C and thermograms are recorded for PTMF-II sample at Sophisticated Testing Instrumentation Centre (STIC), Kochi. Thermal activation energies (Ea) and order of reaction (n) Calculated by using thermogravimetric data. Also other thermodynamic parameters such as entropy change (ΔS), apparent entropy change (S*) and frequency factor (z) are determined and reported in the Table 1.

Theoretical considerations

To provide further evidence regarding the degradation system of analyzed compounds, we derived the TG curves by applying an analytical method proposed by Sharp-Wentworth and Freeman-Carroll.

Freeman–Carroll method

Freeman and Carroll method used to derive the straight line equation [12], which is in the form of

$$\frac{\Delta \log dW/dt}{\Delta \log Wr} = n - \frac{Ea}{2.303R}.\frac{\Delta(1/T)}{\Delta \log Wr} \quad \ldots\ldots\ldots\ldots\ldots\ldots (1)$$

Where,

dW/dt = rate of change of weight with time.

Wr = Wc-W

Wc = weight loss at completion of reaction.

W = fraction of weight loss at time t.

Ea = energy of activation.

The plot between the terms $\frac{\Delta \log dW/dt}{\Delta \log Wr}$ vs $\frac{\Delta 1/T}{\Delta \log Wr}$ gives a straight line from which slope we obtained energy of activation (Ea) and intercept on Y-axis as order of reaction (n). The change in entropy (ΔS), frequency factor (z), apparent entropy (S*) can also be calculated by further calculations.

Sharp–Wentworth method

Using the equation derived by Sharp and Wentworth [13]

$$\log \frac{dC/dT}{1-C} = \log A/\beta - \frac{Ea}{2.303R}.\frac{1}{T} \quad \ldots\ldots\ldots\ldots\ldots\ldots (2)$$

Where,

dC/dT = rate of change of fraction of weight with change in temperature

β = linear heating rate dT/dt. By plotting the graph between log $\frac{dC/dT}{1-C}$ vs $\frac{1}{T}$

we obtained the straight line which give energy of activation (Ea) from its slope.

III. RESULTS AND DISCUSSION

The resin sample was white in color, insoluble in commonly used solvent, but was soluble in DMF, DMSO, THF, pyridine, concentrated H_2SO_4. No precipitation and degradation occurs of resin in all the solvents. These resins were analyzed for carbon, hydrogen and nitrogen content.

Characterization of copolymer

Molecular weight of copolymer was estimated by conductometric titration. The degree of polymerization ($\overline{DP}$) and the number average molecular weight $(\overline{Mn})$ were evaluated from the conductometric titration curves. Following formula used to determine the degree of polymerization.

$$\overline{DP} = \frac{\text{Total meq. of base required for complete neutralization}}{\text{Meq. of base required for smallest interval}}$$

$\overline{Mn}$ = $\overline{DP}$ x Repeat unit weight.

$(\overline{Mn})$ = $\overline{DP}$ x Repeat unit weight.

The molecular weight of PTMF-II is 3894.75. Fig.2.

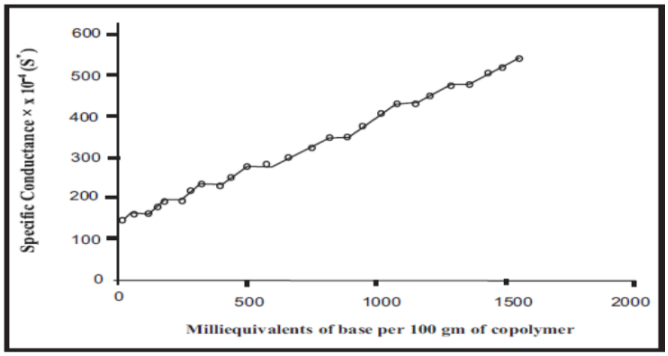

Fig. 2. Conductometric Titration Curves of PTMF-II Copolymer Resins

The composition of copolymer (represented in scheme 1) obtained on the basis of the elemental analysis data was found to be in good correlation to that of the calculated values:

Calculated for $C_{23}H_{19}O_8N_6$: Found : C: 54.02% H: 3.98% N: 16.82%

Calculated : C: 54.44% H: 3.75% N: 16.57%

The UV- Visible spectrum of the purified PTMF-II copolymere has been recorded in DMF. The broad of UV- Visible spectra is shown in figure 3. It shows two bands at 220 and 320 nm. The observed positions of the absorption bands with different intensities indicate the more intense band 220 nm is due to ($\pi \rightarrow \pi^*$) allowed transition which readily attains coplanarity and shoulder merging (loss of fine structure) and also due to chromophore groups like >C=C groups are in conjugation with an aromatic nucleus (aromatic ring) and the less intense band at 320 nm may be due to ($n \rightarrow \pi^*$) forbidden transition in >C=N, –C=O and –OH groups. The appearance of former band (more intense) can be accounted for ($\pi \rightarrow \pi^*$) transition while the latter band (less intense) may \be due to $n \rightarrow \pi^*$ electronic transition. The shift from the basic value (viz 220 and 320 nm, respectively) may be due to conjugation effect, and presence of Ar-COOH hydroxy group (auxochrome) is responsible for hyperchromic effect, i.e. higher $\in_{max}$ [14] . The $\in_{max}$ value gradually increases in the order PTMF-I < PTMF -II. This increasing order of $\in_{max}$ values may be due to introduction of more and more chromophores and auxochromes (- OH group of Ar-COOH) in the repeat unit of the terpolymer [15]. This observation is in good agreement with the proposed most probable structures of these terpolymer.

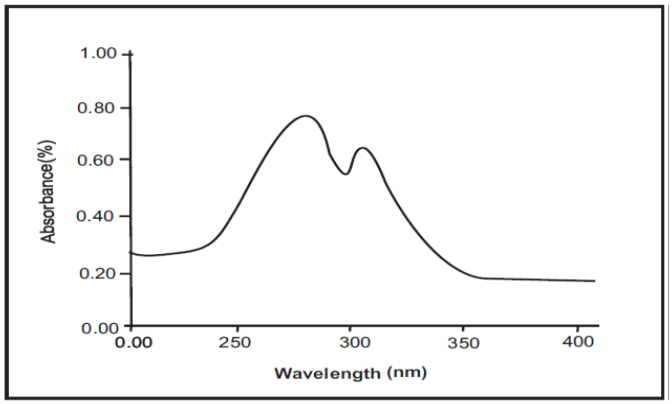

Fig.3. UV-Visible Spectra of PTMF-II Terpolymer Resins

The IR spectra of PTMF-II copolymer is presented in figure 4. The IR spectra revealed this copolymers give

rise to nearly similar pattern of spectra. The copolymer spectrum showed a broad band appeared in the range of 3254 cm^{-1} is assigned to the –NH stretching modes. The broad band appeared in the range of 3624.56 cm^{-1} is assigned to the –OH of Ar-COOH in stretching modes. The strong band is at 1884 cm^{-1} is due to the presence of carbonyl group of aromatic ring stretching mode and a strong band at 1527.24 cm^{-1} is attributed to C=N stretching of melamine ring. The 1, 2, 4. 6 tetra substituted aromatic ring ring is confirmed by sharp, medium/weak absorption bands appeared between 1204–886 cm^{-1}. A band appeared at 2852.35 cm^{-1} is due the –CH stretching vibrations of the aromatic ring. The band appeared at 1063 cm–1 is assigned to –C–N (I) stretching vibration. The bands appeared in the region of 2945 cm^{-1} are attributed to $–CH_2$ asymmetric and symmetric vibrations present in the terpolymer. The presence of $–CH_2$ bending vibration in $Ar–CH_2–N$ bridge in the spectrum is confirmed by the absorption band appeared at 1450 cm^{-1}.

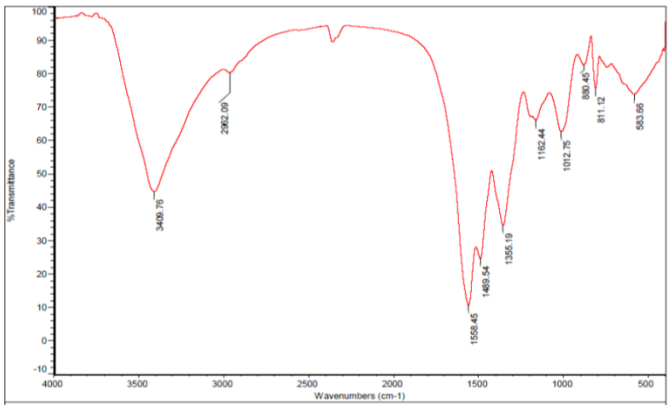

Fig.4. Infra Red Spectra of PTMF-II Terpolymer Resins

^1H NMR spectra of PTMF-II terpolymers show a weak multiple signal (unsaturated pattern) in the region 8.22 to 8.30 (δ) ppm that is due to aromatic protons. Weak signal in the range of appeared in the range at 10.32 to 10.62 (δ) ppm may be due to the proton of CO(OH) in Ar-COOH . The much downfield chemical shift for aromatic carboxyl –OH indicates clearly the intramolecular hydrogen bonding of -OH group. Triplet signal appeared in the region 5.35 (δ) ppm can be assigned to amine proton of – C – NH – C - linkage. Intense signal appeared in the region 3.98 to 4.30 (δ) ppm may be due to protons of methylenic bridges (CH2) of polymer chain.

Thermogravimetric analysis of the terpolymer

The thermal stability of copolymer is evaluated by dynamic thermo-gravimetric analysis in air atmosphere with heating rate of 10^0C min-1. Thermogram of PTMF-II copolymer is shown in Fig. 5. Thermogram of copolymer depicts three steps decomposition after loss of water molecule in the temperature range 40^0C – 800^0C. All decomposition stage depicted in table 2.

Thermo-analytical data

A plot of percentage mass loss versus temperature is shown in the Fig. 5 for a representation of PTMF-II copolymer resin. Sharp-Wentworth and Freeman-Caroll method was adopted to obtain the relative thermal stability of the copolymer. The thermal stability of copolymer, based on the initial decomposition temperature, has also been used here to define their relative thermal stability, neglecting the degree of decomposition.

For calculating activation energy (Ea) thermal decomposition data has been used and then applying above methods. 'Average Ea' by Sharp-Wentworth is nearly double than 'average Ea' calculated by Freeman-Carroll methods. The activation energy calculated by these methods is depicted in Table 2. However the error in activation energies obtained from the Sharp-Wentworth isoconversional method is significant and largely increases as far as conversion increases. On the other hand, it has been considered of interest to analyze the behavior of the process constitute by two competitive reactions that would lead to an apparent dependence between Ea and α when analyzed by isoconversional method, in spite such dependence is not real [16].

A representative thermal activation energy plot of Sharp-Wentworth (Fig. 8) and Freeman-Carroll (Fig.

6-7) method for the copolymer has been shown. Thermodynamic parameters such as entropy change (ΔS), frequency factor (z), apparent entropy change (S*) calculated on the basis of thermal activation energy (Ea) using equations (3), (4), (5). These values are given in (Table 1).

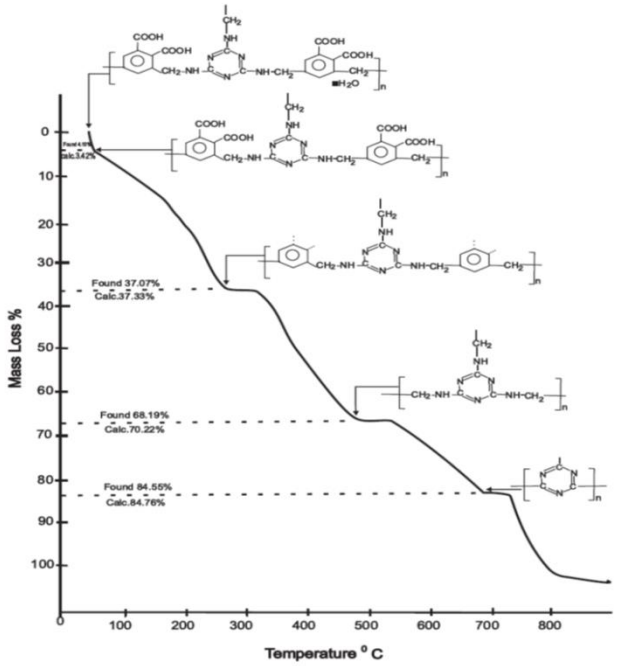

Fig.5. Decomposition Pattern of PTMF-II Copolymer Resin

Entropy Change (*ΔS*):

$$Intercept = log\frac{kR}{h\phi Ea} + \frac{\Delta S}{2.303R} \quad \text{..... (3)}$$

Where, $k = 1.3806 \times 10^{-16}$ erg.deg^{-1}.mol^{-1},
$R = 1.987$ cal.deg^{-1}.mol^{-1},
$h = 6.625 \times 10^{-27}$ erg.sec,
$\phi = 0.166$,

ΔS = entropy change,
Ea = activation energy from graph.

ii. Frequency Factor (z):

$$B_{2/3} = \frac{log\, z.Ea}{R\phi} \quad \text{..... (4)}$$

$$B_{2/3} = log\ 3 + log[1\text{-}3\sqrt{1-\alpha}] - log\ p(x) \quad \text{.....(a)}$$

Where, z = frequency factor,
B = calculated from eq [a],
$log\ p(x)$ = calculated from Doyle table corresponding to activation energy.

iii. Apparent entropy change (S*):

$$S^* = 2.303R\ log\frac{zh}{RT^*} \quad \text{.....(5)}$$

Where, T^* = temp at which half of the compound decomposed.

It may be concluded that decomposition reaction of PTMF-II copolymer can be classed as a 'slow' reaction if the abnormally low value of frequency factor [17, 18]. By using the two methods obtained good straight-line plots. This is expected since the decomposition of copolymer is known not to obey first order kinetic perfectly [19, 20].

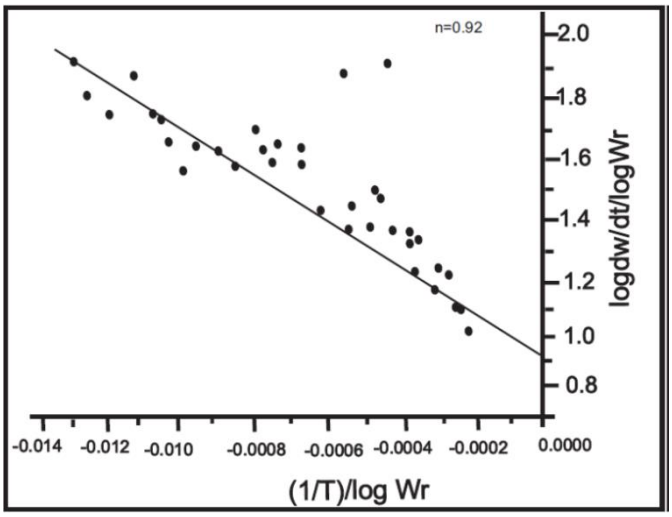

Fig. 6. Freeman-Carroll Plot of PTMF-II Terpolymer.

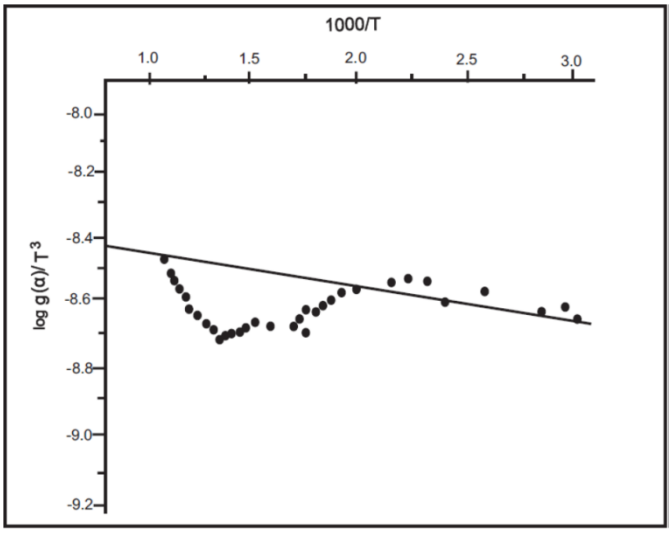

Fig. 7. Thermal Activation Energy Plot of PTMF-II Terpolymer

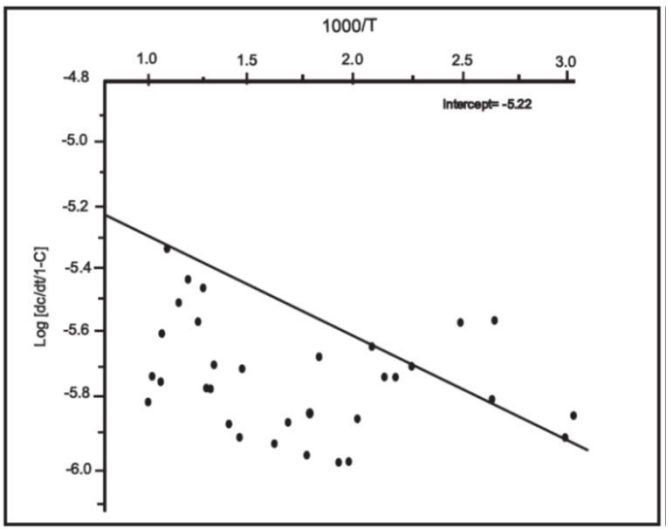

fig.8. Sharp-Wentworth Plot of PTMF-II Terpolymer Resins

Table 1: Thermogravimetrical Parameters Corresponding to Heating Rate of 10°C/min. of PTMF-II copolymers

Copolymer	Entropy change ΔS(J)	Free energy ΔF (KJ)	Frequency Z (S^{-1})	Apparent entropy (S*)	Order reaction (n)
PTMF-II	-161.37	55.46	732.22	-22.48	0.88

Table 2: Comparison of Activation Energy (Ea) of Degradation at Different Stages by Different Methods of PTMF-II Copolymers

Copolymer	Stage	Temp range	Group loss	Wt. Loss (%)	Activation Energy Ea (KJ)/mol	
					sharp-wentworth	Freeman-Carroll
PTMF-II	1st	40-170	H_2O molecule entrapped	4.10	24.05	22.34
	2nd	170-340	degradation of two –COOH group with another two–COOH group	37.07	26.23	24.75
	3rd	340-560	loss of aromatic ring along with -CH2 groups	68.19	9.02	7.14
	4th	560-800	loss of melamine moiety	84.55	34.45	32.12

IV. CONCLUSION

The Pthalic acid–melamine–formaldehyde (PTMF-II) copolymer was prepared with good yield. By various spectral techniques copolymer have been successfully characterized to propose their plausible structure. The calculated activation energies of the copolymer and its metal complexes are in good agreement with each other and their values are in accordance with their order of thermal stability. Based on the comparative Ea values calculated by SW and FC, the thermal degradation mechanism for both the PTMF-II copolymer was proposed. The copolymer follow nearly a first order kinetics.

V. REFERENCES

[1]. Takaji K., Tomita I., Endo T., Macromolecules, 30 (1997) 7386.

[2]. N. Ayrilmis, “Enhancement of dimensional stability and mechanical properties of light MDF by adding melamine resin impregnated paper waste,” International Journal of Adhesion and Adhesives, vol. 33, pp. 45–49, 2012.

[3]. J. Bishopp, “13-Adhesives for aerospace structures,” in Handbook of Adhesives and Surface Preparation, S. Ebnesajjad, Ed., pp. 301–344, William Andrew Publishing, Oxford, UK, 2011.

[4]. W. Clad, “Developments and problems in adhesives used for particle board manufacture,”

International Journal of Adhesion and Adhesives, vol. 3, no. 3, pp. 127–131, 1983.

[5]. Sami Ullah,1 M. A. Bustam,1 M. Nadeem,2 M. Y. Naz,3 W. L. Tan,1 and A. M. Shariff Volume 2014 |Article ID 940502, scientific world journal, Hindawi .

[6]. P.P. Kalbende,1 M. V. Tarase,2 and A.B. Zade, Journal of Chemistry, Volume 2013 ,Article ID 846327

[7]. R. N. Singaru, A. B. Zade, W. B. Gurnule, July 2008 Journal of Applied Polymer Science 109(2):859 - 868

[8]. V.R. Bisen, W. B. Gurnule,December 2014,Emerging Materials Research 3(6):271-281

[9]. Khobragade JV, Ahamed M, Gurnule WB. J Chem Pharma Res 2014; 6(8): 364

[10]. Rahandale S. S., Gurnule W. B., Zade A. B., Ind. J. Chem., 48(A) (2009).

[11]. Rahandale S. S., Gurnule W. B., Zade A. B., E. J. Chem., 6(3) (2009).

[12]. Freeman ES, Caroll BJ. Chem Rev 1958; 62: 394.

[13]. Sharp JB, Wentworth SA. Anal Chem 1969; 41: 2060.

[14]. Dudley H., William, Fleming. I., “Spectroscopic Methods in Organic Chemistry”, McGraw Hill Book Co. U.K. (1975)

[15]. Dudly H., Fleming. I. Spectroscopic methods in organic chemistry; Mc-Graw Hill;UK (1975)

[16]. Criado JM, Sanchez-Jimenez PE, Perez-Maqueda LA. J Them Anal Cal 2008; 92: 199.

[17]. Tonbul Y, Yardakoc K. Turk J Chem 2001; 25: 332.

[18]. Zhao H, Wang YZ, Wang DY, Wang B, Wu B, Chen DQ. Polym Degrad Stab 2003; 80: 135.

[19]. Singru RN, Zade AB, Gurnule WB. J App Polym Sci 2008; 109(2): 859.

[20]. J. V. Khobragade, W. B. Gurnule, S. V. Hunge , 2021 JETIR March 2021, Volume 8, Issue 3 (ISSN-2349-5162)

International Virtual Conference on Materials and Nanotechnology
In Association with International Journal of Scientific Research in Science and Technology
Volume 9 | Issue 4 | Print ISSN: 2395-6011 | Online ISSN: 2395-602X (www.ijsrst.com)

Synthesis and Physio-Chemical Aspects of Chlorosubstituted 1-Phenyl-Δ2-Pyraoles and 1-Phenyl-Δ2-Pyraolines on Plant Pathogen Cerscopora Personata

Amol D. Bhoyar*[1], Vishal S. Bhoyar[2], Smita A. Patil[1], Nilesh R. Thakare[1]

*[1]Department of Science and Humanities, P. R. Pote college of Engineering & Mgmt., Amravati, Maharashtra, India

[2]Department of Chemistry, Vidhyabharti Mahavidyalaya, Amravati, Maharashtra, India

ABSTRACT

Cerscopora genus are the plant pathogens that cause disease in the peanut plant which belongs to the family leguminose. They cause tikka or leaf spot. Plants suffering from this disease have dark brown or black spot are formed on the upper and lower surface of leaf. This infection leads to the early death of leaves or plants which results in the low yields. Cerscopora personata.was procured from genuine agricultural agencies. The compound synthesis in part I was screened invitro for their antifungal & antifungal activities by disc diffusion method.The newly prepare 1-phenyl-Δ2-pyraoles and 1-phenyl-Δ2-pyraolines were more effective against Cerscopora personata. The result in the present study suggest that 1-phenyl-Δ2-pyraoles and 1-phenyl-Δ2-pyraolines can be used for treating disease cause by Cerscopora personata.

Keywords : Cerscopora Personata. Antifungal and Antibacterial Activities , Pyrazoles, Pyrazolines

I. INTRODUCTION

Material and method

All melting points were determined in open capillary tubes and are uncorrected. I.R. spectra were recorded on a Perkin Elmer Infra Red Spectrophotometer 1310 using KBr disc. ^{1}H NMR on silica gel G and the solvent system used was benzene.

2-Aroyloxyacetophenone (3a – c)

2 hydroxy-3,5-dichloroacetophenone (0.04 mol) and benzoyl chloride (0.05 mol) where dissolved in dry pyridine (30 ml) with $POCl_3$ in NaOH (10%) (3a), 2 hydroxy-3,5-dichloroachoro -acetophenone (0.04 mol) and anisic acid (0.05 mol) where suspended in dry pyridine (30 ml) with $POCl_3$ in NaOH (10%) 30 ml (3b) and 2 hydroxy-3,5-dichloroacetophenone (0.04 mol) and valeric acid (0.05 mol) where suspended in dry pyridine (30 ml) with $POCl_3$ in NaOH (10%) 30 ml (3c). All the above reaction mixture was kept overnight and then worked up by dilution and acidification with Ice cold HCl (50%) to neutralize pyridine. the solid product was filtered, washed with water followed by sodium bicarbonate (10%) washing finally again with water. It crystallized from ethanol to obtained 2-Aroyloxyacetophenone (3a-c).

1-(2 hydroxy-3,5-dichlorophenyl)-3-aryl-1,3-propanedione (4a-c)

When 2-Aroyloxyacetophenone (3a-c) (0.05 mol) was dissolved in dry pyridine 40 ml. the solution was warmed upto 60^{0}C and pulvariesd KOH (15 g) was added slowly with constant stirring. After 4hr the reaction mixture was acidified by adding acid cold HCl (1:1). The product thus separated was filtered washed with sodium bicarbonate solution (10%) and finally again with water. It was then crystallized from ethanol- acetic acid mixture to get 1-(2 hydroxy-3,5-dichlorophenyl)-3-aryl-1,3-propanedione (4a-c) respectively.

4b – IR spectrum recorded in KBr (cm $^{-1}$) 3429, (s), -OH ; 2981, (s), -CH ; 1261, (s), > C=O ; 772, (s), -C-Cl . PMR spectrum recorded in δ $CDCl_3$ 3.90, (s), 2H –CO-CH_2-CO- ; 2.65, (s), 1H, -O-CH_3- ; 8.06 - 7.27, (m), 6H, -Ar-H ; 12.72, (s), 1H, -Ar-OH. TLC : Solvent (Benzene) height 3.4.cm, solute height :2.4 cm ; Rf value : 0.70, m.p. 96^{0}C, yield 82 %.

3-Aroylflavanone (5 a-d)

A mixture of 1-(2-hydroxy-3,5-dicholorophenyl)-3-phenyl-1,3-propanidione (4a) (0.01 mol) and benzaldehyde (0.02 mol) was refluxed in ethanol (25 ml) and piperidine (0.5 ml) for 15-20 min. yield 3-benzoyl-2-phenyl-6,8-dichloroflavanone (5a) . 1-(2-hydroxy-3,5-dicholorophenyl)-3-(4'methoxyphenyl)-1,3-propanedione (4b) (0.01 mol) and anisaldehyde (0.02 mol) was refluxed in ethanol (25 ml) and piperidine (0.5 ml) for 15-20 min. yield 3-anisoyl-(4'-methoxyphenyl)-6,8-dichloroflavanone (5b). 1-(2-hydroxy-3,5-dicholorophenyl)-3-butyl-1,3-propanedione (4c) (0.01 mol) and propionaldehyde (0.02 mol) was refluxed in ethanol (25 ml) and piperidine (0.5 ml) for 15-20 min. yield 3-valeroyl-2-ethyl-6,8-dichlorocromanone (5c). 1-(2-hydroxy-3,5-dicholorophenyl)-3-butyl-1,3-propanedione (4c) (0.01 mol) and valeraldehyde (0.02 mol) was refluxed in ethanol (25 ml) and piperidine (0.5 ml) for 15-20 min. yield 3-valeroyl-2butyl-6,8-dichlorocromanone (5d). all above reactions after refluxing, cooling the mixture was acidified with dil HCl (1:1). The product thus separated was filtered washed with sodium bicarbonate solution (10%) and finally again with water. It is then crystallized from ethanol-acetic acid mixture.

5a – IR spectrum recorded in KBr (cm $^{-1}$)

3070, (s), -C-H ; 1773, (s), >C=O ; 1699, (s), >C=O ; 1296, (s), -C-O ; 767, (s), -C-Cl . PMR spectrum recorded in δ $CDCl_3$ 5.40, (D), 1H –CH-CH ; 5.60, (d), 1H, -CH-CH- ; 6.48 – 8.21, (m), 14H, -Ar-H ; TLC : Solvent (Benzene) height 2.6.cm, solute height :1.2 cm ; Rf value : 0.46, m.p. 152^{0}C, yield 75 %.

4-Aroyl-Δ^2-pyrazolines (6 a-b) and 4-alkoyl-Δ^2-pyrazolines (6 c-d)

3-benzoyl-2-phenyl-6,8-dichloroflavanone (5a) (0.01 mol) and phenylhydrazine hydrochloride (0.02 mol) was refluxed in ethanol (20 ml) and piperidine (0.5 ml) for 1.5 hr. yield 3-(2-hydroxy-3,5-dichlorophenyl)-4-benzoyl-1,5-diphenyl-Δ^2-pyrazolines (6a). 3-anisoyl-2-(4'-methoxyphenyl)-6,8-dichloro-flavanone (5b) (0.01 mol) and phenylhydrazine hydrochloride (0.02 mol) was refluxed in ethanol (20 ml) and piperidine (0.5 ml) for 1.5 hr. yield 3-(2-hydroxy-3,5-dichlorophenyl)-4-anisoyl-5-(4'methoxyphenyl)-1-phenyl-Δ^2-pyrazolines (6b). 3-valeroyl-2-ethyl-6,8-dichlorocromanone (5c) (0.01 mol) and phenylhydrazine hydrochloride (0.02 mol) was refluxed in ethanol (20 ml) and piperidine (0.5 ml) for 1.5 hr. yield 3-(2-hydroxy-3,5-dichlorophenyl)-4-valeroyl,5-ethyl-1-phenyl-Δ^2-pyrazolines (6c). 3-valeroyl-2butyl-6,8-dichlorocromanone (5d) (0.01 mol) and phenylhydrazine hydrochloride (0.02 mol) was refluxed in ethanol (20 ml) and piperidine (0.5 ml) for 1.5 hr. yield 3-(2-hydroxy-3,5-dichlorophenyl)-4-valeroyl-5-butyl-1-phenyl-Δ^2-pyrazolines (6d). all above reactions after refluxing, cooling the mixture was acidified with dil HCl (1:1). The product thus separated was filtered washed with sodium bicarbonate solution (10%) and finally again

with water. It is then crystallized from ethanol-acetic acid mixture.

6a – IR spectrum recorded in KBr (cm $^{-1}$)

3208, (vb), -OH ; 3003, (s), -C-H ; 1675, (s), >C=O ; 1599, (m), >C=N ; 764, (s), -C-Cl . PMR spectrum recorded in δ $CDCl_3$ 5.10, (D), 1H –CH-CH ; 5.45, (d), 1H, -CH-CH- ; 6.8 – 8.2, (m), 20H, -Ar-H ; 13.4, (m), 1H, -Ar-OH ; TLC : Solvent (Benzene) height 2.9.cm, solute height :1.5 cm ; Rf value : 0.51, m.p. 165^{0}C, yield 85 %.

3-Aroylflavanone (7a-d)

3-Aroyl-6,8-dichloroflavanone (5 a-d) was refluxed for 10 minutes in ethanol (20 ml) with crystal of iodine. all above reactions after refluxing, cooling the mixture was acidified with dil HCl (1:1). The product thus separated was filtered washed with sodium thiosulphate solution (10%) and finally again with water. It is then crystallized from ethanol to get 3-Aroylflavanone (7a-d) .

7a – IR spectrum recorded in KBr (cm $^{-1}$)

3070, (vb), -C-H ; 1694, (s), >C=O ; 1663, (s), >C=O ; 1587, (s), -C=C ; 750, (s), -C-Cl . PMR spectrum recorded in δ $CDCl_3$ 3.1, (D), 1H –CH-CH ; 3.5, (d), 1H, -CH-CH- ; 6.8 – 8.2, (m), 12H, -Ar-H ; TLC : Solvent (Benzene) height 2.1.cm, solute height :1.3 cm ; Rf value : 0.62, m.p. 172^{0}C, yield 80 %.

4-Aroylflavanones (8 a-b) and 4-Alkoylpyrazoles (8 c- d)

3-benzoyl-2-phenyl-6,8-dichloroflavone (7a) (0.01 mol) and phenylhydrazine hydrochloride (0.02 mol) was refluxed in ethanol (20 ml) and piperidine (0.5 ml) for 1.5 hr. yield 3-(2-hydroxy-3,5-dichlorophenyl)-4-benzoyl-1,5-diphenyl-Δ^2-pyrazoles (8a). 3-anisoyl-2-(4'-methoxyphenyl)-6,8-dichloro-flavone (5b) (0.01 mol) and phenylhydrazine hydrochloride (0.02 mol) was refluxed in ethanol (20 ml) and piperidine (0.5 ml) for 1.5 hr. yield 3-(2-hydroxy-3,5-dichlorophenyl)-4-anisoyl-5-(4'methoxyphenyl)-1-phenyl-Δ^2-pyrazoles (8b). 3-valeroyl-2-ethyl-6,8-dichlorocromone (7c) (0.01 mol) and phenylhydrazine hydrochloride (0.02 mol) was refluxed in ethanol (20 ml) and piperidine (0.5 ml) for 1.5 hr. yield 3-(2-hydroxy-3,5-dichlorophenyl)-4-valeroyl,5-ethyl-1-phenyl-Δ^2-pyrazoles (8c). 3-valeroyl-2-butyl-6,8-di-chlorocromanone (7d) (0.01 mol) and phenylhydrazine hydrochloride (0.02 mol) was refluxed in ethanol (20 ml) and piperidine (0.5 ml) for 1.5 hr. yield 3-(2-hydroxy-3,5-dichlorophenyl)-4-valeroyl-5-butyl-1-phenyl-Δ^2-pyrazoles (8d). All above reactions after refluxing, cooling the mixture was acidified with dil HCl (1:1). The product thus separated was filtered washed with sodium bicarbonate solution (10%) and finally again with water. It is then crystallized from ethanol-acetic acid mixture.

8a – IR spectrum recorded in KBr (cm $^{-1}$)

3228, (vb), -OH ; 1674, (s), >C=O ; 1598, (s), >C=N ; 1441, (m), >C=C< ; 749, (s), -C-Cl . PMR spectrum recorded in δ $CDCl_3$ 6.5 – 8.2, (m), 13H, -Ar-H ; 11.4, (s), 1H, -Ar-OH ; TLC : Solvent (Benzene) height 2.5.cm, solute height :1.9 cm ; Rf value : 0.76, m.p. 175^{0}C, yield 80 %.

Photochemical Study :

The photochemical screening of Cerscopora personata reported in the presence of alkaloids, tannins, steroids, prines, carbohydrates and proteins.

Antifungal Assay

The well diffusion method was used to determine the antifungal activity of Cerscopora personata.

The culture media for pathogens was prepared by using folloeing composition for one liter distilled water.

Peptone	:	5.0 g/lit
Sodium Chloride	:	5.0 g/lit
Beef extract	:	1.5 g/lit
Yeast extract	:	1.5 g/lit
Agar	:	15.0 g/lit
pH (Approximately)	:	7.4 $\pm$ 0.2

The culture medium thus prepared was sterilized in autoclaves at 15 lbs/inch pressure and 121^{0}C temp. for

15 min. After sterilization , it was cooled down to about 50^{0}C and poured into pre sterilized petri plates of 8.5 cm in diameter each and allowed to solidify the nutrient agar medium of about 14mm depth. The petri plates were kept with nutrient broth at 37^{0}C for 4 hr. in an incubator.

The plates were dried again for 30 min. and without further delay discs soaked in the test compound . the plates were kept in incubator at 37^{0}C for about 18 – 24 hrs. soon after incubation period is over the degree of sensitivity to get compound was determined by measuring the visible clear area of growth free zones produces by the diffusion of the antibodies in to media from the discs by vernier caliper in mm. the result obtained are tabulated in the following table.

II. RESULT AND DISCUSSION

The newly synthesized compound is assayed against Cerscopora personata. And the antifungal effects were effects under controlled laboratory conditions. On comparison of the result , the dominant inhibitory effect of butyl group substituted compounds against Cerscopora personata is found remarkable. The cholorosubstituted pyrazoles and pyrazolines showed their prominent effect against E. amylovora and A. tumefacience.

III.CONCLUSION

The fungus causes disease in crop plant , which affects on yield. Plants are natural source of remedy of fungal diseases. *Cerscopora personata* is comes widely in nature. The antifungal study was carried out with an objective to investigate antifungal potentials. The butyl and chloro group substituted compounds shows better activity than other substituents against fungi.

Sr. No.	Test Compounds	Zone of inhibitions (mm) *Cerscopora personata*
1	6a	12
2	6b	11
3	6c	13
4	6d	11
5	8a	11
6	8b	13
7	8c	14
8	8d	10

IV. REFERENCES

[1]. Stocks E J and Ridgeway G L , Clinical Bacterio ,1099 , 5 'h Ed, Edward Arnold ltd. (1975) 211
[2]. Smiti Duliyedi Siddiqui, I R , Indian I.Heterocyclic chem. (2005),14, 251.
[3]. Mandal N K , Sinha R, Baneqee K P, Chem abstra, 1986, 104, 34034 v.-
[4]. Ahluwalia M D, Chem nbsfra.1991, 114, 8166 u.
[5]. Howe K R, Chem abstra. 1979, 90, 16859 w.
[6]. Archaaa V K , Shrivastava R C and Kumar A, Indian I c/tem.2002, 41B, 2325.
[7]. Noel B, Groth C and Seigfried, chem. Abstra.1999, 102 .
[8]. Mulwad V V , Choudhari B P , , Indian I ches. 2005, 44B, 1074
[9]. Bose P K, I Indian Chem Soc, 1958,35, 367.
[10]. Schuda P F , Top Org Chem, 1980,91,75.
[11]. Mogilaiah K & Babu-Rao, Indian I Chem, I 998,37B, 894.
[12]. Morgan G T & Micklehwait F M G , J Chem Soc, , 1904, 85, 12

International Virtual Conference on Materials and Nanotechnology
In Association with International Journal of Scientific Research in Science and Technology
Volume 9 | Issue 4 | Print ISSN: 2395-6011 | Online ISSN: 2395-602X (www.ijsrst.com)

Synthesis and Antifungal Activity of Chlorosubstituted 1-Phenyl-Δ2-Pyraoles and 1-Phenyl-Δ2-Pyraolines on Plant Pathogen Alternaria Solani

Amol D. Bhoyar*[1], Vishal S. Bhoyar[2], Nilesh R. Thakare[1], Amol Nande[3]

*[1]Department of Science and Humanities, P. R. Pote college of Engineering & Mgmt., Amravati, Maharashtra, India

[2]Department of Chemistry, Vidhyabharti Mahavidyalaya, Amravati, Maharashtra, India

[3]Department of Physics, Guru Nanak College of science, Ballarpur, Dist. Chandrapur, Maharashtra, India

ABSTRACT

Alterneria leaf blight is one of the most important disease of potato worldwide. During 2009 – 2010 in the Kashmir valley surveyed that he disease was prevalent in all the potato growing areas. The overall mean disease incidence and intensity ranged from 24.54 to 28.23%. In early stages of disease development , small irregular to circular dark brown spot on lower leaves appear meaning 0.5 mm in size. The aim of the present study was to investigate the antifungal and antibacterial activities on Alterneria solani. Alterneria solani was procured from genuine agricultural agencies. The compound synthesis in part I was screened invitro for their antifungal & antifungal activities by disc diffusion method.

Keywords : Alterneria Solani , Antifungal and Antibacterial Activities , Pyrazoles, Pyrazolines

I. INTRODUCTION

In order to synthesized flavanones , flavones, Pyrazolines and Pyrazoles the reaction sequence were followed as out line in the scheme I. The required 1-(2-hydroxy-3,5-dichoroacetophenone which on condensation is converted into 2-aroyl-3,5-dicholoroacetophenone (3) were reacted under BVT in the presence of KOH with pyridines gives 1-(2-hydroxy-3,5dichorophenyl)-3-substituted-1,3-propanedione (4) and then converted into 3-aroylflavanones (5) by using different aromatic aldehyde in the presence of ethanol-piperidine. The reaction of (5) and the iodine in the presence of ethanol yield flavones (7). The condensation of (7) and phenylhydrazine hydrochloride in the presence of ethanol and piperidine gives pyrazoles (8) . The compounds prepare were characterized and characterized and screened for their antifungal activity.

II. METHOD AND MATERIAL

All melting points were determined in open capillary tubes and are uncorrected. I.R. spectra were recorded on a Perkin Elmer Infra-Red Spectrophotometer 1310 using KBr disc. ^{1}H NMR on silica gel G and the solvent system used was benzene.

2-Aroyloxyacetophenone (3a – c).

2 hydroxy-3,5-dichloroacetophenone (0.04 mol) and benzoyl chloride (0.05 mol) where dissolved in dry pyridine (30 ml) with $POCl_3$ in NaOH (10%) (3a), 2 hydroxy-3,5-dichloroachoro -acetophenone (0.04 mol) and anisic acid (0.05 mol) where suspended in dry pyridine (30 ml) with $POCl_3$ in NaOH (10%) 30 ml (3b) and 2 hydroxy-3,5-dichloroacetophenone (0.04 mol) and valeric acid (0.05 mol) where suspended in dry pyridine (30 ml) with $POCl_3$ in NaOH (10%) 30 ml (3c). All the above reaction mixture was kept overnight and then worked up by dilution and acidification with Ice cold HCl (50%) to neutralize pyridine. the solid product was filtered, washed with water followed by sodium bicarbonate (10%) washing finally again with water. It crystallized from ethanol to obtained 2-Aroyloxyacetophenone (3a-c).

1-(2-hydroxy-3,5-dichlorophenyl)-3-aryl-1,3-propanedione (4a-c)

When 2-Aroyloxyacetophenone (3a-c) (0.05 mol) was dissolved in dry pyridine 40 ml. the solution was warmed upto 60^0C and pulvariesd KOH (15 g) was added slowly with constant stirring. After 4hr the reaction mixture was acidified by adding acid cold HCl (1:1). The product thus separated was filtered washed with sodium bicarbonate solution (10%) and finally again with water. It was then crystallized from ethanol- acetic acid mixture to get 1-(2 hydroxy-3,5-dichlorophenyl)-3-aryl-1,3-propanedione (4a-c) respectively.

4b – IR spectrum recorded in KBr (cm^{-1}) 3429, (s), -OH ; 2981, (s), -CH ; 1261, (s), > C=O ; 772, (s), -C-Cl . PMR spectrum recorded in δ $CDCl_3$ 3.90, (s), 2H – $CO\text{-}CH_2\text{-}CO$- ; 2.65, (s), 1H, -O-CH_3- ; 8.06 - 7.27, (m), 6H, -Ar-H ; 12.72, (s), 1H, -Ar-OH. TLC : Solvent (Benzene) height 3.4.cm, solute height :2.4 cm ; Rf value : 0.70, m.p. 96^0C, yield 82 %.

3-Aroylflavanone (5 a-d)

A mixture of 1-(2-hydroxy-3,5-dicholorophenyl)-3-phenyl-1,3-propanidione (4a) (0.01 mol) and benzaldehyde (0.02 mol) was refluxed in ethanol (25 ml) and piperidine (0.5 ml) for 15-20 min. yield 3-benzoyl-2-phenyl-6,8-dichloroflavanone (5a) . 1-(2-hydroxy-3,5-dicholorophenyl)-3-(4'methoxyphenyl)-1,3-propanedione (4b) (0.01 mol) and anisaldehyde (0.02 mol) was refluxed in ethanol (25 ml) and piperidine (0.5 ml) for 15-20 min. yield 3-anisoyl-(4'-methoxyphenyl)-6,8-dichloroflavanone (5b). 1-(2-hydroxy-3,5-dicholorophenyl)-3-butyl-1,3-propanedione (4c) (0.01 mol) and propionaldehyde (0.02 mol) was refluxed in ethanol (25 ml) and piperidine (0.5 ml) for 15-20 min. yield 3-valeroyl-2-ethyl-6,8-dichlorocromanone (5c). 1-(2-hydroxy-3,5-dicholorophenyl)-3-butyl-1,3-propanedione (4c) (0.01 mol) and valeraldehyde (0.02 mol) was refluxed in ethanol (25 ml) and piperidine (0.5 ml) for 15-20 min. yield 3-valeroyl-2butyl-6,8-dichlorocromanone (5d). all above reactions after refluxing, cooling the mixture was acidified with dil HCl (1:1). The product thus separated was filtered washed with sodium bicarbonate solution (10%) and finally again with water. It is then crystallized from ethanol-acetic acid mixture.

5a – IR spectrum recorded in KBr (cm^{-1})

3070, (s), -C-H ; 1773, (s), >C=O ; 1699, (s), >C=O ; 1296, (s), -C-O ; 767, (s), -C-Cl . PMR spectrum recorded in δ $CDCl_3$ 5.40, (D), 1H –CH-CH ; 5.60, (d), 1H, -CH-CH- ; 6.48 – 8.21, (m), 14H, -Ar-H ; TLC : Solvent (Benzene) height 2.6.cm, solute height :1.2 cm ; Rf value : 0.46, m.p. 152^0C, yield 75 %.

4-Aroyl-Δ^2-pyrazolines (6 a-b) and 4-alkoyl-Δ^2-pyrazolines (6 c-d)

3-benzoyl-2-phenyl-6,8-dichloroflavanone (5a) (0.01 mol) and phenylhydrazine hydrochloride (0.02 mol) was refluxed in ethanol (20 ml) and piperidine (0.5 ml) for 1.5 hr. yield 3-(2-hydroxy-3,5-dichlorophenyl)-4-benzoyl-1,5-diphenyl-Δ^2-pyrazolines (6a). 3-anisoyl-2-(4'-methoxyphenyl)-6,8-

dichloro-flavanone (5b) (0.01 mol) and phenylhydrazine hydrochloride (0.02 mol) was refluxed in ethanol (20 ml) and piperidine (0.5 ml) for 1.5 hr. yield 3-(2-hydroxy-3,5-dichlorophenyl)-4-anisoyl-5-(4'methoxyphenyl)-1-phenyl-Δ^2-pyrazolines (6b). 3-valeroyl-2-ethyl-6,8-dichlorocromanone (5c) (0.01 mol) and phenylhydrazine hydrochloride (0.02 mol) was refluxed in ethanol (20 ml) and piperidine (0.5 ml) for 1.5 hr. yield 3-(2-hydroxy-3,5-dichlorophenyl)-4-valeroyl,5-ethyl-1-phenyl-Δ^2-pyrazolines (6c). 3-valeroyl-2butyl-6,8-dichlorocromanone (5d) (0.01 mol) and phenylhydrazine hydrochloride (0.02 mol) was refluxed in ethanol (20 ml) and piperidine (0.5 ml) for 1.5 hr. yield 3-(2-hydroxy-3,5-dichlorophenyl)-4-valeroyl-5-butyl-1-phenyl-Δ^2-pyrazolines (6d). all above reactions after refluxing, cooling the mixture was acidified with dil HCl (1:1). The product thus separated was filtered washed with sodium bicarbonate solution (10%) and finally again with water. It is then crystallized from ethanol-acetic acid mixture.

6a – IR spectrum recorded in KBr (cm $^{-1}$)

3208, (vb), -OH ; 3003, (s), -C-H ; 1675, (s), >C=O ; 1599, (m), >C=N ; 764, (s), -C-Cl . PMR spectrum recorded in δ $CDCl_3$ 5.10, (D), 1H –CH-CH ; 5.45, (d), 1H, -CH-CH- ; 6.8 – 8.2, (m), 20H, -Ar-H ; 13.4, (m), 1H, -Ar-OH ; TLC : Solvent (Benzene) height 2.9.cm, solute height :1.5 cm ; Rf value : 0.51, m.p. 165^{0}C, yield 85 %.

3-Aroylflavanone (7a-d)

3-Aroyl-6,8-dichloroflavanone (5 a-d) was refluxed for 10 minutes in ethanol (20 ml) with crystal of iodine. all above reactions after refluxing, cooling the mixture was acidified with dil HCl (1:1). The product thus separated was filtered washed with sodium thiosulphate solution (10%) and finally again with water. It is then crystallized from ethanol to get 3-Aroylflavanone (7a-d) .

7a – IR spectrum recorded in KBr (cm $^{-1}$)

3070, (vb), -C-H ; 1694, (s), >C=O ; 1663, (s), >C=O ; 1587, (s), -C=C ; 750, (s), -C-Cl . PMR spectrum recorded in δ $CDCl_3$ 3.1, (D), 1H –CH-CH ; 3.5, (d), 1H, -CH-CH- ; 6.8 – 8.2, (m), 12H, -Ar-H ; TLC : Solvent (Benzene) height 2.1.cm, solute height :1.3 cm ; Rf value : 0.62, m.p. 172^{0}C, yield 80 %.

4-Aroylflavanones (8 a-b) and 4-Alkoyl-pyrazoles (8 c- d)

3-benzoyl-2-phenyl-6,8-dichloroflavone (7a) (0.01 mol) and phenylhydrazine hydrochloride (0.02 mol) was refluxed in ethanol (20 ml) and piperidine (0.5 ml) for 1.5 hr. yield 3-(2-hydroxy-3,5-dichlorophenyl)-4-benzoyl-1,5-diphenyl-Δ^2-pyrazoles (8a). 3-anisoyl-2-(4'-methoxyphenyl)-6,8-dichloro-flavone (5b) (0.01 mol) and phenylhydrazine hydrochloride (0.02 mol) was refluxed in ethanol (20 ml) and piperidine (0.5 ml) for 1.5 hr. yield 3-(2-hydroxy-3,5-dichlorophenyl)-4-anisoyl-5-(4'methoxyphenyl)-1-phenyl-Δ^2-pyrazoles (8b). 3-valeroyl-2-ethyl-6,8-dichlorocromone (7c) (0.01 mol) and phenylhydrazine hydrochloride (0.02 mol) was refluxed in ethanol (20 ml) and piperidine (0.5 ml) for 1.5 hr. yield 3-(2-hydroxy-3,5-dichlorophenyl)-4-valeroyl,5-ethyl-1-phenyl-Δ^2-pyrazoles (8c). 3-valeroyl-2-butyl-6,8-di-chlorocromanone (7d) (0.01 mol) and phenylhydrazine hydrochloride (0.02 mol) was refluxed in ethanol (20 ml) and piperidine (0.5 ml) for 1.5 hr. yield 3-(2-hydroxy-3,5-dichlorophenyl)-4-valeroyl-5-butyl-1-phenyl-Δ^2-pyrazoles (8d). All above reactions after refluxing, cooling the mixture was acidified with dil HCl (1:1). The product thus separated was filtered washed with sodium bicarbonate solution (10%) and finally again with water. It is then crystallized from ethanol-acetic acid mixture.

8a – IR spectrum recorded in KBr (cm $^{-1}$)

3228, (vb), -OH ; 1674, (s), >C=O ; 1598, (s), >C=N ; 1441, (m), >C=C< ; 749, (s), -C-Cl . PMR spectrum recorded in δ $CDCl_3$ 6.5 – 8.2, (m), 13H, -Ar-H ; 11.4, (s), 1H, -Ar-OH ; TLC : Solvent (Benzene) height

2.5.cm, solute height :1.9 cm ; Rf value : 0.76, m.p. 175^{0}C, yield 80 %.

Photochemical Study :

The photochemical screening of *Alterneria solani* reported in the presence of alkaloids, tannins, steroids, prines, carbohydrates and proteins.

Antifungal Assay

The well diffusion method was used to determined the antifungal activity of *Alterneria solani.*

The culture media for pathogens was prepared by using folloeing composition for one liter distilled water.

Peptone	:	5.0 g/lit
Sodium Chloride	:	5.0 g/lit
Beef extract	:	1.5 g/lit
Yeast extract	:	1.5 g/lit
Agar	:	15.0 g/lit
pH (Approximately)	:	7.4 $\pm$ 0.2

The culture medium thus prepared was sterilized in autoclaves at 15 lbs/inch pressure and 121^{0}C temp. for 15 min. After sterilization , it was cooled down to about 50^{0}C and poured into pre sterilized petri plates of 8.5 cm in diameter each and allowed to solidify the nutrient agar medium of about 14mm depth. The petri plates were kept with nutrient broth at 37^{0}C for 4 hr. in an incubator.

The plates were dried again for 30 min. and without further delay discs soaked in the test compound . the plates were kept in incubator at 37^{0}C for about 18 – 24 hrs. soon after incubation period is over the degree of sensitivity to get compound was determined by measuring the visible clear area of growth free zones produces by the diffusion of the antibodies in to media from the discs by vernier caliper in mm. the result obtained are tabulated in the following table.

III. RESULT AND DISCUSSION

The newly synthesized compound is assayed against *Alterneria solani.* And the antifungal effects were effects under controlled laboratory conditions. On comparison of the result , the dominant inhibitory effect of butyl group substituted compounds against *Alterneria solani* is found remarkable. The cholorosubstituted pyrazoles and pyrazolines showed their prominent effect against *E. amylovora* and *A. tumefacience*.

IV. CONCLUSION

The fungus causes disease in crop plant , which affects on yield. Plants are natural source of remedy of fungal diseases. *Alterneria solani* is comes widely in nature. The antifungal study was carried out with an objective to investigate antifungal potentials. The butyl and chloro group substituted compounds shows better activity than other substituents against fungi.

Table 1 : Antifungal activity data of compound 6 a – d and 8 a- d .

Sr. No.	Test Compounds	Zone of inhibitions (mm) *Alterneria solani*
1	6a	13
2	6b	14
3	6c	14
4	6d	14
5	8a	11
6	8b	12
7	8c	13
8	8d	13

V. REFERENCES

[1]. Stocks E J and Ridgeway G L , Clinical Bacterio ,1099 , 5 'h Ed, Edward Arnold ltd. (1975) 211

[2]. Smiti Duliyedi Siddiqui, I R , Indian I.Heterocyclic chem. (2005),14, 251.

[3]. Mandal N K , Sinha R, Baneqee K P, Chem abstra, 1986, 104, 34034 v. -

[4]. Ahluwalia M D, Chem nbsfra.1991, 114, 8166 u.

[5]. Howe K R, Chem abstra. 1979, 90, 16859 w.

[6]. Archaaa V K , Shrivastava R C and Kumar A, Indian I c/tem.2002, 41B, 2325.

[7]. Noel B, Groth C and Seigfried, chem. Abstra.1999, 102 .

[8]. Mulwad V V , Choudhari B P , , Indian I ches. 2005, 44B, 1074

[9]. Bose P K, I Indian Chem Soc, 1958,35, 367.

[10]. Schuda P F , Top Org Chem, 1980,91,75.

[11]. Mogilaiah K & Babu-Rao, Indian I Chem, I 998,37B, 894.

[12]. Morgan G T & Micklehwait F M G , J Chem Soc, , 1904, 85, 12

International Virtual Conference on Materials and Nanotechnology
In Association with International Journal of Scientific Research in Science and Technology
Volume 9 | Issue 4 | Print ISSN: 2395-6011 | Online ISSN: 2395-602X (www.ijsrst.com)

Recent Development and Scope of Transition Metal Oxide Based Cathode Material - A Review

Nitesh P. Sawadekar[1]*, Anil R. Bari[1], Sushil P. Bhavsar[2]

*[1]Department of Physics, Arts, Commerce and Science College, Bodwad 425310, Maharashtra, India

[2]R. C. Patel Anudanit Secondary and Higher Secondary Ashram School Waghadi, Shirpur 425405, Maharashtra, India

ABSTRACT

In the recent years number of research groups have concentrated on cathode material of LIBs. The batteries are promissible power source which can be used in portable electronic devices, electric vehicles and to store the energy from the natural sources. The capacity of LIBs varies with material to material. Nowadays most used LIBs cathodes are based on transition metal oxides. In these review, we describe the different types of cathode material for LIBs as well as their working efficiency.

I. INTRODUCTION

Nowadays, the world is facing the problems of energy crises, such as limited source fossil fuel and pollution by CO_2 emission another serious issue in point of view of environment. To overcome these issues, we are shifting towards the efficient in use of renewable energy sources, such as solar energy, wind energy and other renewable energy sources. But renewable energy sources are depends on whether, so it is need to develop the energy storage device which can be used to store the energy generated from renewable sources, in the portable electronics devices, electric vehicle with high energy density and energy conversion efficiency with the less self-loss and higher safety. Development of energy storage devices is in focus of number of research groups.

Among the various energy storage system, Lithium ion battery are considered among the best choice due to their high operating voltage, high energy density, power density, good cycle rate and relatively good safety[1]. However the current Lithium ion batteries (LIBs) have already reached their practical limits. Therefor a new class of material for cathode for lithium ion batteries needs to be developed with higher specific capacity, high operating voltage, high power density, good cycle rate, high thermal stability, higher safety and low cost.

II. EARLY DEVELOPMENT IN CATHODE MATERIAL

The idea of reversibility was first proposed by Armand in the 1970, using the intercalation materials of different potential for two electrodes [2]. Then Nazzari and Scrosati developed a lithiated tungsten

dioxide electrode and Titanium disulfide electrode [3] as cyclable cell up to 60 cycles although with limited charge voltage 2.2 V and discharge haunted 1.6 V.
Goodenough laboratory [4] discover the family of lithiated transition metal oxide of $NaFeO_2$ structure of rechargeable lithium ion battery with relatively high potential. Transition metal Nickel and Cobalt with mixture of Mn, Al, Fe, etc. were formed the active positive material of Sony's lithium ion battery.

Slightly later J. C. Hunter of everyday laboratory covered a new form of MnO_2 with spinel structure and prepared from $LiMn_2O_4$ that could be reversibly charge and discharge in no aqueous electrolyte at high potential, similar to that of $LiCoO_2$ with a similar capacity which is used in commercial application.

III. NEW GENERATION OF CATHODE FOR Li-ION BATTERIES

The commonly used Lithium ion batteries include graphite anode and cathode from $LiCoO_2$, $LiMnO_3$ and $LiMn_2O_4$. In the present day, material for the cathode includes $LiCoO_2$, $LiMn_2O_4$ and most developing material $LiNi_xMn_yCo_{1-x-y}O_2$. Among the cathode material layered oxides provides high energy density. Moreover Manganese oxides are more intensively explored high energy density, low toxicity and safety, which shows promising electrochemical properties during cycles [5-13]. $LiMnO_3$ combined with $LiMO_2$ (where, M- Transition metals) [14-16] offers higher energy density than the conventional layered oxide electrodes.

The improper selection of the metal oxide reduces the capacity [17-21] so that the capacity can be improved by selecting appropriate transition metal in $LiMO_2$ (where, M- Transition metals) structure.

The various compounds substituted with nickel such as $Li[Li_{0.2}Ni_{0.2}Mn_{0.6}]O_2$ ($0.5Li_2MnO_3{\cdot}0.5LiNi_{0.5}Mn_{0.5}O_2$) and substituted with both nickel and cobalt: $Li[Li_{0.2}Mn_{0.54}Ni_{0.13}Co_{0.13}]O_2$, ($0.5Li_2MnO_3{\cdot}0.5LiNi_{0.33}Mn_{0.33}Co_{0.33}O_2$) or $Ni[Li_{0.05}Ni_{0.31}Co_{0.31}Mn_{0.31}]O_2$ ($0.1Li_2MnO_3{\cdot}0.9LiMn_{0.26}Ni_{0.37}Co_{0.37}O_2$) have been studied by many authors [22-24]. In which Ni and Co addition are used for providing cycling stability with the high capacity. Moreover, the use of the cobalt helps in reducing the electrode polarization [25].

New stoichiometric Li-rich layered oxides ($xLi_2MnO_3{\cdot}(1-x)LiMn_{0.5}Ni_{0.25}Co_{0.25}O_2$ or $Li[Li_yMn_{1-y-2z}Ni_zCo_z]O_2$) were proposed as high-energy density cathode materials for Li-ion batteries. The analysis of the charge-discharge tests shows that $Li[Li_{0.2}Mn_{0.6}Ni_{0.1}Co_{0.1}]$ O_2 electrode delivers nearly 350 mAh·g–1 for the first discharge process and 250mAh·g–1 for following cycles. The investigation of the kinetics of the electrode reactions by means of CV and EIS methods confirmed that $Li[Li_{0.2}Mn_{0.6}Ni_{0.1}Co_{0.1}]O_2$ exhibits highest lithium diffusion coefficients, what with obtained electrochemical cycling tests suggest optimal chemical composition of this material ensuring high energy density along with long-term endurance [26].

Lithium-rich layer oxide, $Li_{1.2}Ni_{0.16}Mn_{0.56}Co_{0.08}O_2$ (NMC), is a potential cathode candidate for high-energy density batteries. The synthesis of Cr-doped lithium-rich phases $Li_{1.2}Ni_{0.16}Mn_{0.56}Co_{0.08-x}Cr_xO_2$ (where x=0.00, 0.01, and 0.02) (NMC-Cr) by the sol-gel technique. The Cr-doped materials exhibit much better cycling stability with 100% capacity retention versus 44% for the undoped sample after 50 cycles [27].a

New generation Li-insertion cathode materials includes,

1. $LiMn_{1.5}Ni_{0.5}O_4$ spinel.
2. Layered integral materials comprising Li_2MnO_3 and $LiMO_2$.
3. $LiMPO_4$ olivines, M ¼ Mn, Mn and Fe, Co.

The spinel structure (3D solid-state diffusion options for Li ions) ensures high rate capability. Hence, it is possible to develop high voltage Li-ion cells, based on this cathode material with graphite anodes. It should be noted that during the last decade, considerable experience with this material has been acquired by a number of research groups throughout the world [1]. The safety features of this material are similar to those lithiated transition metal oxides (Li_xMO_2).

Another important novel material for advanced Li-ion batteries is the integrated layered–layered cathode materials, which were developed recently at the Argonne National Laboratory in the United States [28]. It is possible to synthesize composite materials of the stoichiometry, $[Li_2MnO_3]x$ [LiMO2]y and other possible combinations of transition metal cations.

The three composite structures of $[Li_2MnO_3]x$ $[LiMn_{1/3}Ni_{1/3}Co_{1/3}O_2]y$, is Having the optimal composition is around Li_2MnO_3—$LiMn_{1/3}Ni_{1/3}Co_{1/3}O_2$. Intensive studies of these materials are underway, to a much higher capacity and energy density, compared to the first generation of these battery systems. These new cathode materials exhibit the surface chemistry typical of all kinds of Li_xMO_y cathode materials.

IV. CONCLUSION

The rigorous study is going on Li-ion batteries cathode material. There are many challenges for developing cathode material for Lithium ion batteries regarding to new materials that can bring these batteries to high density, high charge-discharge rate, higher safety and that can open for fully EV. There are much more scope to develop the better combination of Li2MnO3 and LiMO2. LiFePO4 is suggested as super cathode in terms of the rate of capability, high capacity, low price, and high thermal stability, nevertheless LiFePO4 can be replaced by other better material.

With the high performance of batteries safety is most important. So, it is need to develop materials with high performance with high safety, so that we can move towards the use green energy.

V. REFERENCES

[1]. Vinodkumar Etacheri, Rotem Marom, Ran Elazari, Gregory Salitra and Doron Aurbach* "Challenges in the development of advanced Li-ion batteries: a review" 10th June 2011 DOI: 10.1039/c1ee01598b.

[2]. George E. Blomgren "The Development and Future of Lithium Ion Batteries" Journal of The Electrochemical Society, 164 (1) A5019-A5025 (2017).

[3]. M. Lazzari and B. Scrosati "A Cyclable Lithium Organic Electrolyte Cell Based on Two Intercalation Electrodes" J. Electrochem. Soc., 127, 773 (1980).

[4]. K. Mitzushima, P. C. Jones, P. J. Wiseman, and J. Goodenough "LixCoO2 (0 < x < –1): A new cathode material for batteries of high energy density." Materials Res. Bull., 15, 783 (1980).

[5]. H. Zhao, J. Wang, G. Wang, S. Liu, M. Tan, and X. Liu "Facile synthesis of orthorhombic LiMnO2 nanorods by in-situ carbothermal reduction: Promising cathode material for Li ion batteries" Ceram. Int., 43, 10585 (2017).

[6]. H. Zhao, S. Liu, X. Liu, M. Tan, Z. Wang, Y. Cai, and S. Komarneni "Orthorhombic LiMnO2 nanorods as cathode materials for lithium-ion batteries: Synthesis and electrochemical properties." 42, 9319 (2016).

[7]. X.Li,Z.Su, and Y.Wang "ElectrochemicalpropertiesofmonoclinicandorthorhombicLiMnO2 synthesized by a one-step hydro thermal method." J.AlloysCompd.,735, 2182 (2018).

[8]. J. Molenda, M. Ziemnicki, J. Marzec, and W. Zaj "Electrochemical and high temperature

physicochemical properties of orthorhombic LiMnO2." J. Power Sources. 173, 707 (2007)

[9]. Z. Yu and L. Zhao "Structure and electrochemical properties of LiMn2O4." Trans. Nonferrous Met. Soc. China., 17, 659 (2007).

[10]. P. Ram, R. Singhal, and R. Kumar "Science Direct Preliminary study of dysprosium doped LiMn2O4 spinel cathode materials". Mater. Today Proc., 4, 9365 (2017).

[11]. J. Molenda, W. Ojczyk, M. Marzec, J. Marzec, J. Przewoz, R. Dziembaj, and M. Molenda "Electrochemical and chemical deintercalation of LiMn2O4". Solid State Ionics. 157, 73 (2003).

[12]. J. Molenda and W. Kucza "Transport properties of LiMn2O4". Solid State Ionics. 117, 41 (1999).

[13]. M. Bakierska, K. Chudzik, M. Lis, and M. Molenda "Enhancing the lithium ion di ff usivity in LiMn2O4–ySy cathode materials through potassium doping". Solid State Ionics. 317, 190 (2018).

[14]. Q. Zhang, T. Peng, D. Zhan, and X. Hu "Synthesis and electrochemical property of xLi2MnO3•(1 - X)LiMnO2 composite cathode materials derived from partially reduced Li2MnO3" J. Power Sources., 250, 40 (2014).

[15]. F. Yang, Q. Zhang, X. Hu, and T. Peng "Synthesis of layered xLi2MnO3•(1–x)LiMnO2 nanoplates and its electrochemical performance as Lirich cathode materials for Li-ion battery". Electrochim. Acta., 165, 182 (2015).

[16]. W. C. West, R. J. Staniewicz, C. Ma, J. Robak, J. Soler, M. C. Smart, and B. V. Ratnakumar "Implications of the first cycle irreversible capacity on cell balancing for Li2MnO3-LiMO2 (M=Ni, Mn, Co) Li-ion cathodes."J. Power Sources., 196, 9696 (2011).

[17]. M. Oishi, K. Yamanaka, I. Watanabe, K. Shimoda, T. Matsunaga, H. Arai, Y. Ukyo, Y. Uchimoto, Z. Ogumi, and T. Ohta "Direct observation of reversible oxygen anion redox reaction in Li-rich manganese oxide, Li2MnO3, studied by soft X-ray absorption spectroscopy". J. Mater. Chem. A., 4, 9293 (2016).

[18]. K. Kleiner, B. Strehle, A. R. Baker, S. J. Day, C. C. Tang, I. Buchberger, F. F. Chesneau, H. A. Gasteiger, and M. Piana "Origin of High Capacity and Poor Cycling Stability of Li-Rich Layered Oxides: A Long-Duration in Situ Synchrotron Powder Diffraction Study." Chem. Mater., 30, 3656 (2018).

[19]. M. Sauban`ere, E. McCalla, J.-M. Tarascon, and M.-L. Doublet "The intriguing question of anionic redox in high-energy density cathodes for Li-ion batteries." Energy Environ. Sci., 9, 984 (2016).

[20]. G. Assat and J. M. Tarascon "Fundamental understanding and practical challenges of anionic redox activity in Li-ion batteries." Nat. Energy., 3, 373 (2018).

[21]. W. E. Gent, K. Lim, Y. Liang, Q. Li, T. Barnes, S. J. Ahn, K. H. Stone, M. McIntire, J. Hong, J. H. Song, Y. Li, A. Mehta, S. Ermon, T. Tyliszczak, D. Kilcoyne, D. Vine, J. H.Park,S. K.Doo,M. F.Toney,W.Yang,D.Prendergast,andW. C.Chueh "Coupling between oxygen redox and cation migration explains unusual electrochemistry in lithium-rich layered oxides." Nat. Commun., 8, 2091 (2017).

[22]. K.Luo,M.R.Roberts,N.Guerrini,N.Tapia-Ruiz,R.Hao,F.Massel,D.M.Pickup, S.Ramos,Y. S.Liu,J.Guo,A. V.Chadwick,L. C.Duda,andP. G.Bruce "Anion Redox Chemistry in the Cobalt Free 3d Transition Metal Oxide Intercalation Electrode Li[Li0.2Ni0.2Mn0.6]O2." J. Am. Chem. Soc., 138, 11211 (2016).

[23]. W. C. West, J. Soler, and B. V. Ratnakumar "Preparation of high quality layered composite Li2MnO3-LiMO2 (M = Ni, Mn, Co) Li-ion cathodes by a ball milling-annealing process." Journal of The Electrochemical Society, 166 (3) A5333-A5342 (2019).

[24]. S. Kim, C. Kim, J. K. Noh, S. Yu, S. J. Kim, W. Chang, W. C. Choi, K. Y. Chung, and B. W. Cho

"Synthesis of layered-layered xLi2MnO3(1-x)LiMO2 (M=Mn, Ni, Co) nanocomposite electrodes materials by mechanochemical process". J. Power Sources., 220, 422 (2012).

[25]. J. Wang, X. He, E. Paillard, N. Laszczynski, J. Li, and S. Passerini "Lithium- and Manganese-Rich Oxide Cathode Materials for High-Energy Lithium Ion Batteries." Adv. Energy Mater., 6, 1600906 (2016).

[26]. Katarzyna Redel, Andrzej Kulka, Anna Plewa, and Janina Molend "High-Performance Li-Rich Layered Transition Metal Oxide Cathode Materials for Li-Ion Batteries." Journal of The Electrochemical Society 166 (3) A5333-A5342 (2019)

[27]. Umair Nisar1 & Ruhul Amin2 & Abdul Shakoor1 & Rachid Essehli2 & Siham Al-Qaradawi3 & Ramazan Kahraman4 & Ilias Belharoua "Synthesis and electrochemical characterization of Cr-doped lithium-rich Li1.2Ni0.16Mn0.56Co0.08-xCrxO2 cathodes." Emergent Materials (2018) 1:155–164.

International Virtual Conference on Materials and Nanotechnology
In Association with International Journal of Scientific Research in Science and Technology
Volume 9 | Issue 4 | Print ISSN: 2395-6011 | Online ISSN: 2395-602X (www.ijsrst.com)

Raman Spectroscopic Technique for Cancer Diagnosis

Patil S A[1], Thakare N R[1], Bhoyar A D[1]
[1]P. R. Pote College of Engineering and Management, Amravati, Maharashtra, India

ABSTRACT

Raman Spectroscopic technique can be applied for the cancer diagnosis as it can probe the molecular changes associated with diseased tissue. The molecular and cellular changes occurring in the disease result in distinct Raman Spectra. We have recorded the Raman Spectra of 4 samples at different positions. The Raman features and intensity differs for normal and malignant cells which can be attributed to the variation in the chemical composition of the cells.

Keywords : Raman Spectra, Cancer, Molecular Change

I. INTRODUCTION

Raman Spectroscopy is a vibrational spectroscopic technique that can be used to optically probe the molecular changes associated with diseased tissue. Early cancer detection and localization with effective treatment is crucial to increasing the survival rates. However because early cancers i.e. precancer such as dysplasia and carcinoma in situ (CIS) are only a few cell layer thick (0.2 to 1mm) they can be very difficult to visually detect by conventional diagnostic methods. Tissue fluorescence spectroscopy can be successfully used in vivo to diagnose early lung cancers.[1,2] But it has some draw back. Tissue auto fluorescence spectral features are broad and show less specific difference between normal and pathologic tissues. The Raman effect is an inelastic light scattering process whereby a small proportion of incident of photons are scattered with a corresponding change in frequency. The difference between the incident and scattered frequencies corresponds to the vibrational modes of molecules participating in the interaction. The presence of the neighbouring molecules also change the frequency, intensity and bandwidth of the scattered light and hence give information about the corresponding interaction.

Raman spectra are depicted by plotting the intensity of the scattered photons as a function of the frequency shift. Raman spectra can capture a finger print of specific molecular species and can therefore be potentially used for biomedical applications. Most biologic molecules are Raman active scatterers, each with its own spectral fingerprint Raman spectra usually exhibit sharp spectral features that are characteristic of specific molecular structures and confirmation of tissues[3,4] thus providing more specific molecular information about a given tissue or disease state. Raman spectroscopy is particularly amenable for in vivo analysis because the power and wavelength of the lasers used do not cause injury. Raman spectroscopy can provide information about

the conformation of macromolecules such as proteins, nucleic acid and lipids.

Near infrared Raman spectroscopy has certain advantages such as relative insensitivity to tissue water contents and deeper penetration depth in to the tissue.

That justify its increasing popularity for biomedical application.[5,6] In recent years NIR Raman spectroscopy has been investigated for invitro diagnosis of malignant tissue from various organs (e.g. brain, breast, bladder, colon, larynx, cervix and skin)[7-9] These studies show that specific features of tissue Raman Spectra can be related to the molecular and structural changes associated with neoplastic transformation.[10, 11]

II. DIFFERENCE BETWEEN RAMAN AND FLUORESCENCE SPECTROSCOPY

Raman Scattering and Fluorescence emission are 2 competing phenomena, which have similar origin. Generally a laser photon bounces off a molecule and looses a certain amount of energy that allows the molecule to vibrate (Stokes process). The scattered photon is therefore less energetic and associated light exhibits a frequency shift. The various frequency shifts associated with different molecular vibration gives rise to the spectrum that is characteristic of certain compound.

In contrast fluorescence or luminescence emission follows an absorption process. For better understanding one can refer to the diagram below.

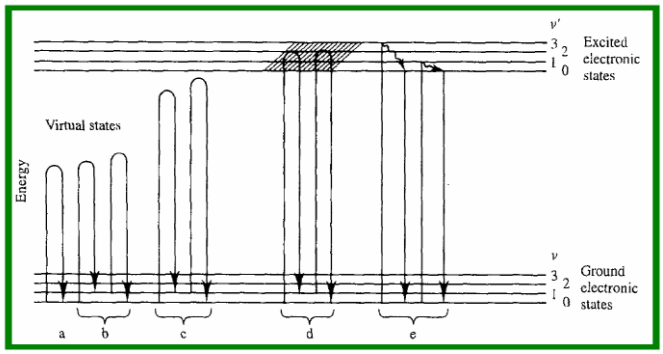

Figure 5(a) : Mechanisms of various light scattering processes. (a) Rayleigh, (b) nonresonance Raman, (c) pre-resonance Raman, (d) resonance Raman resonance fluorescence and (e) relaxed fluorescence.

Virtual states have to be considered to explain Raman Scattering. This is related to the fact that the interaction of the photon with the molecule and the re-emission of the scattered photon occur almost simultaneously. The existence of such virtual states also explains why the non-resonance Raman effect does not depend on the wavelength of the excitation, since no real states are involved in the interaction mechanism. In fact, the Raman spectrum generally does not depend on the laser excitation.

However when the energy of the excitation photon gets close to the transition energy between two electronic state one then deals with the resonance Raman or resonance fluorescence (Figure 1 cased (d)).

The basic difference between these two processes is related to the time scale involved, as well as with the nature of the so called intermediate states. In contrast with resonant fluorescence, relaxed fluorescence results from the emission of a photon from the lowest vibrational level of an excited electronic state, fallowing a direct absorption of a photon and relaxation of the molecule from its vibrational excited level of the electronic state back to the lowest vibrational level of the electronic state. A fluorescence process typically requires more than 10 Sec.[9] In contrary Raman transition is completed within a picoseconds or less.

It clearly appears that, depending on the laser wavelength, resonance effects (Raman or fluorescence), may or may not exist. If the excitation photon does not provide sufficient energy to the molecule, the required transition to generate fluorescence will not take place. However, if fluorescence is generated, it is often much more intense than Raman scattering, hiding Raman features. But because the Raman spectrum tends to be more informative than fluorescence, the Raman spectroscopist is continually searching for methods to avoid fluorescence.

One method to avoid fluorescence condition is to select the laser excitation wavelength. For most examples the choice of Near I.R. (NIR) or UV laser wave length can avoid exciting fluorescence. In the second case the fluorescence may be excited, but the emission is widely separated in energy from the Raman signal so that the Raman spectrum can be recorded without fluorescence interference.

Several biological molecules such as nucleic acids, proteins, and lipids have distinctive Raman features that yield structural and environmental information. These molecules have been studied in solutions and in their natural microscopic environments[11]. The molecular and cellular changes that occur with disease result in distinct Raman spectra that can be used for diagnosis. The transitional changes in precancerous tissues as well as benign abnormalities such as inflammation can also yield characteristic Raman features that allow their differentiation.

III. REVIEW OF LITERATURE

Several groups have indicated the potential of vibrational spectroscopy for disease diagnosis in various organ sites. These groups have shown that features of the vibrational spectrum can be related to molecular and structural changes associated with disease. Raman spectroscopy has been studied extensively for tissue diagnosis in four main organ sites; breast [12] esophagus[13] (and the GI tract), cervix (other gynecological tissues)[14] and skin[15].

Several groups have studied the potential of Raman spectroscopy for pathologies of the breast, from detection of breast cancers to study of capsules from breast implants. Using an FT-Raman system, Alfano et_al. obtained the 1st Raman spectra from excised normal human breast tissues and benign and malignant breast tumors and discussed the feasibility of using FT-Raman spectroscopy for different eating normal and malignant breast tissues.[10]

Redd et_al[16] employed Raman spectroscopy using visible excitation to study excised human breast tissues. Spectra were also obtained from pure compounds and the features observed in tissue spectra were determined to be primarily due to carotenoids myoglobin and lipids.

Feld and colleagues[6] have done extensive work on using Raman spectroscopy for breast cancer diagnosis.

FT-Raman spectroscopy of various gynecologic tissues was also first studied by Affano et_al. Characteristic Raman feature of normal tissues and malignant tumors from the cervix, uterus, endometrium and ovary were described.

A lot of work has been done in diagnosing skin cancer. A study exploring the use of confocal Raman microspectroscopy for skin cancer detection has also been reported.[11] Many researchers have applied NIR Raman Spectroscopy in vitro, exvivo as well as in vivo for the diagnosis of cancer with varying degree of successes.

There is indication that Raman spectroscopy is poised to follow through on its potential to provide real time, non-invasive, automated diagnosis of various cancers Although the process of developing automated classification algorithms has proved arduous, new cutting edge classification algorithms suggest that with enough data, this type of diagnosis will be soon possible.

Researchers also are beginning to understand the biological basis of Raman spectral differences between normal and malignant tissues with the help of techniques like spectral mapping and using tissue model systems. This would enable improved understanding of the progression of cancer.

IV. EXPERIMENTAL ARRANGEMENT

Different samples of tissues were collected and they were recorded using the laser Raman instrumentation. In this set up, a diode laser (785nm, l00mw) is used for excitation of the samples. The scattering is spectrum analyzed by HR320 spectrograph. The scattered radiation is detected by the intense radiation of nitrogen cooled CCD camera. A holographic filter

was used to filter the excitation source. A notch filter is used for removing the Raleigh scattering. Baseline corrected, smoothened, calibrated and normalized spectra (to the highest peak) were subjected to multivariate statistical analysis PC A for objective classification of normal, malignant and benign tissues.

The spectrograph used in the Raman spectrophotometer is highly specialized. The intensity of Rayleigh scattered light is about ten thousand times more than the Raman scattered light. The Raman lines may be obscured by the Rayleigh lines. In order to avoid the overlap of the lines two gratings have been employed in the design of spectrograph.

V. RESULT AND DISCUSSION

Raman scattering cross section is very small and therefore high power laser is utilized as the source of light. When laser radiation having a particular frequency is incident on the sample it undergoes Raman scattering as well as Rayleigh scattering. The Rayleigh scattering light is eliminated by the holographic notch plus filter and the Raman signal is detected by CCD and the spectra is displayed on the P.C.

We record the Raman spectra of 4 samples which are displayed in figures 5.6(a), 5.7(a), 5.8(a) and 5.9(a). We record spectra of normal sample and at 5 different positions of the malignant samples. Considering the degree of malignancy directly proportional to the height of the peak we display the degree of malignancy in Figure 5.6(d), 5.7(d), 5.8(d) and 5.9(d) of the samples 1, 2, 3 and 4 respectively.

From the graph of Raman scattered light it can be observed that the curve indicating the normal sample has more no. of peaks than cancerous sample. But the peaks of normal curve are at lower intensity whereas the peak of cancerous samples is at higher intensities.

Table 5.1 to 5.4 shows the wave numbers of each peak of both normal and cancerous tissue. To better understand the molecular basis of the observed Raman spectra, Table 5.5 lists tentative assignments for the observed Raman bands according to literature data. Thus distinctive Raman features and intensity differences for tumor verses normal tissue can reflect molecular and cellular changes associated with normal and malignant transformation. For instance let us consider graphs 5.6(a) the peak 1425 cm^{-1} in normal tissue can probably be attributed to collagen. However in malignant tissue collagen band was found to shift to 1445cm^{-1} The band at 1445 cm^{-1} are the characteristic of the CH_2-CH_3 bending modes of collagen and phospholipids and their intensities are high in cancerous tissue. Let us consider the example of graph 5.9(a). The peak at 1075 cm^{-1} in normal tissue can be attributed to v(c-c) as v(c-0) phospholipids. But in case of cancerous tissue this peak is shifted to 1087 cm^{-1}.

The observation of the figures 5.6(c) to 5.9(c) show that at the centre of the region the malignancy is maximum and as the point of observation moves away from the center the malignancy goes on decreasing.

The comparison between Raman spectra of two different breast cancer i.e. Figure 5.6(a) and 5.7(a) shows that the number of peaks observed in the spectra is different. Further it is seen that peaks are obtained at different positions showing that the two samples either differ in positions in the breast or they differ in degree of malignancy. The shift in the peak positions shows that the vibrational constant of the molecule change and therefore the neighboring situation is changed as the tissue transforms from normal to malignant condition.

VI. CONCLUSION

The position, intensity and shape of peaks in the Raman spectra of cancerous tissue were significantly different compared with those of normal tissues. From the above discussion it is clear that, the detail study of vibrational levels of Amino acid, structural proteins, and lipids may help in the study of the chemical composition morphology of tissue of cancerous as well as normal tissues.

The analysis of the experimental work suggests that the intensity mapping can be done in case of the Raman Spectra by using proper filters. The variation in the intensity ratio might help in the determination of degree of malignancy.

Continued development of Raman Spectroscopic instrumentation is needed to per format the level necessary for clinical use including the design of a complete hardware apparatus which is compact and can be easily integrated into the clinical setting.

Development of Raman instrumentation is also needed to make it reasonable so that it becomes affordable to the people.

If more Raman spectra are recorded and investigated the mechanism of progress of disease can be studied and the reasons behind the cancer of different organs can be found out.

The interaction between the tissues of the human organ with the external agencies and the effect produced by the external agencies may be explored. Depending upon the type of interaction between tissues and external agencies the people can be divided into different categories. The cancer prone people can be also be found out and they can also be divided into various categories.

Thus finally we may conclude based on the Raman spectra, we are able to discriminate normal versus cancer tissue and observe changes in signature Raman peak representing structural changes of macromolecules.

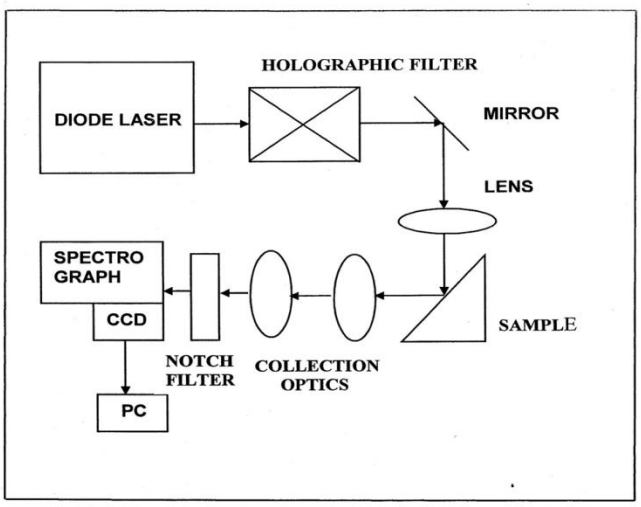

Figure 5(b): Block diagram of the Raman Spectrophotometer.

Table 5.1: The details about peaks in the Raman Spectra of Sample 1

Sr. No.	Peak No.	Normal Energy cm^{-1}	Cancer Energy cm^{-1}
1.	1	-	850
2.	2	-	1075
3.	3	1275	1300
4.	4	1425	1445
5.	5	1650	1650

Table 5.2: The details about peaks in the Raman Spectra of Sample 2

Sr. No.	Peak No.	Normal Energy cm^{-1}	Cancer Energy cm^{-1}
1.	1	825	850
2.	2	-	1100
3.	3	-	1275
4.	4	1450	1462
5.	5	1650	1670

Table 5.3: The details about peaks in the Raman Spectra of Sample 3

Sr. No.	Peak No.	Normal Energy cm^{-1}	Cancer Energy cm^{-1}
1.	1	827	850
2.	2	900	937.5
3.	3	-	1237
4.	4	1425	1450
5.	5	1637	1650

Table 5.4: The details about peaks in the Raman Spectra of Sample 4

Sr. No.	Peak No.	Normal Energy cm^{-1}	Cancer Energy cm^{-1}

1.	1	-	850
2.	2	-	937
3.	3	1075	1087
4.	4	-	1312
5.	5	1412	1450
6.	6	1637	1662

Table 5.5: Peak positions and tentative assignments of major vibrational Bands observed in normal and Tumor bronchial tissue.

Peak position (Cm^{-1})	Protein assignments	Lipid assignments	Others
1745w		v(c=o) gnmento v(c=o) phopholipids	
1655 vs	v(c=o) amid1, x-helix, collagen, elastin		
1618S(sh)	v(c=c), tryptophan		v(c=c), paphyrin
1602ms(sh)	δ(c=c), phenylalanine		
1582 ms(sh)	δ(c=c), phenylalanine		
1552ms (sh)	v(c=c), tryptophan		v(c=c) porphyrin v(c=c), carotenoid
1445vs	$\delta(CH_2)$, $\delta(CH_3)$,	$\delta(CH_2)$ serssoring,	
	Collagin	phospholipids	
1335(sh)	Ch_3CH_2 wagging, collagen		Ch_3CH_2 wagging, nudric acid
1322s	Ch_3CH_2 twisting, collogen		
1302vs	δ (CN), δ(NH) twisting, wagging, collagen	δ(c+b) twisting, wagging phospholipids	
1265s(sh)	δ (CN), δ(NH) amide III, x-helix, collagen, tryptophan.		
1223mw(sh)			Vas(Po2), nudlic acids
1208w(sh)	v(c=c6h_5), tryptophan, phenylalanine		
Peak position (Cm^{-1})	Protein assignments	Lipid assignments	Others
Peak position (Cm^{-1})	Protein assignments	Lipid assignments	Others
1172vw	δ(C-H), tyroscine		
1152w	v(c-N), proteins		

1123w	v(c-N), proteins		
1078ms		v(c-c) or v(c-o), phospholipids	
1031mw(sh)	δ(C-H), phenylolin e		
1004ms	vs(c-c), symm etricring breathing, phenylaline.		
963w	unassigned		
935w	v(c-c), x-helix, praline, valine		
876w(sh)	v(c-c), praline δ(CCH) ring breathing tyrosine		Polysaccharide
823w	Out of plane ring breathing, tyrosine		
752w	Symmetric breathing tryptophan.		

v, stretching mode, vs, symmetric stretch, vas, asymmetric stretch, δ bending mods, v, very, s, strong, m, medium, w, weak, sh, shoulder.

VII. REFERENCES

[1]. Lam S, Kennedy T, Urger M. Miller YE, Germont D, Rusch V, "Localization of bronchial intraepithelial neoplastic usionsty fluorescence bronchioscopy", (1998)

[2]. Hung J, Lam S, Le Riche JC, Palcic B, "Autofluorence of normal and Malignant bronchial tissue, Laser Surg." Med. (1991)

[3]. Peno JR, Grygon CA, Spiro TG, "Raman Excitation Profiles for the nucleotides and for the nudlic acid duplexes poly (rA)-poly (rU) and poly (dG-dC) J. Physchon" (1989) V93.

[4]. Tu AT, Peptide backbone conformation and microenvironment of Pritein side chain. "Spectroscopy of biological Systems", New York John Willey and Sons, (1986)

[5]. Frank CJ, McCreery R/s, Redd-DC, Raman Spectroscopy of normal and diseased human breast tissues. Anal Chem. 1995, 67.

[6]. Manocharan R, Shafer K, Perelmon L, Wu J, Chen K, Denium G, Fitzmarice M, Myles J, Crowe J, Darari R, Fold MS, "Raman Spectroscopy and fluorescence photon migration for breast cancer diagnosic and imaging" Photochem Photobio, (1998), 67, 15-22.

[7]. Schrader B, Keller S, Loechte T, Fendels, Moore DS, Simon A, Sawatzki J., NIRFT Raman Spectroscopy in medical diagnosis. J. Mol Struct (1995), DP 348-293-6.

[8]. Mahadevan-Jansen A, Mitchell MF, Ramanujan N, Malpica A, Thomsen S, Utzinger J, Richard Kortum R. Near infrared Raman spectroscopy for in vitro detection of cervical precanars. Photochem Photobio. (1998) 68.

[9]. Lau DP, Hang Z, Luitl, MonCS, Poerean K, Morrison MD, Zeng H, "Raman spectroscopy for early detection of laryngeal malignancy : preliminary result, Laryngoscope (2000), 110.

[10]. Alfano RR, Liu CH, Sha WL, Zhu D, Akins L, "Human breast tissues studied by IR Flowerer transform Raman Spectroscopy" Lasers Life Sci.(1991).

[11]. Mahadevan Gansen A, Richards Kortum R, "Raman Spectroscopy for the detection of cancer and precancer "J Biomed Opt. (1996).

[12]. Shafer-Pettier, K.E. Haka, A.S. Fitzmauria, M, Crowe J., Myles J., Dasari R.R. and Feld M.S. "Raman Micro spectroscopic model of human breast tissue, implications for breast cancer diagnosis in vivo", J.Raman Spectros. 33 (2002).

[13]. Stone N., Kendall C., Shepherd N., Crow P., Bars H., "Near-infrared Raman Spectroscopy for the classification of epithelial pre-can as and cancers", J.Raman Spectrosc, 33, 564, 2002.

[14]. Utginger U., Heintzelman D.L., Mahadevan Gansen A., Malpica A., Follen M. and Richards Kortum, "NTR spectroscopy for in vivo detection of cervical precancers", Appl. spectrosc. 55, 955 (2001).

[15]. Nijssen A, Bakker Schut, T.C. Heuls F., Caspers P.J., Hayes D.P., Neumann M.H., and Puppels G.J., "Discriminating basal cell carcinoma from its surrounding tissue by Raman spectroscopy, J.Invest. Dermatot, 119, 64, 2002.

[16]. Trans R.C.M, McCrery R.L. and Redd D.C. "Raman spectroscopy of normal and diseased human breast tissues, "Anal.Chem, 67, 777, 1995.

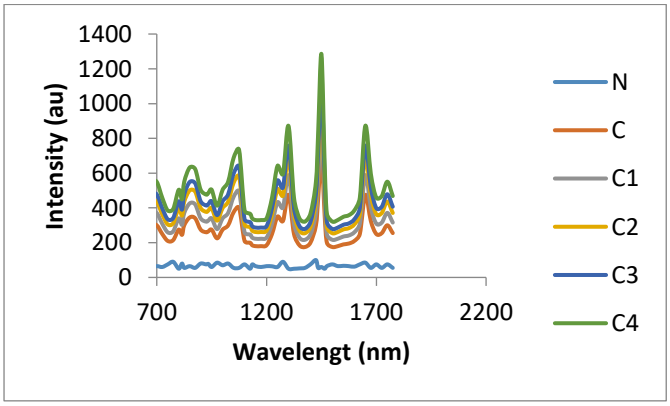

Figure (5.6a) Intensity of Raman scattered light as a function of energy (sample 1)

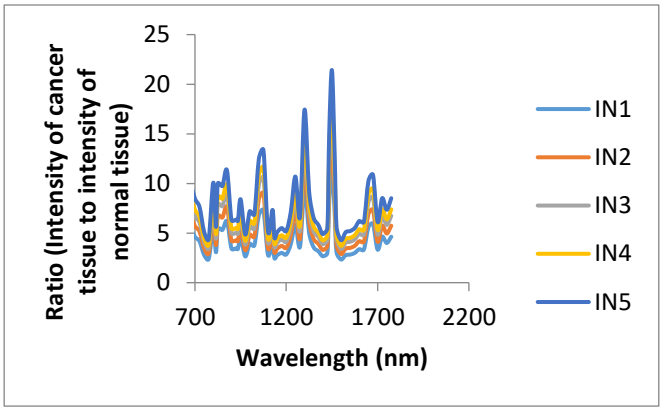

Figure (5.6b) Ratio of intensity of Raman scattered light as a function of energy (sample 1)

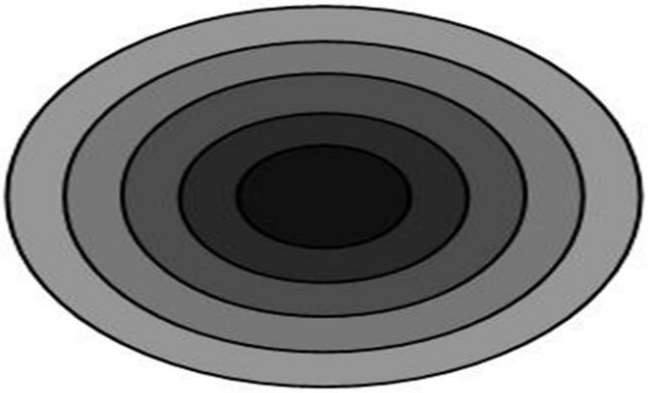

Figure (5.6c) spatial distribution of fluorescence intensity at peak wavelength

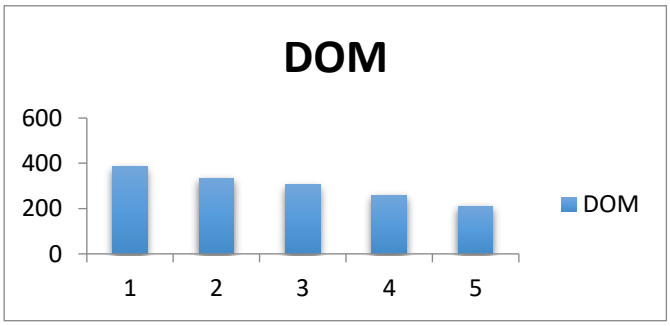

Figure (5.6d) spatial variation of degree of malignancy (sample 1)

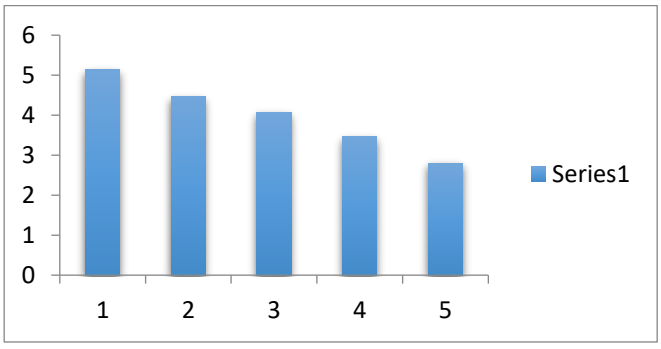

Figure (5.6e) spatial variation of ratio of intensity (sample 1)

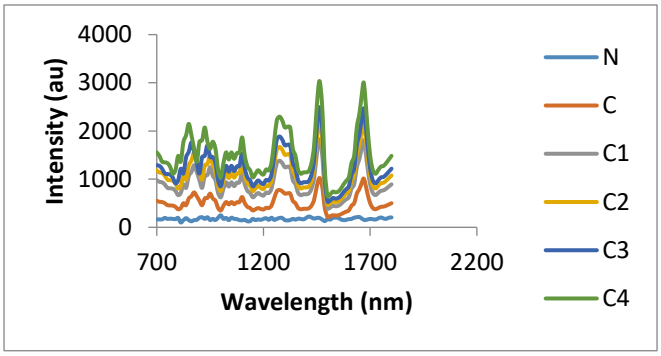

Figure (5.7a) Intensity of Raman scattered light as a function of energy (sample 2)

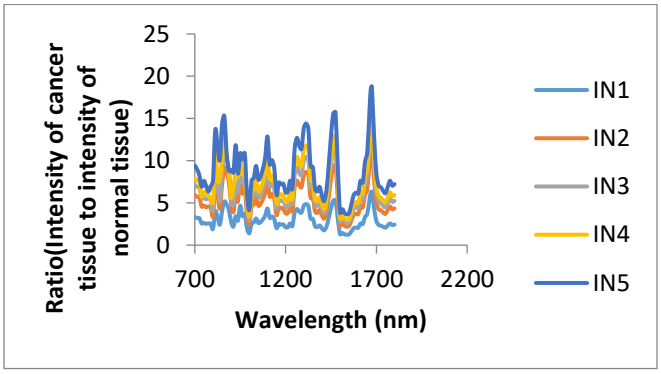

Figure (5.7b) Ratio of intensity of Raman scattered light as a function of energy (sample 2)

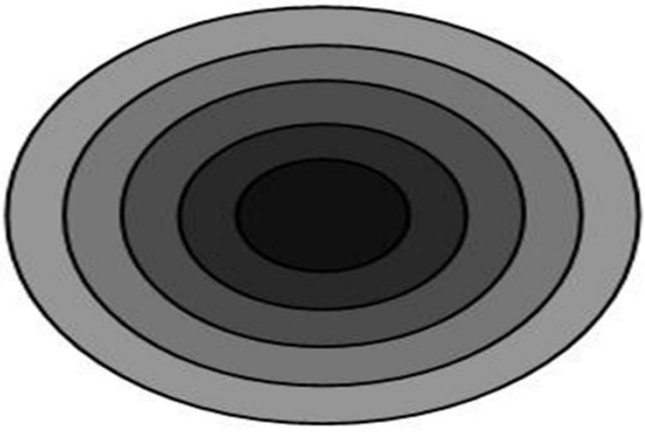

Figure (5.7c) spatial distribution of fluorescence intensity at peak wavelength

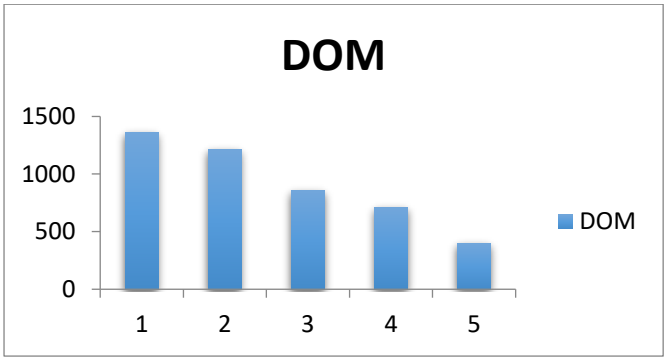

Figure (5.7d) Spatial variation of degree of malignancy (sample 2)

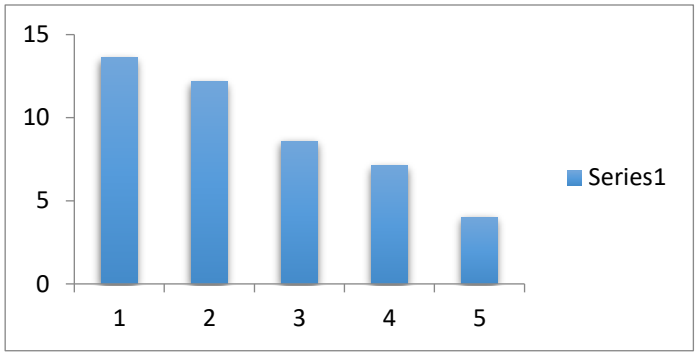

Figure (5.7e) spatial variation of ratio of intensity (sample 2)

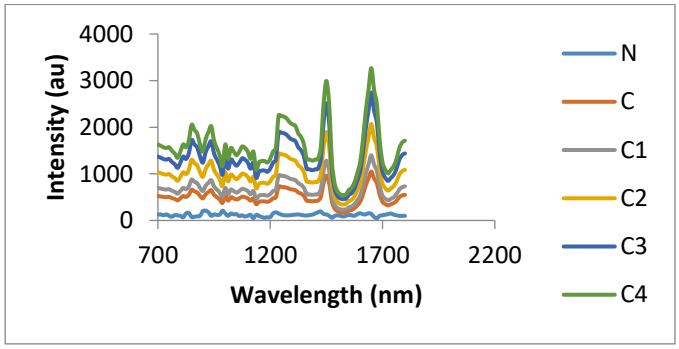

Figure (5.8a) Intensity of Raman scattered light as a function of energy (sample 3)

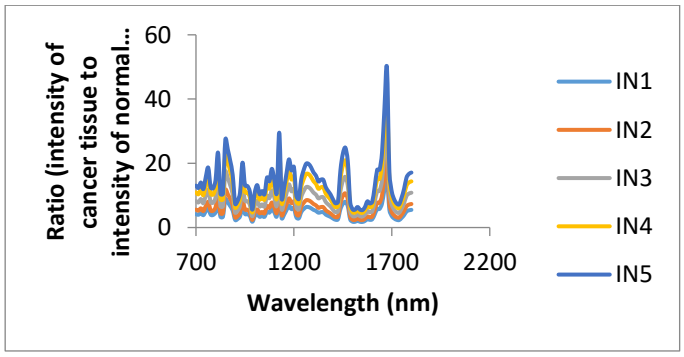

Figure (5.8b) Ratio of intensity of Raman scattered light as a function of energy (sample 3)

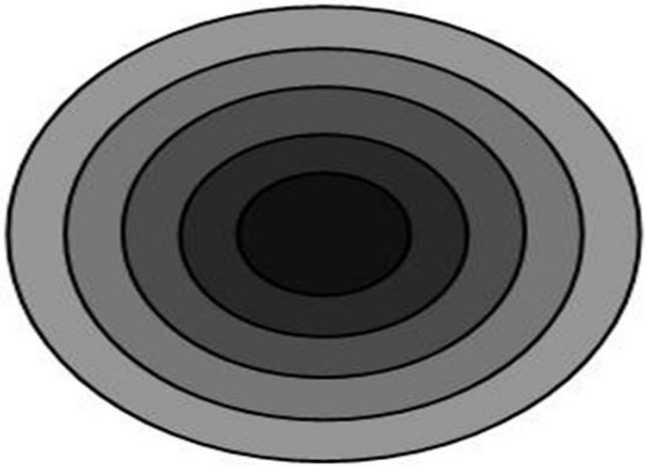

Figure (5.8c) spatial distribution of fluorescence intensity at peak wavelength

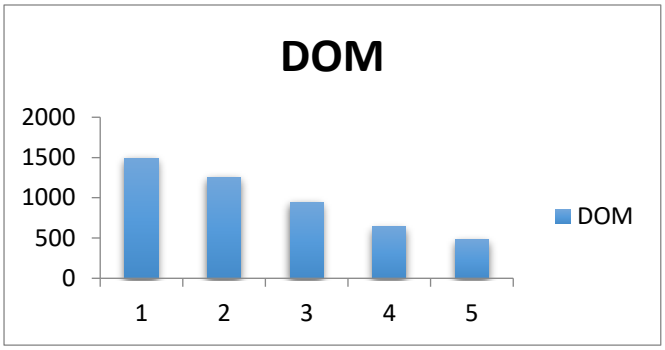

Figure (5.8d) spatial variation of degree of malignancy (sample 3)

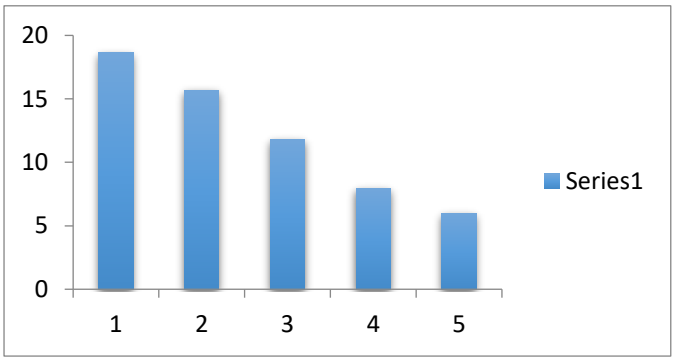

Figure (5.8e) Spatial variation of ratio of intensity (sample 3)

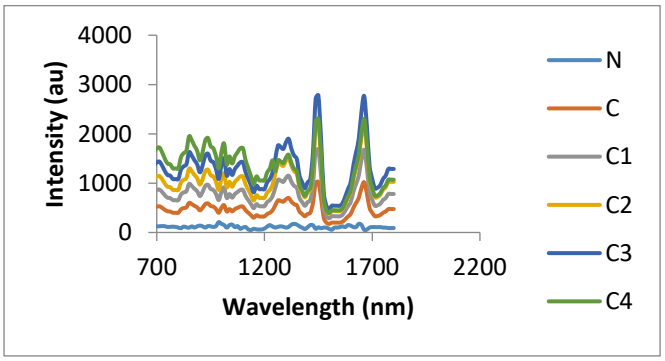

Figure (5.9a) Intensity of Raman scattered light as a function of energy (sample 4)

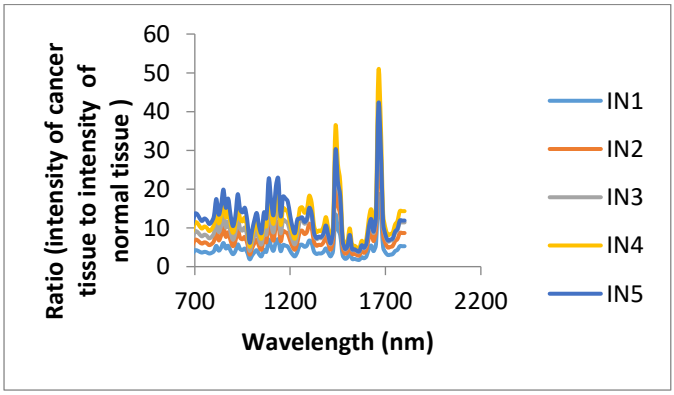

Figure (5.9b) Ratio of intensity of Raman scattered light as a function of energy (sample 4)

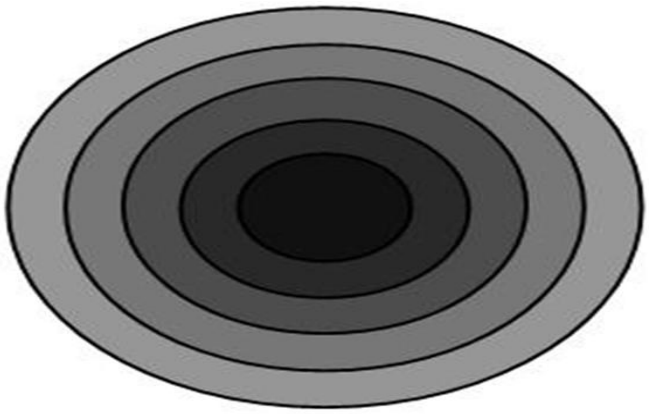

Figure (5.9c) Spatial distribution of fluorescence intensity at peak wavelength

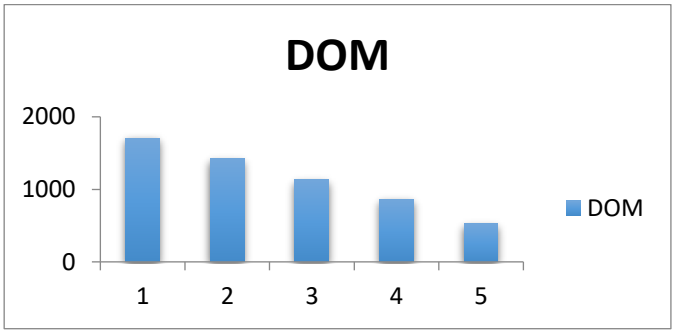

Figure (5.9d) Spatial variation of degree of malignancy (sample 4)

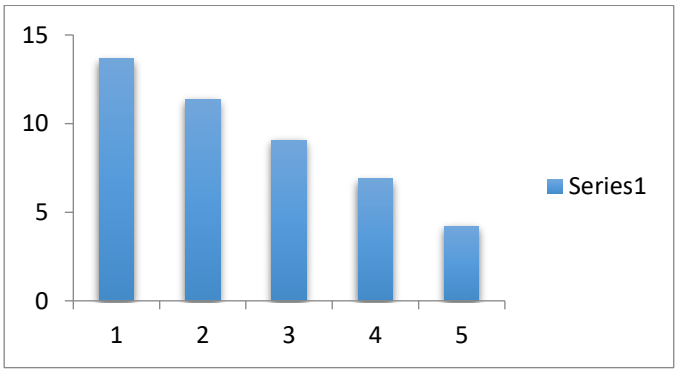

Figure (5.9e) Spatial variation of ratio of intensity (sample 4)

International Virtual Conference on Materials and Nanotechnology
In Association with International Journal of Scientific Research in Science and Technology
Volume 9 | Issue 4 | Print ISSN: 2395-6011 | Online ISSN: 2395-602X (www.ijsrst.com)

Generalized Fractional Sine Transform and its Applications

Dr. S. A. Khapre[1], Milind K.Tatte[2]
[1]Department of Mathematic, P. R. Pote College of Engineering and Management, Amravati, Maharashtra, 444604, India
[2]Department of Computer Engineering, Government Polytechnic, Arvi Wardha, Maharashtra 442201, India

ABSTRACT

This paper is concerned with the generalization fractional Sine transform, in this study we propose a definition of testing function space and distributional generalized one-dimensional fractional Sine transform. Along with this we have proved Inversion formula and Analyticity theorem for the one-dimensional fractional Sine transform. Some properties are verified and applications on generalized one-dimensional fractional Sine transform are discussed.

Keywords : - Fractional Fourier Transforms, Fractional Cosine Transform, Fractional Sine Transform.

I. INTRODUCTION

Fractional calculus can be categorized as applicable mathematics. The properties and theory of these fractional operators are proper objects of study in their own right. Scientists and applied mathematicians in the last decade found the fractional calculus useful in various field: quantative biology, electrochemistry, scattering theory, diffusion, transport, theory of probability, potential theory and elasticity. The unitarity property of transforms is useful in many applications (source compression, transmission, watermarking, to name a few). In many cases, when a transform is applied on real-valued data, it is very useful to obtain real-valued coefficients (i.e. a reality-preserving transform). In most applications, the decor relation property of the transform is of importance and it would be very useful to control it under some transform's parameter (e.g. in Joint source-channel coding).

In the literature there are numerous integral transform and widely used in physics astronomy as well as in Engineering. In order to solve differential equation, the integral transform were extensively used and thus there are several works on the theory and application of the integral transform such as Laplace, Fourier-Mellin & Hankel, Cosine and Sine transform to name but a few. In the sequence of these transform, Pei Soo-Chang redefined the fractional Sine and fractional Cosine transform based on fractional Fourier transform in 2001[12]. The fractional Cosine transform and Sine transform, which are useful, signal processing tools, was defined based on the fractional operations decomposition and eign function[10]. Many mathematician works on discrete cosine and sine transform as well as fractional cosine and sine transform motivated from theses

mathematician we worked on fractional sine and cosine transform. The paper is organized as follows. In the section 2 mathematical pre-requisites, Section 3 gives analyticity theorems for fractional sine transform and inversion formula. Section 4 related with some properties of fractional sine transform [16, 17, and 18].

II. MATHEMATICAL PRE-REQUISITES

2.1. One dimensional generalized fractional Sine transform

One dimensional fractional Sine transform with parameter α. $f(x)$ denoted by $FS_\alpha(u)$ perform a linear operation given by the integral transform.

$FS_\alpha\{f(x)\}(u) = \int_{-\infty}^{\infty} f(x)\, k_\alpha(x,u)dx$ (2.1)

Where the kernel,

$k_\alpha(x,u) =$

$\sqrt{\frac{1-icot\alpha}{2\pi}}\, e^{\frac{i(x^2+u^2)cot\alpha}{2}}\, e^{i(\alpha-\frac{\pi}{2})} \sin(cosec\alpha.ux)$ (2.2)

2.2. One dimensional generalized fractional Cosine transform

One dimensional fractional Cosine transform with parameter α. f(x) denoted by F(u) perform a linear operation given by the integral transform.

$FC_\alpha\{f(x)\}(u) = \int_{-\infty}^{\infty} f(x)\, k_\alpha(x,u)dx$ (2.3)

where the kernel,

$k_\alpha(x,u) = \sqrt{\frac{1-icot\alpha}{2\pi}}\, e^{\frac{i(x^2+u^2)cot\alpha}{2}} \cos(cosec\alpha.ux)$ (2.4)

2.3. The test function space E

An infinitely differentiable complex valued function $\emptyset$ on R^n belongs to $E(R^n)$ if for each compact set $I \subset S_a$ where,

$S_a = \{x: x \in R^n, |x| \le a, a > 0\}, I \in R^n$

$\gamma_{E_p}(\emptyset) = \sup_x \left|D_x^p \emptyset(x)\right| < \infty$, where, p=1, 2, 3….

Thus $E(R^n)$ will denote the space of all $\emptyset \in E(R^n)$ with support contained in S_a

Note that: The space E is complete and therefore a Freechet space. Moreover, we say that f is a fractional Sine transformable, if it is a member of E^*, the dual space of E.

2.4. Distributionalone-dimensional fractional Sine transform

The one dimensional distributional fractional Sine transform of $f(x) \in E^*(R^n)$ defined by

$FS_\alpha\{f(x)\} = \langle f(x), k_\alpha(x,u)\rangle$ (2.5)

$k_\alpha(x,u) =$

$\sqrt{\frac{1-icot\alpha}{2\pi}}\, e^{\frac{i(x^2+u^2)cot\alpha}{2}}\, e^{i(\alpha-\frac{\pi}{2})} \sin(cosec\alpha.ux)$ (2.6)

Where , RHS of equation (2.5) has a meaning as the application of $f \in E^*$to $K_\alpha(x,u,) \in E$.

III. ANALYTICITY AND INVERSION FORMULA OF GENERALIZED FRACTIONAL SINE TRANSFORM

3.1. Analyticity theorem

Let $f(x,) \in E^*(R^n)$ and its generalized fractional Sine transform be defined by,

$FS_\alpha\{f(x)\}(u) = FS_\alpha(u) = \langle f(x), K_\alpha(x,u)\rangle$ Then $FS_\alpha(u,)$ is analytic on C^n if $suppf \subset S_{a,}$,

Where

$S_a = \{x,: x, \in R^n, |x| \le a,, a > 0,\}$ .Moreover,$FS_\alpha(u)$ is differentiable and $D_u^p FS_\alpha(u) = \langle f(x), D_u^p K_\alpha(x,u)\rangle$.

3.2. Inversion formula of generalized fractional Sine transform

The fractional sine transform is given by

$FS_\alpha\{f(x)\}(u)$

$= \int_{-\infty}^{\infty} f(x) \sqrt{\frac{1-icot\alpha}{2\pi}}\, e^{\frac{i(x^2+u^2)cot\alpha}{2}} e^{i\left(\alpha-\frac{\pi}{2}\right)} \sin(cosec\alpha.ux)dx$

then by inversion it is possible to recover $f(x)$ by means of the inversion formula

$f(x) = \frac{2}{\pi}\int_{-\infty}^{\infty} FS_\alpha(u)\widetilde{K_\alpha}(x,u)du$, where

$\widetilde{K_\alpha}(x,y,u,v) = e^{\frac{-i(x^2+u^2)cot\alpha}{2}}$

$e^{i\left(\alpha-\frac{\pi}{2}\right)} \sqrt{\frac{2\pi}{1-icot\alpha}} \sin(cosec\alpha.ux).$

Proof:

$FS_\alpha\{f(x)\}(u)$

$= \sqrt{\frac{1-icot\alpha}{2\pi}} \int_{-\infty}^{\infty} f(x) e^{\frac{i(x^2+u^2)cot\alpha}{2}} e^{i\left(\alpha-\frac{\pi}{2}\right)} \sin(cosec\alpha.ux)\,dx$

$FS_\alpha\{f(x)\}(u)e^{\frac{-i}{2}(u^2)} = C_k \int_{-\infty}^{\infty} f(x) e^{\frac{i(x^2)cot\alpha}{2}} e^{i\left(\alpha-\frac{\pi}{2}\right)} \sin(cosec\alpha.ux)\,dx$

where, $C_k = \sqrt{\frac{1-icot\alpha}{2\pi}}$

$= \int_{-\infty}^{\infty} g(x) e^{i(\alpha-\frac{\pi}{2})} \sin(cosec\alpha.ux)\,dx,$

where $g(x) = C_k e^{\frac{i(x^2)cot\alpha}{2}} f(x)$

$= [Cg(x)](cosec\alpha.u)$

Let $cosec\alpha.u = \eta$; $d\eta = cosec\alpha.du$ and

$FS_\alpha\{f(x)\}(u)e^{\frac{-i}{2}(u^2)} = [Cg(x)](\eta)]$

$FS_\alpha(\frac{\eta}{cosec\alpha})e^{\frac{-i}{2}(u^2)cot\alpha} = G(\eta)$ (3.1)

The right hand side is the Sine transform of g(x) with argument η. Invoking the sine inversion we can write,

$g(x) = \frac{2}{\pi}\int_{-\infty}^{\infty} G(\eta)\sin(\eta x)\,d\eta$

$C_k e^{\frac{i(x^2)cot\alpha}{2}} f(x)$

$= \frac{2}{\pi}\int_{-\infty}^{\infty} FS_\alpha\left(\frac{\eta}{cosec\alpha}\right) e^{i\left(\alpha-\frac{\pi}{2}\right)} e^{\frac{-i}{2}(u^2)cot\alpha} \sin(\eta x)\,d\eta$

$= \frac{2}{\pi}\int_{-\infty}^{\infty} FS_\alpha\left(\frac{\eta}{cosec\alpha}\right) e^{i\left(\alpha-\frac{\pi}{2}\right)} e^{\frac{-i}{2}(u^2)cot\alpha} \sin(\eta x)$

$cosec\alpha.du$

$f(x)$

$= \frac{2}{\pi}\int_{-\infty}^{\infty}\int_{-\infty}^{\infty} e^{\frac{-i(x^2+u^2)cot\alpha}{2}} C_k^{-1} FS_\alpha(u)\sin(cosec\alpha.ux)$

$cosec\alpha.du$

$f(x) = \frac{2}{\pi}\int_{-\infty}^{\infty} FS_\alpha(u)\,\widetilde{K_\alpha}(x,u)du$,

Where ,

$\widetilde{K_\alpha}(x,y,u,v)$

$= e^{\frac{-i(x^2+u^2)cot\alpha}{2}} e^{i(\alpha-\frac{\pi}{2})} \sqrt{\frac{2\pi}{1-icot\alpha}} \sin(cosec\alpha.ux)$

IV. PROPERTIES

4.1 Scaling property:

$$\boldsymbol{FS_\alpha(f(ax))(u) = \sqrt{\frac{1-icot\alpha}{1-icot\theta}}\frac{1}{a} e^{\frac{iu^2cot\alpha}{2}\left(1-\frac{cos^2\theta}{cos^2\alpha}\right)}}$$

$$\boldsymbol{e^{i(\alpha-\theta)} FS_\theta(f(ax))\left(\frac{sin\theta}{sin\alpha}\frac{u}{a}\right)}$$

Proof: Consider

$FS_\alpha(f(ax))(u)$

$= \int_{-\infty}^{\infty} f(ax)\sqrt{\frac{1-icot\alpha}{2\pi}} e^{\frac{i(x^2+u^2)cot\alpha}{2}} e^{i\left(\alpha-\frac{\pi}{2}\right)} \sin(cosec\alpha.ux)\,dx$

$= AB\int_{-\infty}^{\infty} f(ax)\sqrt{\frac{1-icot\alpha}{2\pi}}\sin(cosec\alpha.ux)\,dx$

where A= $\sqrt{\frac{1-icot\alpha}{2\pi}} e^{i\left(\alpha-\frac{\pi}{2}\right)}$, B= $e^{\frac{i(u^2)cot\alpha}{2}}$

Let $ax = T$, $x = \frac{T}{a}$, $dx = \frac{dT}{a}$

$if\ \ x = -\infty$, then $T = -\infty$,

if $x = \infty$, then $T = \infty$ etc.

$= AB\int_{-\infty}^{\infty} f(T) e^{\frac{i}{2}\left(\frac{T^2}{a^2}\right)cot\alpha} \sin\left(cosec\alpha.u\frac{T}{a}\right)\frac{dT}{a}$

$= \frac{AB}{a}\int_{-\infty}^{\infty} f(T) e^{\frac{i}{2}\left(\frac{T^2}{a^2}\right)cot\alpha} \sin\left(csc\theta\left(\frac{csc\alpha}{csc\theta}.\frac{u}{a}\right)T\right)dT$

where, $\frac{cot\alpha}{a^2} = cot\theta$

$= \frac{AB}{a}\int_{-\infty}^{\infty} f(T) e^{\frac{i}{2}(T^2)cot\theta} \sin\left(csc\theta\left(\frac{csc\alpha}{csc\theta}.\frac{u}{a}\right)T\right)dT$

where $P = \frac{csc\alpha}{csc\theta}\frac{u}{a}$ $\quad P = \frac{sin\theta}{sin\alpha}\frac{u}{a}$

$= \frac{AB}{a}\int_{-\infty}^{\infty} f(T) e^{\frac{i}{2}(T^2)cot\theta} \sin(csc\theta PT)\,dT$

$= \frac{AB}{a}\int_{-\infty}^{\infty} f(T) e^{\frac{i}{2}(T^2+P^2-P^2)cot\theta} \sin(csc\theta PT)\,dT$

$= \sqrt{\frac{1-icot\alpha}{1-icot\theta}}\sqrt{\frac{1-icot\theta}{2\pi}}\frac{1}{a}$

$e^{\frac{i}{2}(u^2)cot\alpha} e^{\frac{-i}{2}(P^2)cot\theta} e^{i\left(\alpha-\frac{\pi}{2}\right)}$

$\int_{-\infty}^{\infty} f(T) e^{\frac{i}{2}(T^2+P^2)cot\theta} \sin(csc\theta PT)\,dT$

$= \sqrt{\frac{1-icot\alpha}{1-icot\theta}}\frac{1}{a} e^{\frac{i}{2}(u^2cot\alpha-P^2cot\theta)} e^{i(\alpha-\theta)}$

$$\int_{-\infty}^{\infty}\sqrt{\frac{1-icot\theta}{2\pi}}f(T)\,e^{\frac{i}{2}(T^2+P^2)cot\theta}$$

$$\sin(csc\theta PT)\,e^{i\left(\theta-\frac{\pi}{2}\right)}\,dT$$

$$=\sqrt{\frac{1-icot\alpha}{1-icot\theta}}\frac{1}{a}\,e^{\frac{i}{2}(u^2cot\alpha-P^2cot\theta)}$$

$$e^{i(\alpha-\theta)}FS_\theta\big(f(T)\big)(P)$$

$$=\sqrt{\frac{1-icot\alpha}{1-icot\theta}}\frac{1}{a}\,e^{\frac{i}{2}\left(u^2cot\alpha-(\frac{sin\theta u}{sin\alpha a})^2cot\theta\right)}$$

$$e^{i(\alpha-\theta)}FS_\theta\big(f(ax)\big)\left(\frac{sin\theta}{sin\alpha}\frac{u}{a}\quad\right)$$

$$=\sqrt{\frac{1-icot\alpha}{1-icot\theta}}\frac{1}{a}\,e^{\frac{iu^2cot\alpha}{2}\left(1-\frac{cos^2\theta}{cos^2\alpha}\right)}e^{i(\alpha-\theta)}$$

$$FS_\theta\big(f(ax)\big)\left(\frac{sin\theta}{sin\alpha}\frac{u}{a}\quad\right)$$

4.2 Shifting Property:

$$FS_\alpha\{f(x+a)\}(u)$$
$$=e^{\frac{i(a^2)cot\alpha}{2}}\cos(csc\alpha ua)\,FS_\alpha\big(f(t)e^{-itacot\alpha}\big)(u)$$
$$-e^{i\left(\alpha-\frac{\pi}{2}\right)}e^{\frac{i(a^2)cot\alpha}{2}}\sin(csc\alpha ua)$$
$$FC_\alpha(f(t)e^{-itacot\alpha})$$

Proof:

$$FS_\alpha\{f(x+a)\}(u)=\sqrt{\frac{1-icot\alpha}{2\pi}}\,e^{\frac{i(u^2)cot\alpha}{2}}e^{i\left(\alpha-\frac{\pi}{2}\right)}$$
$$\int_{-\infty}^{\infty}f(x+a)e^{\frac{i(x^2)cot\alpha}{2}}\sin(cosec\alpha.ux)\,.dx$$
$$=AB\int_{-\infty}^{\infty}f(x+a)e^{\frac{i(x^2)cot\alpha}{2}}\sin(cosec\alpha.ux)\,.dx$$

where, $A=\sqrt{\frac{1-icot\alpha}{2\pi}}\,e^{i\left(\alpha-\frac{\pi}{2}\right)}$, $B=e^{\frac{i(u^2)cot\alpha}{2}}$

Let $x+a=t, dx=dt$, If $x\to-\infty to\infty$, then $t\to-\infty to\infty$,

$$=AB\int_{-\infty}^{\infty}f(t)e^{\frac{i(t^2+a^2-2ta)cot\alpha}{2}}\sin\big(cosec\alpha.(ut-ua)\big).dt$$
$$=AB\int_{-\infty}^{\infty}f(t)e^{\frac{i}{2}(t^2+a^2)cot\alpha}\,e^{-itacot\alpha}$$
$$\begin{bmatrix}\sin(csc\alpha.ut)\cos(csc\alpha ua)\\-\cos(csc\alpha ut)\sin(csc\alpha ua)\end{bmatrix}.dt$$
$$=AB\cos(csc\alpha ua)\int_{-\infty}^{\infty}f(t)e^{\frac{i}{2}(t^2+a^2)cot\alpha}\,e^{-itacot\alpha}\sin(csc\alpha.ut)\,dt$$
$$-AB\sin(csc\alpha ua)\int_{-\infty}^{\infty}f(t)e^{\frac{i}{2}(t^2+a^2)cot\alpha}\,e^{-itacot\alpha}$$
$$\cos(csc\alpha ut)dt$$
$$=\sqrt{\frac{1-icot\alpha}{2\pi}}e^{i\left(\alpha-\frac{\pi}{2}\right)}e^{\frac{i(u^2)cot\alpha}{2}}\cos(csc\alpha ua)$$
$$\int_{-\infty}^{\infty}f(t)e^{\frac{i}{2}(t^2+a^2)cot\alpha}\,e^{-itacot\alpha}\sin(csc\alpha.ut)\,dt-$$
$$\sqrt{\frac{1-icot\alpha}{2\pi}}e^{i\left(\alpha-\frac{\pi}{2}\right)}e^{\frac{i(u^2)cot\alpha}{2}}\sin(csc\alpha ua)$$
$$\int_{-\infty}^{\infty}f(t)e^{\frac{i}{2}(t^2+a^2)cot\alpha}\,e^{-itacot\alpha}\cos(csc\alpha ut)dt$$
$$=\sqrt{\frac{1-icot\alpha}{2\pi}}e^{\frac{i(a^2)cot\alpha}{2}}\cos(csc\alpha ua)$$
$$\int_{-\infty}^{\infty}f(t)e^{\frac{i}{2}(t^2+u^2)cot\alpha}\,e^{-itacot\alpha}e^{i\left(\alpha-\frac{\pi}{2}\right)}\sin(csc\alpha.ut)\,dt$$
$$-\sqrt{\frac{1-icot\alpha}{2\pi}}e^{i\left(\alpha-\frac{\pi}{2}\right)}e^{\frac{i(a^2)cot\alpha}{2}}\sin(csc\alpha ua)$$
$$\int_{-\infty}^{\infty}f(t)e^{\frac{i}{2}(t^2+u^2)cot\alpha}\,e^{-itacot\alpha}\cos(csc\alpha ut)dt$$
$$=e^{\frac{i(a^2)cot\alpha}{2}}\cos(csc\alpha ua)\,FS_\alpha\big(f(t)e^{-itacot\alpha}\big)(u)$$
$$-e^{i\left(\alpha-\frac{\pi}{2}\right)}e^{\frac{i(a^2)cot\alpha}{2}}\sin(csc\alpha ua)\,FC_\alpha(f(t)e^{-itacot\alpha})$$

4.3 Derivative

$$FS_\alpha\big(f'(x)\big)(u)$$
$$=-csc\alpha ue^{i\left(\alpha-\frac{\pi}{2}\right)}FC_\alpha\big(f(x)\big)(u)$$
$$-icot\alpha FS_\alpha\big(xf(x)\big)$$

Proof:

$$FS_\alpha\big(f'(x)\big)(u)$$
$$=\int_{-\infty}^{\infty}f'(x)\sqrt{\frac{1-icot\alpha}{2\pi}}\,e^{\frac{i(x^2+u^2)cot\alpha}{2}}e^{i\left(\alpha-\frac{\pi}{2}\right)}$$
$$\sin(cosec\alpha.ux)\,dx$$
$$=AB\int_{-\infty}^{\infty}f'(x)e^{\frac{i(x^2)cot\alpha}{2}}\sin(cosec\alpha.ux)\,dx$$

where $A=\sqrt{\frac{1-icot\alpha}{2\pi}}\,e^{i\left(\alpha-\frac{\pi}{2}\right)}$, $B=e^{\frac{i(u^2)cot\alpha}{2}}$

$$=AB\int_{-\infty}^{\infty}f'(x)e^{\frac{i(x^2)cot\alpha}{2}}\sin(cosec\alpha.ux)\,dx$$
$$=AB\{\left[e^{\frac{i(x^2)cot\alpha}{2}}\sin(cosec\alpha.ux)f(x,y)\right]_{-\infty}^{\infty}$$

$$-\int_{-\infty}^{\infty}\left(e^{\frac{i(x^2)cot\alpha}{2}}\cos(csc\alpha ux)\,(csc\alpha.u)+ ixcot\alpha e^{\frac{i(x^2)cot\alpha}{2}}\sin(csc\alpha ux)\right)f(x)dx\}$$

$$\text{Here}\left[e^{\frac{i(x^2)cot\alpha}{2}}\sin(cosec\alpha.ux)f(x,y)\right]_{-\infty}^{\infty}=0$$

$$= AB[-csc\alpha u\int_{-\infty}^{\infty} f(x)e^{\frac{i(x^2)cot\alpha}{2}}\cos(cosec\alpha.ux)\,dx$$

$$-icot\alpha\int_{-\infty}^{\infty} xf(x)e^{\frac{i(x^2)cot\alpha}{2}}\sin(cosec\alpha.ux)dx]$$

$$= -csc\alpha u\sqrt{\frac{1-icot\alpha}{2\pi}}e^{i\left(\alpha-\frac{\pi}{2}\right)}$$

$$\int_{-\infty}^{\infty} f(x)e^{\frac{i(x^2+u^2)cot\alpha}{2}}\cos(cosec\alpha.ux)\,dx$$

$$-icot\alpha\sqrt{\frac{1-icot\alpha}{2\pi}}e^{i\left(\alpha-\frac{\pi}{2}\right)}$$

$$\int_{-\infty}^{\infty} xf(x)e^{e^{\frac{i(x^2+u^2)cot\alpha}{2}}}\sin(cosec\alpha.ux)dx]$$

$$= -csc\alpha u e^{i\left(\alpha-\frac{\pi}{2}\right)}FC_\alpha(f(x))(u) - icot\alpha FS_\alpha(xf(x))$$

4.4 Application of fractional Sine transform to solve the Differential Equation

$\boldsymbol{P(D_x w(x)) = f(x).}$

Consider the differential equation

$P(D_x w(x)) = f(x)$, where $f \in E^*$ (4.1)

$P(D) = \sum_{|\alpha|\le n} a_\alpha D^\alpha$ is linear differential operator of order m and n with constant coefficients a_α respectively.

Suppose that the equation (4.1) possesses a solution w. applying the fractional Sine transform to (4.1) and using

$$D_x^p k_\alpha(x,u) = \begin{bmatrix} \sqrt{\frac{1-icot\alpha}{2\pi}}\,e^{\frac{i}{2}(x^2+u^2)cot\alpha}e^{i\left(\alpha-\frac{\pi}{2}\right)} \\ \sum_{l=0}^{p}\sum_{r=0}^{l}\binom{p}{l}\frac{\left(\frac{i}{2}cot\alpha\right)^{l-r}l!(2x)^{l-2r}}{r!(l-2r)!} \\ (ucosec\alpha)^{p-l} \\ sin\left(ucosec\alpha x+\frac{(p-l)\pi}{2}\right) \end{bmatrix} \quad (4.2)$$

$$FS_\alpha\{P(D_{x,})w\} = FS_\alpha f(x) = f^\wedge(x).\ (say) \quad (4.3)$$

we can reform them to the l fractional Sine transform and hence we get

$P(D_x).w^\wedge = f^\wedge$

$P(D_x)FS_\alpha\{w(x)\} = f^\wedge$

where $w^\wedge = FS_\alpha\{w(x)\}$

$\therefore P(D_x)w^\wedge(x) = f^\wedge(x)$ (4.4)

Under the assumption that the polynomial P is such that,

$P\left(D_x^p k_\alpha(x,u)\right) < \in$, for $\in > 0$ and

for, $u = (u_1, u_2 \dots \dots u_n) \in R^n$ (4.5)

using (4.4) gives

$$w^\wedge = \left[P\left(D_x^p k_\alpha(x,u)\right)\right]^{-1} \quad (4.6)$$

Applying inversion of fractional Sine transform to (4.6)

We get $w = [FS_\alpha]^{-1}\left[\frac{f^\wedge}{P(D_x^p k_\alpha(x,u))}\right]$ (4.7)

To show that w satisfies (4.1), we apply two dimensional fractional Sine transform to both sides of (4.7) and (4.6), we have obtained (4.3) and applying inversion of fractional Sine transform to (4.3), we will get the given differential equation.

4.5 Application:

Transforms with cosine and sine functions as the transform kernels represent an important area of analysis. It is based on the so-called half-range expansion of a function over a set of cosine or sine basis functions. Because the cosine and the sine kernels lack the nice properties of an exponential kernel, many of the transform properties are less elegant and more involved than the corresponding ones for the Fourier transform kernel [20]. Despite these basic mathematical limitations, sine and cosine transforms have their own areas of applications. In spectral analysis of real sequences, in solutions of some boundary value problems, and in transform domain processing of digital signals, both cosine and sine transforms have shown their special applicability. In particular, the discrete versions of these transforms have found favor among the digital signal-processing

community. Recently, DCT has been employed as the main processing tool for data compression/decompression in international image and video coding standards [14].

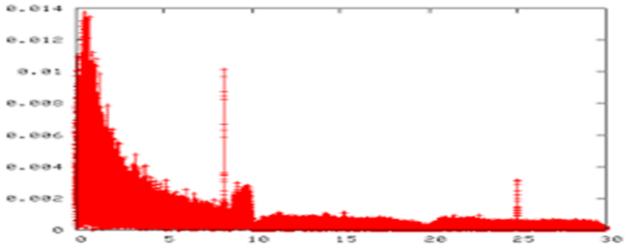

Video compression

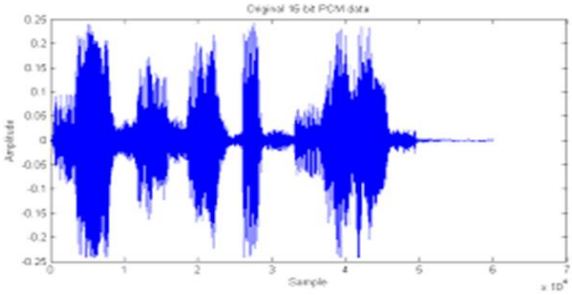

Audio Compression

An alternative transform used in transform coding systems is DST. In fact, the alternate use of modified forms of DST and DCT has been adopted in the international audio coding standards MPEG-1and MPEG-2 (Moving Picture Experts Group) [11, 14].

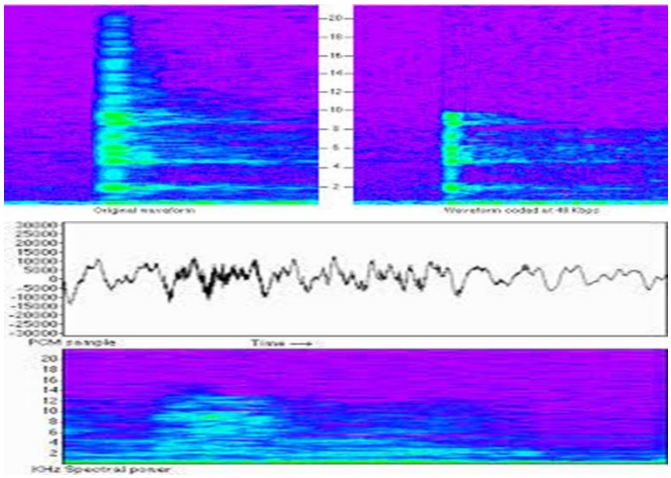

MPEG –Audio Compression using DST & DCT

The authentic techniques that are required to transmit and store visual information's. Such type of transmission and visual information has been increased by the increasing usability of images in the continuous development of multimedia applications [3] because transmission and visual information is directly proportional to usability of image of multimedia. However, the downloading multimedia files from internet is an extremely time consuming. Because of this necessity, image compression has become an important factor and the need for efficient algorithms that can produce large compression ratio with low loss has increased [7]. Multimedia communication contains a major portion of image data which consumes more bandwidth during transmission of techniques [8]. Therefore, the composition of authentic techniques for image compression has become important paradigm [2]. Various image compression techniques have been developed in response to increasing need for medical and microbial consortial images, virtual conferencing and multimedia.

The pre-existing techniques focused on analyzing two dimensional singularities and achieving the fascinating characteristics such as high peak-signal-to-noise ratio (PSNR).

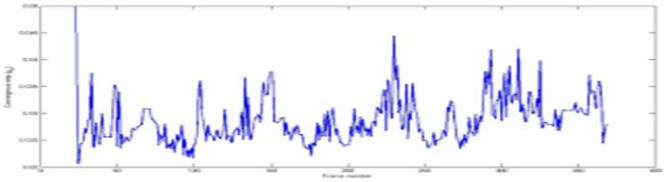

Peak-Signal-to-noise Ratio (PSNR)

Discrete cosine transform (DCT) [1] is very important form the prospective of compressions and it is an adaptation of Fourier series. The DCT is provides accurate approximation of a signal with fewer transform coefficients [13]. Discrete sine transform (DST) is a complementary transform of DCT. DST is used as audio coding and low rate image in compression applications [4, 6]. Discrete Walsh Hadamard transform (DWHT) is the simplest transform, but its energy compaction is poorer than that of DCT, so it does not have a potential to be used for data or image compression [19,9]. Karhunen-Loeve transforms KLT, DST and DCT are linear orthogonal blocked transformations which eliminate the interrelating data points or pixels inside the block.

These transforms do not care of interrelating over the block boundaries [5]. The hybrid fractal image compression technique [15]. Which required more execution time due to its high complexity of images.

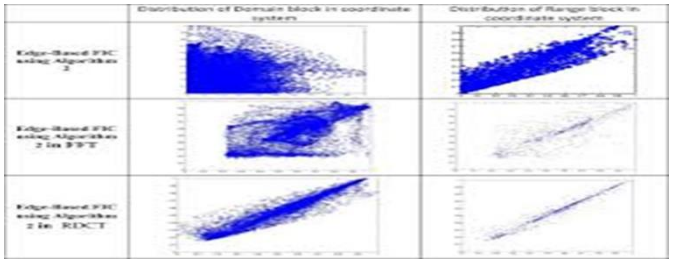

Hybrid fractal image compression technique

This paper focuses on fractional sine transforms, as tools for obtaining such properties. We propose a methodology for obtaining them and obtain variants of the Fractional Cosine (Sine) Transform which share real-valuedness as well as most of the properties required for a fractional transform matrix. Fractional sine transform is fast and its energy compaction is good. This transform is very useful for compressing images.

V. CONCLUSION

In this paper we have developed the fractional one dimensional sine transform. Inversion formula is proved for one dimensional fractional Sine transform. Some properties and applications are discussed for Sine transform.

VI. REFERENCES

[1]. Ahmed N., Natarajan T. and Rao K. R., "Discrete cosine transform", IEEE Trans. Comm., 90-93, 1974.

[2]. Ames G., "Image Compression," International Journal of Advancements in Computing Technology, vol. 1, no. 2, pp. 205-220, 2002.

[3]. Annadurai S. and Sundaresan M., "Wavelet Based Color Image Compression using Vector Quantization and Morphology," in Proceedings of the International Conference on Advances in Computing, Communication and Control, USA, pp. 391-396, 2009.

[4]. Bosi M. and G. Davidson, " High quality low bit rate audio transform coding for transmission and multimedia applications", Journal of audio Eng. Soc., pp. 43-50, 1992

[5]. Chan Y. T., "Wavelet Basics", Kluwer Academic Publishers, Norwell, MA, 1995.

[6]. Fanelle P.M. and Jainn A.K, "Recursive block coding: A new approach to transform coding", IEEE Trans. Comm., pp. 161-179, 1986.

[7]. Krikor L., Baba S., Arif T., and Shaaban Z., "Image Encryption using DCT and Stream Cipher," European Journal of Scientific Research, vol. 32, no. 1, pp. 48-58, 2009.

[8]. Loussert A., Alfalou A., El-Sawda R., and Alkholidi A., "Enhanced System for Image's Compression and Encryption by Addition of Biometric Characteristics," International Journal of Software Engineering and its Applications, vol. 2, no. 2, pp. 111-118, 2008.

[9]. Macwilliams F. J. and Slone N.J., "The Theory of Error Correcting Codes", Elsevier, Amsterdam, 1977.

[10]. Pei-Soo-Chang, Jian-Jiun Ding, :(2002) "fractional cosine, sine and Hartley transform IEEE, Trans. On Signal Processing," vol 50, no.7,

[11]. Pei, Ding, etal." A new definition of continuous fractional Hartley transform", Proceeding of IEEE International conf. on Acoustic, Speech and signal processing, 12-15 May 1998, vol 3, 1485-1488.

[12]. Pei, Ding, "Fractional Canonical and simplified fractional transform", IEEE international conf. on Caustics', speech and signal processing, 2001, vol 6, 3545-3548.

[13]. Rao K.R. and Yip P., "Discrete Cosine Transform: Algorithms Advantages and Applications", Academic Press, New York, 1990.

[14]. Rao, K.R. and Hwang, J.J., Techniques and Standards for Image, Video and Audio Coding, Prentice-Hall, Upper Saddle River, NJ, 1996.

[15]. Rawat C.S. And Meher S., "A Hybrid Image Compression Scheme using DCT and Fractal Image Compression", the international Arab Journal of Information Technology, vol.10, no.6, Nov. 2013.

[16]. Sharma V. D., and Khapre S. A., "Analyticity of the Generalized Two Dimensional Fractional Cosine transforms", J. Math. Computer Sci. ISSN., Pp. 1927-5307.

[17]. Sharma V. D., and Khapre S. A., "Distributional Generalized Two Dimensional Fractional Sine Transform and Its Operators" International Journal of Innovative Research in Science, Engineering and Technology Vol. 5, Issue 1, January 2016 ,pp184-193.

[18]. Sharma V. D., Khapre S.A., "Generalized two dimensional fractional Sine transforms", .In Proc. 2012 IJCA. Int. conf, Recent Trends in information Technology and computer science.

[19]. Solomaon, D., "Data Compression: The complete Reference", Springer Verlag, Newyork, 2004.

[20]. Tatiana Alieva and Martin J. B. "Fractional Cosine and sine transforms in relation to the fractional Fourier and Hartley transforms, Proc. of seventh international symposium on signal processing and It's application, vol 1, 1-4 July 2003, 561-564.

International Virtual Conference on Materials and Nanotechnology
In Association with International Journal of Scientific Research in Science and Technology
Volume 9 | Issue 4 | Print ISSN: 2395-6011 | Online ISSN: 2395-602X (www.ijsrst.com)

The Cloud-Based Health Tracking and Monitoring System With AWS

Vaishnavi Raosaheb Thoke*[1], Prof. Prachi V. Kale*[2]

*[1]Department of Computer Science & Engineering P. R. Pote (Patil) College of Engineering & Management, Amravati-444605, Maharashtra, India

*[2]Department of Computer Science & Engineering P. R. Pote (Patil) College of Engineering & Management, Amravati-444605, Maharashtra, India

ABSTRACT

Medical care has a basic situation in living souls particularly for the individuals who have some medical conditions and need a down to earth answer for a superior life. As of late, there is a quick ascent in e-wellbeing advances, for example, Electronic Health Records (EHRs) and some crisis location and reaction strategies for that used AWS cloud for storing and retrieving managing records. One of the advances that can deal with a portion of the difficulties of shrewd medical care as far as security, sharing, files for avoid data leakages and illegal access help of encryption and description algorithm addition security are digital signature . The motivation behind this article is to feature the estimation of inescapable processing, particularly cloud-based frameworks in medical services area. We survey the importance and chances of AWS Services in inescapable medical services.

Keywords : Cloud Computing, Smart Healthcare, E-health, multi-key search, AWS, DES3.

I. INTRODUCTION

Data innovation can assume a principal part in medical care administrations as far as electronic wellbeing. Late advances in e-wellbeing can be predominantly characterized as the use of data and correspondence innovations in medical services frameworks [1]. Utilizing web for putting away, getting to and changing medical services data and digitizing a ton of cycles and assignments that are important strides for realizing e-wellbeing, is a certain interaction. For this situation, we have the benefits of e-wellbeing, for example, improvement in the nature of administrations in maturing social orders; decrease in expense and in clinical blunders and the straight forwardness by which information can be moved to the perfect spot. All things considered, digitizing paper-based records, gathering and putting away clinical data just as absence of appropriate innovation for preventive consideration can turn out to be somewhat testing. For that used as an AWS (Amazon Web Services) is a subsidiary of Amazon providing on-demand cloud computing platforms and APIs to individuals as well as companies.

COVID-19 affects different people in different ways. Most infected people will develop mild to moderate illness and recover without hospitalization. The first known infections from SARS-CoV-2 were discovered

in Wuhan, China and within year its get spread all over glob these is because many factor but among those are not proper medicinal treatment. Experts believe the virus that causes COVID-19 spreads mainly from person to person for avoid that scenario that patient and doctor without getting physical involved to get best treatment and with proper time span is "Smart healthcare systems on improving the efficiency of healthcare services".

The Cloud market is growing rapidly and has accepted AWS to a great extent in recent years. AWS package has been turned as a huge revenue earner for Amazon as it is being used by most of the companies worldwide for migrating applications over cloud. For Assibilate and security as well many aspect cloud (AWS) is best solution:

- AWS is an Ease of Use, Incredibly Diverse Array of Tools, Unlimited Server Capacity, and Reliable Encryption & Security.
- To provide the Hospital (patient need-preference), e-Blood Bank and Patient Profile(file, daily report) applications to hospitals
- To provide online patient portal for delivery of citizen centric services like online appointment booking, access to lab reports online and blood availability status.

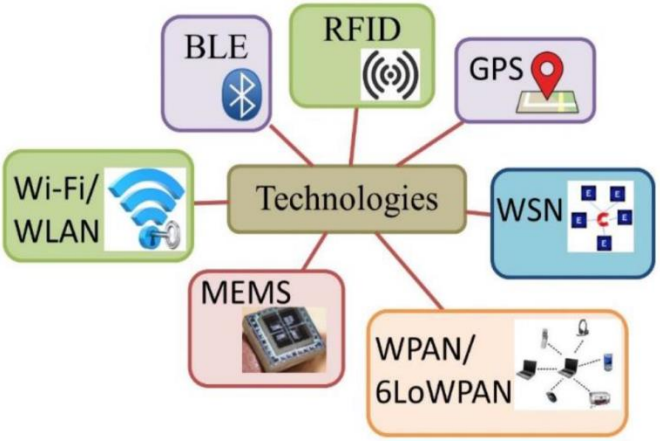

FIGURE 1. Different Technologies used to Deploy Smart Healthcare

Cloud-based healthcare system is build a consumer-focused integrated primary health care system; Improve access and reduce inequity; Increase the focus on health promotion and prevention. In health care System we design Cloud and Admin Module screening that maintain Doctor and Patient record information and other some operation to achieve quality, safety, performance and accountability. For example the heart disease core reasons are many but most affective are physical fitness; low or high cholesterol level vary blood pressure that not affect daily routine but cause major problem after average time such as heart attack, to avoid such scenarios that uses cloud computing to treat, manage and control patients. The systems are supported and consisted of different algorithms such as Authentication Algorithms (the process or action of verifying the identity of a patient or process.)For patient record safety and cloud infrastructures (AWS) for store patient data/record, smart devices, and sensors and initiate different service types according to their context and environment.

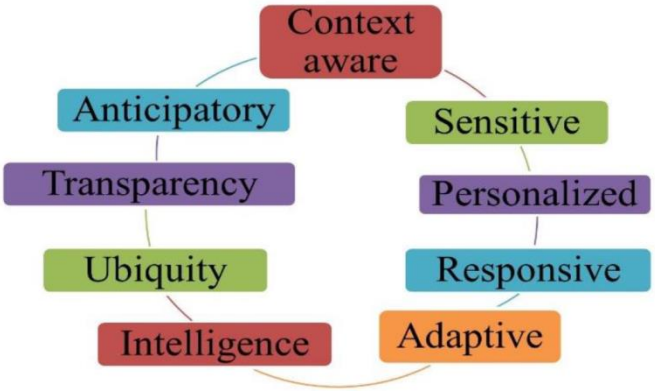

FIGURE 2: Characteristics of Smart Healthcare.

II. LITERATURE SURVEY

A. Cloud Computing (CC)

There are many recent new technologies including mobile computing [1] [2], Cloud Computing, and wireless communications changed people lives everywhere the world and made it easier [3][4]. The concept of Cloud Computing (CC) relies on a

network-based resource sharing to extend resource availability and reduce financial and management costs [5].

There are several examples for emerging Cloud computing infrastructures/ platforms like Microsoft Azure, Amazon EC2, Google App Engine, and Aneka [6]. Cloud Computing utilizes a good range of various computing technologies, and involves distributed systems, virtualization, storage, networking, security, management and automation, service oriented architecture (SOA), and service-level agreement (SLA). Furthermore, CC helps companies improve the IT services, develop applications to realize unlimited scalability and automaticity on demand services of the IT infrastructure, and increase their revenues.

There are many advantages for adopting the cloud environment like [5]: Storage, Backup and Recovery: Location Flexibility: Time Efficiency and price saving.

B. Mobile Cloud Computing

The development and therefore the spread of mobile devices allow the users to profit from wide selection of useful services and mobile applications at any time and from anywhere within the world. People use mobile devices to accomplish sort of daily tasks like online shopping, business management, educating and also health monitoring.

Mobile Cloud Computing (MCC) integrates mobile devices to utilize the cloud unlimited service and to enable information access for mobile devices users [7]. The Cloud Computing depends on network-connected resources pooled to maximise their utilization leading to reduced management and capital costs. Many sectors can enjoy MCC including the cloud-healthcare system. As an example, there's a MCC healthcare system that was built to watch and analyse real time biomedical signals (such as ECG) for users in multiple locations. A customized healthcare application is installed on the mobile device, and health data are being synchronized into the healthcare cloud computing service to be stored and analysed [8].

There are many limitations facing portable mobile device that prevent taking advantage of their portability feature in many sectors including the healthcare. First, portable devices are restricted by their short battery lifetime, computational and storage capacity, which prevents them from performing complicated tasks, computation-intensive applications, and image processing, in social networking and organize meeting. Second, portable devices are operated on heterogeneous wireless networks, which cause the difference of network bandwidth capacity and communication quality; device mobility further affects the network connectivity and cloud resource availability [9]. In other words, MCC increases the capabilities of the mobile devices and overcomes their limitations, therefore the users won't worry about the specified CPU power and memory size to run intensive tasks.

To mitigate the requirements of mobile devices in computing capacity and resources, the mobile cloud computing (MCC) paradigm allows the computing, data storage and mass information science be offloaded to the cloud platform for enhancing the reliability and availability of services while minimizing the energy and computational requirements in mobile devices [10].

There are other challenges associated with storing data on the cloud, essentially is about data privacy and deny unauthorized access and malicious attacks. The supply of the owners' data in the least times for any request is challenge. Also, the integrity of the info and stop alternation or modification on the info by intruders is another issue. These information security concerns might be solved by using cryptographic techniques [11].

Although all the good features of the MCC, the MCC faces some challenges like the delay between the mobile device request and cloud service response especially when there's a far distance between the cloud and therefore the mobile device. Also, there are inherited challenges of wireless network like variable data rates and fewer throughputs.

A cloudlet may be a recent concept that would be considered an answer for a few of the challenges facing the normal mobile cloud computing model. A cloudlet is little resource rich equipped cloud to be placed between the enterprise cloud and therefore the mobile device, to scale back the connection latencies and mobile power consumption [12]. The subsequent section highlights the cloudlet concept.

C. Cloudlet

The cloudlet's concept may be a closer cloud with many advantages and capabilities to avoid several limitations of the remote cloud. It's believed that the cloudlet scheme which is taken into account as a middle stage between the enterprise cloud and therefore the mobile device has a superb chance to beat the challenges related to MCC like power consumption and latencies [8].

But, in some cases, the mobile user has got to connect on to the EC even when it's connected to the cloudlet. This happens when:

The mobile device must update files stored within the Enterprise Cloud. So, the mobile device sends the request for the precise file, then the file is going to be downloaded from the EC to the Cloudlet, and therefore the mobile device can process it.

Requesting specific services that aren't available within the Cloudlet. Motivated by the cloudlet concept, the authors in [12] proposed a mobile cloud system for university applications.

Their system uses different sensors to hold out many tasks. They introduced and implemented two main applications in traffic management and fire detection inside a university whereas the info from sensors is processed within the mobile cloud system.

In the same context, the researcher in [8] introduced an efficient cloudlet MCC model during which the mobile users communicate on to the cloudlet rather than the enterprise cloud. Their model is applicable in many environments including hospitals were saving and processing big amounts of knowledge. There's a replacement concept of massive Data that's associated with the large amounts of stored/obtained data thanks to the advances in several technologies including cloud computing, social media, and wireless communication [13].

On the opposite hand, processing of massive amount of knowledge might be offline or real-time operation of some applications like healthcare applications where the info analysis and extracting the proper decisions make a difference between patient's life and death [14]. Figure 2 shows a general plot for the thought of using Mobile cloud computing for healthcare big data applications [15]. During this MCC model, the cloudlets are placed nearby the hospital and canopy a neighbourhood which will be accessed by authorized people that can access the patients' information and monitor their status remotely.

D. Cloud-based Healthcare Systems

The healthcare sector and usually many other areas like transportation, finance industry, etc. have skilled a rapid climb recently thanks to the exponential growth in ICT.

The increasing role and benefits of ICT in healthcare are getting visible within the enhancement and emergence of technologies like health informatics, epidemiology, bioengineering and Healthcare Information Systems (HIS). we will now imagine a near future where healthcare providers can port powerful analytics and decision support tools to mobile computing devices (smartphones, tablets, laptops, etc.) aiding clinicians at the purpose of care helping them with synthesis of knowledge from multiple sources, optimization of clinical workflows, and context-aware deciding . the gang sourcing technologies also are coming to healthcare augmenting people in their deciding processes for his or her wellbeing though the complexity of such a setting in healthcare domain, including appropriate models (reimbursement, who holds the liability), are posing challenges [16].

Aminian and Naji (2013) [17] propose a hospital healthcare monitoring system supported wireless sensor networks. Specifically, the monitoring system monitors physiological parameters from multiple patient bodies through a coordinator node attached to the patient's body that collects the signals from the wireless sensors and sends them to the bottom station.
A presented mobile healthcare application in [18] to manage patient health records and medical images. The mobile application is developed using Android OS. The Amazon's S3 cloud service is employed during this mobile application. Authors in [19] discussed networked healthcare and the way mobile cloud computing could enable it. They presented the motivation and development of networked healthcare applications with the adoption of cloud computing. They described a usable cloudlet-based mobile cloud-computing infrastructure for dedicated healthcare applications. They utilized the cloud model in building fall detection system for elderly people.
In [20], the authors discussed EHR sharing and integration in healthcare clouds and related concepts. They analyzed the critical security and privacy issues in EHRs accessing and managing. An EHR security reference model was described to manage healthcare cloud security issues. They presented HER security reference model through a use-case scenario and described the corresponding security countermeasures and state of the art of applicable security techniques which will be primary security guards.
As an infrastructure for assistive healthcare, the Mobile Cloud for Assistive Healthcare (MoCAsH) is proposed in [21]. MoCAsH deployed intelligent mobile agents, context-aware middleware, and collaborative protocol for efficient resource sharing. MoCAsH deployed P2P paradigm to federate cloud to manage security issues like data protecting and data ownership preserving.
Authors in [22] proposed a framework for secure health data system supported big data analytics in mobile cloud computing environment. This framework provides a high level of integration, availability, interoperability, and sharing of healthcare data among healthcare stakeholders. Thanks to the huge size of healthcare data and therefore the complexity of healthcare data types, the proposed framework employs big data analytics to assist physicians take critical decision at the proper time.
The authors in [23] proposed a Real-time face recognition acceleration architecture that integrates mobile devices, cloudlets, and cloud servers. They utilized the features of cloudlet-mobile cloud model and developed Cloud-Vision system to reinforce the vision related operations. Their results showed improvements in real-time face recognition by reducing the reaction time during face recognition process.
The authors in [24] proposed a Cloudlet based MCC system getting to reduce the facility consumption and therefore the network delay while using MCC. The MCC concepts are merged with the proposed Cloudlet framework and propose a replacement framework for the MCC model. The author of [25] presented an efficient software based mobile cloud computing which will be utilized in many useful different applications including: education and healthcare.
A Scalable Cloudlet-based Mobile Computing Model is proposed in [26]. The model utilizes the scalability feature where the number of deployed cloudlets can be adjusted based on the design requirements and the number of users in the region to be covered. The authors in [27] proposed a solution to automate patients' vital data collection by using sensors attached to existing medical equipment. These data are transformed to cloud for processing. The authors in [28] proposed a framework for the unified middleware over heterogeneous networks.

III.CONCLUSION

There are also a lack of research on the various issues of this area as in recent studies showed. Generally speaking, cloud-based pervasive healthcare is a new paradigm in healthcare sector and has many potential and beneficial features, but there are still several problems and challenges that need to be addressed by researchers in the future. These can be summarized into the following open research directions that should be focused upon in the future:

- As we described above, there are various service types in healthcare sector, such as monitoring, daily life assistance, medical assistance, pervasive access, emergency management and smart hospital. Designing a functional healthcare system for managing emergency situations or assisting medical cares is very important.
- Access to private context types like patient medical information by illegal persons should be banned. Security and privacy for sharing health records and access rights for both patients and professionals are other essential issues.

IV. REFERENCES

[1]. Susmit Paul, Asmita Sharma, "Concept of Wireless Sensor AD-HOC Network Focusing on Mobile Computing," ISTP Journal of Research in Electrical and Electronics Engineering (ISTP-JREEE) 1st International Conference on Research in Science, Engineering & Management (IOCRSEM 2014), 2014, pp. 137-147.

[2]. Amit Kumar, Dr. Yunfei Liu, Dr. Jyotsna Sengupta, Divya." Evolution of Mobile Wireless Communication Networks: 1G to 4G," International Journal of Electronics & Communication Technology, 2010, pp.68-72. Doi: 0910/101/124.

[3]. Zimmerman, James B., "Mobile Computing: Characteristics, Business benefits, and the mobile framework,"University of Maryland European Division-Bowie State 10, 1999.

[4]. N. D. Lane, E. Miluzzo, H. Lu, D. Peebles, and A. T. Campbell, "A survey of mobile phone sensing'' IEEE Commun. Mag., vol. 48, no. 9, pp. 140_150, Sep. 2010.

[5]. P. Mell and T. Grance, "The NIST Definition of Cloud Computing" Recommendations of the National Institute of Standards and Technology (Technical Report No. Gaithersburg, MD, USA: NIST, 2011.

[6]. Copeland, Marshall, Julian Soh, Anthony Puca, Mike Manning, and David Gollob. "Microsoft azure and cloud computing." In Microsoft Azure, pp. 3-26. Apress, Berkeley, CA, 2015.

[7]. Bahwaireth, Khadijah, and Lo'ai Tawalbeh. "Cooperative models in cloud and mobile cloud computing." InTelecommunications (ICT), 2016 23rd International Conference on, pp. 1-4. IEEE, 2016.

[8]. Lo'ai, A. Tawalbeh, Waseem Bakhader, Rashid Mehmood, and Houbing Song. "Cloudlet-based mobile cloud computing for healthcare 2016 IEEE, pp. 1-6. IEEE, 2016.

[9]. Tawalbeh, Lo'ai, Norah Alassaf, Waseem Bakheder, and Alaa Tawalbeh. "Resilience Mobile Cloud Computing: Features, Applications and Challenges." In e-Learning (econf), 2015 Fifth International Conference on, pp. 280-284. IEEE, 2015.

[10]. Qi, Han, and Abdullah Gani, "Research on mobile cloud computing: Review, trend and perspectives," Digital Information and Communication Technology and it's Applications (DICTAP) 2012 Second International Conference on, Bangkok, 2012, pp. 195-202.

[11]. L. A. Tawalbeh, N. Darwazeh, R. Al-Qassas, F. Dosari, " A Secure Cloud Computing Model based on Data Classification". In the Int. Workshop on Mobile Cloud Computing Systems, Management, and Security (MCSMS-2015). Procedia Computer Science, Vol.52, pp 1153–1158, UK. June 2015.

[12]. Lo'ai, A. Tawalbeh, and Waseem Bakhader. "A mobile cloud system for different useful applications." In Future Internet of Things and Cloud Workshops (FiCloudW), IEEE International Conference on, pp. 295-298. IEEE, 2016.

[13]. A. Zaslavsky, C. Perera, and D. Georgakopoulos. (2013). ``Sensing as a service and big data.'' [Online]. Available: https://arxiv.org/abs/1301.0159 <Last accessed 18/6/2017>

[14]. M. Chen, S. Mao, and Y. Liu, "Big data: A survey,'' Mobile Netw. Appl., vol. 19, no. 2, pp. 171_209, Apr. 2014.

[15]. L. A. Tawalbeh, W. Bakheder, and H. Song, ``A mobile cloud computing model using the cloudlet scheme for big data applications,'' in Proc. IEEE 1st Int. Conf. Connected Health, Appl., Syst. Eng. Technol. (CHASE), Jun. 2016, pp. 73_77.

[16]. D. Fluckinger, "Pulse Strategic insight for health IT leaders," TechTarget Inc, 2014.

[17]. M. Aminian, "A Hospital Healthcare Monitoring System Using Wireless Sensor Networks," J. Health Med. Inform., vol. 04, no. 02, 2013.

[18]. C. Doukas, T. Pliakas, & I. Maglogiannis "Mobile healthcare information management utilizing Cloud Computing and Android OS". In Engineering in Medicine and Biology Society (EMBC), 2010 Annual International Conference of the IEEE (pp. 1037-1040). IEEE.

[19]. F. Muheidat, Lo'ai Tawalbeh, and H. Tyrer. "Context-Aware, Accurate, and Real Time Fall Detection System for Elderly People". In the proceedings of the 12th IEEE International Conference on Semantic Computing, Jan 31st 2018,Laguna Hills, CA,USA

[20]. Zhang, Rui, and Ling Liu. "Security models and requirements for healthcare application clouds." In Cloud Computing (CLOUD), 2010 IEEE 3rd International Conf. on, pp. 268-275. IEEE, 2010.

[21]. Hoang, Doan B., and Lingfeng Chen. "Mobile cloud for assistive healthcare (MoCAsH)." In Services Computing Conference (APSCC), 2010 IEEE Asia-Pacific, pp. 325-332. IEEE, 2010.

[22]. L. A. Tawalbeh, R. Mehmood, E. Benkhelifa, and H. Song. "Mobile Cloud Computing Model and Big Data Analysis for Healthcare Applications." IEEE Access Journal., Vol 4, pp 6171-6180, Sept 2016.

[23]. T. Soyata, R. Muraleedharan, C. Funai, M. Kwon, and W. Heinzelman, "Cloud-Vision: Real-time face recognition using a mobile-cloudlet cloud acceleration architecture," in 2012 IEEE Symposium on Computers and Communications (ISCC), 2012, pp. 59–66.

[24]. Y. Jararweh, L. Tawalbeh, F. Ababneh, and F. Dosari, "Resource Efficient Mobile Computing Using Cloudlet Infrastructure," in 2013 IEEE Ninth International Conference on Mobile Ad-hoc and Sensor Networks (MSN), 2013, pp. 373–377.

[25]. F. Macias and G. Thomas, "Cloud Computing Advantages in the Public Sector: How Today's Government, Education, and Healthcare Organizations Are Benefiting from Cloud Computing Environments," Cisco Systems, Inc., White Paper, 2011.

[26]. Y. Jararweh, L. Tawalbeh, F. Ababneh, A. Khreishah, and F. Dosari, "Scalable Cloudlet-based Mobile Computing Model," Procedia Comp. Sci.,(34), pp. 434–441, 2014

[27]. C. O. Rolim, , F. L. Koch, C. B. Westphall, J. Werner, A. Fracalossi , & G. S. Salvador. (2010, February). A cloud computing solution for patient's data collection in health care institutions. In eHealth, Telemedicine, and Social Medicine, 2010. ETELEMED'10. Second International Conference on (pp. 95-99). IEEE.

[28]. A. Soomro and R. Schmitt, "A framework for mobile healthcare applications over heterogeneous networks," in 2011 13th IEEE International Conference on e-Health

Networking Applications and Services (Healthcom), 2011, pp. 70–73.

[29]. Bahwaireth, Khadijah, and Lo'ai Tawalbeh. "Cooperative models in cloud and mobile cloud computing." In Telecommunications (ICT), 2016 23rd International Conference on, pp. 1-4. IEEE, 2016.

[30]. King Faisal Specialist Hospital and Research Center. [Online].<Last Accessed: 1/8/2018> Available: http://www.kfshrc.edu.sa

[31]. N. Saquib, and at al. , "Chronic disease prevalence among elderly Saudi men," International Journal of Health Sciences, vol. 11, no. 5, pp. 11–16, 2017.

[32]. Z. A. Memish and at.al, "Obesity and associated factors – kingdom of saudi arabia, 2013," Preventing Chronic Disease, vol. 11, p. E174, Oct. 2014.

[33]. M. N. Koukias, and D. K. Lymberopoulos, Biomedical Engineering. Available from: InTech, 2009, ch. Requirements and Solutions for Advanced Telemedicine Applications, pp. 645–658.

[34]. Alesanco and J. GarcÃ a, "Clinical assessment of wireless ECG transmission in real-time cardiac telemonitoring," IEEE Transactions on Information Technology in Biomedicine, vol. 14, no. 5, pp. 1144–1152, Sept 2010.

[35]. Sensor and data transmission needs and technologies for patient monitoring in the operating room and intensive care unit," in 2005 IEEE Engineering in Medicine and Biology 27th Annual Conference, Jan 2005, pp. 5182– 5185.

[36]. K. Kumar and Y. H. Lu, "Cloud computing for mobile users: Can offloading computation save energy?" Computer, vol. 43, no. 4, pp. 51–56, April 2010.

[37]. T. Muhammed and R. A. Shaikh, "An analysis of fault detection strategiesin wireless sensor networks," Journal of Network and Computer Applications, vol. 78, pp. 267 – 287, Jan. 2017.

[38]. J. Sametinger, J. Rozenblit, R. Lysecky, and P. Ott, "Security challenges for medical devices," Commun. ACM, vol. 58, no. 4, pp. 74–82, March, 2015.

International Virtual Conference on Materials and Nanotechnology
In Association with International Journal of Scientific Research in Science and Technology
Volume 9 | Issue 4 | Print ISSN: 2395-6011 | Online ISSN: 2395-602X (www.ijsrst.com)

A Study of Green Inhibitor for Acidic Corrosion of Mild Steel

R. Anto Maria Jesili[1], J. Antony Rajam[1]*

[1]Department of Chemistry, St. Mary's College (Autonomous), Thoothukudi, Affiliated to Manonmaniam Sundaranar University, Abishekapatti, Tirunelveli, Tamilnadu, India

ABSTRACT

The inhibition efficiency of *Euphorbia hirta* leaves on the corrosion of mild steel in hydrochloric acid (1M) was investigated by the weight loss method. Potentiodynamic polarization and electrochemical impedence were studied to evaluate the corrosion inhibition performance of the *Euphorbia hirta* leaf extract. The results revealed that *Euphorbia hirta* acts as a corrosion inhibitor in 1M HCl. The inhibition efficiency increases with increase of extract temperature and contact time but decreases with the concentration of the leaf extract. The inhibition action was attributed to the adsorption of the chemical compounds present in the leaf extract on mild steel. The formation of an adsorbed film on a steel surface was investigated using scanning electron microscopy (SEM) and FT – IR.

Keywords : Corrosion inhibitor, Mild steel, *Euphorbia hirta*, Polarization, 1M HCl, Electrochemical Impedence Spectroscopy.

I. INTRODUCTION

In the Chemical or electro chemical reaction between the materials, usually a metal and its environment that causes a deterioration of the material and its properties. To stop metals (especially steel) from corroding we can try to stop the oxygen and water from coming in contact with the metal. Areas that are humid (more moisture in the air) will have more corrosion than areas that are dry. Corrosion is also faster when there are more ions present in the water. The minimization of corrosion by coating with a protective coating, with an oxide or phosphide or similar substance or with a protective paint or by rendering the metal passive is known as corrosion control. Protective coatings are the most widely used corrosion controlled by modifying the metal and environment. Natural products such as amino acids, proteins, biopolymers and plant extracts have been reported to be efficient corrosion inhibitors [1]. Plant extracts are viewed as rich source of naturally synthesized chemical compounds that can be extracted by simple procedures with low cost [2]. Plants are sources of naturally occurring compounds, some with complex molecular structures and having different chemical, biological and physical properties. The naturally occurring compounds are mostly used because they are environmentally acceptable, cost effective and have abundant availability. These advantages are the reason for use of extracts of plants and their products as corrosion inhibitors for metals and alloys under different environment. Different plant extracts can be used as corrosion inhibitors commonly known as green corrosion inhibitors [3-16]. Green

corrosion inhibitors are biodegradable and do not contain heavy metals or other toxic compounds.

In this view, we have chosen *Euphorbia hirta* as green inhibitor for mild steel in 1 molar hydrochloric acid. The corrosion rate was studied by weight loss method. To ascertain the inhibition efficiency of the leaf extract, we have varied the concentration of the extract, temperature and time duration.

II. EXPERIMENTAL PROCEDURE

About 10g of powdered leaves of *Euphorbia hirta* was boiled in 100mL of water for 1 hr. Then it was cooled and filtered. The extract was used to prepare various concentrations of inhibitors by diluting 2, 4, 6, 8, 10 mL and blank in 1M HCl in 50 mL SMF. About 25mL of made up solution was taken and the mild steel was dipped in different concentrations in the beaker.

2.1. Weight loss measurements

Mild steel specimens of size 2.5 cm, with a small hole of about 1 cm diameter near its upper edge were used for weight loss studies. The specimens were cut abraded with scrubbed, rinsed with water before they were dried. The pre-cleaned and weighed specimens were suspended in beakers containing the test solutions. Tests were conducted under immersion test in 150 mL of the aerated and unstirred test solutions. Immersion of time was varied from 5 hrs to 72 hrs (3 days) in 1M HCl. The specimens were retrieved from test solutions after 5, 10, 24, 48, 72 hrs appropriately cleaned, dried and reweighed. The weight loss was taken to be the difference between the weight of the specimens at a given time and its initial time. The effect of temperature on mild steel corrosion and corrosion inhibition was investigated by repeating experiments 303, 313, 323, 333, 343K respectively. All tests were run in duplicate and the data obtained showed good reproducibility.

$$\textbf{Corrosion rate (mmpy)} = 87.6 \times \frac{W}{DAT} \qquad (1)$$

Where, mmpy - millimeter per year; W - Weight loss in mg; D - Density in gm/cm^{-3};

A - Area of specimen cm^2;

T - Time in hours;

R_{corr} - Corrosion Rate

The inhibition efficiency (% IE) and degree of surface coverage (Θ) were calculated using equations below respectively.

$$\% IE = W_1 - W_2 / W_1 \times 100 \qquad (2)$$

$$\Theta = W_1 - W_2 / W_1 \qquad (3)$$

W_1 and W_2 are weight losses in the absence and presence of the inhibitor respectively.

III. RESULT AND DISCUSSION

3.1. Weight loss method

The weight loss method of monitoring corrosion rate is useful because of its simple application and reliability. Several authors have been reported on comparable agreement between weight loss technique and the other technique of corrosion monitoring. The corrosion rate can be determined by using equation (1). The effect of addition of inhibitors at different concentration on the corrosion of mild steel in 1M HCl studied by weight loss method at blank HCl and HCl with the leaf extract for immersion period of 5 hours. A decrease in corrosion rate is observed in the presence of inhibitor to the blank.

Table: 1 Effect of leaf extract on corrosion rate

Medium used	Weight loss (g)	Corrosion rate (g/cm^2)
1M HCl	0.23	0.0410
HCl with extract	0.14	0.0267

3.1.1 Effect of concentration of extract

The effect of concentration of the leaf extract was studied by varying the concentration from 2, 4, 6, 8, 10 ppm in 1 M HCl at room temperature for 5 hrs. The corrosion rate decreases and then increases, so that inhibition efficiency increases and then decreases with decrease in inhibitor concentration. This is better because it means low concentration of green

inhibitors can be used, thus making them cheaper and eco-friendly. By using equations (2) and (3), inhibition efficiency (IE) and the degree of surface coverage (Θ) can be calculated respectively. Table 2 depicts the value of corrosion rate, weight loss, IE and Θ. The trend of IE with concentration of leaf extract is given by figure 1.

Table 2 Effect of concentration of *Euphorbia hirta* leaf extract

Concentration of inhibitor ppm	R_{Corr} g/cm^2	Weight loss g	I.E %	Θ
2	0.0374	0.21	14.4827	0.1448
4	0.0267	0.15	11.1111	0.1111
6	0.0339	0.19	12.8378	0.1283
8	0.0339	0.19	12.9251	0.1292
10	0.0310	0.16	10.6771	0.1006

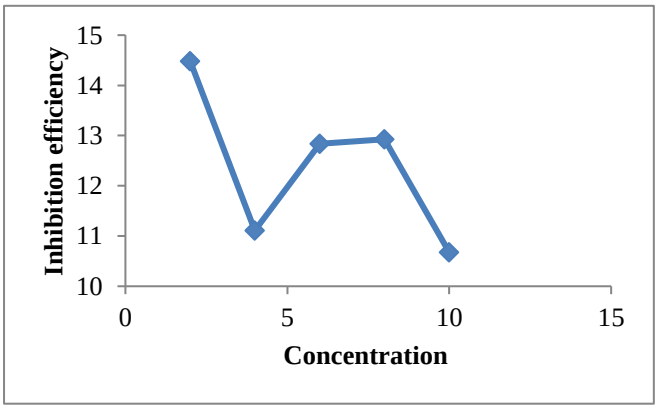

Figure 1 Plot of Inhibition Efficiency (%) vs Concentration of leaf extract

3.1.2 Effect of Temperature

The inhibition efficiency increased with an increase in temperature. This is an advantage, where mild steel can be used in high temperature applications. The corrosion rate, weight loss, percentage inhibition efficiencies and surface coverage for different temperatures in 2 ppm of the leaf extract concentration for 5 hours are given in Table 3. With an increase in temperature, more active molecules of the reactants (acid and mild steel surface) become available for the reaction. Thus, the observed trend may also be due to the fact that rates of chemical reactions generally increase with temperature (Figure 2).

Table 3 Effect of temperature on corrosion rate

Temperature °C	R_{corr} g/cm^2	Weight loss g	IE %	Θ
30	0.0267	0.15	10.6771	0.1006
40	0.0339	0.19	12.4183	0.1241
50	0.0374	0.21	14.4827	0.1448
60	0.0553	0.31	21.2328	0.2123
70	0.0607	0.34	23.2876	0.2328

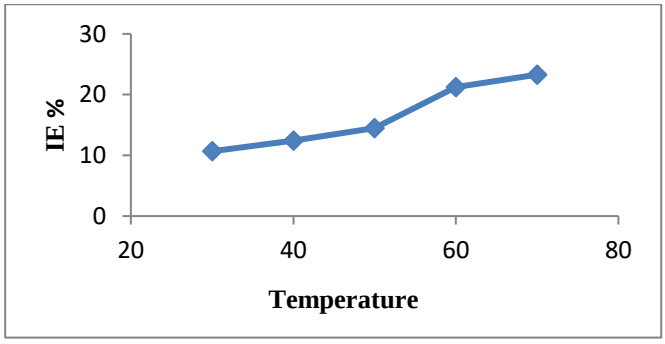

Figure 2 Plot of Inhibition Efficiency (%) vs Temperature

3.1.3 Effect of Contact time

The effect of contact time on inhibition efficiency was carried out in 2 ppm leaf concentration at 308K for 5 to 72 hours. It can be seen that inhibition efficiency (%) increases with increasing time. This shows that the inhibitors are adsorbed on the surface when it is in contact with the mild steel for a long time (Table 4). Figure 3 gives the trend of corrosion rate with time.

Table 4 Effect of contact time on corrosion rate

Contact Time Hours	R_{Corr} g/cm^2	Weight loss g	IE %	Θ

5	0.0267	0.15	10.6771	0.1006
10	0.0178	0.20	14.0845	0.1408
24	0.0085	0.23	15.7534	0.1575
48	0.0042	0.23	15.8620	0.1586
72	0.0032	0.26	17.8082	0.1780

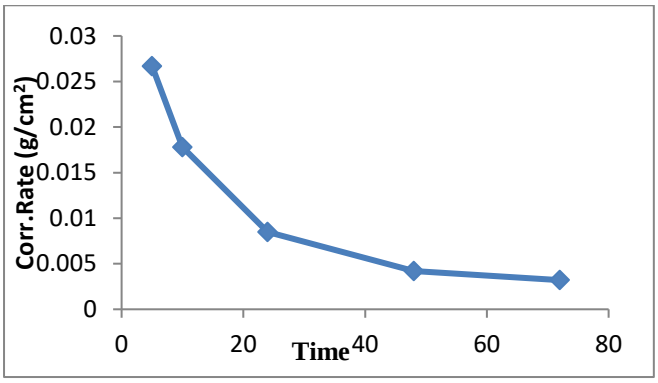

Figure 2 Plot of Corrosion Rate vs Time

3.2. Adsorption Isotherm

The nature of corrosion inhibition has been deduced in terms of the adsorption characteristics of the inhibitors. The adsorption of an organic compound adsorbed and a metal surface is regarded as a substitution adsorption process between the organic molecule in the aqueous solution and water molecule adsorbed on the metallic surface.

$Org_{(sol)} + x\ H_2O_{(ads)} \rightarrow Org_{(ads)} + x\ H_2O$

Where, x is the size ratio representing the number of water molecule replace by one molecule of organic compound adsorbed. The adsorption of organic compounds can be described by two main types of interaction. They are physisorption and chemisorption.

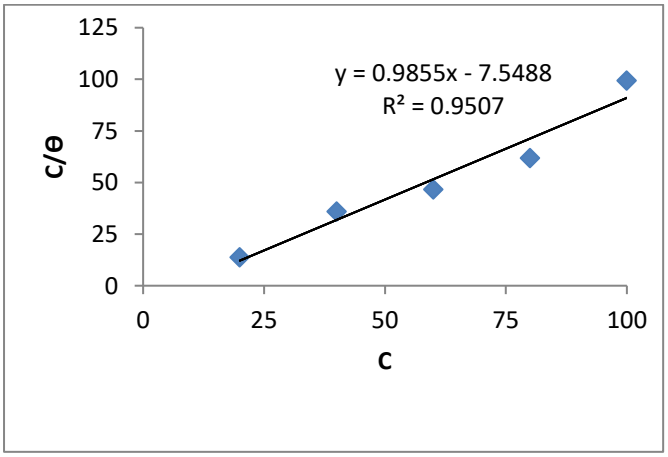

Figure 3 Plot of C/Θ vs C (Langmuir adsorption isotherm)

3.3. Electrochemical Impedence study

The impedence measurement has been applied to the study of pitting and other localized corrosion. Polarization resistance R_p can be used to determine the resistance of the metal under investigation against corrosion. From the impedance and polarization study, we get the polarization resistance value. From that value we can calculate C_{dl} value using the formula

$$C_{dl} = 1/2\ \pi\ f_{max}\ R_{ct}$$

Where, C_{dl} – Double layer capacitance; f_{max}- Maximum frequency; R_{ct} - Charge transfer C_{dl} values are used to study about corrosion efficiency. The values obtained for the bare (1M HCl) corresponds to 0.2345, bare (1M HCl), with extracts corresponds to 1.7483.The AC impedance spectra of mild steel immersed in HCl, in the presence and absence of inhibitors, are shown in Figure 4. The AC impedance parameters namely charge transfer resistance (R_{ct}) and double layer capacitance (C_{dl}) are given in Table 5. When the mild steel is immersed in acid, the R_{ct} values are 0.561 Ω cm^2 in 1M HCl and the C_{dl} values are 0.2345 Fcm^{-2} in 1M HCl. When the leaf extract is added to HCl, the R_{ct} value is increased to 1.549 Ω cm^2 for 1M HCl. The increase in R_{ct} value confirms that a protective film is formed on metal surface.

Table 5 Electrochemical Impedance measurements in 1M HCL

Coating Sample	R_{ct}	f_{max}	C_{dl}	IE %	Surface coverage
Blank (1M HCl)	0.561	0.2663	0.2345	-	-
HCl with extract	1.549	0.7189	1.7483	63.78 %	0.6378

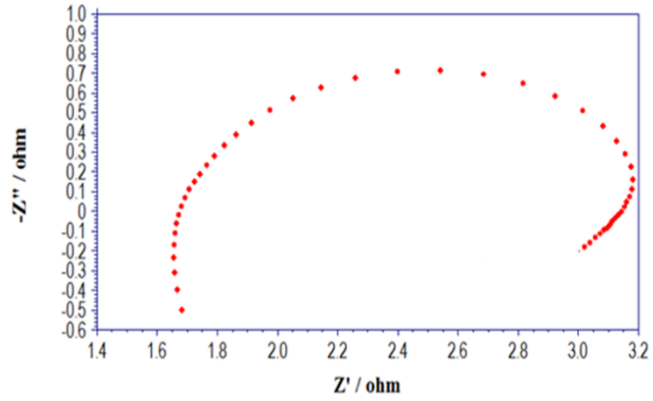

Figure 4 Nyquist plot for Bare 1M HCl with leaf extract

3.4. Potentiodynamic polarization study

The potentiodynamic polarization behaviourof mild steel in 1MHCl . Figure 5 shows that the potentiodynamic polarization behaviour of mild steel in 1MHCl containing different concentration of *Euphorbia hirta* inhibitor and observed data.

Table 6 Potentiodynamic polarization measurements in 1 M HCl with leaf extract

Coating sample	E_{corr}	I_{corr}	PE %
Bare (1M HCl)	-0.9185	0.0274	-
Bare with leaf extract	-0.9205	0.0902	69.62%

The polarization curves of carbon steel immersed in 1M HCl in the presence and absence of inhibitors are shown. The corrosion parameters are given in Table 6. When mild steel is immersed in 1M HCl, the corrosion potential is – 0.9185 V vs saturated calomel electrode (SCE). When the leaf extract is added to 1M HCl, the corrosion potential shifted to the cathodic side (– 0.9205 V vs SCE). That is 0.8944 V to 0.9014 V vs SCE. This suggests that this formulation controls the cathodic reaction predominantly.

When carbon steel immersed in 1M HCl, the corrosion current, I_{corr} from 0.02747 to 0.02902 Acm^{-2}. This indicates that protective film formed on the mild steel strongly in 1M HCl.

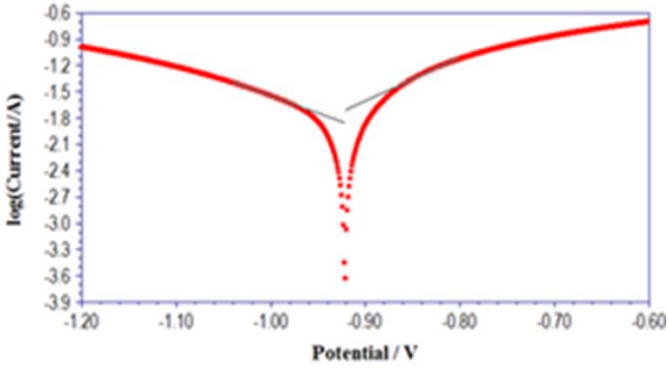

Figure 5 Tafel plot for Bare 1M HCl with leaf extract

3.5. FT-IR Spectroscopy

The peak values obtained from FT-IR analysis are shown in the figure 4.25. The broad peaks are obtained 3695.61 to 3332.99 cm^{-1} assigned to the presence of a superfacial absorbed water, stretching mode of an OH and C-H. The peaks at 3695and 2978 corresponds to stretching vibration of aliphatic aromatic OH and C-H. The peaks at 2978, 2823, 2360, 1627 cm^{-1} corresponds to C-H stretch in the presence of alkanes, C-H stretch in the presence of aldehyde, -NH, -C=O stretching. The peaks at 671, 601, 470, 432 cm^{-1} corresponds to C-Cl stretching in the presence of alkyl halides. The peaks at 948, 1157, 1242, 1512 cm^{-1} corresponds to O-H bend in the presence of carboxylic acids, C-N stretching in the presence of aliphatic amines, $-CH_2X$ in the presence of alkyl halides, -N-O asymmetric stretch in the presence of nitro compound. Almost all the peak observed for plant extract is also noticed in mild steel immersed in 1M HCl acid with plant extract as shown in the figure 6.

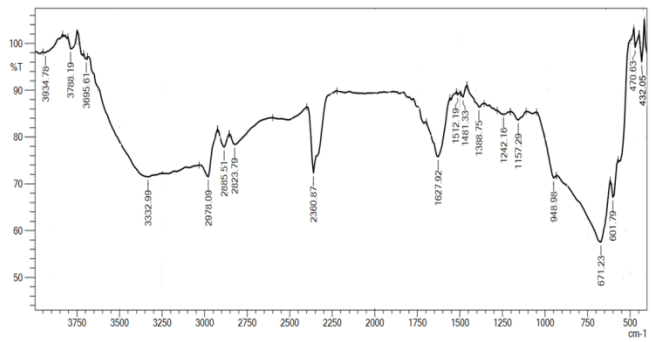

Figure 6 FT-IR Spectrum of leaf extract

3.6. SEM Analysis

Surface morphology of the mild steel surface was studied by scanning electron microscopy. Figure 7 shows that the SEM micrographs of mild steel surface after immersion in 1M HCl respectively. SEM photographs showed that the surface of metal has number of pits and cracks are visible in the surface may be belongs to the plug type of corrosion. But in presence of inhibitor the dissolution process significantly reduced by the formation of thin film covered on the entire surface of the metal.

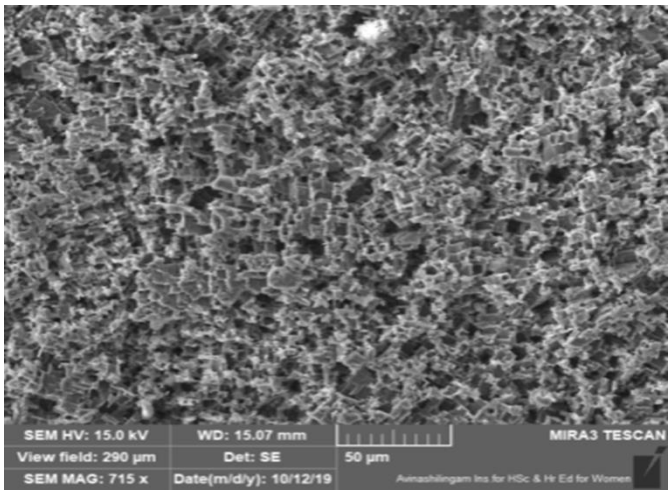

Figure 7 SEM image of leaf extract

IV. CONCLUSION

The current investigation shows that the chosen plant is very effective in inhibiting corrosion of mild steel in 1M HCl. The major conclusions of this experiment are;

- All natural compounds act as inhibitors and the highest efficiency was observed at 1M HCl in the *Euphorbia hirta* leaves.
- The corrosion inhibition process follows Langmuir isotherm suggest that one molecule of the inhibitor occupying one active site.
- Inhibitors of the *Euphorbia hirta* leaves are easily available, non-toxic and eco-friendly as well as having good inhibition efficiency.
- The AC impedence spectra reveal that plant leaves form protective film on mild steel.
- The surface morphology of the corrosion inhibition is characterized by SEM analysis and suggested different morphological structures.
- From the tafel plot, potentiodynamic polarization nature of the corrosion inhibition is examined.

V. REFERENCES

[1]. G. Sı˘gırcık, T. T¨uken, and M. Erbil, Assessment of the inhibition efficiency of 3,4-diaminobenzonitrile against the corrosion of steel, Corrosion Science, vol. 102, pp. 437–445, 2016.

[2]. K. Krishnaveni and J. Ravichandran, Effect of aqueous extract of leaves of Morinda tinctoria on corrosion inhibition of aluminium surface in HCl medium, Transactions of Nonferrous Metals Society of China, vol. 24, no. 8, pp. 2704–2712, 2014.

[3]. Rekha. N Nair, Green corrosion inhibitors for mild steel in acidic medium, International Journal of Modern Trends in Engineering and Research, vol. 04, no. 12, pp. 216-221, 2017.

[4]. Marko Chigondo, Fidelis Chigondo, Recent Natural Corrosion Inhibitors for Mild Steel: An Overview, Journal of Chemistry, Vol. 2016, Article ID 6208937, 1-7.

[5]. M. S. Al-Otaibi, A. M. Al-Mayouf, M. Khan, A. A. Mousa, S. A. Al-Mazroa e H. Alkhathlan, Corrosion inhibitory action of some plant extracts on the corrosion of mild steel in acidic media, Arabian Journal of Chemistry, pp. 1-7, 2012.

[6]. Alfred. I. Onen, Dzaradiya. U. Yakubu, Cleome gynandra and Solanum scabrum Leaf Extracts as Corrosion Inhibitor of Mild Steel in Hydrochloric Acid Solutions, Chem Sci Rev Lett, 4(16), 1069-1078, 2015.

[7]. A. M. Al-Fakih, M. Aziz, H.M. Sirat, Turmeric and ginger as green inhibitors of mild steel corrosion in acidic medium, Journal of Materials

and Environmental Science, vol. 6, no. 5, pp. 1480–1487, 2015.

[8]. K. C. Ajani, A. S. Abdulrahman, and E. Mudiare, Inhibitory action of aqueous Citrus aurantifolia seed extract on the corrosion of mild steel in H2SO4 Solution, World Applied Sciences Journal, vol. 31, no. 12, pp. 2141–2147, 2014.

[9]. E. E. Oguzie,M. A. Chidiebere, K. L. Oguzie, C. B. Adindu, and H. Momoh-Yahaya, Biomass extracts for materials protection: corrosion inhibition ofmild steel in acidic media by Terminalia chebula extracts, Chemical Engineering Communications, vol. 201, no. 6, pp. 790–803, 2014.

[10]. Z. V. P. Murthy and K. Vijayaragavan, Mild steel corrosion inhibition by acid extract of leaves of Hibiscus sabdariffa as a green corrosion inhibitor and sorption behavior, Green Chemistry Letters and Reviews, vol. 7, no. 3, pp. 209–219, 2014.

[11]. K. K. Anupama, K. Ramya, A. Joseph, Electrochemical and computational aspects of surface interaction and corrosion inhibition of mild steel in hydrochloric acid by Phyllanthus amarus leaf extract (PAE), Journal of Molecular Liquids, vol. 216, pp. 146–155, 2016.

[12]. Abeng, F. E., Ekpe, U. J., Ikeuba, A. I., Ugi, B. U., Nna, P. J. Inhibitive action of alkaloid and non-alkaloid fractions of ethanolic extracts of Phyllanthus amarus on the corrosion of mild steel in HCl solution, Global Journal of Pure and Applied Sciences, vol. 19, 2013.

[13]. Kamal, C., Gopalakrishnan, M., A bis-indol alkaloid as a green inhibitor for corrosion of mild steel in HCl solution from Caulerpa racemosa, Journal of Hazardous Materials, vol. 2, no. 3, pp. 54-60, 2012.

[14]. Ghazoui, A., Saddik, R., Benchat, N., Guenbour, M., Hammouti, B., Al-Deyab, S.S., Zarrouk, A. Comparative study of pyridine and pyrimidine derivatives as corrosion inhibitors of C38 steel in molar HCl, Int. J. Electrochem. Sci. vol. 7, pp. 7080-7097, 2012.

[15]. P. M. Ejikeme, S. G.Umana, M. C.Menkiti, O.D.Onukwuli, Inhibition ofmild steel and aluminium corrosion in 1MH2SO4 by leaves extract of African Breadfruit, International Journal of Materials and Chemistry, vol. 5, no. 1, pp. 14–23, 2015.

[16]. M. Prabakaran, S.H. Kim, K. Kalaiselvi, V. Hemapriya, I.M. Chung, Highly efficient Ligularia fischeri green extract for the protection against corrosion of mild steel in acidic medium: electrochemical and spectroscopic investigations, Journal of the Taiwan Institute of Chemical Engineers, vol. 59, pp. 553–562, 2016.

International Virtual Conference on Materials and Nanotechnology
In Association with International Journal of Scientific Research in Science and Technology
Volume 9 | Issue 4 | Print ISSN: 2395-6011 | Online ISSN: 2395-602X (www.ijsrst.com)

A Comparative Analysis of Optimization Technique in Large Scale Transportation Problem to Optimize Mathematical Manipulation

Prof. Yogita D. Shahakar
Assistant Professor, Department of Electrical Engineering, P.R. Pote (Patil) College of Engineering & Management, Amravati, Maharashtra, India

ABSTRACT

Transportation problem is one of the classical optimization technique in which the objective is that the problem of deciding the quantities to be transport from different source to various destinations so as to minimize the total cost of transformation. I.e. to transport some goods from source to destination in such a way that minimizes the total cost while satisfying supply and demand constraints. There are various tabular methods to solve the transportation problem like NWCM, LCM, VAM, Stepping stone & MODI Method etc.. In this, an approach is presented to solve transportation problem as a LPP by considering the optimization tool of MATLAB and compare it with tabular methods of transportation. The complexity reduction is done by eliminating the large number of steps. By using proposed technique, the calculation part has been completely avoided and we can achieve the results in considerable duration. By using optimization tool in MATLAB used for transportation problem as a LPP. The objective of the study was to find out how these proposed algorithms behave in terms of accuracy and speed when a large-scale transportation problem is being solved.

Index Term: Transportation Problem, LPP, Optimization tool, Tabular methods

I. INTRODUCTION

Optimization technique is a mathematical approach to solve the problem for finding the best possible solution out of the available alternatives under the given circumstances. Optimization technique plays a vital role in operational as well as in strategic decision making in business, agriculture, manufacturing, production, transportation, investment policy etc. The transportation Problem is one of the optimization problem where the objective is to determine the total transportation cost means to minimize the total transportation cost ,while satisfying supply and demand constraints. A typical Transportation Problem has the various elements like Source(s) , Destination(s) Weighted edge(s). There are various classical methods to solve transportation problem using optimization technique like North West corner, least cost, voogles approximation, stepping stone & MODI method etc. Most real life problems formulated as an LP model have more than two variables and therefore need a more efficient method to get optimal solution. So Optimization tool in MATLAB for LPP is very efficient, time consuming, most accurate tool to solve the transportation problem as a LPP.

Transportation problem converted as a LP model in which the objective function and constraint are strictly linear. The linear programming technique is used in a variety of applications, and in areas such as economics, transportation, production, and social sciences. A Linear Programming (LP) problem of transportation problem consists of Objective function, Design variables and Constraints.

Simple Network Representation

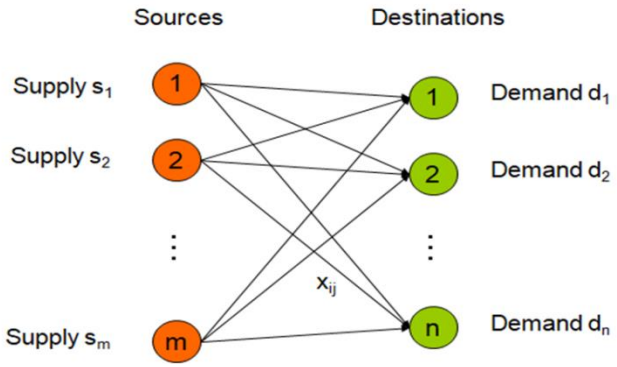

	D1	D2	D3	D4	Supply
S1	50	75	30	45	12
S2	65	80	40	60	17
S3	40	70	50	55	11
Demand	10	10	10	10	

Transportation problem is simple and it can be solved without taking much effort. In practical transportation problem, networks are much more complicated and therefore simplified techniques are needed to solve this problem.. Another method to solve transportation problems by using Linear Programming method. By using optimization tool in MATLAB used for linear programming, we can easily solve the transportation problem without any complications and less computation time & iterations.

II. CLASSICAL/TABULAR METHODS OF TRANSPORTATION PROBLEM

There are various tabular/classical methods to solve the transportation problem to minimize the total cost of transportation. To find the initial basic feasible solution, there are three methods

A. North West Corner Method
B. Least Cost Method
C. Vogel's Approximation Method

To find the optimum solution of transportation problem, there are two methods

D. Stepping Stone Method
E. MODI Method

A. North West Corner Method

It is a simple & efficient method to obtain an initial basic feasible solution. This method does not take into account the cost of transportation on any routs of transportation.

Steps:-

1. Verify that problem is balanced is balanced or not. If problem is not balanced, then balanced it.
2. Start with the cell upper left corner (North West) of the transportation table and allocate as much as possible equal to the minimum of the first row and first column. i.e. min (a1 ,b1)
3. If min (a1, b1) = a1, then X11 = a1. Cross off the first row and adjust the requirement of the first column as b1 – a1
4. If min (a1, b1) = b1, then X11 = b1. Cross off the first column and adjust the requirement of the first row as a1- b1
5. If a1 = b1, then X11 = a1 = b1. Cross off the first column as well as of the first row
6. Continue this procedure step by step till the allocation is made in the south east corner cell of the transportation table. After completion all availabilities will be exhausted and all requirements will be satisfied

B. Least Cost Method (LCM)

In this method to minimize the total transportation cost we must try to transport as much as possible through those roots (cells) where the unit transportation cost is minimum. This method takes into the minimum unit cost.

C. Vogel's Approximation Method (VAM)

In this method, each allocation is made on the basis of the opportunities or penalty or extra cost that would have incurred if allocation in certain cell s with minimum transportation cost is missed. In this method, allocations are made so that the penalty cost is minimized. The advantage of this method is that it nearer to an optimum solution or is the optimum solution itself.

Steps:

1. Calculate the penalty for each row and each column by taking the difference between smallest and next smallest unit transportation cost in the same row or column. This difference indicates the penalty or extra cost which has to be paid if one fails to allocate to the cells with the minimum unit transportation cost
2. Select the row or column with largest penalty and allocate as much as possible in the cell having the least cost in the selected row or column. If there is a tie in the values of penalty then it can be broken by selecting the cell where maximum allocations can be made.
3. Balance the supply and demand and cross out the satisfied row or column. If row or column satisfied simultaneously then cross them simultaneously.
4. Repeat step 1 and 3 until the entire available supply at various sources and demand at various destinations are satisfied.

D. Stepping stone method:

It is the most accurate method to find the exact optimum solution than other methods. By using this method, we can easily find the minimum transportation cost.

Steps:

1. Find the cost change for each unoccupied cell by allocating one unit to that cells.
2. If all the cost changes are positive it indicate that optimum solution is reached.
3. If all the cost changes are positive, some are zero it indicate that there are multiple optimum solution and the present solution is one of them .
4. If some cost changes are negative then further optimization is possible.
5. Choose the cell giving most negative cost change.
6. Allocate maximum possible unit to that cell.
7. Modify the allocations of other cells.
8. Again find the cost change for other cell.

III. IMPLEMENTATION OF TABULAR METHODS

Case study

Example:

Power Company has three electric power plants that supply the electric needs of four cities. The power plant supply of each plant and demand of each city is given in the table 1. The cost of sending 1 million kwh of electricity from a plant to a city depends on the distance the electricity must travel. A transportation problem consists of supply, demand, and the shipping costs. So the relevant data can be presented in a transportation table. The transportation table represents the supply and demand constraints and the shipping cost between each demand and supply.

Table 1: Shipping cost, Supply and Demand for Power Company Example

From	To				
	City 1	City 2	City 3	City 4	Supply(Million kwh)
Plant 1	$8	$6	$10	$9	35
Plant 2	$9	$12	$13	$7	50
Plant 3	$14	$9	$16	$5	40
Demand (Million kwh)	45	20	30	30	

1. North West Corner Method

By using the mentioned steps, we can find the total transportation cost.

Total Transportation Cost = 35*8+10*9+20*12+20*13+ 10*16+30 *5 = **1180 Rs**

2. Least Cost Method:

In similar way, we can find the total transportation cost by using LCM Method according to the given steps.

Total Transportation Cost = 30*5+20*6+15*8+30*9+20*13+10*16 = **1080 Rs**

3. VAM Method:

In similar way, we can find the total transportation cost by using VAM Method according to the given steps.

Total Transportation Cost = 30*5+10*9+10*6+45*9+5*13+25*10 = **1020 Rs**

Stepping stone method:

To apply the stepping stone method, first to find IBFS by using NWCM, LCM or VAM method. By using VAM method, it takes only one iteration to find the optimum solution. NWCM & LCM methods take more iteration to find the optimum solution.

By using the mentioned steps, the total transportation cost is given by, =1020 RS.

IV. COMPUTATIONAL DIFFICULTIES

Any Linear Programming problem can be solved by using the Simplex method, two phase simplex method, dual simplex method, revised simplex method, Big M method , graphical etc... There are various tabular methods to solve the transportation problem like NWCM, LCM, VAM, Stepping stone and MODI method. When we apply all these tabular methods, it requires too much computation time to solve large-scale transportation problems .There is possibility to get inaccurate solution because of complicated calculations. If there are large numbers of sources and destination, then calculation part makes complicated. So it is necessary to apply another advanced method, which reduces computation time & iterations and also get the exact optimum solution. In MATLAB, there are various optimization tools are available, that can apply to linear programming, nonlinear programming problem of optimization to get the optimum solution in less time and iterations. For that we have to convert given transportation problem into linear programming problem. For linear programming problem, the proper syntax is given in MATLAB. By using this syntax we can easily find the exact optimum solution.

V. PROPOSED METHODOLOGY

Optimization techniques for Transportation problem consist of various methods to find optimum solution. By using NWCM, LCM, VAM, Stepping stone &

MODI method, we can find the total transportation cost by using these methods and also compare the solution. But when there are large number of sources & destinations, then it is difficult to find the solution of transportation problem. In this case we can formulate the transportation problem as a linear programming problem. To solve the linear programming problem, there are various tabular methods like simplex, two phase simplex, dual simplex and graphical method etc. But again the because of large number of variables, it is difficult to apply all these methods. To avoid all these situations, there are various tools are available in MATLAB to solve the each & every complicated problem. To solve the linear programming problem, optimization tools are available in MATLAB. The advantage of these optimization tools is that, it takes very less computation time & iteration. & there are no chances to get the inaccurate solution. Another advantage is that , When we solve the transportation problem by using tabular methods of transportation and also as a linear programming problem by using tabular methods , first there is need to identify the separate methods of LPP like simplex , two phase simplex , dual simplex & graphical method etc. according to the algorithms. But when we use the optimization tools in MATLAB, there is no need to identify each method separately only to identify it is linear or nonlinear programming problem.

A. Implementation of Proposed Methodology

To apply proposed methodology, consider the same example i.e. power company example that used in tabular methods

1. Decision Variable

We have to determine how much electricity is sent from each source (plant) to each destination (city);

X_{ij} = Amount of electricity produced at plant i and sent to city j

2. Objective function

Here we want to minimize the total cost of shipping from different plants to various to cities;

$MinimizeZ=8X_{11}+6X_{12}+10X_{13}+9X_{14}+9X_{21}+12X_{22}+13X_{23}+7X_{24}+14X_{31}+9X_{32}+16X_{33}+5X_{34}$

3. Supply Constraints

Each supply has a limited production capacity;

$X_{11}+X_{12}+X_{13}+X_{14} <= 35$

$X_{21}+X_{22}+X_{23}+X_{24} <= 50$

$X_{31}+X_{32}+X_{33}+X_{34} <= 40$

4. Demand Constraints

Since each supply point has a limited production capacity;

$X_{11}+X_{21}+X_{31} >= 45$

$X_{12}+X_{22}+X_{32} >= 20$

$X_{13}+X_{23}+X_{33} >= 30$

$X_{14}+X_{24}+X_{34} >= 30$

5. Sign Constraints

Since a negative amount of electricity cannot be shipped all Xij's must be non-negative;

$Xij >= 0$ (i= 1, 2, 3; j= 1, 2, 3, 4)

B. LP Formulation of Powerco's Problem

$MinZ=8X_{11}+6X_{12}+10X_{13}+9X_{14}+9X_{21}+12X_{22}+13X_{23}+7X_{24}+14X_{31}+9X_{32}+16X_{33}+5X_{34}$

S.T.:

$X_{11}+X_{12}+X_{13}+X_{14} <= 35$ (Supply Constraints)

$X_{21}+X_{22}+X_{23}+X_{24} <= 50$

$X_{31}+X_{32}+X_{33}+X_{34} <= 40$

$X_{11}+X_{21}+X_{31} >= 45$ (Demand Constraints)

$X_{12}+X_{22}+X_{32} >= 20$

$X_{13}+X_{23}+X_{33} >= 30$

$X_{14}+X_{24}+X_{34} >= 30$

$Xij >= 0$ (i= 1, 2, 3; j= 1, 2, 3, 4)

To apply the proposed methodology in transportation problem, first it can be formulated as a linear programming problem. To solve the any linear programming problem, the optimization toolbox is

available in MATLAB. There is specific syntax for the linear programming problem is as follows

Syntax for LPP

x = linprog(f,A,b)

x = linprog(f, A, b, Aeq, beq)

x = linprog(f, A, b, Aeq, beq, lb, ub)

Sr. No.	Parameter	Description
1	f	Objective function (Coefficient vector)
2	A	Linear inequality constraints (LHS of the constraints)
3	B	Linear inequality constraints (RHS of the constraints)
4	Aeq	Linear equality constraints(LHS of the constraints)
5	Beq	Linear equality constraints (RHS of the constraints)
6	lb	Lower bound
7	ub	Upper bound

To solve the any linear programming problem by using optimization tool in MATLAB, it is necessary to convert given problem into standard form.

VI. ANALYSIS OF TRANSPORTATION PROBLEM USING OPTIMIZATION TOOLBOX

Transportation Problem as a linear programming problem

$MinZ=8X_{11}+6X_{12}+10X_{13}+9X_{14}+9X_{21}+12X_{22}+13X_{23}+7X_{24}+14X_{31}+9X_{32}+16X_{33}+5X_{34}$

S.T.

$X_{11}+X_{12}+X_{13}+X_{14} <= 35$ (Supply Constraints)

$X_{21}+X_{22}+X_{23}+X_{24} <= 50$

$X_{31}+X_{32}+X_{33}+X_{34} <= 40$

$X_{11}+X_{21}+X_{31} >= 45$ (Demand Constraints)

$X_{12}+X_{22}+X_{32} >= 20$

$X_{13}+X_{23}+X_{33} >= 30$

$X_{14}+X_{24}+X_{34} >= 30$

Conversion to standard Form

$MinZ=8X_{11}+6X_{12}+10X_{13}+9X_{14}+9X_{21}+12X_{22}+13X_{23}+7X_{24}+14X_{31}+9X_{32}+16X_{33}+5X_{34}$

S.T.

$X_{11} + X_{12} + X_{13} + X_{14} <= 35$ (Supply Constraints)

$X_{21} + X_{22} + X_{23} + X_{24} <= 50$

$X_{31} + X_{32} + X_{33} + X_{34} <= 40$

$-X_{11} - X_{21} - X_{31} <= -45$ (Demand Constraints)

$-X_{12} - X_{22} - X_{32} <= -20$

$-X_{13} - X_{23} - X_{33} <= -30$

$-X_{14} - X_{24} - X_{34} <= -30$

Problem Using optimization Toolbox

```
f=[8 6 10 9 9 12 13 7 14 9 16 5];

A = [1 1 1 1 0 0 0 0 0 0 0 0; 0 0 0 0 1 1 1 1 0 0 0 0 ; 0 0 0 0 0 0 0 0 1 1 1 1 ; -1 0 0 0 ; -1 0 0 0 ; -1 0 0 0 ; 0 -1 0 0 ; 0 -1 0 0 ; 0 -1 0 0 ; 0 0 -1 0 ; 0 0 -1 0 ; 0 0 -1 0; 0 0 0 -1; 0 0 0 -1; 0 0 0 -1] ;

b=[ 35 50 40 -45 -20 -30 -30];

lb=[0 0 0 0 0 0 0 0 0 0 0 0];

[x, fval ] =linprog(f , A , b , [ ] , [ ] , lb)
```

Output

X = 0, 10 , 25, 0, 45, 0, 5, 0, 0, 10, 0, 30 fval= 1020 Rs.

Comparison of Transportation Problem Methods

Methods →	Tabular Methods			Proposed Method
Type of solution ↓	North West Corner Method	Least Cost Method	Voggles Approximation Method	Optimization Toolbox in MATLAB Used for LPP
`IBFS	**1180**	**1080**	**1020**	

(Transportation Cost in Rs.)	**Rs**	**Rs.**	**Rs**	**1020 Rs.**
	Stepping Stone Method			
Optimum Solution (Transportation Cost in Rs.)	**1020 Rs.**			

From the above table, it is clear that if we compare the tabular methods of transportation problem to find the initial basic feasible solution, then VAM is the best optimum method to find the minimum transportation cost. And if we used stepping stone method to find the optimum solution, then we get the same cost as VAM method.

If we find the solution by using proposed methodology, & compare with the tabular methods, then It is clear that, the proposed methodology gives the exact optimum solution in less computation time and iteration. And also clear that we can apply this method for large number of variables which is not possible by using tabular methods.

But when we apply all these tabular methods, it takes more computation time & iteration. There is possibility to get inaccurate solution because of complicated calculations. If there are large number of sources and destination , then calculation part makes complicated.

VII. CONCLUSION

In this, a new approach of optimization technique i. e. optimization toolbox in MATLAB used for LPP, has been discussed to minimize the total transportation cost in large scale transportation problem. Thus obtained results have been compared with existing technique (Tabular methods) and results are reported. The proposed technique has been conducted through MATLAB coding using optimization tools used for LPP and verified with tabular methods. The proposed technique is able to minimize the total transportation cost & find the exact optimum solution than tabular methods.

Due to which the proposed technique is more efficient and convenient and can find the exact optimum solution in less time and iteration. In this calculation part is completely avoided finally proposed technique gives better results than other specified techniques in less time & iteration.

VIII. REFERENCES

[1]. Gautahman p. , " Optimization Technique for Transportation Problem" International Journal of Engineering ,Research & Applications, Vol 7 , issue 6 , (Part 1) June 2017 , pp 424-25

[2]. Chaudhuri, Arindam. "A Comparative study of Transportation Problem under." Journal of mathematics and computer science, 2011: 256-267.

[3]. Namrata Tripathi & Namita Shrivastav "Optimization problem solved by different platform say optimum toolbox (MATLAB) & Excel solver" International Research Journal of Engineering & Technology. vol 4 , issue 9 sep 2017 .

[4]. Nikolaos Ploskas & Nikolaos Samaeas "Linear Programming Using MATLAB (Springer Optimization & its applications)" 1st edition 2017

[5]. Optimization in Practice with MATLAB, Achille Messle

[6]. Barnes,J, W, and R.M. Crisp, "Linear Programming: A Survey of General Purpose Algorithms,"AIIE Transactions,

[7]. D. Gay, A Variant of Karmarkar's Linear Programming Algorithm for Problems in Standard form, Mathematical Programming 37 (1987) 81-90

[8]. E.D. Anderson and K.D. Anderson. Presolving in Linear Programming, Mathematical Programming, 71 (1995), pp. 221-245.

[9]. E.R. Barnes, A Variation on Karmarkar's Algorithm for Solving Linear Programming problems, Mathematical Programming 36, 1986, p. 174-182 .

[10]. Hillier, Frederick S and Lieberman, Gerald. Introduction to Operations Research. 2005. Boston: McGraw-Hill. ISBN: 0-07-123828-X.

[11]. Charles Copper & Henderson,1963, An Introduction to Linear programming, John Willy,New York

[12]. Optimization Toolbox™ 4 User's Guide

[13]. Cesar Parez Lopez "MATLAB Optimization Technique: Springer.

[14]. Singereshu S. Rao, "Engineering Applications: Theory & Practice", Fourth Edition ,John Wiley & Sons.

[15]. D.S. Hira. and P.K. Gupta. Operations research, Seventh revised Edition 2014. ISBN: 81-219-0281-9

[16]. Taha, H. A. , " Operations Research An Introduction " , Macmillan publishing co., Inc. United States , 1982.

International Virtual Conference on Materials and Nanotechnology
In Association with International Journal of Scientific Research in Science and Technology
Volume 9 | Issue 4 | Print ISSN: 2395-6011 | Online ISSN: 2395-602X (www.ijsrst.com)

Synthesis, Spectral and Thermal Degradation Kinetics Studies of Copolymer Resin

Jyotsana Khobragade[1], W. B. Gurnule[2]
[1]Department of Chemistry, Gurunanak Science College, Ballarpur, Maharashtra, India
[2]Department of Chemistry, Kamla Nehru Mahavidyalaya, Nagpur-440024, Maharashtra, India

ABSTRACT

Terpolymer (PTFM-II) has been synthesized by using the three monomers pthalic acid, melamine and formaldehyde in 2:1:4 molar proportions. The structure of PTFM-II copolymer has been elucidated on the basis of elemental analysis and various physicochemical techniques, i.e. UV–Visible, FT-IR and H^1-NMR spectroscopy. Thermal degradation study of the new copolymer has been carried out for its thermal stability. The activation energy (*Ea*) and thermal stability calculated by using the Sharp-Wentworth and Freeman-Carroll methods. Thermodynamic parameters such as entropy change (ΔS), apparent entropy change (S^*) and frequency factor (*z*) have also been evaluated on the basis of the data of Freeman-Carroll method.

Keywords : PTMF-II, copolymer; Synthesis; characterization; Sharp–Wentworth method; Freeman–Carroll method, Thermal degradation.

I. INTRODUCTION

Copolymers, very special class of polymer, are known for their versatile uses and are found to be amorphous, crystalline or resinous in nature. Due to their exciting features such as high thermal stability of copolymer resin which is considerable attention has been paid in the past two decades. The study of thermal behaviour of polymers in air at different temperature provides important information about its practical applicability. The thermal stability of the synthesized compounds was determined by thermo gravimetric analysis [1]. Thermo gravimetric analysis (TGA) has been proved to be a useful and efficient technique for the estimation of lifetimes of polymers. Phenol-formaldehyde resins were the first synthetic polymers to be commercialized. Phenolic are still very important industrial polymers, though their most common use today is in adhesives for the bonding of plywood and other structural wood products.

Melamine-formaldehyde resin is hard, thermosetting and water soluble resin. These are formed by the polymerization of melamine with formaldehyde.

In more than 70% of all wood-based materials in use today, adhesives and the physicochemical phenomenon of adhesion play an important role [2, 3]. This adhesives also used in paper products, paints, and finishes. The forest products industry have been used natural adhesives derived from starch, soybeans, animal waste, and byproducts of the meat processing, tanning industries, casein from skim milk [4]. In

many respects, the chemistry of the formation of melamine-based resins is very similar to that of UF resins.

MF resins have versatile applications such as in preparing kitchen utensil, table ware, furniture, automotive industry, clutch facing, brake pads, friction materials, for clutch and break, coated abrasive, grinding wheels, laminated paper and cloth, wood panel industry, composite wood panels, electrical molding, binder for leather tanning. Melamine resin is often used in kitchen utensils and plates. MF resins (also known as amino resins) are water soluble and, hence, find use as sizing agents and textiles-finishing resins. They are also used in paper industry, plywood industry and as adhesives. A considerable attention has been paid in the past two decades to the synthesis of copolymer resin due to their exciting features such as high thermal stability. Sami Ullah and coworker studied the thermal decomposition kinetics study of melamine-formaldehyde resin [5]. A. B. Zade and coworker studied the thermal degradation of copolymer resin (*p*-NP-4,4′-MDA-F) from p-nitrophenol (*p*-NP) and 4,4′-methylene dianiline (4,4′-MDA) with formaldehyde (F)[6] .

R. N. Singaru and coworker synthesis, characterization, and thermal degradation studies of copolymer resin derived from p-cresol, melamine, and formaldehyde[7]. Synthesis, characterisation and thermal degradation studies of copolymer resin by Wasudeo B. Gurnule and Vaishali R. Bisen Synthesised by monomers 2,4-dihydroxybenzoic acid, phenyl hydrazine and formaldehyde[8]

The objective of this work is synthesis and characterization of PTMF-II resins at 2:1:4 molar ratios of pthalic acid, melamine and formaldehyde and determination of the morphology, molecular weight synthesized resin samples. The synthesised resin samples were characterized by using molecular weight determination by conductoetric titration, and thermogravimetric analysis (TGA). The elemental analysis has been carried out to ascertain the molecular formula and the spectral studies have been used to characterize the complete structure of the PTMF-II resins. After treating the thermal degradation data with Sharp–Wentworth (S-W) and Freeman–Carroll (F-C) methods, activation energy and kinetic parameters such as ΔS, z, S* and n (order of reaction) have been evaluated [9].

II. MATERIALS AND METHOD

Materials and samples

All the chemicals used were of analytical grade. Pthalic acid, melamine and formaldehyde which are purchased from Merck Chemicals, India. Solvents like N-,Ndimethylformamide and dimethylsulphoxide purchased from SD Fine Ltd, Mumbai, India, were used after distillation.

Synthesis of PTMF-II copolymer resin

The PTMF-II copolymer was synthesized by condensing pthalic acid (0.2 mol) – melamine (0.1 mol) – formaldehyde (0.4 mol) (PTMF) copolymers in the presence glacial acetic acid (200 ml) as a reaction medium at 126 ± 2°C in oil bath for 5 hours [10-11].

The resinous product so obtained was repeatedly washed with cold distilled water, dried in air and powdered with the help of mortar and pestle. The powdered sample was washed many times with boiling water and methanol to remove unreacted monomers. The air dried powdered then extracted with diethyl ether and then with petroleum ether to remove melamine formaldehyde copolymer which might be present along with PTMF copolymer resin. It was further purified by dissolving in 8% NaOH solution, filtered and reprecipitated by gradual drop wise addition of ice cold 1:1 (v/v) concentrated HCl/distill water with constant and rapid stirring to avoid lump formation. The process of reprecipitation was repeated thrice. The resulting polymer sample was filtered, washed several time with boiling water, dried in air, powdered and kept in vacuum over silica

gel. The yield of these copolymer resins found to be 85%. The reaction is shown as follows.

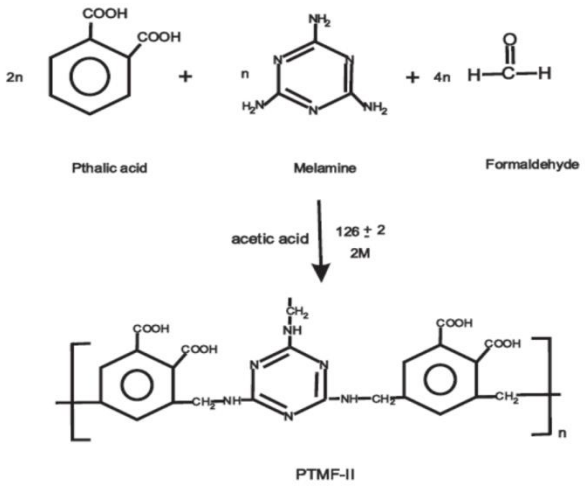

Fig.1 Synthesis of PTMF-II Terpolymer Resin

Analytical and physicochemical studies

The elemental analysis was carried out on a Perkin Elmer 2400 Elemental Analyzer instrument. The UV–Visible studies were out carried using Scimadzu UV-1800 Spectrophotometer in the range 200-800 nm. The Infrared spectrum was recorded in the region of 500–4000 cm-1 on Shimadzu Affinity-1 FTIR Spectrophotometer at Department of Chemistry, Kamla Nehru Mahavidyalaya, Nagpur. 1H-NMR studied using Bruker Avance-II FT-NMR Spectrometer in DMSO-d6 solvent. All the analytical and spectral studies for the newly synthesized copolymer were carried out at Sophisticated Testing Instrumentation Centre (STIC), Kochi.

Instrumentation

The nonisothermal thermogravimetric analysis was performed in air atmosphere with heating rate of 10 ^{0}C. min-1 using 5 - 6 mg of samples in platinum crucible from temperature of 40 ^{0}C to 800 ^{0}C and thermograms are recorded for PTMF-II sample at Sophisticated Testing Instrumentation Centre (STIC), Kochi. Thermal activation energies (Ea) and order of reaction (n) Calculated by using thermogravimetric data. Also other thermodynamic parameters such as entropy change (ΔS), apparent entropy change (S*) and frequency factor (z) are determined and reported in the Table 1.

Theoretical considerations

To provide further evidence regarding the degradation system of analyzed compounds, we derived the TG curves by applying an analytical method proposed by Sharp-Wentworth and Freeman-Carroll.

Freeman–Carroll method

Freeman and Carroll method used to derive the straight line equation [12], which is in the form of

$$\frac{\Delta \log dW/dt}{\Delta \log Wr} = n - \frac{Ea}{2.303R}.\frac{\Delta(1/T)}{\Delta \log Wr} \quad \text{.....(1)}$$

Where,

dW/dt = rate of change of weight with time.

Wr = Wc-W

Wc = weight loss at completion of reaction.

W = fraction of weight loss at time t.

Ea = energy of activation.

The plot between the terms $\frac{\Delta \log dW/dt}{\Delta \log Wr}$ vs $\frac{\Delta 1/T}{\Delta \log Wr}$ gives a straight line from which slope we obtained energy of activation (Ea) and intercept on Y-axis as order of reaction (n). The change in entropy (ΔS), frequency factor (z), apparent entropy (S*) can also be calculated by further calculations.

Sharp–Wentworth method

Using the equation derived by Sharp and Wentworth [13]

$$\log \frac{dC/dT}{1-C} = \log A/\beta - \frac{Ea}{2.303R}.\frac{1}{T} \quad \text{..... (2)}$$

Where,

dC/dT = rate of change of fraction of weight with change in temperature

β = linear heating rate dT/dt. By plotting the graph between log $\frac{dC/dT}{1-C}$ vs $\frac{1}{T}$

we obtained the straight line which give energy of activation (Ea) from its slope.

III. RESULTS AND DISCUSSION

The resin sample was white in color, insoluble in commonly used solvent, but was soluble in DMF, DMSO, THF, pyridine, concentrated H_2SO_4. No precipitation and degradation occurs of resin in all the solvents. These resins were analyzed for carbon, hydrogen and nitrogen content.

Characterization of copolymer

Molecular weight of copolymer was estimated by conductometric titration. The degree of polymerization ($\overline{DP}$) and the number average molecular weight $(\overline{Mn})$ were evaluated from the conductometric titration curves. Following formula used to determine the degree of polymerization.

$$\overline{DP} = \frac{\text{Total meq. of base required for complete neutralization}}{\text{Meq. of base required for smallest interval}}$$

$\overline{Mn}$ = $\overline{DP}$ x Repeat unit weight.

$(\overline{Mn})$ = $\overline{DP}$ x Repeat unit weight.

The molecular weight of PTMF-II is 3894.75. Fig.2.

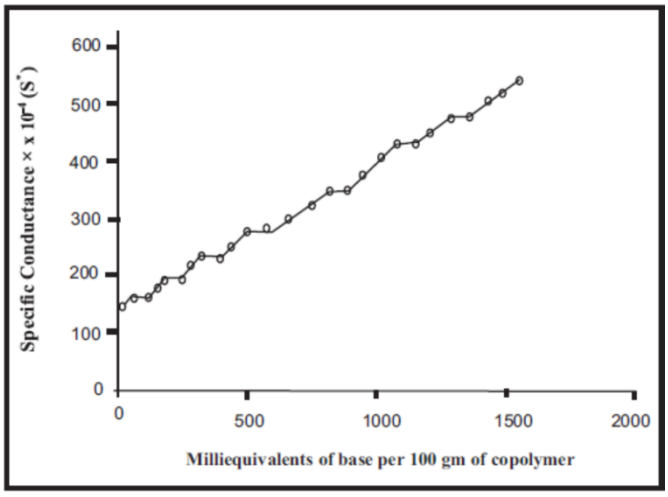

Fig. 2. Conduct metric Titration Curves of PTMF-II Copolymer Resins

The composition of copolymer (represented in scheme 1) obtained on the basis of the elemental analysis data was found to be in good correlation to that of the calculated values:

Calculated for $C_{23}H_{19}O_8N_6$: Found: C: 54.02% H: 3.98% N: 16.82%

Calculated: C: 54.44% H: 3.75% N: 16.57%

The UV- Visible spectrum of the purified PTMF-II copolymere has been recorded in DMF. The broad of UV- Visible spectra is shown in figure 3. It shows two bands at 220 and 320 nm. The observed positions of the absorption bands with different intensities indicate the more intense band 220 nm is due to ($\pi \rightarrow \pi^*$) allowed transition which readily attains coplanarity and shoulder merging (loss of fine structure) and also due to chromosphere groups like >C=C groups are in conjugation with an aromatic nucleus (aromatic ring) and the less intense band at 320 nm may be due to ($n \rightarrow \pi^*$) forbidden transition in >C=N, –C=O and –OH groups. The appearance of former band (more intense) can be accounted for ($\pi \rightarrow \pi^*$) transition while the latter band (less intense) may \be due to $n \rightarrow \pi^*$ electronic transition. The shift from the basic value (viz 220 and 320 nm, respectively) may be due to conjugation effect, and presence of Ar-COOH hydroxy group (auxochrome) is responsible for hyperchromic effect, i.e. higher $\in_{max}$ [14] . The $\in_{max}$ value gradually increases in the order PTMF-I < PTMF -II. This increasing order of $\in_{max}$ values may be due to introduction of more and more chromophores and auxochromes (- OH group of Ar-COOH) in the repeat unit of the terpolymer [15]. This observation is in good agreement with the proposed most probable structures of these terpolymer.

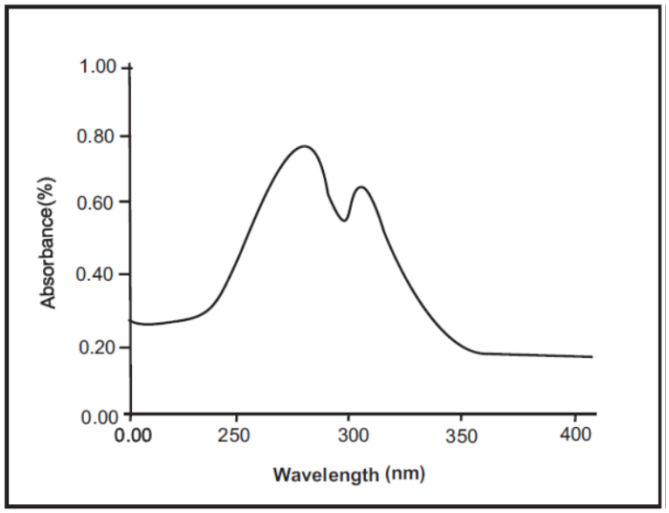

Fig.3. UV-Visible Spectra of PTMF-II Terpolymer Resins

The IR spectra of PTMF-II copolymer is presented in figure 4. The IR spectra revealed this copolymers give rise to nearly similar pattern of spectra. The copolymer spectrum showed a broad band appeared in the range of 3254 cm^{-1} is assigned to the –NH stretching modes. The broad band appeared in the range of 3624.56 cm^{-1} is assigned to the –OH of Ar-COOH in stretching modes. The strong band is at 1884 cm^{-1} is due to the presence of carbonyl group of aromatic ring stretching mode and a strong band at 1527.24 cm^{-1} is attributed to C=N stretching of melamine ring. The 1, 2, 4. 6 tetra substituted aromatic ring ring is confirmed by sharp, medium/weak absorption bands appeared between 1204–886 cm^{-1}. A band appeared at 2852.35 cm^{-1} is due the –CH stretching vibrations of the aromatic ring. The band appeared at 1063 cm–1 is assigned to –C–N (I) stretching vibration. The bands appeared in the region of 2945 cm^{-1} are attributed to $–CH_2$ asymmetric and symmetric vibrations present in the terpolymer. The presence of $–CH_2$ bending vibration in $Ar–CH_2–N$ bridge in the spectrum is confirmed by the absorption band appeared at 1450 cm^{-1}.

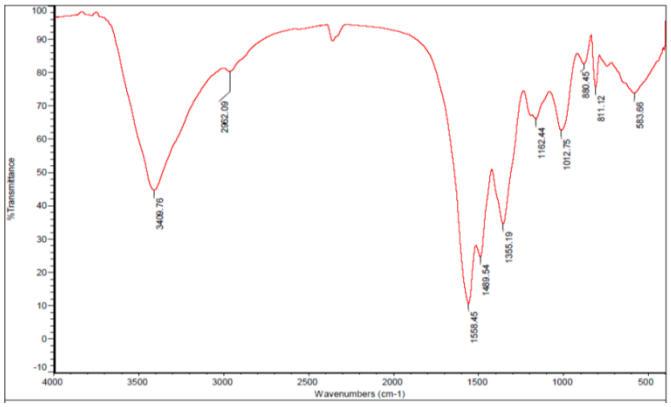

Fig.4. Infra Red Spectra of PTMF-II Terpolymer Resins

^1H NMR spectra of PTMF-II terpolymers show a weak multiple signal (unsaturated pattern) in the region 8.22 to 8.30 (δ) ppm that is due to aromatic protons. Weak signal in the range of appeared in the range at 10.32 to 10.62 (δ) ppm may be due to the proton of CO(OH) in Ar-COOH . The much downfield chemical shift for aromatic carboxyl –OH indicates clearly the intramolecular hydrogen bonding of -OH group. Triplet signal appeared in the region 5.35 (δ) ppm can be assigned to amine proton of – C – NH – C - linkage. Intense signal appeared in the region 3.98 to 4.30 (δ) ppm may be due to protons of methylenic bridges (CH2) of polymer chain.

Thermogravimetric analysis of the terpolymer

The thermal stability of copolymer is evaluated by dynamic thermo-gravimetric analysis in air atmosphere with heating rate of 10^0C min-1. Thermogram of PTMF-II copolymer is shown in Fig. 5. Thermogram of copolymer depicts three steps decomposition after loss of water molecule in the temperature range 40^0C – 800^0C. All decomposition stage depicted in table 2.

Thermo-analytical data

A plot of percentage mass loss versus temperature is shown in the Fig. 5 for a representation of PTMF-II copolymer resin. Sharp-Wentworth and Freeman-Caroll method was adopted to obtain the relative thermal stability of the copolymer. The thermal stability of copolymer, based on the initial decomposition temperature, has also been used here to define their relative thermal stability, neglecting the degree of decomposition.

For calculating activation energy (Ea) thermal decomposition data has been used and then applying above methods. 'Average Ea' by Sharp-Wentworth is nearly double than 'average Ea' calculated by Freeman-Carroll methods. The activation energy calculated by these methods is depicted in Table 2. However the error in activation energies obtained from the Sharp-Wentworth isoconversional method is significant and largely increases as far as conversion increases. On the other hand, it has been considered of interest to analyze the behavior of the process constitute by two competitive reactions that would lead to an apparent dependence between Ea and α

when analyzed by isoconversional method, in spite such dependence is not real [16].

A representative thermal activation energy plot of Sharp-Wentworth (Fig. 8) and Freeman-Carroll (Fig. 6-7) method for the copolymer has been shown. Thermodynamic parameters such as entropy change (ΔS), frequency factor (z), apparent entropy change (S*) calculated on the basis of thermal activation energy (Ea) using equations (3), (4), (5). These values are given in (Table 1).

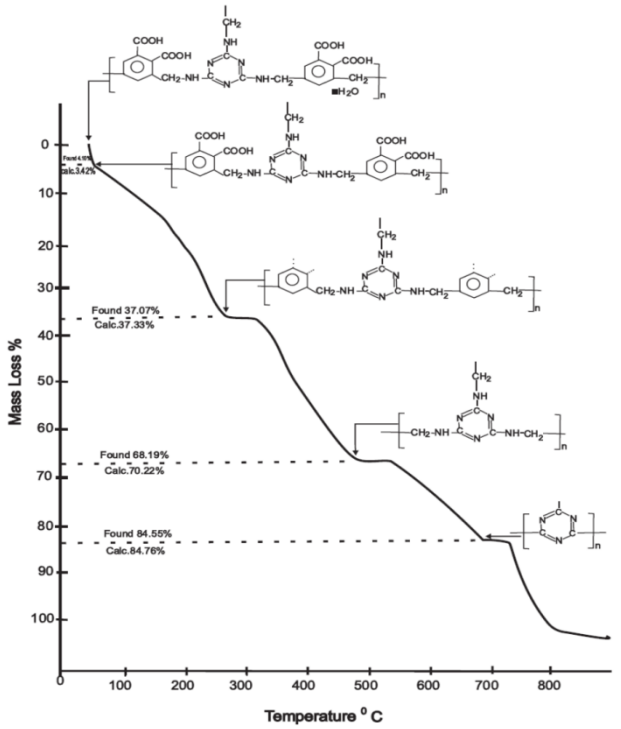

Fig.5. Decomposition Pattern of PTMF-II Copolymer Resin

Entropy Change (ΔS):

$$Intercept = log\frac{kR}{h\phi Ea} + \frac{\Delta S}{2.303R} \quad \text{..... (3)}$$

Where, $k = 1.3806 \times 10^{-16}$ erg.deg^{-1}.mol^{-1},
$R = 1.987$ cal.deg^{-1}.mol^{-1},
$h = 6.625 \times 10^{-27}$ erg.sec,
$\phi = 0.166$,

ΔS = entropy change,
Ea = activation energy from graph.

ii. Frequency Factor (z):

$$B_{2/3} = \frac{log\, z.Ea}{R\phi} \quad \text{..... (4)}$$

$$B_{2/3} = log\, 3 + log[1-3\sqrt{1-\alpha}] - log\, p(x) \quad \text{.....(a)}$$

Where, z = frequency factor,
B = calculated from eq [a],
$log\, p(x)$ = calculated from Doyle table corresponding to activation energy.

iii. Apparent entropy change (S*):

$$S^* = 2.303R\, log\frac{zh}{RT^*} \quad \text{.....(5)}$$

Where, T^* = temp at which half of the compound decomposed.

It may be concluded that decomposition reaction of PTMF-II copolymer can be classed as a 'slow' reaction if the abnormally low value of frequency factor [17, 18]. By using the two methods obtained good straight-line plots. This is expected since the decomposition of copolymer is known not to obey first order kinetic perfectly [19, 20].

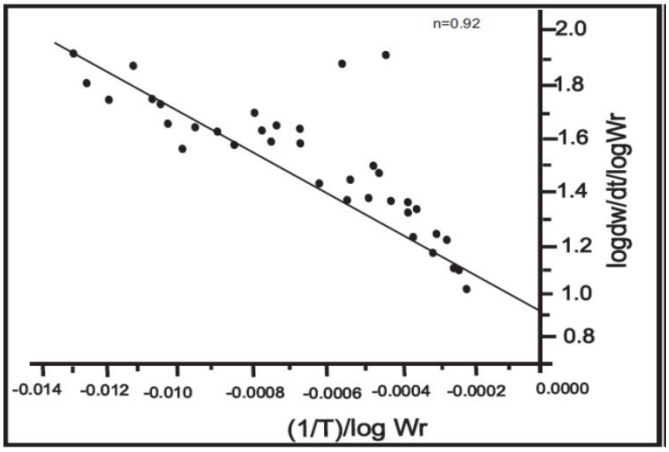

Fig. 6. Freeman-Carroll Plot of PTMF-II Terpolymer.

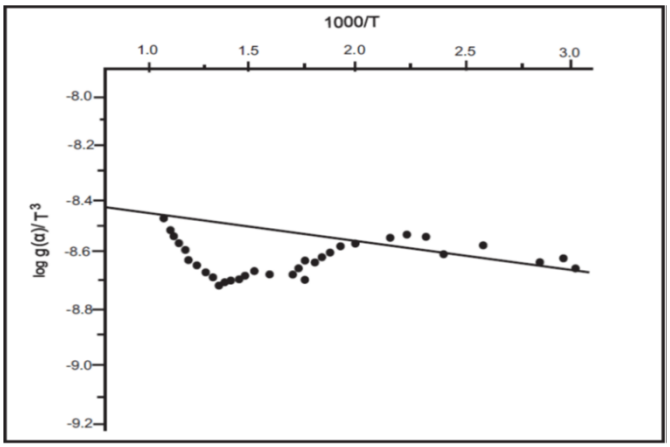

Fig. 7. Thermal Activation Energy Plot of PTMF-II Terpolymer

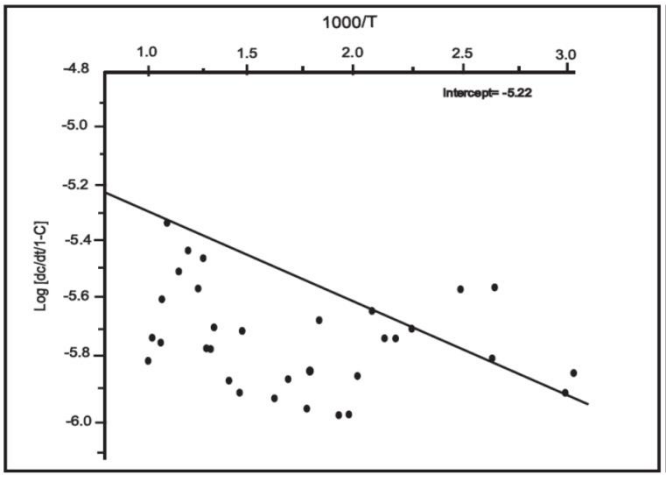

fig.8. Sharp-Wentworth Plot of PTMF-II Terpolymer Resins

Table 1: Thermo gravimetrical Parameters Corresponding to Heating Rate of 10°C/min. of PTMF-II copolymers

Copolymer	Entropy change ΔS(J)	Free energy ΔF (KJ)	Frequency Z (S^{-1})	Apparent entropy (S*)	Order reaction (n)
PTMF-II	-161.37	55.46	732.22	-22.48	0.88

Table 2: Comparison of Activation Energy (Ea) of Degradation at Different Stages by Different Methods of PTMF-II Copolymers

Copolymer	Stage	Temp range	Group loss	Wt. Loss (%)	Activation Energy Ea (KJ)/mol	
					sharp-wentworth	Freeman-Carroll
PTMF-II	1st	40-170	H_2O molecule entrapped	4.10	24.05	22.34
	2nd	170-340	degradation of two –COOH group with another two –COOH group	37.07	26.23	24.75
	3rd	340-560	loss of aromatic ring along with -CH2 groups	68.19	9.02	7.14
	4th	560-800	loss of melamine moiety	84.55	34.45	32.12

IV. CONCLUSION

The Pthalic acid–melamine–formaldehyde (PTMF-II) copolymer was prepared with good yield. By various spectral techniques copolymer have been successfully characterized to propose their plausible structure. The calculated activation energies of the copolymer and its metal complexes are in good agreement with each other and their values are in accordance with their order of thermal stability. Based on the comparative Ea values calculated by SW and FC, the thermal degradation mechanism for both the PTMF-II copolymer was proposed. The copolymer follow nearly a first order kinetics.

V. REFERENCES

[1]. Takaji K., Tomita I., Endo T., Macromolecules, 30 (1997) 7386.

[2]. N. Ayrilmis, "Enhancement of dimensional stability and mechanical properties of light MDF by adding melamine resin impregnated paper waste," International Journal of Adhesion and Adhesives, vol. 33, pp. 45–49, 2012.

[3]. J. Bishopp, "13-Adhesives for aerospace structures," in Handbook of Adhesives and Surface Preparation, S. Ebnesajjad, Ed., pp. 301–344, William Andrew Publishing, Oxford, UK, 2011.

[4]. W. Clad, "Developments and problems in adhesives used for particle board manufacture," International Journal of Adhesion and Adhesives, vol. 3, no. 3, pp. 127–131, 1983.
[5]. Sami Ullah,1 M. A. Bustam,1 M. Nadeem,2 M. Y. Naz,3 W. L. Tan,1 and A. M. Shariff Volume 2014 |Article ID 940502, scientific world journal, Hindawi .
[6]. P.P. Kalbende,1 M. V. Tarase,2 and A.B. Zade, Journal of Chemistry, Volume 2013 ,Article ID 846327
[7]. R. N. Singaru, A. B. Zade, W. B. Gurnule, July 2008 Journal of Applied Polymer Science 109(2):859 - 868
[8]. V.R. Bisen, W. B. Gurnule,December 2014,Emerging Materials Research 3(6):271-281
[9]. Khobragade JV, Ahamed M, Gurnule WB. J Chem Pharma Res 2014; 6(8): 364
[10]. Rahandale S. S., Gurnule W. B., Zade A. B., Ind. J. Chem., 48(A) (2009).
[11]. Rahandale S. S., Gurnule W. B., Zade A. B., E. J. Chem., 6(3) (2009).
[12]. Freeman ES, Caroll BJ. Chem Rev 1958; 62: 394.
[13]. Sharp JB, Wentworth SA. Anal Chem 1969; 41: 2060.
[14]. Dudley H., William, Fleming. I., "Spectroscopic Methods in Organic Chemistry", McGraw Hill Book Co. U.K. (1975)
[15]. Dudly H., Fleming. I. Spectroscopic methods in organic chemistry; Mc-Graw Hill;UK (1975)
[16]. Criado JM, Sanchez-Jimenez PE, Perez-Maqueda LA. J Them Anal Cal 2008; 92: 199.
[17]. Tonbul Y, Yardakoc K. Turk J Chem 2001; 25: 332.
[18]. Zhao H, Wang YZ, Wang DY, Wang B, Wu B, Chen DQ. Polym Degrad Stab 2003; 80: 135.
[19]. Singru RN, Zade AB, Gurnule WB. J App Polym Sci 2008; 109(2): 859.
[20]. J. V. Khobragade, W. B. Gurnule, S. V. Hunge , 2021 JETIR March 2021, Volume 8, Issue 3 (ISSN-2349-5162)

International Virtual Conference on Materials and Nanotechnology
In Association with International Journal of Scientific Research in Science and Technology
Volume 9 | Issue 4 | Print ISSN: 2395-6011 | Online ISSN: 2395-602X (www.ijsrst.com)

Dielectric Behaviour of Amides in Hexane: A Theoretical Study

Sanjay H Bagade*
Department of Physics, Bajaj College of Science, Wardha-442001, Maharashtra, India

ABSTRACT

A system of organic binary mixture containing various polar amides(b) dissolved in nonpolar solvent(a) is studied here to ascertain their dielectric response in the presence of static low frequency electric field. Amides like formamide, acetamide, N-methyl acetamide, N-N-dimethyl acetamide, acetanilide are dissolved in nonpolar solvent Hexane. Dielectric behaviour is studied by computing the static dipole moment μ_s from the knowledge of static relative permittivity ε_{0ab} ,high frequency permittivity $\varepsilon_{\infty ab}$ for different weight fraction of polar solute at 30^0 C. The Debye model for polar liquid molecules has been employed in the present study. The calculated static dipole moment μ_s are compared with μ_b,which has been obtained from conductivity measurements and μ_t which are derived from available bond angle and bond moments. Intramolecular charge distribution is caused due to inductive, mesomeric and electromeric effect, and is responsible for dipole moment μ_t. Good agreement between μ_s, μ_b and μ_t validates the correctness of study to estimate the dielectric response of amides-nonpolar organic binary solutions.

Keywords : Dielectric Properties, Dipole Moment, Polar Amide, Nonpolar Solvents, Molecular Interactions.

I. INTRODUCTION

Study of amides is important as it find wide application in medical, Pharmaceutical, industrial and various biological fields. Proteins and enzymes which are vital to living organisms are basically made up of amide like structures and the stability of protein molecules depends upon its interaction with solvents within body. [1-2] Amides possess large dielectric constant which is the result of its interaction with surrounding and the individual molecular dipole. [2-4] Large dielectric constant of binary organic mixtures indicates its response to static low frequency electric field. [3,5-7,17,22] Information about dielectric properties of binary liquid mixtures is important to ascertain the kinematics of the sample, the molecular processes and interactions involved and to understand its practical applications. [8-16]

The knowledge about static dipole moment μ_s in low frequency electric field provides information about the solute-solvent and solute-solute molecular associations. Dielectric response of organic mixture of amides in nonpolar solvent was investigated on the basis of Kirkwood correlation factor g, where the g values can be derived from dipole moment measurement.[6-8] The dielectric constant of amides dissolved in nonpolar solvents gives significant information about the hydrogen bonding, molecular interactions and dipolar orientation among the unlike molecules in the liquid binary mixtures. [16,18,21] The relaxation behaviour of amides dissolved in nonpolar

solvent at high frequency electric field had already been studied using conductivity measurement technique and the associated dipole moment μ_b have been reported.[7,9,11,16-18] Static relative permittivity ε_{0ab} and high frequency permittivity $\varepsilon_{\infty ab}$ of several amides dissolved in various nonpolar solvent were already measured for different mole fractions.[16,21] However studies related to the dielectric behaviour of several primary, secondary, tertiary amides dissolved in nonpolar solvents in static low frequency electric field are very few. The bond angle and value of dipole moment μ_t based on bond angle had been reported before. [16-20]

In the present paper, the dielectric response of certain amides dissolved in nonpolar solvent Hexane [$CH_3(CH_2)_4CH_3$], has been studied at static low frequency electric field by making use of static relative permittivity ε_{0ab} and high frequency permittivity $\varepsilon_{\infty ab}$ for several weight fraction w_b of solute at temperature 30^0 C. Hexane is taken in the study as it is an important solvent readily miscible in water and has wide applications. The static dipole moment μ_s under low frequency electric field was estimated in terms of slope $p_1$of graph between static experimental parameter X_{ab} against weight fraction $w_b$within the framework of Debye model for polar-nonpolar liquid mixture. The purpose of above study is to theoretically investigate dielectric response of some amides dissolved in nonpolar solvent Hexane, on the basis of the calculated value of μ_s,based on Debye theory. μ_s values are compared with μ_t and μ_b to understand the effect of electric field frequency on dipole moment of molecules for validity of present work.

II. THEORY

The static dipole moment μ_s of polar solute(a) dissolved in nonpolar solvent(b) under low frequency electric field at T Kelvin according to Debye [16,19,20] is

$$\frac{\varepsilon_{0ab}-1}{\varepsilon_{0ab}+2}-\frac{\varepsilon_{\infty ab}-1}{\varepsilon_{\infty ab}+2}=\frac{\varepsilon_{0a}-1}{\varepsilon_{0a}+2}-\frac{\varepsilon_{\infty a}-1}{\varepsilon_{\infty a}+2}+\frac{N{\mu_s}^2 C_b}{9\varepsilon_0 K_B T} \quad (1)$$

Where ε_0 =absolute permittivity of free space = $8.854\text{x}10^{-12}$ Fm^{-1}, all other symbols carry their usual meanings and SI units are used. The molar concentration C_b can be expressed in terms of solution density ρ_{ab} and weight fraction W_b of polar solute as

$$C_b = \frac{\rho_{ab} W_b}{M_b} \quad (2)$$

and the solution density ρ_{ab} as in [16]

$$\rho_{ab} = \rho_a(1-\Upsilon W_b)^{-1} \quad (3)$$

Weight fraction W_a and W_b of the solvent and solute are

$W_a = \frac{W_a}{W_a+W_b}$, and $W_b = \frac{W_b}{W_a+W_b}$

Now eq. (1) reduces to

$$\frac{\varepsilon_{0ab}-\varepsilon_{\infty ab}}{(\varepsilon_{0ab}+2)(\varepsilon_{\infty ab}+2)} = \frac{\varepsilon_{0a}-\varepsilon_{\infty a}}{(\varepsilon_{0a}+2)(\varepsilon_{\infty a}+2)} + \frac{N\rho_a{\mu_s}^2}{27\varepsilon_0 M_b K_B T} W_b(1-\Upsilon W_b)^{-1}$$

put $\frac{\varepsilon_{0ab}-\varepsilon_{\infty ab}}{(\varepsilon_{0ab}+2)(\varepsilon_{\infty ab}+2)} = X_{ab}$, the static experimental parameter

$$X_{ab} = X_a + \frac{N\rho_a{\mu_s}^2}{27\varepsilon_0 M_b K_B T} W_b + \frac{N\rho_a{\mu_s}^2}{27\varepsilon_0 M_b K_B T} \Upsilon {W_b}^2 + - - - - \quad (4)$$

Eq. (4) is polynomial equation of X_{ab} with respect to W_b and can be expressed as

$$X_{ab} = P_0 + P_1 W_b + P_2 {W_b}^2 + - - - - - \quad (5)$$

On comparison of equation (4) and (5), and equating the coefficient of the first power of W_b,we get static dipole moment μ_s as

$$\mu_s = \left[\frac{27\varepsilon_0 M_b K_B T}{N\rho_a} P_1\right]^{\frac{1}{2}} \quad (6)$$

Where P_1 is slope of $X_{ab} - W_b$ curve for very small W_b as shown in figure1. Higher powers of W_b can be neglected as solute concentration is very small. Here M_b is solute molecular weight, K_B is the Boltzmann Constant ($1.38\text{x}10^{-23}Jk^{-1}$), T is the temperature, N is Avogadro's number and ρ_a the density of nonpolar solvent.

Table1. Static relative permittivity ε_{0ab} , high frequency relative permittivity $\varepsilon_{\infty ab}$, static experimental parameter X_{ab} of certain amides dissolved in Hexane at different weight fractions of solute.

System	Weight fraction W_b of solute	Static relative permittivity ε_{0ab}	High frequency relative permittivity $\varepsilon_{\infty ab}$	Static experimental parameter X_{ab}
Formamide in Hexane	0.0084	2.486	1.913	0.0264
	0.0126	2.752	2.015	0.0358
	0.0168	2.932	2.016	0.0425
	0.021	3.241	2.128	0.0504
	0.0256	3.455	2.135	0.0574
Acetamide in Hexane	0.017	2.662	1.818	0.0410
	0.0234	2.886	1.822	0.0472
	0.0286	3.118	1.949	0.0524
	0.0342	3.262	2.027	0.0574
	0.0384	3.389	2.031	0.0621
N-Methyl Acetamide in Hexane	0.00843	2.541	2.217	0.0103
	0.0103	2.576	2.216	0.0137
	0.0178	2.916	2.216	0.0296
	0.02061	3.152	2.215	0.0393
	0.0347	4.142	2.211	0.072
N-N-Dimethyl Acetamide in Hexane	0.0164	2.504	1.924	0.0272
	0.0345	2.956	1.996	0.0443
	0.0514	3.365	2.006	0.0602
	0.0672	3.805	2.008	0.0744
	0.0751	4.055	2.011	0.0821
Acetanilide in Hexane	0.0062	2.405	2.007	0.0180
	0.0188	2.682	2.115	0.0266
	0.02684	2.777	2.119	0.0315
	0.0324	2.828	2.122	0.0354
	0.0356	2.906	2.124	0.0386

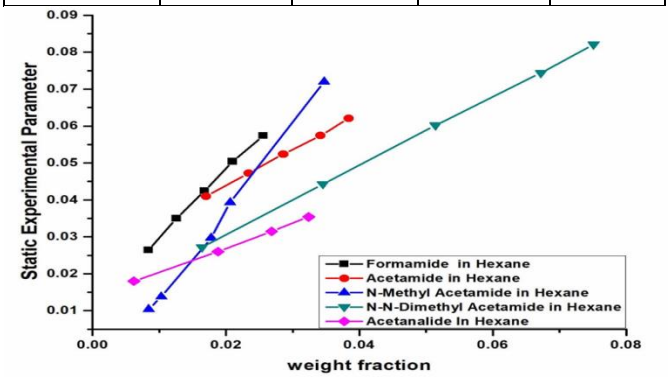

Figure 1. Graph between the static experimental parameter X_{ab} against weight fraction W_b for different amides dissolved in nonpolar solvent Hexane.

Table2. Coefficient P_1 from $X_{ab} - W_b$ curve, reported dipole moment μ_b from conductivity measurement, theoretical dipole moment μ_t from bond angle, calculated static dipole moment μ_s for some amides in nonpolar solvent Hexane.

System	coefficient P_1 from $X_{ab} - W_b$ curve	Reported dipole moment μ_b x10^{30} C-m	Theoretical dipole moment from bond angle μ_t x10^{30} C-m	Calculated static dipole moment μ_s x10^{30} C-m
Formamide in Hexane	1.3564	13.65	12.56	12.85
Acetamide in Hexane	1.1840	12.10	10.70	11.24
N-Methyl Acetamide in Hexane	1.8412	16.82	18.55	17.62
N-N-Dimethyl Acetamide in Hexane	1.0215	12.44	13.02	12.56
Acetanilide in Hexane	0.5642	11.09	10.89	12.15

III. RESULT AND DISCUSSION

Table .1 gives the values of ε_{0ab} and $\varepsilon_{\infty ab}$ for different weight fraction W_b of the solute along with static experimental parameters X_{ab} . The

concentration of polar solute in solute-solvent binary mixture is taken extremely low as the Debye theory for polar molecules holds good at lower concentrations only. The plotted graph between static experimental parameter X_{ab} against W_b of the solute are nearly parabolic in nature as shown in figure.1. Static dipole moment μ_s are directly proportional to square root of slope P_1 of $X_{ab} - W_b$ curves. Higher values of μ_s for formamide and N-Methyl acetamide indicates solute-solute(dimer) molecular association through hydrogen bonding in Hexane, with increasing concentration. Higher values of μ_s for these two compounds can also be expected due to higher values of slope P_1 of $X_{ab} - W_b$ curves for them. The hydrogen bonding causes alignment of polar amide molecules to increase the polarization and hence increase the dielectric properties and dipole moment.

The almost similar nature of curves in figure1., indicate similar magnitude of slope for the graphs, which indicates a similar polarity for solute molecules. A good agreement is observed between the values of calculated static dipole moment μ_s ,the reported dipole moment μ_b from conductivity measurement technique and μ_t the dipole moment from bond angle. Small discrepancies in value of μ_s, μ_b, μ_t may be due to the effect of frequency of applied electric field.

The primary and secondary amides show solute-solute (dimer) interaction through hydrogen bonding in nonpolar solvent Hexane. Intramolecular charge distribution is introduced due to dipole adjacent to polar group or formation of π bonds in molecules. This intramolecular charge distribution is caused due to inductive, mesomeric and electromeric effect, and is responsible for bond moments or dipole moment.

IV. CONCLUSION

The theoretical formulations on the basis of Debye theory of polar molecules explains the polarisation and dipole moments of dilute solution of polar-nonpolar organic mixture, of certain amides dissolved in Hexane, which is observed from nearly correct value of μ_s. Inductive, mesomeric and electromeric effects are responsible to cause a change in bond angle and impart a bond moment or dipole moment to above investigated polar-nonpolar binary mixtures. This study of dielectric behaviour of amides and form amides based on Debye theory of polar –nonpolar liquid mixture can be used in manufacture of batteries and super capacitors.

V. REFERENCES

[1]. A.E. Garcia, K.Y. Sanbonmatsu, Proc Natl Acad. Sci. U S A,2002, 99(5),2782–2787.

[2]. T.Z. Lwin, R. Luo, Protein science: a publication of the Protein Society,2006, 15(11), 2642–2655.

[3]. I.N. Daniels, Z. Wang, B.B. Laird, J. Phys. Chem. C,2017, 121(2), 1025–1031.

[4]. G. Chae, K. Kim, S. Cho, B. Walker, J. Seo, Journal of the Korean Physical Society, 2016, 68, 889–895.

[5]. R. Behrends, K. Fuchs, U. Kaatze, J. Chem. Phys.,2006,124, 144512.

[6]. J. Brebels, J.V. Manca, L. Lutsen, D. Vanderzande, W. Maes, Mater. Chem. A, 2017, 5, 24037-24050.

[7]. P. Senthilkumar, T. Ganesh, K. Vinoth, M. Sylvester, A. Karunakaran, P. Hudge, and A. Kumbharkhane, Journal of Physics Communication,2018, 2(3),035042.

[8]. R. Bouteloup, D. Mathieu, Phys. Chem. Chem. Phys.,2019, 21, 11043-11057.

[9]. A. Gomma, A. H. Fawzi, AASCIT Communications ,2015, 2(4), 93-98.

[10]. Y. Yu, A. Jiang, W. Lee, Nanoscale Res Lett,2016, 11, 488.

[11]. Attila Göllei, Progress and Developments in Ionic Liquids,2017, Scott Handy, Intech Open,

[12]. J. Terrones, P. Kiley, J. Elliott, Sci. Rep.,2016, 6, 27406.

[13]. X. Liu, B. Xie, C. Duan, Y. Cao, J. Mater. Chem. A,2018, 6, 395-403.
[14]. E. Thoms, P. Sippel, D. Reuter, Sci. Rep.,2017, 7, 7463.
[15]. M. Fisch, C. Braganza, L. Chien, R. Petschek, Journal of Advanced Dielectrics, 2014, 4(3), 1450022.
[16]. M. Malathi, R. Sabesan, S. Krishnan, S. Journal of Molecular Liquids,2004, 109(1),11-18.
[17]. S. Sahoo, 2019 3rd International Conference on Trends in Electronics and Informatics (ICOEI),2019.
[18]. A. Deshmukh, R. Shinde, S. Ingole, M. Lokhande, A. Sarode, Indian Journal of Pure and Applied Physics, 2018, 56, 346-352.
[19]. N. Hill, A. Price, H. Davis, Dielectric Properties and Molecular Behaviour, Van Nostrand Co. London,1969.
[20]. R.C. Weast, Handbook of chemistry and physics, CRC Press, Princeton University, Princeton,1988.
[21]. M.Malathi, P. Mohan Kumar, Der Pharma Chemica,2012, 4 (1),76-84.
[22]. C.J. Bottcher, Theory of Electric Polarization Vol-1, Elsevier Amsterdam,1973.

International Virtual Conference on Materials and Nanotechnology
In Association with International Journal of Scientific Research in Science and Technology
Volume 9 | Issue 4 | Print ISSN: 2395-6011 | Online ISSN: 2395-602X (www.ijsrst.com)

Photo catalytic Degradation of Methylene Blue Using Mixed Metal Nano Ferrite

S. B. Narde
Dhote Bandhu Science College, Gondia, Maharashtra, India

ABSTRACT

The present work demonstrates the photo degradation of methylene blue dye solution using cubic spinel mixed metal ferrite NixZn1-xFe2O4 (x= 0.4) as photocatalyst. The ferrite was synthesized by sol-gel auto combustion method at pH 7. The ferrite sample was characterized using XRD, FTIR, SEM- EDX and TEM techniques. The photo catalytic study was carried out in the presence of short wave UV light. The effect of operating parameters such as initial pH, amount of catalyst, initial dye concentration on the rate of dye degradation was studied. The photocatalyst showed excellent photocatalytic activity against methylene blue dye (96%) for 120 min contact time. The stability of the catalyst was checked by performing repetitive experiments. The pseudo first order kinetics for photo degradation was observed using Langmuir-Hinshelwood model.

Keywords : Methylene blue, Ni-Zn Nano Ferrite, Photo Catalytic Degradation.

I. INTRODUCTION

Colour effluent containing synthetic dyes from various industries such as textile, leather, paint and printing industries is one of the major pollutants for ground and surface water [1]. Up to 20% dyes are lost across the world during dyeing process and contaminate water resources and create serious environmental problems. Methylene blue is a basic cationic thiazine dye extensively used in the textile industry. Its exposure may cause headache, vomiting, confusion, shortness of breath, and high blood pressure, etc [2]. Thus, colour effluents should be treated at the source before their discharge into water resources. Wide range of conventional methods is available for removal of dyes but they need further treatment [3]. Recently, semiconductor-assisted photo-catalysis has come up as one of the favourable method over the traditional wastewater treatment. It has attracted the researchers due to its ability to convert toxic waste into nontoxic products [4]. The different metal oxides like TiO_2, ZnO are commonly used semiconductors. The present study demonstrates photo catalytic efficiency of the novel ferrite material viz. Nickel zinc ferrite Nanoparticles having formula $Ni_{0.6}Zn_{0.4}Fe_2O_4$ synthesized by sol gel auto combustion method against methylene blue dye [5].

II. METHODS AND MATERIAL

Materials: AR Grade Iron (III) nitrate nonahydrate $Fe(NO_3)_3.9H_2O$, Nickel (II) nitrate hexahydrate $Ni(NO_3)_2.6H_2O$, Zinc (II) nitrate hexahydrate $Zn(NO_3)_2.6H_2O$, citric acid $C_6H_8O_7$ and liquor

ammonia, methylene blue were purchased from SD fine-chem limited and used as received.

Synthesis: Nickel zinc ferrite Nanoparticles having formula $Ni_{0.6}Zn_{0.4}Fe_2O_4$ were synthesized by sol gel auto-combustion method using nitrate precursors and citric acid (molar ratio 1:1) at pH = 7 and sample was annealed at 800°C in a muffle furnace for 2 hrs (Fig. 1,2).

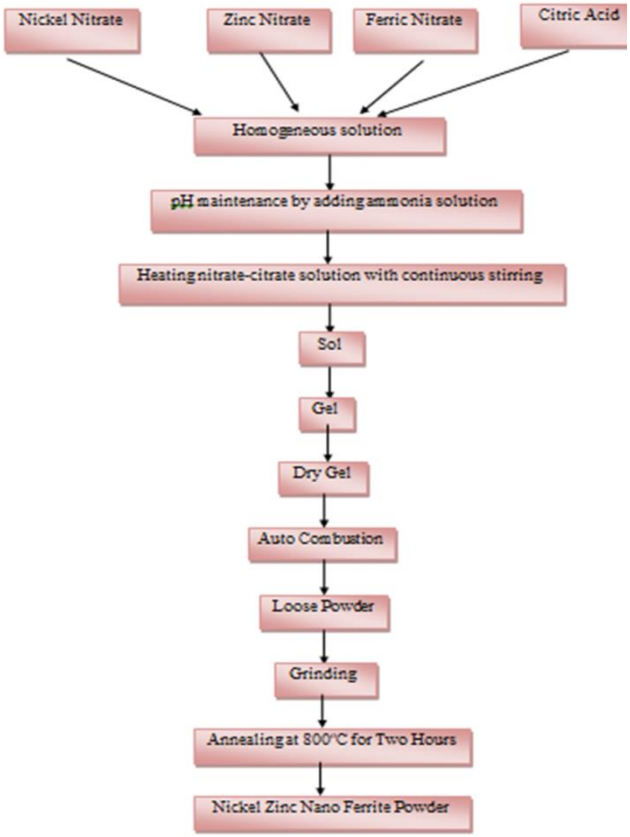

Fig. 1: Flow chart for the synthesis of Ni-Zn Nano ferrites

Fig.2: Synthesis of Ni-Zn Nano ferrites by Auto combustion method

Characterization Techniques: The X-ray diffraction studies of ferrite was performed using Bruker AXS, D8 Advance spectrophotometer with Cu-Kα radiation (λ=1.5418 Å) in a wide range of Bragg's angle (20-80°C) at room temperature. An infrared spectrum of the powder sample was recorded using Fourier Transform Infra-Red Spectrophotometer (FTIR Nicolet, Avatar 370 model) by the KBr pellet method. The microstructure of the powdered sample was investigated using Scanning Electron Microscope (JEOL Model JSM-6390LV). Elemental analysis was studied by using Energy Dispersive Spectrometer (JEOL Model JED–2300). TEM studies of the ferrite were performed using Transmission Electron Microscope JEOL Model JSM - 6390LV.

Photocatalytic Experiment: Photo degradation efficiency of zinc substituted nickel ferrite for methylene blue was investigated in the presence of short wavelength UV light (254 nm). The series experiments were performed for 100ml dye solution for 120 min contact time for all tests under different operational parameters such as initial pH, amount of catalyst, initial dye concentration and reuse of catalyst. 0.1N HCl and 0.1N NaOH were used for pH adjustment of dye solution. Aliquots were collected from the dye solution at regular time interval of 30 min, centrifuged for 5min and supernatants were used to record the absorption spectra using Shimadzu UV1800 spectrophotometer in the wavelength range 200-800 nm. The percentage degradation of dye from aqueous solution was determined by the formula:

Percentage degradation= $\{(A_0 - A_t) \div A_0\} \times 100$

where, A_0 is the initial absorbance of the dye solution, A_t is the absorbance at time interval 't'.

The pHpzc value of ferrite was determined by salt addition method [6]. It was found at pH=2.

III. RESULTS AND DISCUSSION

Characterization of ferrite: Single phase cubic spinel structure of ferrite sample is confirmed by XRD

spectrum shown in the Fig.3. It is matched with JCPDS standard powder diffraction card No. 52-0278 having space group Fd3m (227). The average crystallite size of the ferrite samples was found to be 24.03 nm by applying Debye Scherer's formula for most intense peak (311) at 2θ value of 35.51° [7].

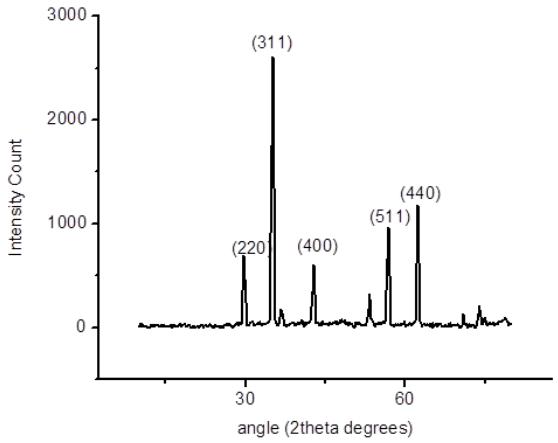

Fig. 3:- XRD spectrum of ferrite sample

Spinel structure of synthesized ferrite sample is supported by FT-IR spectrum of the ferrite sample shown in Fig.4. The intense peak at 566.61 cm^{-1} indicates intrinsic Fe-O vibration of tetrahedral Fe^{3+} and the peak near 400 cm^{-1} to that of octahedral Fe^{2+} sites [8].

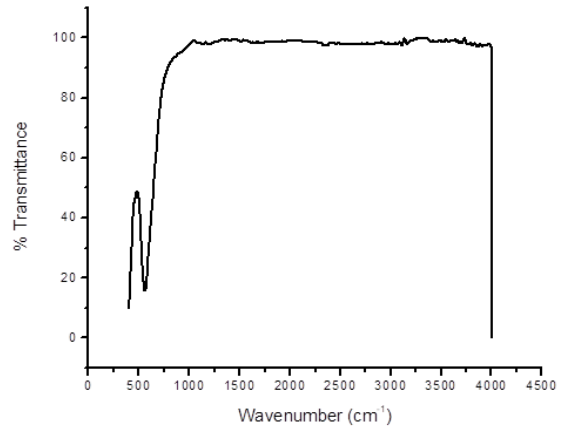

Fig.4:- FTIR spectrum of ferrite sample

SEM image and EDX pattern of ferrite sample are shown in Fig.5.a-b, respectively. SEM micrograms show formation of agglomerated well defined nanoparticles with irregular morphology. The elemental composition of the sample was analyzed by energy dispersive X-ray spectroscopy (EDX) technique showing purity of sample and presence of Ni, Zn, Fe and O as major elements.

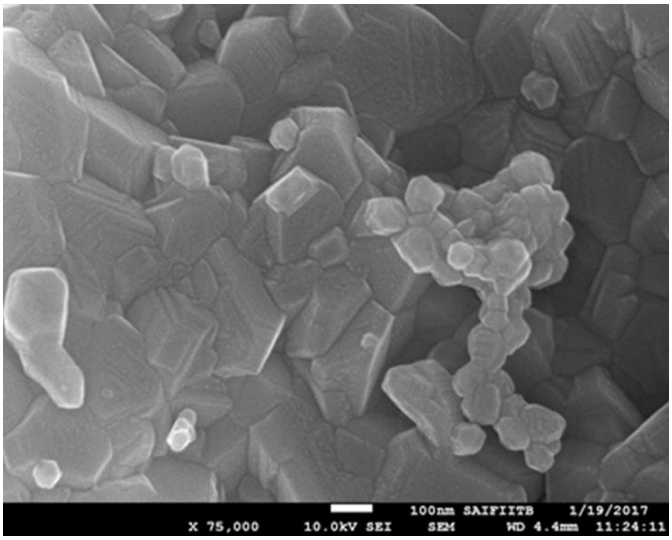

Fig. 5a:- FE-SEM image of ferrite system

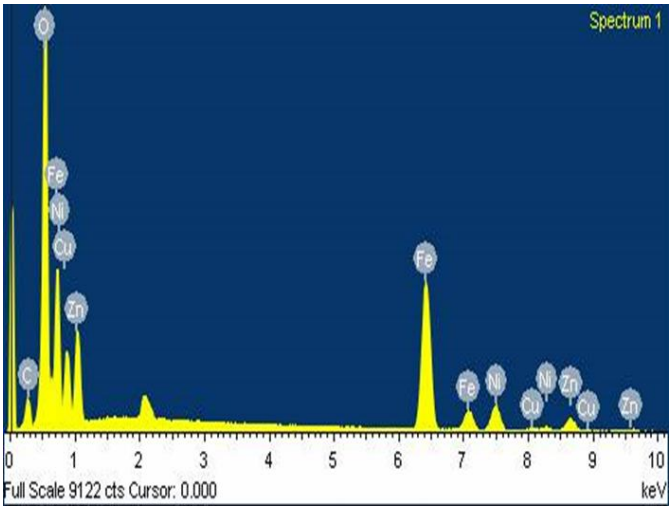

Fig. 5b:- EDX pattern of ferrite system

Fig. 6a-b show the TEM images of ferrite sample. Tem studies reveal that particles are in nano-meter scale and are mostly of elongated spherical shape with a narrow size distribution and agglomeration. The results obtained are in good agreement with the size calculated from peak broadening in X-ray diffractogram. Also, the selected area electron diffraction pattern (SAED) consists of concentric rings with bright spots over the rings indicating polycrystalline nature of the sample. The rings are

consistent with the cubic spinel structure with an intense ring pattern from (hkl) plane [9].

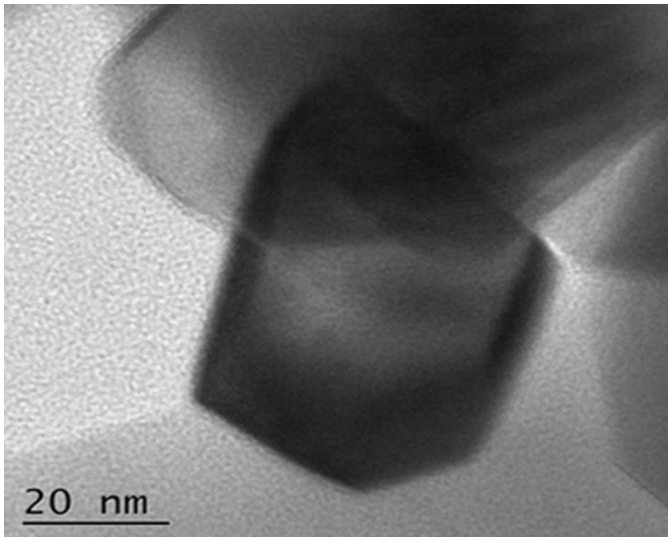

Fig.6a:- TEM image of ferrite system

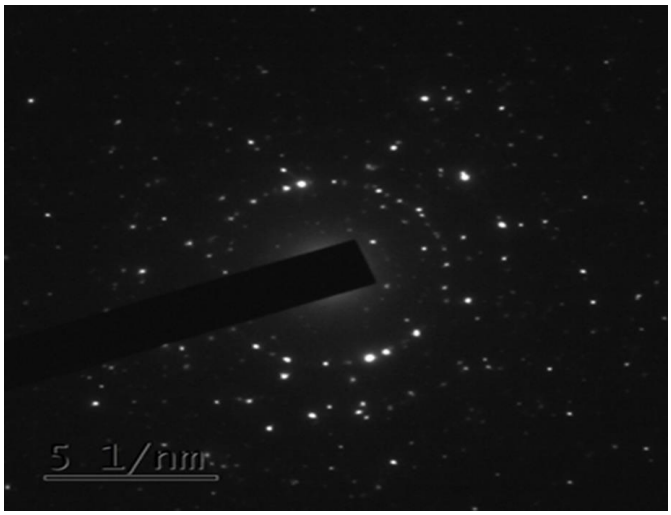

Fig.6b:- SAED pattern of ferrite system

Photo degradation of methylene blue: Several parameters affecting photo catalysis such as initial pH of dye solution, amount of catalyst, initial dye concentration were studied. Further, the possibility for reuse of catalyst was tested.

Effect of pH: The influence of pH on photo catalytic degradation of methylene blue assisted by synthesized ferrite in aqueous solution over the pH range 2-10 was studied in presence of short wave UV light for 100 ml dye solution. Fig. 7a-b show the influence of initial solution pH on photo degradation of MB using ferrite $Ni_{0.6}Zn_{0.4}Fe_2O_4$. Percentage degradation and pseudo first order kinetic parameter of MB dye w. r. t. pH are presented in Table 1. The maximum photocatalytic activity onto ferrite was observed at pH = 2 and decreases gradually up to pH = 8 and further increase is observed for pH = 9 and 10. The results obtained are in accordance with the pHpzc value of the ferrite (pH = 2).

Generally, the effect of pH on organic degradation assisted by the semiconductor oxides has been related to the establishment of acid-base equilibrium governing the surface chemistry of metal oxides in water. It can be explained in terms of electrostatic interaction between the catalyst surface and the target substrate. The results revealed that the photo degradation efficiency decreases with the increase in pH. At low pH value (pH = 2) the photo degradation efficiency reached to 92.54% and it reaches to 78.17% at pH = 4 and then falls rapidly at higher pH values. This is because the methylene blue is negatively charged in acidic medium, whereas above pH = 2, the charge on ferrite changes to negative charge. Consequently, the photo catalytic activity decreases due to the increase of the electrostatic repulsion between ferrite and anionic dye gradually. In addition, the increase of pH may increase electron-hole recombination rate and thus decrease the photo catalytic activity [10, 11].

The degradation kinetics of MB dye in aqueous solution was studied by Langmuir-Hinshelwood (L-H) model [12]. Accordingly, the apparent rate constant of a pseudo first order reaction is expressed as

$$\ln \frac{Ao}{At} = kapp \times t$$

where, A_o is initial absorbance and A_t is absorbance at time t.

The reaction rate constants (K_{app}) at different pH were determined from the slope of the linearly fitted curves by means of linear regression Table 1. All the plots show a linear relationship with good correlation coefficient ($R^2 > 0.9$), indicating pseudo-first order kinetic model is followed by ferrite for MB degradation under UV light. Also, the results obtained

are reliable with highest k_{app}, $7.1x10^{-3}min^{-1}$ with R^2 value 0.90439 calculated for pH 2 of dye solution (Fig.8).

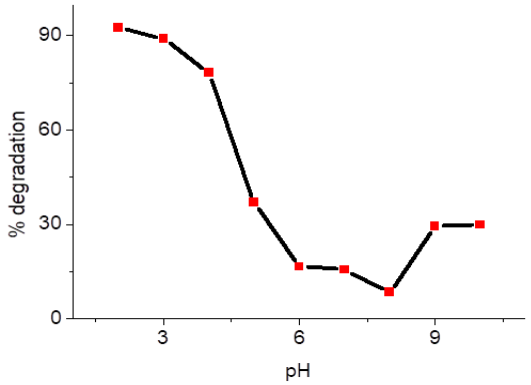

Fig.7a: Variation in % degradation of MB solution w. r. t. pH

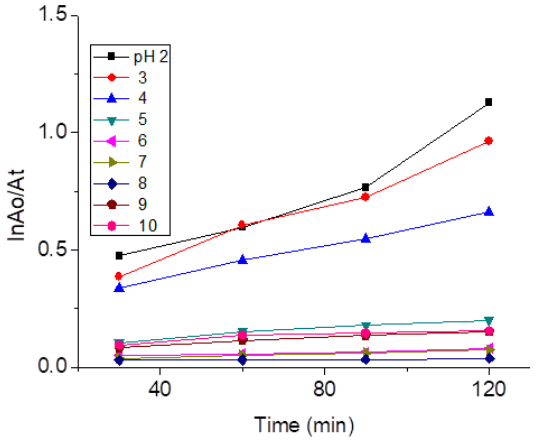

Fig.7b: Degradation kinetics of MB solution w. r. t. pH

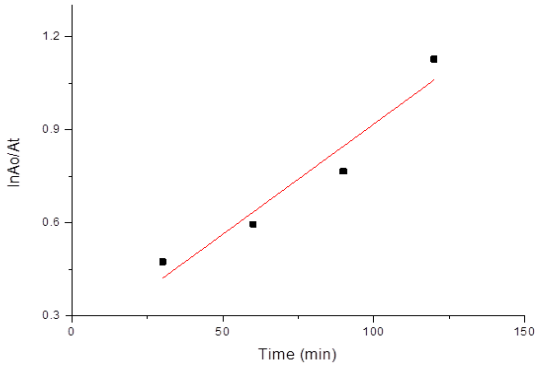

Fig. 8: Linear graph of degradation kinetics of MB solution at pH=2

Table 1: Percentage degradation and pseudo first order kinetic parameter of MB dye w. r. t. pH

Sr. No.	pH	% Degradation	$K_{app}(min^{-1})$	R^2
1.	2	92.54	7.1×10^{-3}	0.90439
2.	3	89.09	6.18×10^{-3}	0.97986
3.	4	78.17	3.56×10^{-3}	0.99604
4.	5	36.90	1.04×10^{-3}	0.94979
5.	6	16.56	3.14×10^{-4}	0.88212
6.	7	15.60	3.92×10^{-4}	0.99068
7.	8	8.37	9.43×10^{-5}	0.95203
8	9	29.46	7.77×10^{-4}	0.96817
9.	10	29.89	6.23×10^{-4}	0.78707

Effect of photo catalyst loading: The effect of photo catalyst loading was investigated for the ferrite in the range of 0.05-0.3 g for 100 mL of 10 mgL^{-1} dye solution at pH = 3 with 2 hrs contact time for all experiments. The removal of methylene blue at different doses is shown in Fig.9a-b. It was found that with increase in catalyst doses the removal percentage of dye increases. At equilibrium, the percentage of dye removal was found to increase from 26.33% to 82.03% for $Ni_{0.4}Zn_{0.6}Fe_2O_4$ with increase of catalyst doses from 0.05g to 0.3g respectively. This is due to increase in active sites at the catalyst surface with increasing catalyst dosage [13].

At equilibrium, the percentage of dye removal was found to increase with increase in catalyst doses from 64.85% (0.05g) to 97.15% (0.3g). The result is due to increase of sorption active sites at the catalyst surface. Further, it is observed that for increase in catalyst doses from 0.15g to 0.3g, the degradation rate increases minutely (from 95.15% to 97.15). The results are shown in Table 2. Hence, 0.15g catalyst

dose was used for further study. The above results are also verified by pseudo-first order degradation kinetics of MB solution w. r. t. ferrite concentration having good correlation coefficient (R^2 >0.9) and increase in reaction rate constants k_{app} with increased ferrite concentration is observed (Fig.10).

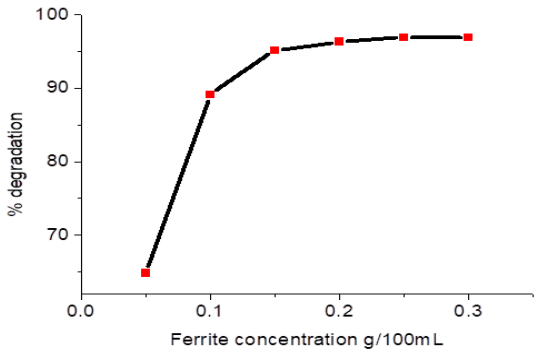

Fig.9a: Variation in % degradation of MB solution w.r.t. ferrite concentration

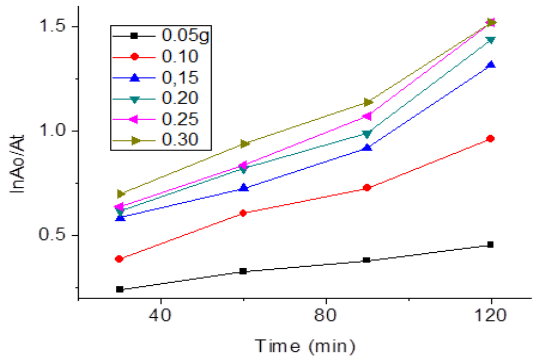

Fig.9b: Degradation kinetics of MB solution w. r. t. ferrite concentration

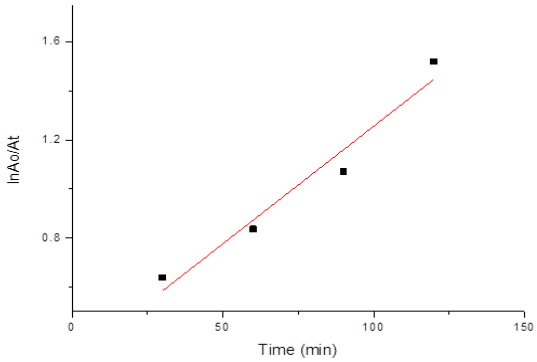

Fig. 10: Linear graph of degradation kinetics of MB solution
w. r. t. ferrite concentration

Table 2: Percentage degradation and pseudo first order kinetic parameter of MB dye w. r. t. ferrite concentration

Sr. No.	Ferrite Conc. (g/100mL)	% Degradation	K_{app} (min^{-1})	R^2
1.	0.05	64.85	1.39×10^{-4}	0.98923
2.	0.10	89.09	5.095×10^{-4}	0.97986
3.	0.15	95.15	1.4×10^{-3}	0.91223
4.	0.20	96.27	1.51×10^{-4}	0.91636
5.	0.25	96.89	1.37×10^{-4}	0.94111
6.	0.30	96.89	9.046×10^{-4}	0.96937

Effect of initial dye concentration: The percentage of photo degradation of methylene blue as a function of initial dye concentration was examined for 100 mL dye solution at pH 3 using 0.15 g ferrite with 10 mgL^{-1} to 50 mgL^{-1} dye solution with 2 hrs contact time for all experiments (Fig.11a-b). Percentage of dye removal was found to decrease from 95.15% (10 mg/L) to 61.80% (50 mg/L). The decrease in removal percentage of dye with increasing dye concentration is attributed to the shielding effect of dye at high concentration that hinders the penetration of solar light to the dye molecules deposited over the catalyst surface [14]. The same results are revealed by pseudo-first order degradation kinetics of MB solution w. r. t. dye concentration, correlation coefficient (R^2 > 0.9), (Fig.12). Further, decrease in reaction rate constant k_{app} is observed with increased dye concentration (Table 3).

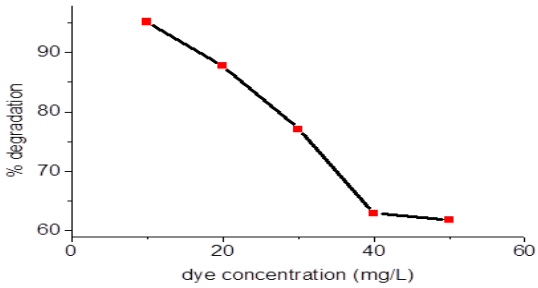

Fig.11a: Variation in % degradation of MB solution w.r.t. dye concentration

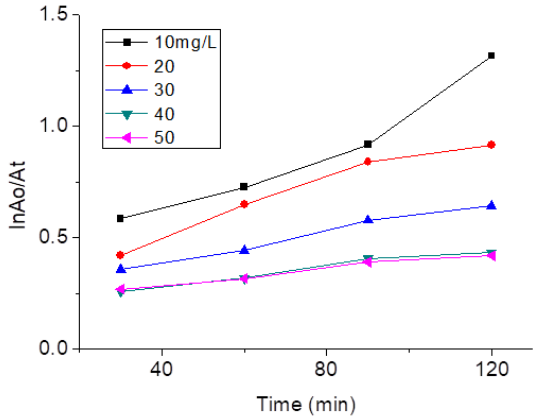

Fig.11b: Degradation kinetics of MB solution w.r.t. dye concentration

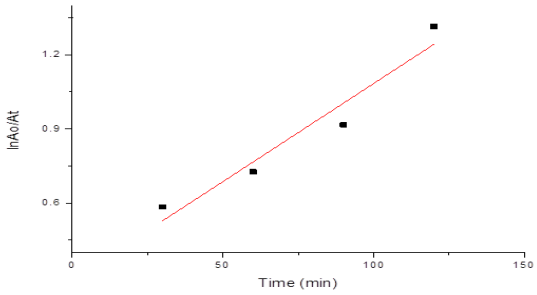

Fig. 12: Linear graph of degradation kinetics of MB solution
for10 mgL^{-1} dye solution

Table 6.20: Percentage degradation and pseudo first order kinetic parameter of MB dye

Sr. No.	Dye Conc. (mg/L)	% Degradation	K_{app} (min^{-1})	R^2
1.	10	95.15	1.40 x 10^{-4}	0.91223
2.	20	87.79	8.35 x 10^{-4}	0.93585
3.	30	77.14	3.09 x 10^{-4}	0.97415
4.	40	62.97	2.96 x 10^{-4}	0.93922
5.	50	61.80	2.05 x 10^{-4}	0.95998

Reuse of photocatalyst: To make the photocatalytic process economical, the stability of photocatalyst was checked by performing the repetitive photo degradation of MB during six consecutive cycles with the previously used photocatalyst. Recycling experiments were carried out using 0.15g/100mL $Ni_{0.4}Zn_{0.6}Fe_2O_4$ for 10mg L^{-1} dye concentration at pH 2. The efficiency of the catalyst was observed to decrease from 95.15% to 50.53% after six cycles. Moreover, it could be used for third time with 69.01% efficiency (Fig. 13).

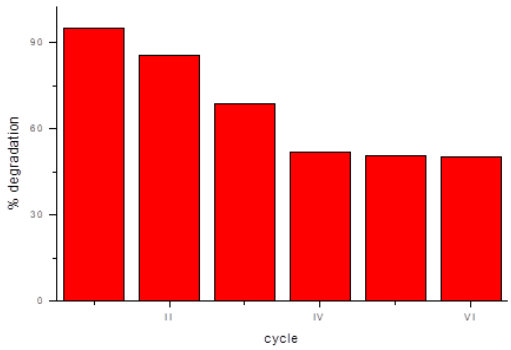

Fig. 13: Recyclability of $Ni_{0.4}Zn_{0.6}Fe_2O_4$ catalyst for degradation of MB

IV. CONCLUSION

Zinc substituted nickel ferrite Ni0.6Zn0.4Fe2O4 nanoparticles have been synthesized successfully by sol gel auto combustion method. The cubic spinel structure of the ferrite nanoparticles was confirmed by XRD, FTIR, SEM-EDX and TEM spectroscopic techniques. The ferrite nanoparticles were successfully employed for photo catalytic degradation of methylene blue dye under various operational conditions by maximum photo catalytic activity of spinel ferrite was observed for 0.3g ferrite for 100 mL dye solution at pH = 2 for 2 hrs contact time. Further, the recycling experiments demonstrated the reuse of photocatalyst which explains the stability of catalyst and hence cost effectiveness of the process. In future, the work can be extended to synthesize variety of metal oxides and more eco-friendly methods can be generated to get fine nanoparticles that can be used for removal of other synthetic dyes and unwanted pollutants present in industrial effluents. So, the process will be helpful to prevent environmental pollution, especially water pollution.

V. REFERENCES

[1]. Yamjala, K., Nainar, M. and Ramisetti, N., 2015, Food Chemistry, 192, 813-824.

[2]. Mathew S., Linhartova L., Raghuraman G., 2006, Anaesthesia, 61, 580-583

[3]. Khan M. Reza, Asw Kurny and Fahmida Gulshan, 2016, International Journal of Environmental Science and Development, Vol. 7, No. 5.

[4]. Yogendra K., Naik S., Mahadevan K.M., Madhu sudhana N., 2011, Int. J. Environ. Sci. Res., 1(1), 11-15.

[5]. Bhukal S., Namgyal T., Mor S., Bansal S., Singhal S., 2012, J. Mol. Struct., 1012, 162-167.

[6]. Jothiramalingam R., Wang M. K., 2007, J. Hazardous Mat, 147, 562.

[7]. Lwin, N., Othman, R., Noor, A. F. M., Sreekantan, S., Yong, T. C., Singh, R., Tin, C. C. 2015, Materials Characterization, 110, 109-115.

[8]. Raming, T. P., Winnubst, A. J. A., Van Kats, C. M., Philipse, P. 2002, Journal of Colloid and Interface Science, 249, 346-350.

[9]. Narde S. B., Lanjewar R. B., Gadegone S. M., Lanjewar M. R., 2019, IJCESR,ISSN (PRINT): 2393-8374, (ONLINE): 2394-0697, VOLUME-6, ISSUE-1,1406-1413.

[10]. El-Bahy Z. M., Ismail A. A., Mohamed R. M., Journal of Hazardous Materials, 2009, 166(1), 138-143.

[11]. Mohamed R. M., Mkhalid I. A., Baeissa E. S., Al-Rayyani M. A., Journal of Nanotechnology, Volume 2012, 1-5, Article ID 329082, doi:10.1155/2012/329082.

[12]. Tanveer, M., Cao, C., Aslam, I., Ali, Z., Idrees, F., Tahir, M., Khan, W. S., Butt, F. K., Mahmood, A. 2014, RSC Adv., 4, 63447–63456.

[13]. Royer, B., Cardoso, N. F., Lima, E. C., Vaghetti, J. C. P.,. Simon, N. M., Calvete, T., Veses, R. C., 2009. J. Hazard. Mater., 164, 1213-1222.

[14]. Tarigh G. D., Shemirani F., Mazhari N. S., RSC Adv., 5, 2015, 35070-35079.

International Virtual Conference on Materials and Nanotechnology
In Association with International Journal of Scientific Research in Science and Technology
Volume 9 | Issue 4 | Print ISSN: 2395-6011 | Online ISSN: 2395-602X (www.ijsrst.com)

Analysis of Heat Transfer and Human Comfort in Warehouse

Vivek Bhide*[1], Prof. Prakash Ingle*[2]
*[1]ME Thermal, SGBAU University/PR POTE Patil College of Engineering & Management, Amravati, Maharashtra, India
[2]ME Thermal, SGBAU University/PR POTE Patil College of Engineering & Management, Amravati, Maharashtra, India

ABSTRACT

With Growth of E-commerce & Global consumer good industry Warehouse demand in India has overtaken supply for the first time in four years. According to a new report by property developer Jones Lang LaSalle (JLL), FY 2018-19 India's total stock of Grade A and B warehousing space increased 22% year on year to 169 million sq ft. "Last year saw India's warehousing sector come of age, outshining some of the conventional real estate asset classes and attracting global investors," the report notes.
With more warehouse coming up the need for improvement in current Operations and maintenance is in high priority by the users. Temperature control is one of the biggest maintenance requirements of running a warehouse. Too much heat causes heat stress, which can make employees less productive. Extreme cold also has its shortcomings, including exposing employees to cold-related illnesses. Depending on the nature of the warehouse inventory, extreme heat can cause damages and hefty losses.
The vast space in a warehouse makes temperature control complicated – and expensive. This paper addresses the complications of air conditioning in a warehouse and suggests efficient remedies which can be implemented before and after construction of Warehouses.
Keywords : Storage Conditions, Human Comfort, Warehouse heat.

I. INTRODUCTION

Basically, a warehouse is great for storing surplus goods, which customers and clients don't need immediately. Most companies usually produce goods in anticipation of demand. This means they'll need adequate storage for their surplus goods until their customers and clients start putting in orders.
Warehouses have unique heating obstacles. They tend to be large buildings with high ceilings and many doors and windows. Additionally, many warehouses accept deliveries or shipments several times a day, exposing the space to outdoor conditions.

A. Processes in a Warehouse

The six fundamental warehouse processes comprise receiving, put-away, storage, picking, packing, and shipping. Optimizing these six processes will allow you to streamline your warehouse operation, reduce cost & errors, and achieve a higher perfect order rate. Below Image shows Process areas inside a warehouse

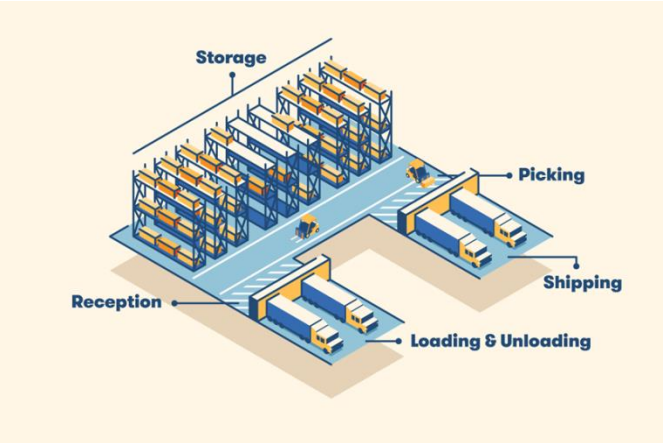

1. Receiving: operations that involve the assignment of trucks to docks, the scheduling and execution of unloading activities
2. Storing: material's movement from unloading area to its designated place in inventory
3. Order Picking: the process of obtaining the right amount of the right products for a set of customer orders. This is the main and the most labour-intensive activity of warehouses
4. Shipping: execution of packing and truck's loading after picking, involving also the assignment of trucks to docks
5. Delivery: the transit time for transportation from the warehouse to the customer.

B. Basic characteristic of Warehouse

1. Made of Steel structure (PEB)
2. Very high height (20 - 30 M)
3. Large space is covered (ranging 10k Sq-ft to 10 Lakh sq-ft)
4. large no of Docks / opening for flow of material
5. Internal structure includes racks and structural steel shelve for storage of material
6. Large no of manpower working inside in 2-3 shifts operation
7. Huge energy consumption for lighting, HVAC & other utilities

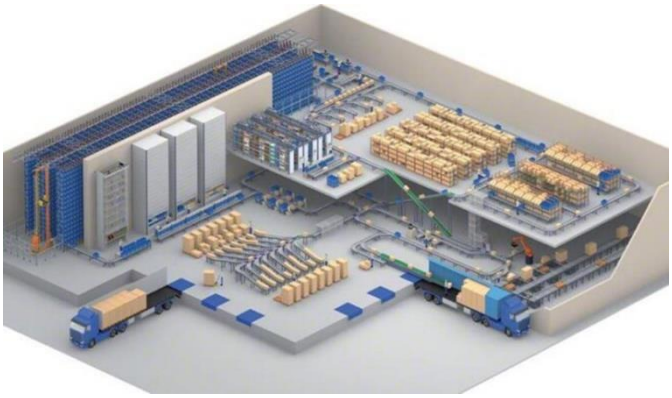

II. METHODS AND MATERIAL

Heat from Sun is transferred by Radiation, Conduction and convection from outside environment to inside the building.

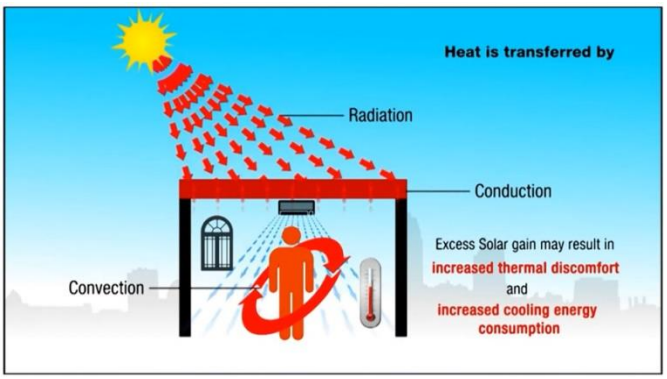

As illustrated in the image. This increases the Thermal discomfort and when we start using the HVAC system the energy Consumption of building increases.

A. Storage Conditions

Below table gives classification of various storage conditions for commodity / material in Open and closed packed state stored in the warehouse require. Any variation in the parameters affect the Physical shape, Appearance & Chemical composition which will further not qualify for shipping it to customer.

Storage condition	Temperature (C)
Cold Temperature	2 to 8
Cool Temperature	8 to 25
Room Temperature	25 to 30
Warm Temperature	30 to 40

Excessive Heat	Above 40
Controlled Room Temperature	15 to 30
Freezer	-20 to -10
Extreme Heat	Above 40
Dry Place	40% Rel Humidity

B. Important Factor for Human comfort Inside a Building

1. Temperature - Humans like to be in the range of 70 to 80 degrees, more or less.
2. Humidity - 40% -60% relative humidity is the ideal range. In addition to decreasing comfort, a relative humidity that's too low or too high increases the likelihood of things like bacteria, mold, dust mites.

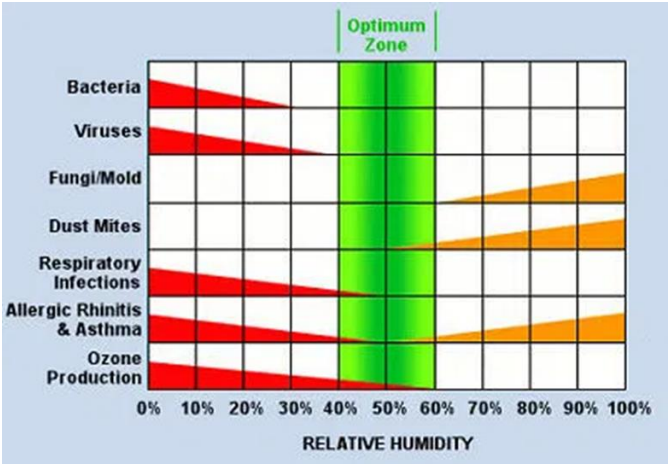

3. Air Movement - Is the air moving across your skin? In the summer, one way that our bodies keep cool is by the evaporation of sweat. A nice breeze or a ceiling fan can keep us comfortable even when the the temperature and humidity are at or above the narrow range we find most comfortable. In the winter, that same air movement will make us uncomfortable.
4. Mean Radiant Temperature - How hot or cold are the surfaces around you? Even if the air temperature in that room is 70 degrees, you may be uncomfortable because the walls keep blasting you with heat. The photo here shows an infrared image of a hot attic kneewall, and you can see from the wide range of colors that the wall is very hot in most places but very cold by the air conditioning vent.

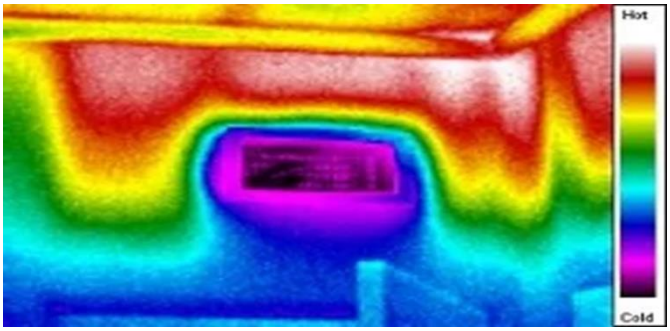

The two things that most affect our comfort in buildings are the building envelope (insulation and air barrier) and the heating and cooling system. Good insulation, properly installed and in contact with the air barrier, and a tight house go a long way to helping. Good HVAC design takes us the rest of the way. When it all works harmoniously together, we're comfortable, and the house is also efficient, durable, and healthful.

III. RESULTS AND DISCUSSION

There are dozens of complications when regulating temperatures in a warehouse. The most common include:

A. Heat collecting around the ceiling

One of the most basic characteristics of heat is its tendency to rise above cold air in a building. This difference in air density can cause problems in a warehouse, especially if it has a high ceiling. When warm air congregates around the ceiling of a building, it doesn't properly heat the lower areas where employees are.

Solution: Destratify the air in your space by increasing airflow. Greater airflow in your warehouse means the air temperature is consistent, or thermal equalized. Bringing the warm air down from the ceiling means that your employees stay warmer without you having to crank up the heater.

B. Maintaining control over heating

You always want to have sufficient control over how much heat is being pumped into your warehouse. It's important to have enough warm air coming in to keep the building comfortable, but if you have too much heating, you'll face high energy bills.

Solution: Invest in a better method of monitoring the heating in your building. A building management system (BMS) is a great way to keep an eye on how much warm air is being pushed into your warehouse. Many of these systems also allow you to remotely adjust heating levels, meaning you can save money by lowering the heat when it's not needed.

C. Getting heat between racks

Many warehouses are used for shipping and receiving, company equipment, or other tools. These items are often stored in racks placed along the floor at equal intervals. Depending on what they're storing, shelving and rack units can be large and wide, creating a challenge for heating around them.

Solution: Before you decide how to properly heat up a warehouse with racking, it's best to create a model using an airflow visualization tool. Typically fans are laid out near the docking areas and in the open areas around the racking. With this layout, the fans are near the heaters and can move the heated air between the racking and throughout the space.

D. Air leaks around windows

Over time, the seal around most windows will begin to wear down. This is especially problematic if you don't know about it, and since many warehouses have high windows that are difficult to reach, leaks can go unnoticed.

Solution: Check the air temperature of the areas around your window at least a few times a year to see if the air is unusually hot or cold. If so, you might have a leak – you'll want to check the insulation around the window and possibly replace or add new weatherstrips.

Above listed complication and solution are being used in industry for regulating the heat transfer. Many solution can be implemented in the warehouse which are already in use. For future warehouse construction few improvement in the design can also help.

IV. APPLICATION FOR REDUCING HEAT TRANSFER

During Building Construction

1. Turbo Ventilators on the roof

2. Side wall louvers

3. Smart HVAC system - with modern ventilation and Heat Mapping

After Building Construction

4. HVLS(High Volume Low Speed) Ceiling Fans

5. Exhaust Fan in the Highly Concentrated heat areas(Between the racks)

6. Roof Insulation - Heat reflective and water proofing Coating on the Roofs

7. Side wall – Insulation

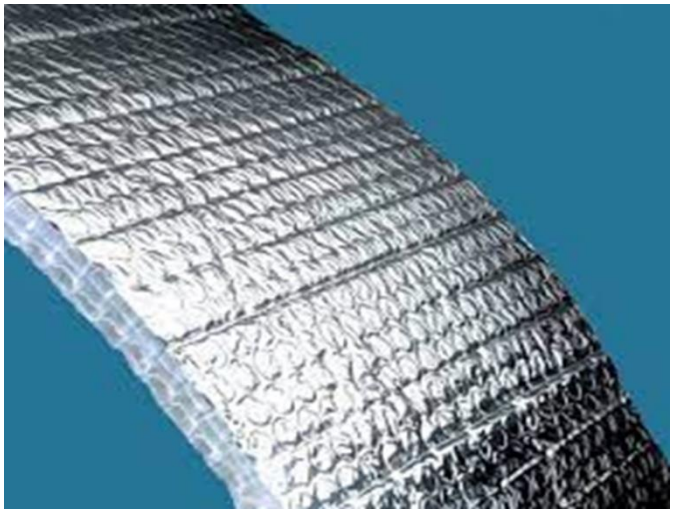

V. CONCLUSION

With new research and developments happening across the world the Warehouse Heat transfer factor are being control using simple solution at various stages of construction. These measure can help in reducing temperature is summer by 3-5 degree C and Heat loss 15-30 % heat losses can also be reduce by insulation..

VI. REFERENCES

[1]. Heat Transfer by J.P. Holman, Tata McGraw Hill Publication,
[2]. Heat and Mass Transfer SI Unit by RK Rajput, S Chand Publication
[3]. Heat & Mass transfer by Arora , Domkundwar, Dhanpat Rai & co Publication.
[4]. http://www.scmdojo.com/warehouse-activities/
[5]. https://www.energyvanguard.com/blog/the-4-factors-of-comfort/
[6]. https://www.reznorhvac.com/efficient-warehouse-heating-cooling-ventilation-tips/
[7]. https://www.youtube.com/watch?v=AnLidGz7sYI&t=182s
[8]. https://www.youtube.com/watch?v=ZPL1c0CdJjQ

International Virtual Conference on Materials and Nanotechnology
In Association with International Journal of Scientific Research in Science and Technology
Volume 9 | Issue 4 | Print ISSN: 2395-6011 | Online ISSN: 2395-602X (www.ijsrst.com)

Comparative Study of Electrical Properties of Substituted Calcium Hexaferrites

Moharkar P.R.[1*], Gawali S.R.[2]

[1*]Department of Physics, Arts, Commerce and Science College, Tukum, Chandrapur, Maharashtra, India

[2]Department of Physics, Dr. Ambedkar College, Chandrapur, Maharashtra, India

ABSTRACT

The two series of samples of substituted calcium hexaferrite with composition $Ca_2Zn_2Fe_{12-x}Me_xO_{22}$ (Me = Al and Co, x=0, 0.3 and 0.7) were prepared by the sol-gel auto combustion method. The microstructure of the both series of prepared samples has been characterized by XRD technique. The XRD data shows the prepared sample are found to be a single phase Y-type hexagonal ferrite. The lattice constants a and c, X- ray density, bulk density and porosity of both series of synthesized sample were measured. The lattice constants of the synthesized sample were found to decrease with increase substitution of Al^{3+} ion for Fe^{3+} ion where as increases with substitution of Co^{3+} ion for Fe^{3+} in calcium hexaferrites, which is attributed to the ionic size differences of cations involved. The dc electrical conductivity measurementsof both series have been carried out the temperature range 300 K-800 K by using impedance analyzer. The electrical conductivity of the sample was explained on the basis of hopping mechanism. The resistivity of the samples was found to be enhancing with the substitution of Al^{3+} ion for Fe^{3+} ion in calcium hexaferrites which has potential applications in microwave devices.

Keywords : Y-type Hexagonal Ferrite, Microstructural property, XRD, Electrical Conductivity and Auto-combustion method etc.

I. INTRODUCTION

Many researchers have shown their interest in hexagonal ferrites due to their use as permanent magnet [1, 2], microwave absorption device material and magneto-optic recording media [2, 5]. The Y-type hexagonal ferrite possesses electrical properties like conductivity, dielectric constant and loss tangent etc., which are useful in the solid-state electronic devices and microwave to radio frequency devices. The low electrical conductivity results into low losses, which are useful for microwave application. The electrical properties give information about the defects in crystal structure conduction mechanism and grain boundaries, which depends on the chemical composition of material, the charges and distribution of ions amongst the various sites. It is possible to prepare a hexaferrite of having specific properties by controlling the chemical composition and substituting metallic element [6].

In current research module, the two series of samples of aluminium and cobalt substituted calcium hexaferrite have been synthesized by sol-gel auto-combustion method. The influence of substitution of

Al3+ and Co3+ ion for Fe3+ ion on structural and electric properties of substituted calcium hexaferrite have been investigated.

II. EXPERIMENTAL

1. Sample preparations

The two series of aluminium and cobalt substituted calcium hexaferrite with composition Ca2Zn2Fe12-xMexO22 (Me = Al and Co, x=0, 0.3 and 0.7) have been synthesized by sol-gel auto-combustion method. The synthesis route involved the combustion of redox mixtures, in which metal nitrates acted as an oxidizing reactant and urea as a reducing reactant. The initial composition of solution containing metal nitrates and urea was based on the total oxidizing and reducing valences of the oxidizer and the fuel using the concept using the concept of propellant chemistry [7].

The stoichiometric amounts of AR grade calcium nitrate Ca(NO3)2 4H2O, iron nitrate Fe(NO3)3 9H2O, aluminum nitrate Al(NO3)3 ·9H2O, cobalt nitrate Co(NO3)2·4H2O and urea CO(NH2)2 dissolved in a minimum quantity of water, were placed in a beaker.

The beaker containing the solution was introduced into a microwave oven. Initially the solution boils and undergoes dehydration followed by decomposition with the evolution of a large volume of gases (N2 , NH3, and HNCO). After the solution reaches the spontaneous combustion, it begins burning and releases lots of heat, vaporizes all the solution instantly and becomes a solid burning at temperatures above 1000 oC. The entire combustion process which produces aluminium substituted calcium hexaferrite powders in microwave oven takes only 15 min [8].

2. Characterization

The samples of both series were analyzed using a Philips X-ray diffractometer (XRD) model (PW-1710) and Cu-Kα radiation with the wavelength λ = 1.54056 Å. The X-ray diffraction is measured in the range from 20 to 70 with a step of 0.02 for 1 second.

The particle morphology of synthesized samples was examined by a transmission electron microscope (TEM).

The electrical conductivity of aluminium substituted calcium ferrite has been measured from 300 to 800K by using impedance analyzer.

III. RESULTS AND DISCUSSION

1. XRD analysis

The XRD patterns of the samples are shown in Fig 1(a) and (b). The crystallographic data are tabulated in Table 1. The data is analyzed by using computer software PCPDF Win, Powder-X and Full proof Suite. By comparing the patterns with JCPDS, the phases in the different samples are determined. The lattice parameters a and c are found to be in the range 5.0404 to 5.0490 Å and 44.1792 to 44.3072 Å for samples. The XRD pattern of both series of samples confirms that the synthesized samples are found to have Y-type hexagonal structure belonging to the space group R m (no. 166).

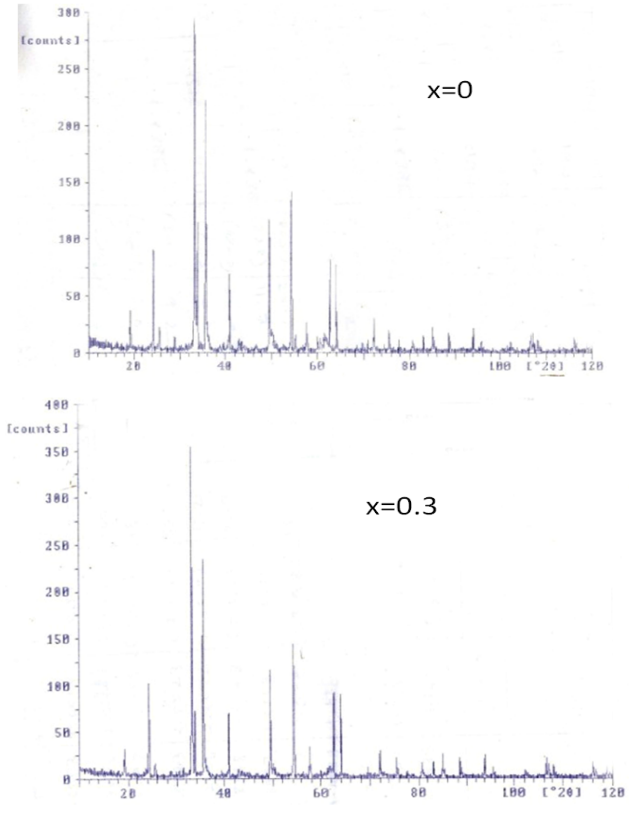

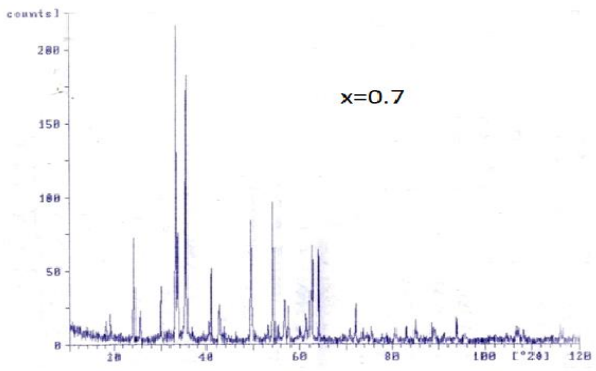

Fig.1. (a) X-ray diffraction spectra of sample Ca2Zn2Fe12-xAlxO22

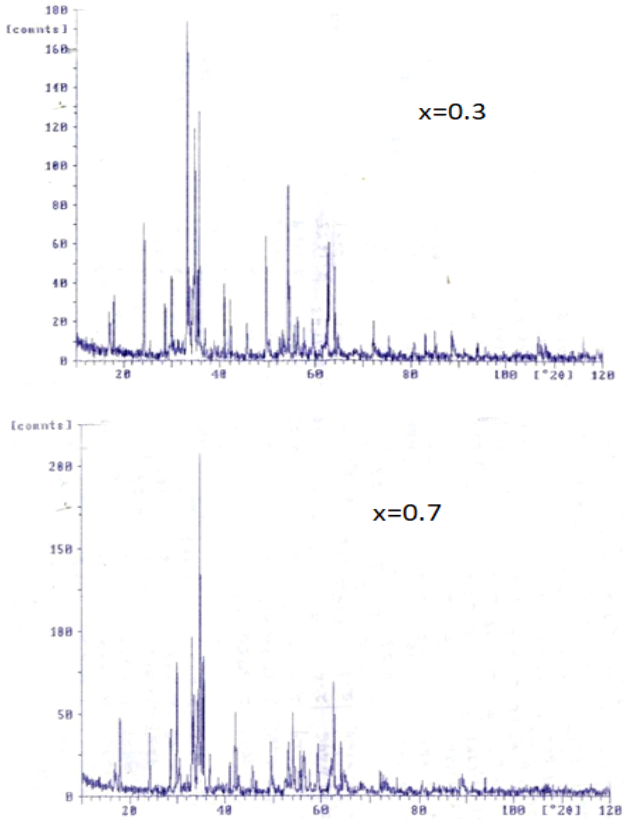

Fig. 1.(b) X-ray diffraction spectra of sample Ca2Zn2Fe12-xCoxO22

The lattice constants a and c, X-ray densities, bulk densities and porosity of the both series of samples at room temperature are given in the Table 1. The lattice parameter 'a' and 'c' shows decreasing trend with increase in concentration of Al+3 ions. This variation in relatively small but can be considered due to smaller ionic radii of Al+3 ions (0.53Å) compared to that Fe+3 ions (0.64Å) for six fold co-ordination. As a result, the cell volume of calcium hexaferrites found to have contraction after being doped with Al+3 ions. Kuhikar [9] reported the values of 'a' and 'c' as 5.884 Å and 43.938 Å for Ca2Co2Fe11LaO22 sample. This is in agreement with the fact that all the hexagonal types exhibit variation in lattice constant after being substituted by variable size ions as reported by Ounnunkad and Winotai [10].

Similarly the lattice parameters 'a' and 'c' increases with increase in the concentration of Co+3 ions as shown in Table 1. The variation in lattice parameters with substitution of Co+3 is also related to larger ionic radii of Co+3 (0.68Å) than Fe+3 ion (0.64Å). The similar results of lattice parameter were reported by Meaz and Koch [11].

It was seen that density and porosity are inversely varies with dopent concentration. This behaviour may be attributed to the fact that introduction of Co+3 ions in hexagonal ferrites may affect the grain size development during firing process and decrease the porosity.. Thus it can be concluded that substitution enhance the firing process and increase the grain size to leading to decrease of porosity.

2. TEM analysis

Fig. 2 (a) and (b) shows TEM images of aluminium and cobalt substituted calcium hexaferrite. The average particle size of the samples is in nanorange with an average diameter of 40 nm.

3. DC conductivity

Fig. 3 (a) and (b) shows that as temperature increases, the conductivity of ferrite increases, indicating that these ferrites have semiconductors like behavior [12]. The conduction in ferrite at room temperature is due to the impurities, where as at high temperature it is due to polaron hopping [13]. The conductivity in ferrites may be explained by Verwey's hopping mechanism. According to Verwey, the electronic conduction in ferrite is mainly due to hopping of electrons between ions of the same element present in

more than one valence state, distributed randomly over crystallographically different lattice sites.

Table 1: Lattice constants (a) and (c), cell volume (V), X-ray density (ρx-ray), bulk density (ρm) and porosity (P) of samples

Sample	a (Å)	c (Å)	V (Å)3	ρx-ray (gm/cm³)	ρm (gm/cm³)	P (%)
Ca2Zn2Fe12O22	5.0490	44.3072	1240.27	4.2239	3.0982	26.67
Ca2Zn2Fe11.7Al0.3O22	5.0472	44.2776	1248.12	4.1257	2.9238	29.14
Ca2Zn2Fe11.3Al0.7 O22	5.0446	44.2236	1245.31	4.1633	3.1118	25.26
Ca2Zn2Fe11.7Co0.3O22	5.0404	44.1792	1241.97	4.2168	3.1092	26.26
Ca2Zn2Fe11.3Co0.7 O22	5.0454	44.2872	1247.79	4.2340	2.5757	38.73

Table 2: Electrical resistivity at room temperature and activation energy of substituted calcium ferrite

Sample	Room Temperature Resistivity (MΩ-cm)	Electrical Conductivity (Ω-1cm-1) x 10-9	Activation Energy ΔE (eV)	
			Ferri	Para
Ca2Zn2Fe12O22	89.8	11.13	0.25	0.37
Ca2Zn2Fe11.7Al0.3O22	108.9	9.18	0.23	0.31
Ca2Zn2Fe11.3Al0.7 O22	118.7	8.42	0.26	0.39
Ca2Zn2Fe11.7Co0.3O22	72.4	13.80	0.28	0.35
Ca2Zn2Fe11.3Co0.7 O22	45.0	22.22	0.26	0.33

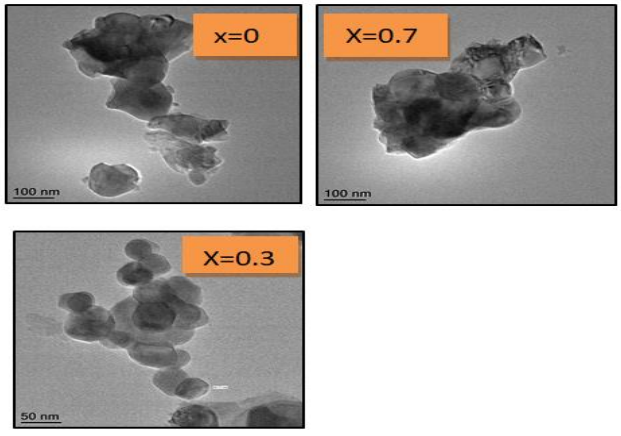

Fig.2(a) TEM images of samples: $Ca_2Zn_2Fe_{12-x}Al_xO_{22}$

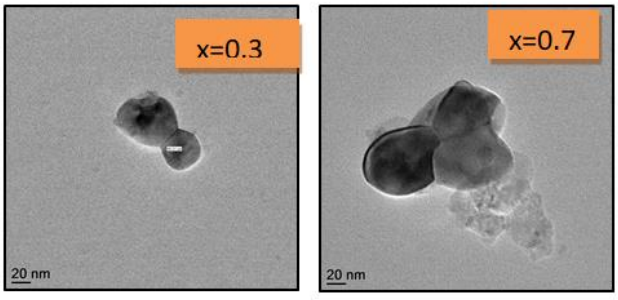

Fig.2(b) TEM images of samples: $Ca_2Zn_2Fe_{12-x}Co_xO_{22}$

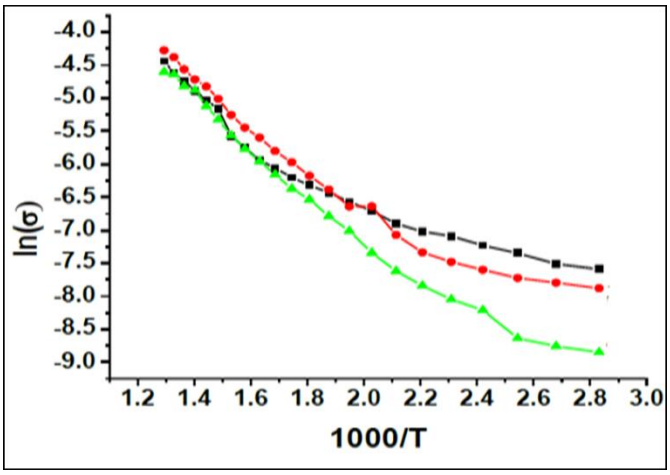

Fig. 3(a) : Variation of ln() with temperature (103/T) of sample Ca2Zn2Fe12-x Alx O22

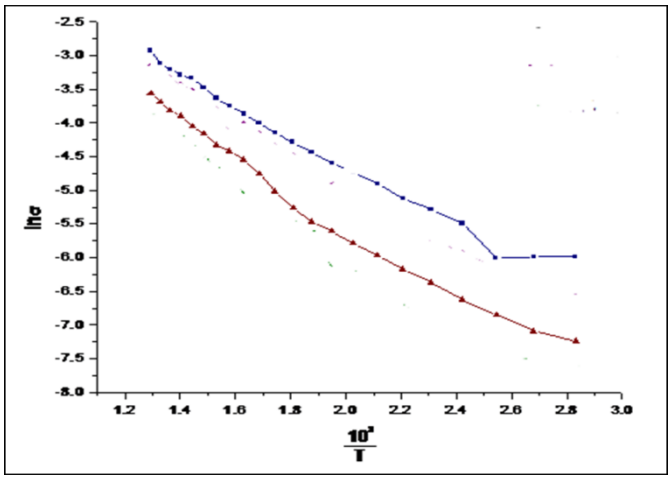

Fig. 3(b): Variation of ln() with temperature (103/T) of sample Ca2Zn2Fe12-x Cox O22

The resistivity of the samples is given in the Table 2. The resistivity of the samples at room temperature increases from 89.8 MΩ to 118.7 MΩ for replacement of Al3+ ion and decreases from 89.8 MΩ to 45.0 MΩ for Co3+ ion for Fe3+ ion. The increase in resistivity may be due to the fact that Al is more resistive than Fe whereas Co is less resistive than Fe [14]. The activation energy of the samples lies in the semiconducting range. The activation energy of the samples in paramagnetic region is more than ferrimagnetic region. Thus the resistivity of the samples was found to be enhancing with the substitution of Al3+ ion for Fe3+ ion whereas the resistivity of samples decreases with substitution of Co3+ ion for Fe3+ ion in calcium hexaferrites.

IV. CONCLUSION

The two series of samples of aluminium and cobalt substituted calcium hexaferrite samples were synthesized by the sol-gel auto-combustion method. The XRD data of both series of samples have confirm the formation of Y-type hexagonal ferrites and the values of a and c of the sample supports this confirmation. TEM analysis reveals that the synthesized samples are in the nanorange. The lattice parameters a and c and cell volume V decreases for substitution of Al3+ ion for Fe3+ ion where as increases for substitution of Co3+ ion for Fe3+ ion in calcium hexaferrites. The resistivity of the samples was found to be enhancing with the substitution of Al3+ ion for Fe3+ ion in calcium hexaferrites which has potential applications in microwave devices.

V. REFERENCES

[1]. Leceabue F, Painzzieri Albanese G, Leo G and Suarez N, 1998. Mat. Res. Bull., 33, 266.

[2]. Kirchmayr H. R., 1996. J. Phys. D. Appl. Phys. 29 pp. 2763-2778.

[3]. Haneda K. and Kojima H, 1971. J. Phys Status Solidi (A) 6 259 b.

[4]. Pardavi- Horvath M, 2000. J. Magn. Magn. Mater. 215-216 pp. 171-183.

[5]. Shankaranarayanan V. K., Pant R. P., Rastogi A. C., 2000. J. Magn. Magn. Mater.220 pp. 72-78.

[6]. Kaura B., Bhata M., Liccib F., Kumarc R., Kulkarni S. D., Joyd P. A., Bamza K. K. Kotrua P. N., 2006. J. Magn. Magn. Mater. 305 pp. 392-402.

[7]. Jain S. R., Adiga K. C. and Pai Verneker V. R., 1981. Combustion Flame, 40 pp. 71-79.

[8]. Moharkar P.R., Gawali S.R., Rewatkar K.G., Sable S.N., and Nanoti V.M., 2012. Inter. J. Know. Engi. 3 (1) pp. 113-115.

[9]. Kuhikar S.V. and Kulkarni D.K. 2005. Ultra Science, 17(2) pp. 333-338.

[10]. Ounnunkad S. and Winotai P, 2006. J.Magn.Magn.Mater. 301, pp. 292-300.

[11]. Meaz T.M., Koch C.B., 2004. Hyp Interact., 156/157, pp. 341-346.

[12]. Abbas T, Islam M. U, Chaudhry M. A., 1995. Mod. Phys. Lett. B 9 (22) pp.14-19.

[13]. Verway E. J. W., De Boer J. H., 1936. Rec. Trans. Chem. Des. Pays. Bas. 55, 531.

[14]. Lakshman A, Subha Rao P.S.V., Rao B. P., Rao K. H., 2005. J. Phys. D. Appl. Phys. 38 673.

International Virtual Conference on Materials and Nanotechnology
In Association with International Journal of Scientific Research in Science and Technology
Volume 9 | Issue 4 | Print ISSN: 2395-6011 | Online ISSN: 2395-602X (www.ijsrst.com)

Solvent (Water) Effect on Geometry Properties of Patuletin Dyes for Formation of Metal Complex by DFT Method

Nilesh U. Jadhao*, Dinesh W. Deshmukh, Manisha M. Jiwatode, B. M. Bahirwar
Guru Nanak College of science, Ballarpur, Dist: Chandrapur-442701, Maharashtra, India

ABSTRACT

For determine the metal complex structure used is the costly and complicated spectrum method but due to DFT method, fast computer we can interested to sketch of metal complex with patuletin ligand in proper solvent over the calculation of geometrical properties by DFT method. The interested result is outcome that, only optimization and charge density properties explain by the probable side attack of metal on ligand.

Keywords : Solvent effect, Geometry, DFT Method, Patuletin dye.

I. INTRODUCTION

Computational chemistry is used in a number of different ways [1]. One particularly important way is to model a molecular system prior to synthesizing the target molecule in the laboratory [2]. Although computational models may not be precisely accurate, but they are often good enough to rule out 90% of possible compounds as being unsuitable for their intended use [3]. This is very useful information because synthesizing a single compound may require months of labour, raw materials cost and also generate toxic waste. A second use of computational chemistry is in understanding a problem more completely [4]. There are some properties of a molecule such as electronic charge distribution, dipoles and vibrations frequency that can be obtained computationally more easily than by experimental means. There are also insights into molecular bonding, which can be obtained from the results of computations, which cannot be obtained from any experimental method. In 2011, Jadhao N.U. and Rathod S.P. were done the quantum mechanical calculation for Schiff bases by DFT method which shows the appropriate result to experimental data and they shows the type of electronic state of UV-Visible spectrum and clear the transition type by the TD-DFT method [5].

For determine the metal complex structure used is the costly and complicated spectrum method but we have been interested to sketch of metal complex with patuletin ligand in proper solvent over the calculation of geometry properties by DFT method. For the above mentioned reasons, optimization in gas phase and water phase will be carried out. Computational calculations will be employed to study charge density properties for patuletin dye.

II. MATERIAL AND METHODS

Computation work was done using the GAUSSIAN 03W program suite. The patuletin studied in C_1 symmetry and molecule was fully optimized with the tight criteria using the DFT (PBE1) level of theory with basis set 3-21G used without solvent and same

parameters are used to optimize the patuletin in water as a solvent with IEFPCM model.

The following is structure of patuletin.

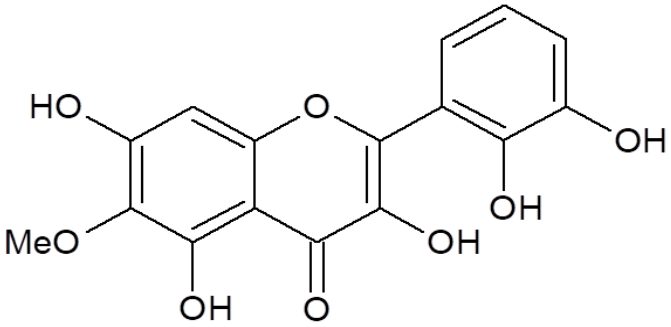

Figure 1.1 Structure of Patuletin

III. RESULT AND DISCUSSION

3.1. MOLECULAR OPTIMIZATION GEOMETRY

We started the geometry optimization of patuletin, without symmetry constraints. Optimized structure converged to C_1 symmetrical species. The geometry was optimized in a singlet ground state by the DFT method with the PBE1function using 3-21G** basis set in gas phase and water phase using with IEFPCM model. The optimized structure in gas phase shown in figure 1.2a and in water phase shown in figure 1.2b.

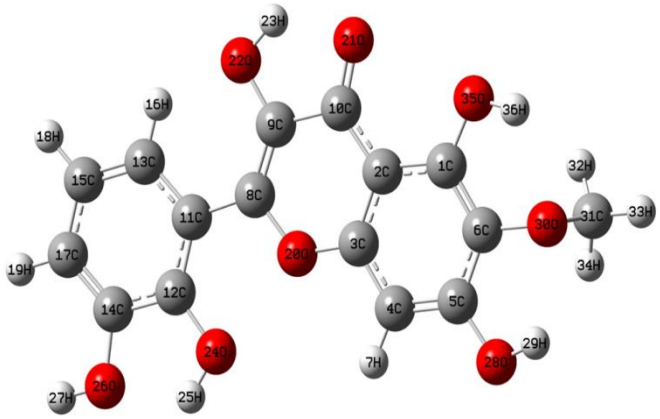

Figure 1.2 a) Optimized structure in gas phase of patuletin.

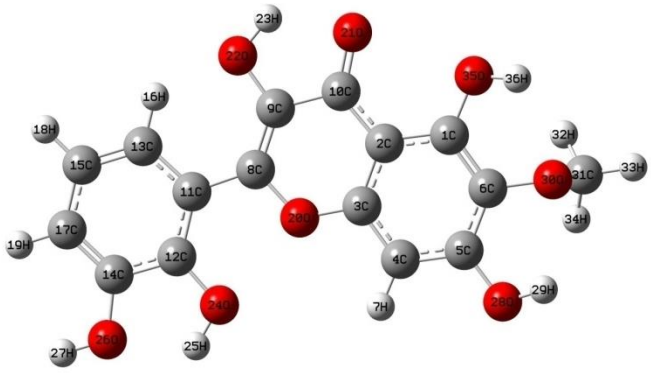

Figure 1.2 b) Optimized structure in water phase of patuletin

In both phases the molecule behaves the planner structure only methyl group is out of plane. The bond length of all O-H bond are higher in water phase as compare to gas phase because in water phase, the H-bonding was occurred due to this bonding all O-H bond length are changed as compare to gas phase moiety are shown in table 1.

The large effect show in 26 – O and 27- H that is in gas phase the bond length between these atoms is 0.984836 Å and in water phase the bond length between these atoms is 1.011795 Å.

So the 27-hydrogen atom in water phase is goes long from 26-oxygen atom and it is good intense towards, breaking of bond with low energy and formation of metal complex.

The optimized geometric all parameters are gathered in following table.

Table 1. Bond length of O-H in Å in water and gas phase

Sr.no.	No. of atom	Bond length of O-H in Å	
		In water phase	In gas phase
1.	22,23	1.023189	1.024274
2.	24,25	1.006361	0.998632
3.	**26,27**	**1.011795**	**0.984836**
4.	28,29	1.009733	0.997015
5.	35,36	1.010088	0.997357

The optimized geometric all parameters are gathered in following table.

Full optimized parameter in gas phase

#	Symbol	NA	NB	NC	Bond	Angle	Dihedral	X	Y	Z
1	C							-2.988753	0.700149	-0.180053
2	C	1			1.408478			-1.581500	0.731382	-0.130326
3	C	2	1		1.408482	117.639461		-0.900294	-0.501406	-0.126732
4	C	3	2	1	1.393131	122.945613	0.898173	-1.555550	-1.729284	-0.188136
5	C	4	3	2	1.382931	118.364344	-0.993369	-2.937693	-1.734807	-0.234482
6	C	1	2	3	1.379311	118.964411	0.092546	-3.628755	-0.521022	-0.220523
7	H	4	3	2	1.079072	119.621492	178.921737	-0.979147	-2.641438	-0.199629
8	C	3	2	1	2.416493	92.245163	-179.888473	1.257083	0.582830	-0.028789
9	C	8	3	2	1.357606	89.633500	-0.157193	0.639895	1.792022	-0.034172
10	C	2	1	6	1.435028	123.514503	-179.900709	-0.817050	1.944944	-0.083537
11	C	8	3	2	1.454500	142.860368	179.700343	2.686371	0.318334	0.023642
12	C	11	8	3	1.403555	122.530631	-0.216167	3.213412	-0.982482	0.032192
13	C	11	8	3	1.414672	119.228100	179.861856	3.589028	1.406630	0.069687
14	C	12	11	8	1.407575	119.120192	-179.899032	4.609242	-1.155677	0.086327
15	C	13	11	8	1.382304	121.455434	179.913342	4.956017	1.208259	0.122180
16	H	13	11	8	1.080951	117.495327	-0.043442	3.170110	2.403083	0.063059
17	C	14	12	11	1.377223	122.184513	-0.016640	5.479577	-0.089253	0.131046
18	H	15	13	11	1.083330	119.928619	179.991533	5.624819	2.059801	0.156579
19	H	17	14	12	1.085499	120.683223	179.996189	6.552160	-0.250995	0.172439
20	O	3	2	1	1.365196	121.123522	-179.796374	0.462929	-0.554193	-0.075767
21	O	10	2	1	1.260671	128.153898	0.101221	-1.240481	3.132359	-0.076967
22	O	9	8	3	1.365325	125.842044	-179.981564	1.261361	3.007006	0.007134
23	H	22	9	8	1.024274	101.380116	-179.836063	0.459965	3.644644	-0.010736
24	O	12	11	8	1.369395	124.542780	0.052026	2.460485	-2.125606	-0.007946
25	H	24	12	11	0.998632	105.404110	179.950117	3.117958	-2.877053	0.009987
26	O	14	12	11	1.394731	111.871634	179.967089	4.965805	-2.504059	0.088348
27	H	26	14	12	0.984836	111.615236	179.777908	5.943088	-2.620833	0.122739
28	O	5	4	3	1.367428	122.018135	179.906781	-3.656336	-2.896447	-0.297760
29	H	28	5	4	0.997015	106.384094	-169.939801	-4.599217	-2.633849	-0.487648
30	O	6	1	2	1.415223	118.968375	178.093274	-5.043580	-0.553430	-0.229306
31	C	30	6	1	1.487317	110.478362	-88.882434	-5.572083	-0.580310	1.160685
32	H	31	30	6	1.094601	109.966538	60.254643	-5.248431	0.314932	1.701003
33	H	31	30	6	1.091157	105.816795	179.800416	-6.658874	-0.600606	1.065305
34	H	31	30	6	1.094714	110.004241	-60.635167	-5.213203	-1.474364	1.680561
35	O	1	6	5	1.362768	119.139350	178.920002	-3.734360	1.840798	-0.191284
36	H	35	1	6	0.997357	106.374600	-10.227444	-4.669500	1.563401	-0.399336

Full optimized parameter in water phase

#	Symbol	NA	NB	NC	Bond	Angle	Dihedral	X	Y	Z
1	C							-3.003452	0.701015	-0.185644
2	C	1			1.413264			-1.591124	0.731355	-0.144109
3	C	2	1		1.407281	117.702158		-0.909910	-0.500055	-0.148076
4	C	3	2	1	1.388718	122.702305	1.381827	-1.567603	-1.721107	-0.218863
5	C	4	3	2	1.388235	118.798839	-1.408448	-2.955220	-1.731973	-0.258829
6	C	1	2	3	1.383830	119.334543	-0.040751	-3.654362	-0.519408	-0.228883
7	H	4	3	2	1.083011	120.042092	178.799368	-0.999207	-2.642763	-0.238575
8	C	3	2	1	2.419824	92.312924	-179.515244	1.251233	0.583546	-0.044073
9	C	8	3	2	1.360446	89.453219	-0.380904	0.630003	1.793866	-0.047467
10	C	2	1	6	1.435377	123.506141	-179.858467	-0.825749	1.944644	-0.094737
11	C	8	3	2	1.458122	142.946310	179.017748	2.683871	0.319083	0.016986
12	C	11	8	3	1.406104	122.593502	-0.011777	3.213804	-0.983271	0.030151
13	C	11	8	3	1.417790	119.273664	-179.701417	3.588409	1.409452	0.072077
14	C	12	11	8	1.413067	119.444000	-179.558676	4.613668	-1.162917	0.099917
15	C	13	11	8	1.382554	121.389472	179.587857	4.954687	1.208966	0.139487
16	H	13	11	8	1.080584	117.697869	-0.265403	3.173569	2.407184	0.062077
17	C	14	12	11	1.379719	121.616237	-0.054642	5.478800	-0.089521	0.154621
18	H	15	13	11	1.086626	119.915737	-179.951535	5.626202	2.062227	0.181558
19	H	17	14	12	1.088028	120.045896	179.969903	6.552460	-0.257370	0.208331
20	O	3	2	1	1.369856	121.135416	-179.477268	0.458035	-0.552930	-0.098727
21	O	10	2	1	1.262415	127.778058	-0.194040	-1.256894	3.131105	-0.083960
22	O	9	8	3	1.367092	124.845825	-179.939315	1.270543	3.000771	-0.002406
23	H	22	9	8	1.023189	103.673240	-179.605120	0.506146	3.680838	-0.013424
24	O	12	11	8	1.367126	124.092475	0.337316	2.455430	-2.119714	-0.018826
25	H	24	12	11	1.006361	106.992711	-179.629300	3.091313	-2.899151	0.011074
26	O	14	12	11	1.378803	112.170304	179.924419	4.967594	-2.495510	0.105430
27	H	26	14	12	1.011795	112.824177	-179.437891	5.967899	-2.635683	0.164333
28	O	5	4	3	1.360398	119.713615	-179.108634	-3.619061	-2.918307	-0.309906
29	H	28	5	4	1.009733	110.690317	-162.773260	-4.572257	-2.780957	-0.613408
30	O	6	1	2	1.405386	118.911030	176.234483	-5.059005	-0.542058	-0.189198
31	C	30	6	1	1.490613	110.075221	-88.961073	-5.530136	-0.596134	1.223968
32	H	31	30	6	1.094460	109.898615	59.605102	-5.167411	0.279466	1.771323
33	H	31	30	6	1.091189	105.719625	178.975509	-6.620107	-0.592188	1.172575
34	H	31	30	6	1.094475	109.841620	-61.729088	-5.171231	-1.513805	1.700354
35	O	1	6	5	1.358005	120.340657	179.402218	-3.714814	1.857687	-0.169742
36	H	35	1	6	1.010088	109.727449	-16.772299	-4.663510	1.678613	-0.466705

3.2. Charge Density:

The atomic charge density gives the information about the oxidation state of atoms and oxidation state is very important to formation of metal complexes.

The figure 1.3 and 1.4 shows the charge density of all atoms present in the patuletin dye in gas phase and water phase respectively.

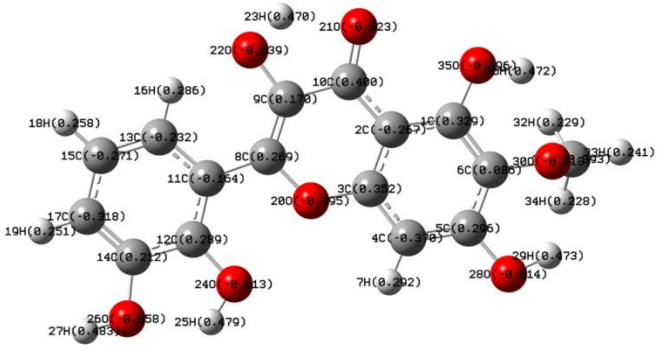

Figure 1.3. Charge density of patuletin in gas phase.

Table 2. Charge density of O-H atom in water and gas phase

Sr. no.	No. of atom	Charge density in water phase		Charge density in gas phase	
		Oxygen	Hydrogen	Oxygen	Hydrogen

1.	22,23	-0.652	0.490	-0.639	0.470
2.	24,25	-0.633	0.502	-0.613	0.479
3.	**26,27**	**-0.680**	**0.544**	**-0.658**	**0.483**
4.	28,29	-0.641	0.520	-0.614	0.473
5.	35,36	-0.630	0.517	-0.596	0.472

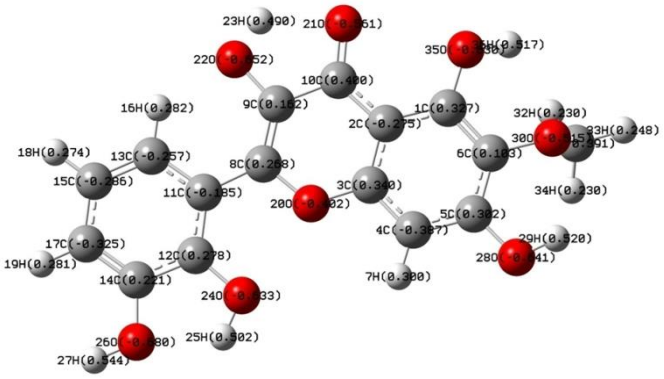

Figure 1.4. Charge density of patuletin in water phase.

In table 2 show the charge density on Oxygen and Hydrogen atom which is involve in O-H bond. From the table 2 , charge density in water phase are higher than gas phase moiety. The large effect show on 26-O and 27-H in water phase that are -0.680 and 0.544 respectively. Due to large negative charge on 26-Oxygen atom, it attract the metal towards itself.

The charge density presented in 26-O and 27-H atoms showing the good intense towards metal complex formation. So the charge density is very much important to study in the metal complex formation.

IV. CONCLUSION

From the present work, we concluded that, the quantum mechanical calculation is very much helpful to sketch the probable metal complex structure with patuletin ligand in water solvent for this only use the optimization and charge density properties by DFT method instead of complicated and costly spectrum method.

V. ACKNOWLEDGEMENTS

The authors very much thankful to principal of Ismail Yusuf college Jogeshwari, Mumbai-60 for providing the necessary facilities.

VI. REFERENCES

[1]. Koch Wolfram and Holthausen Max C., "A Chemist's Guide to Density Functional Theory". Second Edition, Copyright © (2001) Wiley-VCH Verlag GmbH.ISBNs: 3-527-30372-3 (Softcover); 3-527-60004-3 (Electronic).

[2]. Kohn W., Sham L., J. Phys. Rev. A 140 (1965) 1133.

[3]. Frisch M.J. et al., GAUSSIAN 03, Revision B04, Gaussian Inc., Wallingford, CT,(2004).

[4]. Legault C.Y., CYLVIEW, 1.0b , Université de Sherbrooke, (2009).

[5]. Jadhao N.U. and Rathod S.P., The ecosphere, 2 (1&2):103-106, (2011), ISSN: 0976-1578.

[6]. Dennington R., Keith T., Millam J., Eppinnett K., Hovell W.L., Gilliland R., Gaussview, Version 3.09, Semichem, INC., Shawnee Mission, KS, (2003).

[7]. Zhdankin V.V., Crittell C.M., Stang P.J., Tetrahedron Lett. 31 (1990) 4821.

[8]. H. Chermette, Coord. Chem. Rev. 178–180 (1998) 699.

[9]. M.C. Aragoni, M. Arca, T. Cassano, C. Denotti, F.A. Devillanova, F. Isaia, V. Lippolis, D. Natali, L. Niti, M. Sampietro, R. Tommasi, G. Verani, Inorg. Chem. Commun. 5 (2002) 869.

[10]. P. Romaniello, F. Lelj, Chem. Phys. Lett. 372 (2003) 51.

[11]. A. Voigt, U. Abram, R. Bo¨ ttcher, U. Richter, J. Reinhold, R. Kirmse, Chem. Phys. 253 (2000) 171.

[12]. B. Machura, R. Kruszynski, Polyhedron 25 (2006) 1985.

[13]. J. Gancheff, C. Kremer, E. Kremer, O.N. Ventura, J. Mol. Struct. (Theochem) 580 (2002) 107.
[14]. M.J. Frisch et al., GAUSSIAN 03, Revision B04, Gaussian Inc., Wallingford, CT, (2004).
[15]. A. D. Becke, J. Chem. Phys. 98 (1993) 5648.

International Virtual Conference on Materials and Nanotechnology
In Association with International Journal of Scientific Research in Science and Technology
Volume 9 | Issue 4 | Print ISSN: 2395-6011 | Online ISSN: 2395-602X (www.ijsrst.com)

To Study the Effect of Substrate Temperature on Optical Properties of Spray Pyrolitically Deposited $CdZnSe_{2x}Te_{2(1-X)}$ Thin Films for X=0.25

Gaikwad S. A.
Department of Physics, Guru Nanak Science College, Ballarpur, Maharashtra, India

ABSTRACT

Spray pyrolysis is a simple, inexpensive and economical method to produce a thin film on largesubstrate area. Semiconducting thin films of $CdZnSe_{2x}Te_{2(1-x)}$ for x=0.25 have been deposited onto preheated glass substrate by varying substrate temperature from 250°C at an interval of 25°C to 325°C.The optimized deposition temperature is around 300°C. From optical transmission and reflection spectra, absorption coefficient(α) was calculated at various wavelengths ranging from 350 nm to 1100 nm and was of the order of 10^4 cm^{-1}. Band gap energy were determined from absorbance measurement in visible range using Tauc theory. It shows that the main transition at the fundamental absorption edge is a direct allowed transition. At the temperature of 300°C, the optical band gap is found to 2.27 eV. At the temperatures less than or greater than 300°C, the optical band gap goes on increasing. The refractive index(n) and extinction coefficient(k) both decreases as wavelength increases which shows that the optical constants are most suitable for many scientific studies and technological applications such as heat mirrors, transparent electrodes and solar cells. SEM study provide the information regarding the morphology of the material which confirms the formation of nano sized, nanotubes. The value of lattice parameter ' a' is 6.3702 A° for $CdZnSe_{2x}Te_{2(1-x)}$ thin films deposited at substrate temperature 300°C with composition parameter 'x=0.25.'

Keywords : CdZnSe2, thin films, spray pyrolysis, absorption coefficient, optical band gap, refractive index, extinction coefficient.

I. INTRODUCTION

Semiconducting II-VI compounds because of their optoelectronic properties and their possible applications in switching and memory devices, photodiodes and solar cells. The ternary compounds including Cadmium zinc selenide have attracted much more attention in the field of solar cells due to their interesting properties of band gap. The evaluation of any material for application is complete and meaningful only when its structure and composition are precisely known. The growth of ternary compound is a opens up the possibility of their application for novel optoelectronic devices [1-4], solar cells [5], light emitting diodes [6-7], field effect transistors [8], photo electrodes, blue green lasers etc.[9]. The research of the optical properties of CdZnSe2, system forms a basis of the active region of laser and LED. Most of the work has been done on CdZnS2XSe2(1-x) system. To the best of our knowledge, very less work has been reported on selenium CdZnSe2,polycrystalline material. With this

idea in mind we present a detailed study of optical properties of $CdZnSe_{2x}Te_{2(1-x)}$ with x=0.25, in the form of thin films at different substrate temperatures. Several researchers studied properties of II-VI semiconductor films using the variety of methods such as thermal evaporation [10], vapour phase deposition [11], r.f.sputtering [12], spray pyrolysis [13-16], electrodeposition [17], chemical deposition [18]. We have chosen spray pyrolysis due to simple, inexpensive and produce a thin film on large substrate area and it is suitable for scientific studies and for many technological and industrial applications. The advantage of the technique is that just by varying the concentration of precursor and substrate temperature, it is possible to control stoichiometry of the deposits. The present study deals with the effect of substrate temperature on optical band gap of spray pyrolitically deposited $CdZnSe_{0.5}Te_{1.5}$, thin films.

II. EXPERIMENTAL DETAILS

The aquous solutions of Cadmium chloride($CdCl_2$), of Zinc chloride($ZnCl_2$), Selenium dioxide (SeO_2) and Tellurium tetrachloride($TeCl_4$) each of 0.02 M were prepared using ,in double distilled water. Chemicals used were of AR grade. The solutions are mixed in one in the proportion 1:1:1:3 by volume. The film shows a tellurium and selenium deficiency [19-20] if the ratio of proportion of solution was taken as 1:1:0.5:1.5 by volume. Sprayer was mechanically moved to and fro to avoid the formation of droplets on the substrate and insure the instant evaporation from the substrate. The distance between the sprayer nozzle and substrate was kept at 30 cm. The spraying was done in the atmosphere at the spray rate 3.5 ml/min. with a maintaining pressure of 12 Kg/cm^2. The temperature of substrate was maintained at 250°C, 275°C, 3000C, 325°C and was measured by pre-calibrated copper constantan thermocouple. The thicknesses of the films were measured by weighing method on unipan microbalance and were of the order of 0.1695 μm at substrate temperature of 300°C. It was found that as deposited $CdZnSe_{0.5}Te_{1.5}$ thin films had grayish color owing to the presence of more amount of tellurium. Optical transmittance and reflectance was taken on UV-1800-Shimandzu Spectrophotometer in the wavelength range 350 nm to 1100 nm. Analytical method of indexing the X-ray diffraction pattern was used. The copper Kα (λ=1.5418A0) radiation was used for recording the diffraction pattern.

III. RESULTS AND DISCUSSION

In spray pyrolysis technique aqueous solutions of required material are mixed in proper proportion and then sprayed onto preheated substrate. When droplets of sprayed solution reach the hot substrate, owing to pyrolytic decomposition of the solution, well adhered and good quality films are formed on the surface of the substrate.

3.1. Thickness variation

The thickness of $CdZnSe_{0.5}Te_{1.5}$ thin films deposited at various substrate temperatures was measured and the graph was plotted between the thickness of the films and substrate temperature as shown in fig.1

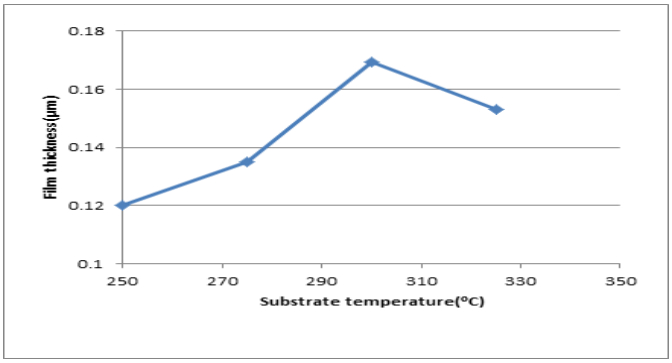

Figure 1: Variation of film thickness of $CdZnSe_{0.5}Te_{1.5}$ thin films with substrate temperature.

It was observed from the Graph that the thickness of as deposited $CdZnSe_{0.5}Te_{1.5}$ thin films increases with temperature, attains the maximum value at 300°C and then decreases with further increase in substrate temperature. At low temperatures (<300°C), the temperature may not be sufficient to decompose the

sprayed droplets from the solution and hence the deposits results into low thickness. At substrate temperature 300°C, deposition occurs at optimum rate resulting in terminal thickness of 0.1695μm. At higher substrate temperatures (>300°C) film thickness decreases due to higher evaporation rate of initial ingredients [21].

3.2. Optical study:-

Transmission spectra-

The optical transmission spectra of $CdZnSe_{0.5}Te_{1.5}$, thin films deposited at different substrate temperature was taken on UV-1800-Shimandzu spectrophotometer in the wavelength range 350 nm to 1100 nm. Fig.2. Shows the transmission versus wavelength of as deposited $CdZnSe_{0.5}Te_{1.5}$ thin films at different substrate temperatures.

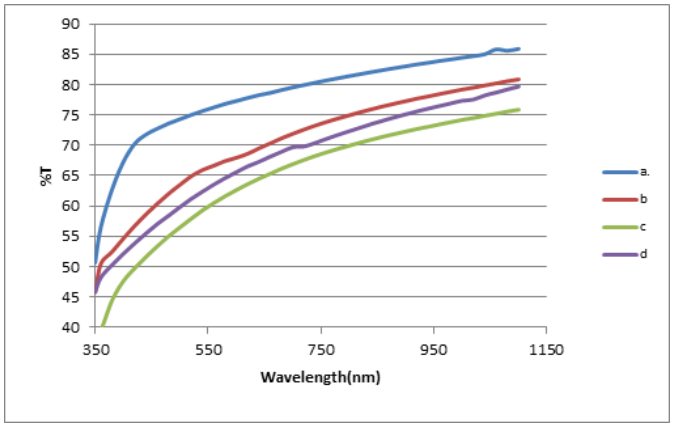

Fig.2. Transmission versus wavelength of as deposited $CdZnSe_{0.5}Te_{1.5}$ thin films at different substrate temperatures. a.250°C, b.275°C, c.300°C, d. 325°C.

The linearity of graphs in high energy region indicates direct type of transitions in the films. It was observed that onset of decrease of transmission gives the optical absorption edge. The optical coefficients were calculated for each wavelength given by relation,

$\alpha = (1/t)^* \ln(1/T)$…… (1)

Where, t- thickness of the films, T- transmittance of the film.

Reflectance spectra:- Reflectance can be calculated using above values of %transmittance and graph is plotted between reflectance(R) and wavelength in nm.

Fig. 3 represents the reflectance spectra of as deposited $CdZnSe_{0.5}Te_{1.5}$ thin films at different Substrate temperatures.

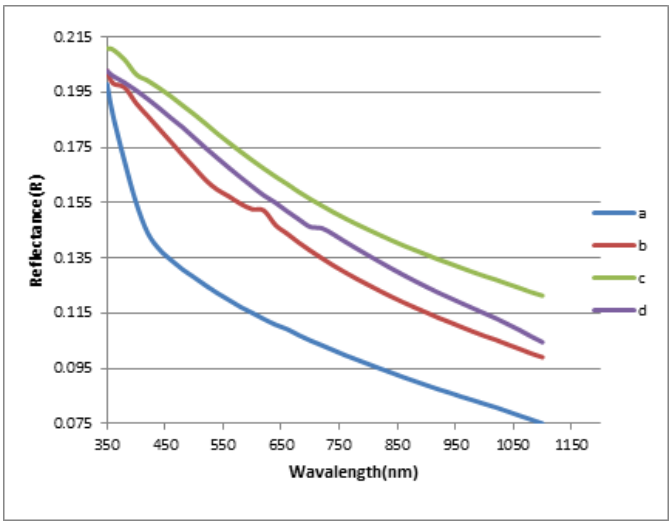

Fig.3. Reflectance spectra of $CdZnSe_{0.5}Te_{1.5}$ thin films at Substrate temperatures a.250°C,b.275°C,c.300°C,d.325°C

From **fig. 3** it was observed that as the wavelength increases there is sharp decrease in the reflectance. The onset of decrease of reflectance gives the approximate value of band gap [22].

Knowing the approximate region of band gap from reflectance curve, α is calculated by using equation (2), from the knowledge of T, R and t.

An analysis of the spectrum showed that the absorption at the fundamental absorption edge can be described by the Taue relation [23],

$\alpha = (A/hv) \times (hv-Eg)^n$ ……(2)

Where hv –photon energy, A-constant which is different for different transitions, n = 1/2 for direct band gap transition and n = 2 for indirect band gap transition.

To calculate the exact value of band gap, a graph is plotted between $(\alpha hv)^2$ versus hv of as deposited $CdZnSe_{0.5}Te_{1.5}$thin film at different substrate temperatures as shown in **fig.4.** The linearity of each graph shows the direct allowed transition, indicating the semiconducting nature of the films. The linear portion of the plot was extrapolated to meet on hv axis yield the band gap energies.

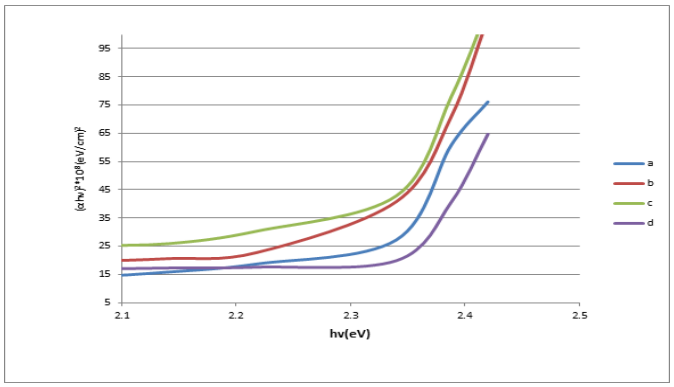

Figure 4: Variation of(αhv)² in (eV/cm)² versus hv in eV for as deposited $CdZnSe_{0.5}Te_{1.5}$ thin films at substrate temperatures a)250°C,b) 275°C,c)300°C,d)325°C

The values of optical band gap energies for as deposited $CdZnSe_{0.5}Te_{1.5}$ thin films at different substrate temperatures are shown in **Figure 5.**

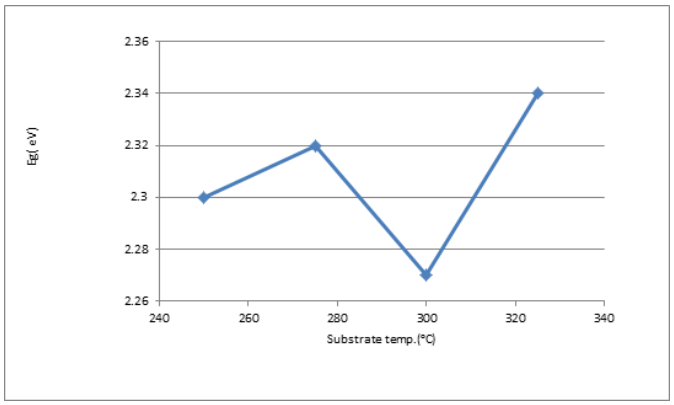

Fig 5: Variation of optical band gap energy (Eg) with substrate temperature of as deposited $CdZnSe_{0.5}Te_{1.5}$ thin films.

It is observed that optical band gaps of $CdZnSe_{0.5}Te_{1.5}$ decreases from 2.34eV to 2.27eV as substrate temperature increases from 250°C to 300°C which is due to increase in grain size with increase in substrate temperature and beyond 300°C, the optical band gap again increases with increase in substrate temperature and attains the value 2.34eV at substrate temperature of 325⁰C as shown in fig.4. These results are found to be in good agreement with that obtained by Umeshkumar *et al.* and Murali *et al.*[24-25].

K.Y.Rajpure *et.al* [26] have also reported optical band gap value vary from 1.73 to 2.58 eV of Cd1-xZnxSe thin films by varying the Zn content prepared by electrodeposition technique.

Extinction coefficient and refractive index:-

The extinction coefficient ' k' is related to absorption coefficient 'α' by the relation[27-29]

$K = \alpha \lambda / 4 \pi$..... (3)

And Refractive index 'n'for the $CdZnSe_{0.5}Te_{1.5}$ thin films at different substrate temperatures are calculated using the relation,

$n = (1 + \sqrt{R})/(1 - \sqrt{R})$..... (4)

where 'α' is the absorption coefficient , 'λ' the wavelength and 'R' the reflectance. The calculated values of extinction coefficient (k) and refractive index (n) at the wavelengths in the range 350 nm - 1100nm are plotted as a function of wavelength as shown in figs.6 and 7 respectively. Figures shows that both k and n decreases with increasing wavelength but at higher wavelengths remains approximately constant. The same results have been also reported byPankove et.al.[30].

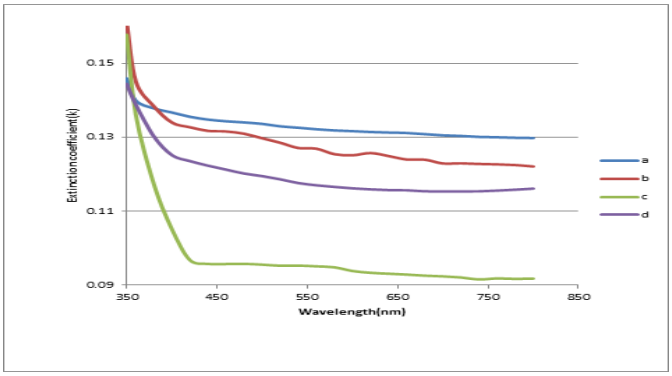

Fig.6 Variation of extinction coefficient as a function of wavelength for $CdZnSe_{0.5}Te_{1.5}$ thin film at substrate temperatures. a.250°C,b.275°C,c.300°C,d.325°C.

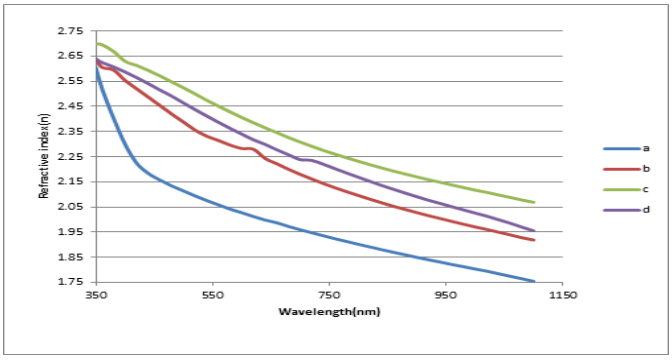

Fig7. Variation of refractive index as a function of wavelength for $CdZnSe_{0.5}Te_{1.5}$ thin films at Substrate temperatures a.250°C,b.275°C,c.300°C,d.325°C.

3.3. SEM study:-

Fig. 8 shows the SEM image if as depositedCdZnSe0.5Te1.5 thin film at the substrate temperature of 300^{0}C.

The SEM images provide the information regarding the morphology of the material which confirms the formation of nano sized, nano-tubes has the smooth surface of the films. The size of nano tubes of the films was about 556 nm.

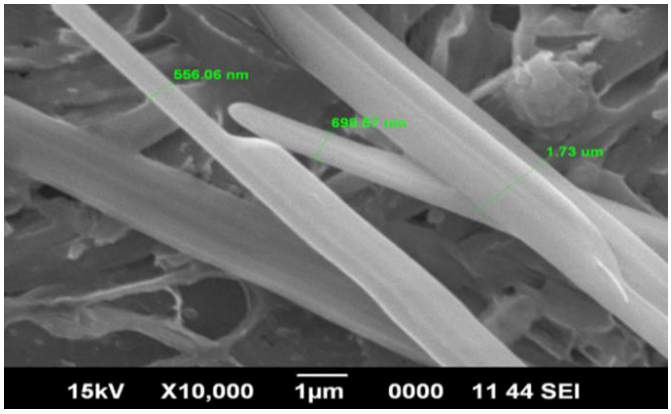

Fig. 8 SEM image if as depositedCdZnSe$_{0.5}$Te$_{1.5}$ thin film at the substrate temperature of 300^{0}C.

3.4. XRD STUDY:-

Phase analysis of deposited thin films is carried out by X-ray diffraction method using C_uK_α radiation (λ=1.5406A.U.) with 2θ=20° to 80°. XRD study of all samples were taken at room temperature. X-ray diffraction (XRD) spectra of as deposited CdZnSe$_{2x}$Te$_{2(1-x)}$ thin films deposited on glass substrate at the substrate temperature 300°C for the composition parameter x= 0.25, is shown in **Fig9**.The XRD pattern shows number of peaks indicating that the films are polycrystalline in nature. The analysis of spectrum indicated that the ternary films are having throughout cubic structure It is observed that two main peaks correspondS to (111) and (220) planes. The experimental d-values for CdZnSe$_{0.5}$Te$_{1.5}$ thin films are calculated using Bragg's relation, by taking θ values from the peaks of XRD pattern; these d-values are compared with the results of other workers [31-37].

$2d_{hkl} \sin\theta = n\lambda$,……..(5)

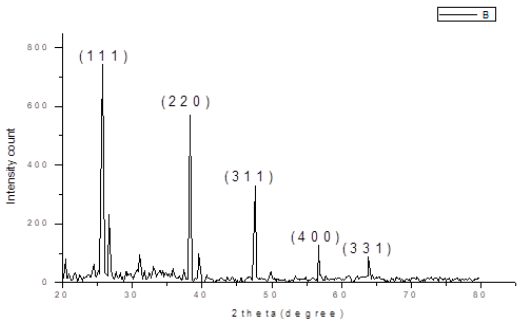

Fig.9 XRD of as deposited CdZnSe$_{2x}$Te$_{2(1-x)}$ thin film with x=0.25

The value of lattice parameter ' a' is found to be 6.3702 A° for for CdZnSe$_{2x}$Te$_{2(1-x)}$ thin films deposited at substrate temperature 300°C with composition parameter 'x=0.25' Hankare et. al.[38] prepared Cd$_{1-x}$ Zn$_x$Se thin films by chemical route method and reported that the films have cubic structure with lattice parameter varying from 6.07 A.U. to 5.66A.U. as composition parameter changes from 0 to 1.

Ibrahim[39] also studied the physical properties of vacuum deposited Cd$_{0.5}$Zn$_{0.5}$Te ternary solid solutions also reported the cubic phases with lattice parameter a=0.629 nm.The results are in good agreement with the results of Nevesha et.al.[40] who prepared Zn$_x$Cd$_{1-x}$Se thin films with various compositions by thermal vacuum evaporation technique and reported lattice parameter a to vary from 0.5676 nm to 0.5875 nm for x=1 to 0.39.

IV. CONCLUSION

Spray pyrolysis is a simple and inexpensive method to produce a thin film. At substrate temperature 300°C, deposition occurs at optimum rate resulting in terminal thickness of 0.1695 μm. . At low temperatures (<300°C), the temperature may not be sufficient to decompose the sprayed droplets from the solution and hence the deposits results into low thickness. At higher substrate temperatures (>300°C) film thickness decreases due to higher evaporation rate of initial ingredients. Optical band gap of CdZnSe0.5Te1.5 thin film at substrate temperature 300°C, was of 2.27 eV .which was calculated from

(αhv)2 versus (hv) plot. The linearity of the plot shows the direct allowed transition. It is observed that optical band gaps of CdZnSe0.5Te1.5 decreases from 2.34eV to 2.27eV as substrate temperature increases from 250°C to 300°C which is due to increase in grain size with increase in substrate temperature and beyond 300°C, the optical band gap again increases with increase in substrate temperature and attains the value 2.34eV at substrate temperature of 3250C. SEM study provides the information regarding the morphology of the material which confirms the formation of nano sized, nanotubes. The XRD pattern shows number of peaks indicating that the films are polycrystallinein nature. The analysis of spectrum indicated that the ternary films are having throughout cubic structure(sphalerite) The value of lattice parameter ' a' is 6.3702 A° for CdZnSe2xTe2(1-x) thin films deposited at substrate temperature 300°C with composition parameter 'x=0.25.'

V. REFERENCES

[1]. O. Haneman., G.H. Wenteraar., R.C. Kainthla., Sol.Energy Mater. Sol. cells 10(1984)69.

[2]. A. Ratari., R. Thangara., A.K. Sharma., B.B. Tripathi.,O. P. Agnihotri., Thin solid films91(1982)55.

[3]. A.Meskauskas., J. Viscalkas., Thin solid films 36 (1976)81.

[4]. M. Yokoyama., N.T. Chen., ALE, Journal of Crystal growth 223 (3), 2001, pp.369-75.

[5]. S. Chavhan., R. Sharma., Solar energy Materials and Solar cells 90 (9), 2006, pp.1241-53.

[6]. R. Mariappan., V.Ponnuswany., M.Ragavendar.,Characterization of CdS1-XSexthin films by chemical bath deposition technique,Optik123 (2012)1196-1200.

[7]. P.P. Hankare., V.M.Bhuse., K.M.Garadkar., S.D.Delekar., P.R. Bhagat., CdHg Sethinfilm preparation, characterization and optoelectronic studies, Semicond.Sci. Tech. 19 (2004)277-284.

[8]. B.Mereu., G.Sarau., E.Pentia., V.Draghici., M.Lisca.,T.Botila., L. Pintilie., Field effect transistor based on nanometric thin CdS films, Matt. Sci. and Engg. B 109(2004)260-263.

[9]. L.I.Maissel., R.Glang., Handbook of thin film technology, Mc Graw-Hill. New York, 1980.

[10]. R. Venugopal., R.P.Vijayalakshimi., D.R.Reddy., B.K.Reddy., J.Mater Sci.31 (1996)4081.

[11]. V.Korostelin Yu., V.I. Kozlovsky., A.S. Nasibov., P.V.Shapkin., J. Crystal Growth 159(1996)181.

[12]. S.G.Hur and E.T.Kim, J.-H.Lee, G.H. Kim and S. G.Yoon. Journal of vaccume science and technology B, Vol.26, No.4, 2008, pp.1334-1337.

[13]. Y.D. Tembhurkar. and J.P. Hirde. Bulletin of Material Science Vol.16, No.3 (1993), pp.177-186.

[14]. Y. D. Tembhurkar.and J. P. Hirde. Bulletin of Material Science Vol.17, No.5 (1994), pp.465-68.

[15]. Y.D. Tembhurkar. and J.P. Hirde. Indian J. of Pure and Appl. Physics, 28(1990) pp. 583-585.

[16]. V. Krishna Kumar., K.Ramamurthi., E.Elangovan.,Preparation of(CdO)1-X(PbO)X and (CdS)1-X(PbS)X thin films by spray pyrolysis technique and their characterization. Solid state comm.132-10(2004)673-677.

[17]. S.D.Chavhan., R.S.Mane., T.Ganesh., W.Lee.,S.H.Han., S.Senthilarasu., S.H.Lee., J.Alloy. Compd. 474 (2009) 210.

[18]. R.B. Kale., C.D. Lokhande., R.S. Mane., S.H.Han., Appl. Surf. Sci., 253(2007)3109.

[19]. Y.D.Tembhurkar and J.P.Hirde.Bull.mat.sci.17(5)465-468.

[20]. Y.D.Tembhurkar., A.S.Meshram. International J. of Scientific Research 4 sept.2016 .

[21]. R.R. Sawant., C.H. Bhosale. Indian J. Pure and Appl.Phys.44 (2006)741-745.

[22]. T.S.Moss, Optical properties of semiconductors
[23]. J.Tauc, Amorphous and liquid Semiconductors., Plenum Press, New York,NY,USA,1974
[24]. Umeshkumar P, Khairnar,Sulakshana S, Behere, Panjabrao H.2011. Pawar."The optical parameters of ZnxCd1-xTe chalcogenide thin films,Journal of surface Engineered Materials and Advanced Technology,1,51-55.
[25]. Murali, K. R., Austine, A. 2009. "Deposition of Cdx Zn1-xSe films by brush electrodeposition and their characteristics"Chalcogenide Letters Vol. 6, No. 1, p. 23 – 28.
[26]. K.Y.Rajpure., S.M. Bamane., C.D. Lokhande and C.H. Bhosale. Indian Journal of Pure and Applied Physics, Vol.37 (1999), pp.413-420.
[27]. T.J.Coutts,, J.S. Ward, D.L.Young, T. A.Dessent and R.Noufi(2001), The search for and potential impact of improved transparaent conducting oxides on thin film solar cells, Technical digest of the 12th international photovoltaic science and engineering conference, Jeju Korea June 11-15.
[28]. B. Mahrov,G.Boschloo,A.Hgfeldt,L.Dloczuk,and Th. Dittrich(2004), Photovoltage study of charge injection from dye Molecules into transparent hole and electron conductors,Appl. Phys. Lett. 84(26),5455-5457.
[29]. Mahrov, B., G. Boschloo, A. Hyfeldt, H. Siegbahn and H. Rensmo (2004), Photoelectron spectroscopy studies of Ru(dcbpyH2)2(NCS)2/CuI and Ru(dcbpyH2)2/CuSCN interfaces for solar cell applications, Journal of Physical Chemistry B, 108 (31), 11604-11610.
[30]. J. I. Pankove, "Optical Processes in Semiconductors", Dover Publications Inc., New York, p- 91.
[31]. S.A.Ringel, R.Sudharsanan, A.Rohatgi, and W.B. Carter. Journal of Electronic Materials,Vol.19.No.3,pp.259-263,1990.
[32]. T. L. Chu, S. S. Chu, C. Ferekides, and J. Britt. Journal of Applied Physics, Vol.71,No.11,pp.5635-5640,1992.
[33]. B.M.Basol,V.K.Kapur,M.L.Ferris. Journal of Applied physics Vol. 66, No.4,pp.1816-1821,1989.
[34]. K.Prasada Rao,O.Md.Hussain, K.T.R.Reddy et.al. Journal of Alloys and Compounds, Vol.218,No.1,pp.86-89,1995.
[35]. A.Haloui, Y.Feutelais,B.Legendre. Journal Alloy. Compd. 260(1997)179-192.
[36]. Haitao Xu, Run Xu, Linjun Wang,Yanyan Zhu. Journal Infrared Millim. W.31(2012)411-416.
[37]. Yaglin Wu,Haitao Xu., Huanhuan Ji., Jian Huang, Jijun Zhang, Zebo Fang, Ke.Tang,Xiaoyan Liang, Run Xu.Linjun Wang.Vacuum 132(2016),106-110.
[38]. P.P.Hankare,P.A.Chate,M.R.Asabe,S.D.Delekar, I.S.Mulla,K.M.Garadkar.J.Mater Sci.:Mater Electron(2006)17,pp.1055-1063.
[39]. A.M.Ibrahim. Vacuum,Volume 49,Number 1, pp.5 to 8(1998).
[40]. D.Nesheva,Z.Aneva,M.J.Scepanovic,Z.Levi,I.Iordanova and Z.V.Popovic. J.Phys.D:Appl.Phys.44(2011)415305(7pp).

International Virtual Conference on Materials and Nanotechnology
In Association with International Journal of Scientific Research in Science and Technology
Volume 9 | Issue 4 | Print ISSN: 2395-6011 | Online ISSN: 2395-602X (www.ijsrst.com)

Intermolecular Interactions between Saline Salts and Fertilizer : An Acoustical Approach

Paritosh L. Mishra[1*], Ajay B. Lad[2], Urvashi P. Manik[3]
[*1]Research Scholar, Department of Physics, Amolakchand Mahavidyalaya, Yavatmal, India
[2]Department of Physics, Amolakchand Mahavidyalaya, Yavatmal, India.
[3]Department of Physics, Sardar Patel Mahavidyalaya, Chandrapur, India

ABSTRACT

An attempt is made to understand the structural/molecular changes of fertilizer in saline salts which results various solute-solvent, solvent-solvent and ion-solvent interactions in order find a way to control the salinity problem. These interactions depend on the nature of solvent, size and structure of ion. For this purpose Potassium Sulfate (PS) fertilizer is being used which contain the 43% of K concentration. The ultrasonic parameters and characterization helps to forecast and understand the behavior of intermolecular interaction, strength as well as the nature of the liquid mixture present in these system. In view of above facts, the ultrasonic velocity (U) and density (ρ) measurements studies on fertilizer (PS) of number of concentrations varying from 0.02-0.2 mol-kg-1 in 0.5M solution of saline soil salts and the results were explored in terms of solute-solvent, solvent-solvent interactions and structure making or breaking effects are of great importance in understanding the extent and nature of solutions.

Keywords : Acoustical properties, Density, Fertilizer, Intermolecular interaction, Sound velocity.

I. INTRODUCTION

The salinity of soil has great effects on nutrients availability to plants or crops and on the ability of plant roots to absorb nutrients. Because of low productivity problems in the salt affected soils, fertilizers are applied to counteract the conditions which limit the plant absorption of nutrients.[1] During literature survey it has been revealed that, a decrease in the ability of the plant to absorb K generally take place in saline soils containing excess amount of Na, Mg or Ca. Therefor application of K fertilizer not only correct the deficiencies but also decrease the adverse effect of Na, Mg and Ca on the plants. Various thermo-acoustic parameters like: adiabatic compressibility, change in adiabatic compressibility, intermolecular free length, and acoustic impedance were calculated. It was occurred that there is certain degree of variation exist in these parameters with change in concentration Therefore the present work aimed to understand the structural (molecular) changes of fertilizer in saline salts solutions which explore various solute-solvent, solvent-solvent and ion-solvent interactions in order find a way to control the salinity problem.

II. EXPERIMENTAL DETAILS

A. MATERIALS

AR grade chemicals (mass fraction purity 99.8%) as Potassium Sulfate (CAS no.: 7778-80-5), Sodium Chloride (CAS no.: 7647-14-5) and Magnesium Chloride (CAS no.: 7786-30-3), were obtained from Himedia Lab. Pvt. Ltd., Mumbai. All chemicals were used as supplied. The concentrations (0.02-0.2 mol-kg^{-1}) of Potassium Sulfate in 0.5M aqueous saline salts were changed by weight. All the glassware's was washed with double distilled water as well as with acetone and dried before use.

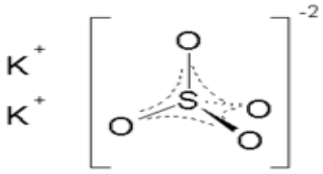

Figure: Structure of Ammonium Sulfate

B. METHOD

A digital ultrasonic velocity interferometer was used for measuring the ultrasonic velocity operating at frequency 2 MHz supplied from Vi Microsystems Pvt. Ltd., Chennai (Model VCT:71) with an overall accuracy 0.0001m/s.

The densities of the solutions were determined using 10ml specific gravity bottle having accuracy ±2*10^{-2} kg/m^3 and digital electronic balance (Contech CA-34) having accuracy ±0.0001gm. An average of triple measurements was taken into account for better accuracy. The experimental temperature was maintained constant by circulating water with the help of an automatic thermostatic water bath supplied by Lab-Hosp. Company Mumbai having an accuracy ±1K temperature.

Table 1: Density and Ultrasonic velocity of water at 288.15K temperature.

Current Work Data		Literature Data	
U. Vel. (U)	Density (ρ)	U. Vel. (U)	Density (ρ)
m/sec	kg/m^3	m/sec	kg/m^3
1466.032	999.103	1466.25	999.1

Table 2: Abbreviations used.

M	Molal Concentration in mol./kg
CAS	Chemical Abstract Service
MHz	Mega Hertz
U_∞	Infinite Value of Ultrasonic Velocity

DEFINING RELATIONS

For the derivation of several acoustical and thermo-dynamical parameters the following defining relations reported in the literature are used:

- Adiabatic Compressibility $(\beta) = 1/(U^2\rho)$
- Change in Adiabatic Compressibility $(\Delta\beta) = \{\beta-\beta_0\}$
- Intermolecular Free Length $(L_f) = K(\beta)^{1/2}$

Where, K be the Jacobson temperature dependent constant.

- Acoustic Impedance $(Z) = U\rho$

III. RESULT AND DISCUSSION

A. ULTRASONIC VELOCITY & DENSITY:

In the present work ultrasonic velocity of pure water has been measured at 288.15K temperature and the observed data tabulated in the Table 1. Comparison of observed data with literature data reported for water indicated that our results are in assent with the literature data.[2] The ultrasonic velocity (U) of fertilizer of varying concentrations (0.02-0.2 mol/kg) in 0.5M solution of both the saline salts solvents: NaCl and $MgCl_2$ measured at 288.15K temperature. The observed data of ultrasonic velocity increases with increase in concentration is tabulated in Table 3. Temperature and concentration affects the ultrasonic wave passing through solution. The increase in sound speed is accredited to the cohesion brought about by

the ionic hydration and the construction of hydrogen bond between the fertilizer-water as well as fertilizer-saline salts. [3]

Density of pure water has been measured at 288.15K temperature and the observed data tabulated in the Table 3. After Comparison of observed data with literature data reported for water indicated that our results are shows well agreement with the literature data. [4, 5] The density (ρ) of both the systems, increases with increase in concentration due to improve in compactness or structure of solvent by the addition of solute molecules. This indicates association occurs between solute and solvent molecules. [6] The increase in density results increase in the molar volume indicating the association in the components of the constituent molecules and confirms the structural rearrangement.

Table 3: Density and Ultrasonic velocity of PS + (0.5M) aq. NaCl/$MgCl_2$. at 288.15K temperature.

CONC. (M)	DENSITY		U. VELOCITY	
	0.5M-NaCl	0.5M-$MgCl_2$	0.5M-NaCl	0.5M-$MgCl_2$
0.00	1019.7	1037.4	1496.1366	1521.688
0.02	1023.0	1046.8	1501.275	1525.827
0.04	1025.8	1049.1	1504.145	1528.797
0.06	1028.6	1052.0	1507.604	1532.377
0.08	1031.4	1054.9	1511.660	1534.773
0.1	1034.1	1057.2	1514.571	1537.779
0.12	1036.4	1059.9	1516.908	1538.984
0.14	1039.7	1062.5	1518.665	1540.796
0.16	1042.6	1065.0	1521.015	1543.826
0.18	1045.0	1067.7	1524.553	1545.650
0.2	1048.0	1070.4	1526.921	1548.088

B. ADIABATIC COMPRESSIBILITY & CHANGE IN ADIABATIC COMPRESSIBILITY:

Physico-chemical properties of liquid can be understood by adiabatic compressibility (β) as the hydrogen bonding between the unlike components in the solutions decreases with the compressibility. In the present case it is found that the adiabatic compressibility decreases with increase in concentration. Because, as water is polar solvent and when salts and fertilizer mixed, the well intermolecular interaction occurred, resulting in close packing of molecules. The decrease values of adiabatic compressibility listed in Table 4 indicate the strong association of fertilize and saline salts molecules. The compressibility of the solvent is higher than that of solution and decreases with increase in concentration of the solution.[7]

After calculating the values of change in adiabatic compressibility against concentration as listed in Table 4 it is found that the negative values of 'Δβ' is due to the solute-solvent interaction. Such an increase in 'Δβ' with increase in concentration may be attributed to an increase in the cohesive forces in solution. [8] The negatively increase in 'Δβ' values confirms the negatively increase of bulk modulus values with concentration indicates that the hydrogen bonding between the unlike components in the solution increases. [9]

Table 4: Adiabatic Compressibility and Change in Adiabatic Compressibility of PS + (0.5M) aq. NaCl/$MgCl_2$. at 288.15K temperature.

CONC. (M)	ADI. COMPRESSIBILITY		CHANGE IN AD. COMPR.	
	0.5M-NaCl	0.5M-$MgCl_2$	0.5M-NaCl	0.5M-$MgCl_2$
0.00	4.38112E-10	4.16296E-10	0	0
0.02	4.33714E-10	4.10323E-10	-4.398E-12	-5.9734E-12
0.04	4.30882E-10	4.07834E-10	-7.230E-12	-8.4622E-12
0.06	4.27739E-10	4.04812E-10	-1.037E-11	-1.1485E-11
0.08	4.24292E-10	4.02439E-10	-1.382E-11	-1.3857E-11
0.1	4.21559E-10	3.99995E-10	-1.655E-11	-1.6301E-11
0.12	4.19328E-10	3.98352E-10	-1.878E-11	-1.7944E-11
0.14	4.17031E-10	3.96443E-10	-2.108E-11	-1.9853E-11
0.16	4.14587E-10	3.93961E-10	-2.352E-11	-2.2335E-11
0.18	4.11717E-10	3.92038E-10	-2.640E-11	-2.4258E-11
0.2	4.09266E-10	3.89819E-10	-2.885E-11	-2.6478E-11

C. INTERMOLECULAR FREE LENGTH & ACOUSTIC IMPEDANCE:

Intermolecular free length (L_f) is one of the important parameter in determining the nature as well as

strength of interaction between the components of solution. It is the average distance between the surfaces of two neighboring molecules, which is called intermolecular free length.[10] Variation of free length is set down in Table 5. It is observed that the free length decreases with increase in concentration of fertilizer in saline solution. This indicates that there exists a significant interaction among the fertilizer and electrolyte solution. Among both the saline salts (NaCl and $MgCl_2$) intermolecular free length values are found low in water, while in the case of electrolyte solutions, it is found low in $MgCl_2$ indicating strong intermolecular interaction of fertilizer with $MgCl_2$. The observed order of variation of intermolecular free length (L_f) in water as well as in salt solution is: $MgCl_2$>NaCl>H_2O

The values of acoustic impedance for fertilizer: Potassium Sulfate of different concentration viz. 0.02-0.2mol/kg in 0.5M solution of aqueous electrolyte solution of NaCl and $MgCl_2$ was calculated and tabulated in Table 5 respectively. It is observed that the acoustic impedance (Z) values of Potassium Sulfate fertilizer increases with increase in concentration of fertilizer in the both 0.5M aqueous electrolyte solutions and the values centered around 1Rayal. The increase in acoustic impedance with the increase in concentration indicates the greater association among solute and solvent through hydrogen bonding. Thus increase in acoustic impedance indicates associative nature of solute and solvent and enhancement in molecular interaction.[11] The order of variation of acoustic impedance (Z) in water as well as in salt solution is: MgCl2>NaCl>H2O.

Table 5 : Intermolecular Free Length and Acoustic Impedance of PS + (0.5M) aq. NaCl/$MgCl_2$. at 288.15K temperature.

CONC. (M)	INTER. FREE LENGTH		ACOUSTIC IMPEDANCE	
	0.5M-NaCl	0.5M-$MgCl_2$	0.5M-NaCl	0.5M-$MgCl_2$
0.00	4.2266E-11	4.1201E-11	1525610.491	1578599.131
0.02	4.2054E-11	4.0904E-11	1535804.325	1597235.704
0.04	4.1916E-11	4.0780E-11	1542951.941	1603860.933
0.06	4.1763E-11	4.0628E-11	1550721.474	1612060.604
0.08	4.1594E-11	4.0509E-11	1559126.124	1619032.038
0.1	4.1460E-11	4.0386E-11	1566217.871	1625739.959
0.12	4.1351E-11	4.0303E-11	1572123.451	1631169.142
0.14	4.1237E-11	4.0206E-11	1578956.001	1637095.75
0.16	4.1116E-11	4.0080E-11	1585810.239	1644174.69
0.18	4.0974E-11	3.9982E-11	1593157.885	1650290.505
0.2	4.0851E-11	3.9869E-11	1600213.208	1657073.395

IV. CONCLUSION

The various acoustical parameters determined by using the measured values of density and ultrasonic velocity of Potassium Sulfate solutions in both electrolyte solution (NaCl and $MgCl_2$). All parameters used to investigate the intermolecular interactions between the Potassium Sulfate fertilizer molecules and saline salts. The impact of concentration on these parameters were observed and studied. In the light of above observations and discussions, it may be concluded that: the concentration, nature of solute, nature of solvent and its position plays an important role in determining the interactions occurring in the solution. Also it is concluded that H-bonding interaction is strong at higher concentration. Moreover, the values of density and compressibility for Potassium Sulfate fertilizer are found to be maximum with $MgCl_2$ coz it has weak interaction with water molecules among the electrolyte solution and ergo can bind with fertilizer molecules more effectively.

V. REFERENCES

[1]. Gowaliker V., Krishnamurthy V.N., Gowarikar S., Dhanorkar M., Pranjape K. (2009). The fertilizer Encyclopedia, John Wiley and Sons, 43-48.

[2]. Greenspan M., Tschiegg C.E. (1957) J. of Research of the National Bureau of Standards, 59(4), 249-254.

[3]. Kumar P., (2012) Rasayan J. Chem., 5(3), 424-431.

[4]. Chauhan S., Kumar K. (2014) J. Mol. Liq., 194, 212-226.

[5]. Naseem B., Jamal A., (2013) J. Mol. Liq., 181, 68-76.

[6]. Malasane P.R., (2013) Res. J. Chem. Sci., 3(8), 73-77.

[7]. Endo H., (1973) Bull. Chem. Soc. Jpn, 46(4), 1106-1111.

[8]. Sumanthi T. and Varalakshmi M.., (2010) Rasayan J. chem., 3(3), 550-555.

[9]. Iqbal M., Venrall R.E.,(1989) Canadian Journal of Chemistry, 64(7), 727-735.

[10]. Thirumaran S., Inbum P., (2011) Ind. J. Pure and Appl. Phys., 49, 451-459.

[11]. Nithiyanathan S., Palanippan L., (2012) Arab. J. Chem, 5, 25-30

IJSRST

INTERNATIONAL VIRTUAL CONFERENCE ON MATERIALS AND NANOTECHNOLOGY IVCMN-2021

Jointly Organized by

Guru Nanak College of Science, Ballarpur

In Association with

P. R. Pote (Patil) College of Engineering and Management, Amravati

Publisher

Technoscience Academy

Website : www.technoscienceacademy.com

Email : editor@ijsrst.com Website : http://ijsrst.com